

This work is protected by copyright and other intellectual property rights and duplication or sale of all or part is not permitted, except that material may be duplicated by you for research, private study, criticism/review or educational purposes. Electronic or print copies are for your own personal, non-commercial use and shall not be passed to any other individual. No quotation may be published without proper acknowledgement. For any other use, or to quote extensively from the work, permission must be obtained from the copyright holder/s.



# Remote control healing for osteoarthritis repair

---

**Iria Echevarria**

Submitted for the Degree of Doctor of Philosophy

October 2022

Keele University

## Abstract

Articular cartilage is a key tissue for the normal functioning of the joints, with a trend for degradation with aging and physical activity. The lack of vascularisation hinders the self-repair, and often a scar tissue replaces the damaged cartilage, failing to fulfill the mechanical and functional needs for normal functioning of the joints. Current therapeutic approaches fail to stop the progression of this chronic disease, and represent a huge economic burden for the health system. The need for a less-invasive treatment for delaying the progression of the disease while improving the life quality of the patient has led to tissue engineering scientists to research for a potential therapy. Currently research has focused on MSCs for their expansion potential, multi-lineage differentiation and low immunogenicity. Despite the promising outcome of novel studied there is still need for techniques that manage to generate tissue matching those properties of the native cartilage.

This work aimed to develop a new technique for cartilage regeneration that could potentially deliver a remote therapy. UC-MSCs were studied as a potential cell source for chondrogenic differentiation using the MICA technology. Cells were labelled with MNPs targeted towards TRPV4, a mechano-sensitive ion channel involved in cartilage homeostasis (1). The channel was activated following MNPs labelling of cells, by using a magnetic force bioreactor that generates an external alternating magnetic field. The force exerted by the activated MNPs trigger the activation of the ion channel, with the subsequent ion exchange and signaling activation pathway.

The effects of the MICA technology on the chondrogenic response were assessed by in-depth histological and immunohistochemical assessment of the cartilage constructs. In addition, gene expression analysis of chondrogenic markers and early transcription factors was performed on several cell sources.

The combination of the MICA technology together with the aid of biochemical cues resulted in constructs showing enhanced deposition of chondrogenic markers at early time points. Elevated

collagen II, proteoglycans and *SOX9* was observed for the 3D constructs without any presence of hypertrophy signs. This was observed for all tested cell sources with a promising potential for UC-MSCs as candidates for cartilage repair. We believe that the work here has a great potential for developing a therapy for cartilage repair based on the combination of MSCs and MNPs with the aid of the MICA technology.

## Contents

|  |       |
|--|-------|
| <i>Abstract</i> .....                              | i     |
| <i>Contents</i> .....                              | iii   |
| <i>Figures</i> .....                               | ix    |
| <i>Tables</i> .....                                | xvi   |
| <i>Supplementary figures</i> .....                 | xvii  |
| <i>Abbreviations</i> .....                         | xviii |
| <i>Publications and presentations</i> .....        | xxi   |
| <i>Acknowledgments</i> .....                       | xxii  |
| <b>Introduction</b> .....                          | 1     |
| 1.1 Joints and Cartilage: Anatomical review.....   | 2     |
| 1.2 Articular cartilage .....                      | 4     |
| 1.2.1 Structure of articular cartilage.....        | 4     |
| 1.2.2 Extracellular matrix.....                    | 7     |
| 1.2.3 Function and Mechanical Properties.....      | 9     |
| 1.3 Osteoarthritis and clinical approaches .....   | 10    |
| 1.3.1 Pharmacological and surgical approaches..... | 13    |
| 1.4 Cartilage tissue engineering .....             | 16    |
| 1.4.1 Cell sources .....                           | 17    |
| Chondrocytes.....                                  | 17    |
| Adult stem cells.....                              | 17    |
| Foetal stem cells .....                            | 20    |
| 1.4.2 Bioreactors and biomaterials.....            | 22    |
| 1.5 Mechanotransduction .....                      | 26    |
| 1.5.1 RGD .....                                    | 29    |

|  |    |
|--|----|
| 1.5.2 TREK .....   | 31 |
| 1.5.3 TRPV4.....   | 33 |
| 1.6 Magnetic nanoparticles .....   | 43 |
| 1.6.1 Magnetic nanoparticle design .....   | 43 |
| 1.6.2 Current applications .....   | 48 |
| 1.6.3 MNPs and Mechanotransduction: Applications in orthopaedics.....                            | 51 |
| 1.7 Concept approach and hypothesis .....  | 57 |
| <b>Materials and methods</b> .....   | 60 |
| 2.1 Materials .....  | 61 |
| 2.2 General cell culture techniques .....  | 66 |
| 2.2.1 Coating tissue culture plastic with fibronectin .....                                      | 66 |
| 2.2.2 Resuscitation and seeding of frozen cells.....   | 67 |
| 2.2.3 Passaging cells .....  | 67 |
| 2.2.4 Cryopreservation of cells .....  | 68 |
| 2.2.5 Manual cell counting .....   | 68 |
| 2.2.6 Automated cell counting .....  | 68 |
| 2.3 Isolation and culture of cells.....  | 69 |
| 2.3.1 Isolation and culture of bone marrow mesenchymal stem cells from bone marrow aspirate..... | 69 |
| 2.3.2 Isolation and culture of ovine chondrocytes from lamb knee .....                           | 69 |
| 2.3.3 Lentiviral transfection and culture of adipose-derived equine mesenchymal stem cells.....  | 70 |
| 2.3.4 Isolation and culture of ovine MSCs.....   | 71 |
| 2.3.5 Culture of human umbilical cord-derived mesenchymal stem cells .....                       | 72 |
| 2.3.6 Monolayers and micromasses formation and culture .....                                     | 73 |
| 2.3.7 Pellet formation and culture .....   | 73 |
| 2.4 Chondrogenic differentiation induction media .....   | 74 |
| 2.4.1 Biochemical activation of TRPV4 .....  | 75 |
| 2.5 Particle labelling.....  | 75 |
| 2.5.1 Magnetic nanoparticle activation.....  | 75 |
| 2.5.2 Magnetic nanoparticle coating with TRPV4, TREK-1 and RGD .....                             | 75 |
| 2.5.3 Magnetic nanoparticle labelling of monolayers.....   | 76 |

|  |    |
|--|----|
| 2.5.4 Magnetic nanoparticle labelling of micromasses and pellets ..... | 77 |
| 2.6 Magnetic activation .....  | 77 |
| 2.7 Histological staining of pellets and tissue sections.....          | 79 |
| 2.7.1 Pellet size .....  | 79 |
| 2.7.2 Sample dehydration and paraffin embedding.....                   | 80 |
| 2.7.3 APES Coating of slides.....                                      | 80 |
| 2.7.4 Sample sectioning and de-paraffinisation .....                   | 80 |
| 2.7.5 Haematoxylin and eosin staining.....                             | 81 |
| 2.7.6 Toluidine blue staining.....                                     | 81 |
| 2.7.7 Alcian blue staining.....  | 81 |
| 2.7.8 Picrosirius red staining.....                                    | 82 |
| 2.7.9 Prussian blue staining .....                                     | 82 |
| 2.7.10 Safranin O staining.....  | 83 |
| 2.8 Histological assessment of monolayers and micromasses.....         | 83 |
| 2.8.1 Sample preservation.....   | 83 |
| 2.8.2 Sample histological staining .....                               | 84 |
| 2.9 Immunohistochemistry.....  | 84 |
| 2.9.1 Antigen retrieval, permeabilisation and blocking .....           | 84 |
| 2.9.2 Primary antibody staining.....                                   | 84 |
| 2.9.3 Secondary antibody and DAPI staining.....                        | 85 |
| 2.9.4 Pellet immunohistochemistry.....                                 | 85 |
| 2.9.5 Fluorescence quantification.....                                 | 86 |
| 2.10 Cell viability and proliferation .....                            | 86 |
| 2.10.1 Presto™ blue .....  | 86 |
| 2.10.2 Live / Dead assay .....   | 87 |
| 2.11 CM-Dil labelling of pellets.....                                  | 88 |
| 2.12 Proteinase K digestion of pellets .....                           | 88 |
| 2.13 DMMB sulphated GAGs assay .....                                   | 89 |
| 2.13.1 Preparation of DMMB solution .....                              | 89 |
| 2.13.2 Preparation of samples.....                                     | 89 |

|   |            |
|---|------------|
| 2.14 PicoGreen double stranded DNA assay .....              | 89         |
| 2.15 RNA isolation from pellets .....                       | 90         |
| 2.15.1 Cell lysis and homogenisation .....                  | 90         |
| 2.15.2 Isolation of RNA using the RNeasy mini kit .....     | 90         |
| 2.16 Reverse transcription.....                             | 91         |
| 2.17 Quantitative real-time polymerase chain reaction ..... | 92         |
| 2.17.1 Preparation of the samples .....                     | 92         |
| 2.17.2 Gene amplification.....                              | 93         |
| 2.17.3 qRT-PCR data analysis.....                           | 94         |
| 2.17.4 qRT-PCR Primer design .....                          | 94         |
| 2.18 Agarose gel electrophoresis .....                      | 96         |
| 2.19 Flow cytometry characterisation.....                   | 96         |
| 2.20 Magnetic nanoparticle characterisation.....            | 97         |
| 2.20.1 Particle size .....                                  | 97         |
| 2.20.2 Particle surface charge .....                        | 98         |
| 2.20.3 Total protein determination .....                    | 98         |
| 2.21 Transmission electron microscopy (TEM).....            | 99         |
| 2.22 Luciferase measurement .....                           | 99         |
| 2.23 RNA sequencing .....                                   | 99         |
| 2.24 Statistical analysis .....                             | 100        |
| <b><i>Cells and MNPs characterisation</i></b> .....         | <b>101</b> |
| 3.1 Introduction .....                                      | 102        |
| 3.2 Aims .....  | 105        |
| 3.3 Methods.....  | 105        |
| 3.3.1 Magnetic nanoparticle characterisation.....           | 105        |
| 3.3.2 Cytotoxicity study of MNPs .....                      | 105        |

|        |  |     |
|--------|--|-----|
| 3.3.3  | Characterisation of MSCs.....  | 106 |
| 3.3.4  | Magnetic activation of MSCs for chondrogenic differentiation.....                                    | 107 |
| 3.3.5  | Gene expression analysis of TC28 cells.....  | 108 |
| 3.3.6  | Statistical analysis.....  | 108 |
| 3.4    | Results.....   | 109 |
| 3.4.1  | Determination of MNPs hydrodynamic size and charge.....  | 109 |
| 3.4.2  | MNPs protein determination.....  | 111 |
| 3.4.3  | Study of the cytotoxic effect of the MNPs.....   | 112 |
| 3.4.4  | TRPV4-MNPs labelling efficiency.....   | 116 |
| 3.4.5  | MSCs characterisation.....   | 117 |
| 3.4.6  | Human MSCs chondrogenic potential following MICA induction.....                                      | 121 |
| 3.4.7  | Chondrogenic early transcription factor study.....   | 127 |
| 3.5    | Discussion.....  | 129 |
| 3.6    | Conclusions.....   | 134 |
|        | <b><i>Assessment of MICA potential for in vitro chondrogenic induction in animal cells</i></b> ..... | 135 |
| 4.1    | Introduction.....  | 136 |
| 4.2    | Aims.....  | 140 |
| 4.3    | Methods.....   | 140 |
| 4.3.1  | Experimental design: Part I.....   | 140 |
| 4.3.2  | Collagen II tracking.....  | 141 |
| 4.3.3  | Histological and immunohistochemical analysis.....   | 142 |
| 4.3.4  | Primer optimisation and gene expression.....   | 142 |
| 4.3.5  | DNA and sGAG analysis.....   | 142 |
| 4.3.6  | Luciferase detection.....  | 143 |
| 4.3.7  | Experimental design: Part II.....  | 143 |
| 4.3.8  | Histological and immunohistochemical assessment.....   | 143 |
| 4.3.9  | Molecular analysis of chondrogenesis.....  | 144 |
| 4.3.10 | Statistical analysis.....  | 144 |
| 4.4    | Results.....   | 145 |
| 4.4.1  | Determination of possible chondro-inductive targets for the MICA technology.....                     | 145 |

|   |            |
|---|------------|
| 4.4.2 MICA activation of TRPV4 channel .....  | 151        |
| 4.4.3 Collagen II expression analysis: Luciferase – Col 2 Reporter .....                        | 161        |
| 4.4.4 Effect of TGF- $\beta$ presence in the culture medium following MICA activation .....     | 164        |
| 4.4.5 Histological determination of TRPV4-MICA activation for chondrogenic differentiation..... | 172        |
| 4.5 Discussion .....  | 172        |
| 4.6 Conclusions .....   | 184        |
| <b><i>Human UC-MSCs as potential candidates for an injectable OA therapy.....</i></b>           | <b>185</b> |
| 5.1 Introduction .....  | 187        |
| 5.2 Aims .....  | 189        |
| 5.3 Methods.....  | 189        |
| 5.3.1 Experimental design .....   | 189        |
| 5.3.2 Histological and immunohistochemical analysis .....                                       | 192        |
| 5.3.3 Gene expression and DNA / sGAGs analysis.....   | 192        |
| 5.3.4 Statistical analysis .....  | 193        |
| 5.4 Results.....  | 194        |
| 5.4.1 Pellet size analysis.....   | 194        |
| 5.4.2 Pellet histology .....  | 195        |
| 5.4.3 Pellets sGAGs and DNA production .....  | 233        |
| 5.4.4 Chondrogenic gene expression .....  | 237        |
| 5.5 Discussion .....  | 239        |
| 5.6 Conclusions .....   | 247        |
| <b><i>Discussion, future work and concluding remarks.....</i></b>                               | <b>248</b> |
| 6.1 Summative discussion.....   | 249        |
| 6.2 Future work .....   | 255        |
| 6.3 Concluding remarks .....  | 258        |
| <b><i>References.....</i></b>   | <b>259</b> |
| <b><i>Appendices .....</i></b>  | <b>300</b> |

## Figures

|   |     |
|---|-----|
| Figure 1-1. Anatomical description of the knee joint in a sagittal view .....   | 3   |
| Figure 1-2. Zonal organisation of articular cartilage.....  | 5   |
| Figure 1-3. Macromolecular structure of proteoglycans embedded on a collagen network .....  | 8   |
| Figure 1-4. Schematic representation of the role of proteoglycans in the cartilage under compressive load .....   | 10  |
| Figure 1-5. Structural and molecular changes in OA.....   | 12  |
| Figure 1-6. Therapeutic strategies to address cartilage repair and regeneration.....  | 16  |
| Figure 1-7. Focal adhesion mediated mechanotransduction .....   | 27  |
| Figure 1-8. Molecular structure of TREK-1 channel and the various stimuli triggering the channel activity .....   | 32  |
| Figure 1-9. Structural composition of the TRPV4 protein located in the membrane.....  | 35  |
| Figure 1-10. Schematic representation of the different magnetic states of the materials without an external magnetic field and in the presence of the magnetic field..... | 45  |
| Figure 1-11. Biomedical applications of MNPs.....   | 50  |
| Figure 1-12. Different methods for MNP actuation on cell mechanotransduction .....  | 54  |
| Figure 1-13. Schematic representation of the magnetic ion channel activation (MICA) principle .....   | 56  |
| Figure 2-1. Schematic diagram of the expansion process of the umbilical cord-derived stem cells. ..   | 72  |
| Figure 2-2. MICA Magnetic Bioreactor and control unit .....   | 79  |
| Figure 2-3. qRT-PCR Thermal cycler programme.....   | 94  |
| Figure 3-1. Surface modification of 250 nm Nanomag particles increases the hydrodynamic size and results in a more stable solution than plain particles.....              | 110 |
| Figure 3-2. MNPs antibody coating was successfully performed.....   | 111 |
| Figure 3-3. Cell viability is not affected by the presence of MNPs .....  | 112 |
| Figure 3-4. Representative images of dead cells cultured in pellets .....   | 113 |

|  |     |
|--|-----|
| Figure 3-5. Decreased proliferation over culture time .....  | 114 |
| Figure 3-6. Quantification of the cell death showed similar levels for all groups and time points....  | 115 |
| Figure 3-7. No toxic effects found when labelling cells with MNPs regardless of the protein<br>functionalisation .....   | 116 |
| Figure 3-8. Internalisation of MNPs observed immediately after cell labelling .....  | 117 |
| Figure 3-9. TRPV4 channel is found among hMSCs .....   | 118 |
| Figure 3-10. TRPV4 channel is present in ovine MSCs.....   | 118 |
| Figure 3-11. TRPV4 channel is found among eMSCs .....  | 119 |
| Figure 3-12. TRPV4 channel is found among hUC-MSCs being present for all visualised cells .....  | 119 |
| Figure 3-13. TRPV4 channel is expressed in both human UC-MSCs and equine MSCs.....   | 120 |
| Figure 3-14. Pellet size decreased over culture time being higher for MICA activated samples in 10%<br>FBS .....   | 121 |
| Figure 3-15. MNPs stay present after 21 days of culture .....  | 122 |
| Figure 3-16. Moderately higher deposition of sGAGs in TRPV4 activated samples cultured in 10% FBS<br>.....   | 123 |
| Figure 3-17. Mechanically and chemically TRPV4 activated samples showed enhanced proteoglycan<br>production. ....  | 124 |
| Figure 3-18. Higher collagen deposition for TRPV4 static samples. ....   | 125 |
| Figure 3-19. Enhanced collagen II production for MICA activated samples in 10% FBS at early time<br>points .....   | 126 |
| Figure 3-20. Decrease of collagen II signal with culture time.....   | 127 |
| Figure 3-21. Chondrogenic transcription factors were activated for TRPV4 activated samples with<br>GSK101 or MICA stimulation with little variation across experiments ..... | 128 |
| Figure 4-1. dTomato marker observed in eMSCs indicates successful transfection of the GFP-Col2<br>reporter.....  | 145 |

|   |     |
|---|-----|
| Figure 4-2. Culture of samples in basic media is not sufficient for chondrogenic induction after 21 days of culture regardless the magnetic activation..... | 146 |
| Figure 4-3. Regardless of the lack of TGF- $\beta$ , TRPV4-labelled samples showed early expression of collagen II at day 10.....                           | 147 |
| Figure 4-4. TRPV4 labelled samples showed enhanced collagen II production at day 21 of culture..  | 148 |
| Figure 4-5. Collagen fibres were observed in all MICA activated samples regardless of the presence of TGF- $\beta$ in the culture medium.....               | 149 |
| Figure 4-6. TRPV4 activated samples cultured with TGF- $\beta$ showed enhanced gene expression for all genes and when compared to all groups .....          | 150 |
| Figure 4-7. The constitutively expressed dTomato fluorescence was visualised from the initiation of culture with no signs of a GFP-Collagen II signal ..... | 151 |
| Figure 4-8. TRPV4 MICA-activated samples showed early expression of collagen II that increased for the duration of the culture time.....                    | 152 |
| Figure 4-9. TRPV4 MICA-activated cells beginning to acquire a chondrocyte-like phenotype from early culture time points. ....                               | 153 |
| Figure 4-10. TRPV4-MNPs labelled samples showed higher collagen production than unlabelled samples.....   | 154 |
| Figure 4-11. Enhanced sGAGs deposition in TRPV4-MNPs labelled samples with a higher density observed for MICA activated micromasses.....                    | 155 |
| Figure 4-12. Enhanced cartilage ECM deposition on TRPV4 MICA-activated samples .....  | 156 |
| Figure 4-13. MNPs of the labelled micromasses were found mostly on the pellets formed by the cells .....  | 157 |
| Figure 4-14. TRPV4 MICA-activated samples showed enhanced proliferation and the TRPV4 channel was present for all treated conditions.....                   | 158 |

|  |     |
|--|-----|
| Figure 4-15. Few differences were found between samples cultured in chondro-inductive media unstimulated and TRPV4 MICA-activated groups for sGAGs production.....                       | 159 |
| Figure 4-16. Higher <i>Col2a1</i> expression was observed for TRPV4 MICA-activated samples, and no differences were found among groups for <i>Acan</i> expression analysis .....         | 161 |
| Figure 4-17. Cells were successfully transfected with the GFP reporter.....  | 162 |
| Figure 4-18. No statistical differences were found among experimental groups for Col2-Luc reporter cell line.....  | 162 |
| Figure 4-19. No toxic effects found when labelling cells with MNPs for any of the cell types .....   | 163 |
| Figure 4-20. Increased pellet size and GAGs deposition for de-differentiated chondrocytes pellets with elevated matrix formation in TREK-1 and TRPV4 activated samples .....             | 165 |
| Figure 4-21. Enhanced collagen production on de-differentiated chondrocytes over MSCs, with elevated deposition for TREK-1 and TRPV4 MICA-activated samples cultured in complete media . | 166 |
| Figure 4-22. Medium organised fibres for all samples with an outer ring formation. ....  | 167 |
| Figure 4-23. Higher production of collagen II for both cell types in TREK-1 and TRPV4 activated samples cultured with or without TGF- $\beta$ .....                                      | 168 |
| Figure 4-24. Enhanced production of aggrecan for MSCs and TREK-1 and TRPV4-MICA activated samples.....   | 169 |
| Figure 4-25. MNPs were present in labelled samples for both cell types.....  | 170 |
| Figure 4-26. Variable gene expression pattern with overall higher expression found among samples cultured with TGF- $\beta$ for both cell types.....                                     | 171 |
| Figure 4-27. Day 1 images.....   | 172 |
| Figure 4-28. Low levels of sGAGs were found for all compared groups.....   | 172 |
| Figure 4-29. Enhanced deposition found among TRPV4 MICA-activated samples with proteoglycans deposited in the periphery .....  | 172 |

|  |     |
|--|-----|
| Figure 4-30. Enhanced collagen production for TRPV4 MICA-activated samples from initial culture time points.....                             | 172 |
| Figure 4-31. Higher intensity of the stain observed in TRPV4 MICA-activated samples from day 7 of culture.....                               | 176 |
| Figure 5-1. Pellet size increases with culture time for all groups with an enhanced size in MICA activated samples cultured with 1% FBS..... | 194 |
| Figure 5-2. MNPs were present after 21 days of culture with some areas of higher aggregation.. .   | 196 |
| Figure 5-3. Clustering of MNPs was present in all samples and similar concentration of particles after 21 days of culture. ....              | 197 |
| Figure 5-4. MNPs were homogeneously distributed on the sections with little clustering observed  | 198 |
| Figure 5-5. Homogeneous distribution of MNPs observed on pellet sections from pooled donors .  | 199 |
| Figure 5-6. Alcian blue staining of a pellet sample at day 0 of culture and human cartilage samples .....                                    | 200 |
| Figure 5-7. TRPV4 activated samples showed enhanced sGAGs deposition.....  | 201 |
| Figure 5-8. MICA activated samples cultured in 10% FBS showed evident increase in sGAGs production .....                                     | 202 |
| Figure 5-9. Lower stain intensity was observed for all studied groups from donor 3 samples.....  | 203 |
| Figure 5-10. Similar sGAG deposition to previous experiments was observed with lower stain levels for control samples.....                   | 204 |
| Figure 5-11. Toluidine blue staining of negative and positive controls.....  | 205 |
| Figure 5-12. Enhanced proteoglycan production observed for TRPV4 stimulated samples.....   | 206 |
| Figure 5-13. Higher GAGs production for groups cultured in 10% FBS than for same groups cultured in 1% FBS.....                              | 207 |
| Figure 5-14. Lower intensity of the stain was found in donor 3 for all studied groups when compared to previous donors.....                  | 208 |

|  |     |
|--|-----|
| Figure 5-15. MICA stimulated samples showed evident enhanced GAGs production.....  | 209 |
| Figure 5-16. Picrosirius red staining of collagen of day 0 pellet and human cartilage controls.....  | 210 |
| Figure 5-17. Higher collagen deposition for TRPV4 activated samples with a homogeneous distribution .....  | 211 |
| Figure 5-18. Samples cultured in 10% FBS showed higher collagen production than the homologous groups cultured in 1% FBS .....   | 212 |
| Figure 5-19. Higher collagen production for samples cultured in 10% FBS with MICA stimulated group showing increased production of the marker .....  | 213 |
| Figure 5-20. Enhanced collagen production at early time points for all studied groups .....  | 214 |
| Figure 5-21. Day 0 pellet and cartilage positive control.....  | 215 |
| Figure 5-22. TRPV4 activated samples showed enhanced collagen II production and little collagen X was detected after 21 days.....  | 216 |
| Figure 5-23. Lower general production of collagen II with enhanced production on MICA activated groups and mild presence of collagen X detected for samples after 21 days of culture ..... | 217 |
| Figure 5-24. High levels of collagen II were detected with more pronounced production of MICA samples cultured in 10 % FBS and low overall collagen X production .....                     | 218 |
| Figure 5-25. Increased levels of collagen II over culture time with higher presence in TRPV4 MNPs-labelled samples and low detection of collagen X.....                                    | 219 |
| Figure 5-26. Lower collagen II in samples cultured in 1% FBS.....  | 220 |
| Figure 5-27. Day 0 pellet and cartilage positive control.....  | 221 |
| Figure 5-28. SOX9 was detected from early time points for MICA activated group cultured in 10% FBS that increased with culture time .....  | 222 |
| Figure 5-29. Early detection of SOX9 in TRPV4 MICA samples cultured in 10% FBS with low overall production over culture time for all groups.....   | 223 |

|   |     |
|---|-----|
| Figure 5-30. Higher SOX9 expression from early time points that was maintained with culture time for all samples cultured in 10% FBS.....                     | 224 |
| Figure 5-31. High presence of SOX9 was detected from day 7 for all groups except for the control with a continuous growth over culture time.....              | 225 |
| Figure 5-32. Variability observed in the results with more consistency found among TRPV4 activated groups .....   | 226 |
| Figure 5-33. Day 0 pellet and cartilage positive control.....   | 227 |
| Figure 5-34. Increased Ki67 presence over culture time for all groups with enhanced presence in TRPV4 activated samples cultured in 10% FBS.....              | 228 |
| Figure 5-35. Increased Ki67 production with culture time for samples labelled with TRPV4 MNPs .   | 229 |
| Figure 5-36. Increased production of Ki67 over culture time with enhanced presence on TRPV4 activated samples and TRPV4 static group cultured in 10% FBS..... | 230 |
| Figure 5-37. Lower levels of Ki67 presence observed when compared to individual donors, with a higher presence in MICA activated samples.....                 | 231 |
| Figure 5-38. Increased proliferation with culture time for samples cultured in 10% FBS.....   | 232 |
| Figure 5-39. Samples cultured in 10% FBS showed higher sGAGs production.....  | 234 |
| Figure 5-40. Gene expression analysis revealed higher expression on TRPV4 activated groups for the SOX9 transcription factor and reduction in collagen X..... | 238 |
| Figure 6-1. Summative conclusion diagram.....   | 258 |

## Tables

|  |     |
|--|-----|
| Table 1-1. Studies based on MICA technology and their application .....                        | 56  |
| Table 2-1. List of reagents, catalogue number and suppliers.....                               | 61  |
| Table 2-2. List of equipment and suppliers/ manufacturers.....                                 | 66  |
| Table 2-3. Supplements for chondrogenic induction media for each cell type.....                | 74  |
| Table 2-4. qRT-PCR equine primer sequences.....  | 95  |
| Table 2-5. qRT-PCR ovine primer sequences.....   | 95  |
| Table 3-1. Human MSCs experimental groups tested for chondrogenic differentiation.....         | 107 |
| Table 3-2. Polydispersity values of Nanomag particles unlabelled and labelled with TRPV4.....  | 110 |
| Table 4-1. Experimental conditions of the eMSC study performed in pellets and micromasses..... | 141 |
| Table 4-2. Statistical analysis of Figure 4-14.....  | 160 |
| Table 5-1. Experimental groups for the 2 different hUC-MSC donors.....                         | 191 |
| Table 5-2. Pooled donors experimental conditions for each studied time point.....              | 192 |
| Table 5-3. Statistical analysis of donor 3 Figure 5-39 (Top).....                              | 235 |
| Table 5-4. Statistical analysis of pooled donors Figure 5-39 (bottom).....                     | 236 |

## Supplementary figures

|   |     |
|---|-----|
| Supplementary figure 1. Higher variability was found among experiments than among experimental conditions .....                               | 301 |
| Supplementary figure 2. DEGs in common between comparisons shown few genes matching the mechanical and chemical activation of TRPV4 .....     | 302 |
| Supplementary figure 3. No signs of collagen or proteoglycan presence were detected on P0 chondrocytes sections after 21 days of culture..... | 302 |
| Supplementary figure 4. Little differences were found among samples MICA activated for 7 days and 21 days.....                                | 303 |
| Supplementary figure 5. Similar expression found among samples MICA-activated for 7 days and 21 days with the exception of collagen II .....  | 303 |

## Abbreviations

|                                |   |
|--------------------------------|---|
| <b>4<math>\alpha</math>PDD</b> | 4 $\alpha$ ,12,13 phorbol didecanoate   |
| <b>2D</b>                      | Two-dimensional   |
| <b>3D</b>                      | Three-dimensional   |
| <b>AC</b>                      | Articular cartilage   |
| <b>ACAN</b>                    | Aggrecan  |
| <b>ACI</b>                     | Autologous chondrocyte implantation   |
| <b>APES</b>                    | 3-aminopropyltriethoxysilane  |
| <b>ARD</b>                     | Ankyrin   |
| <b>ASCs</b>                    | Adult stem cells  |
| <b>ATMSCs</b>                  | Adipose tissue-derived MSCs   |
| <b>BM-MSCs</b>                 | Bone marrow-derived mesenchymal stem cells                                    |
| <b>BMI</b>                     | Body mass index   |
| <b>BMP</b>                     | Bone morphogenetic protein  |
| <b>BSA</b>                     | Bovine serum albumin  |
| <b>C-terminus</b>              | Carboxyl-terminus   |
| <b>CaMBD</b>                   | Calcium-calmodulin binding domain   |
| <b>CMV</b>                     | Citomegalovirus   |
| <b>COL2</b>                    | Collagen type II  |
| <b>COL2A1</b>                  | Collagen type II alpha I gene transcript                                      |
| <b>COL10</b>                   | Collagen type X   |
| <b>DAPI</b>                    | 4',6-Diamidino-2-phenylindole   |
| <b>Dc</b>                      | Critical value  |
| <b>dH<sub>2</sub>O</b>         | Distilled water   |
| <b>DMEM</b>                    | Dulbecco's Modified Eagle Medium  |
| <b>DMMB</b>                    | Dimethyl methylene blue   |
| <b>DMSO</b>                    | Dimethyl sulphoxide   |
| <b>DOTAP</b>                   | 1,2-Dioleoyl-3-trimethylammonium propane                                      |
| <b>ECM</b>                     | Extracellular matrix  |
| <b>EDAC</b>                    | <i>N</i> -Ethyl- <i>N'</i> -(3-dimethylaminopropyl)carbodiimide hydrochloride |
| <b>EDTA</b>                    | Ethylenediaminetetraacetic acid   |
| <b>ERK</b>                     | Extracellular signal-reduced protein kinase                                   |
| <b>ESCs</b>                    | Embryonic stem cells  |
| <b>FAK</b>                     | Focal adhesion kinase   |
| <b>FBS</b>                     | Foetal bovine serum   |
| <b>FDA</b>                     | Food and drug administration  |

|                                    |  |
|------------------------------------|--|
| <b>Fe<sub>2</sub>O<sub>3</sub></b> | Maghemite  |
| <b>Fe<sub>3</sub>O<sub>4</sub></b> | Magnetite  |
| <b>GAG</b>                         | Glycosaminoglycan  |
| <b>GAPDH</b>                       | Glyceraldehyde 3-phosphate dehydrogenase   |
| <b>GFP</b>                         | Green fluorescent protein  |
| <b>GSK101</b>                      | (N-((1S)-1-[[4-((2S)-2-[[[2,4-Dichlorophenyl)sulfonyl]amino]-3-hydroxypropanoyl]-1-piperazinyl]carbonyl]-3-methylbutyl)-1-benzothiophene-2-carboxamide |
| <b>GSK205</b>                      | N-[4-[2-[Methyl(phenylmethyl)amino]ethyl]phenyl]-5-(3-pyridinyl)-2-thiazolamine  |
| <b>HA</b>                          | Hyaluronic acid  |
| <b>Hc</b>                          | Coercive field   |
| <b>HCl</b>                         | Hydrochloric acid  |
| <b>HD</b>                          | Hydrodynamic size  |
| <b>ICRS</b>                        | Cartilage research society   |
| <b>IL-1RA</b>                      | Interleukin 1 receptor antagonist  |
| <b>IL-4</b>                        | Interleukin 4  |
| <b>IL-6</b>                        | Interleukin 6  |
| <b>IL-10</b>                       | Interleukin 10   |
| <b>IL-β1</b>                       | Interleukin β1   |
| <b>IMS</b>                         | Industrial methylated spirits  |
| <b>IP3</b>                         | Inositol triphosphate  |
| <b>ITS</b>                         | Insulin-Transferrin-Selenium-Sodium Pyruvate   |
| <b>iPSCs</b>                       | Induced pluripotent stem cells   |
| <b>K2P</b>                         | Two-pore domain  |
| <b>LBS</b>                         | Ligand binding site  |
| <b>MACI</b>                        | Matrix-induced autologous chondrocyte implantation   |
| <b>MFB</b>                         | Magnetic force bioreactor  |
| <b>MICA</b>                        | Magnetic ion channel activation  |
| <b>Mnp13</b>                       | Manganese peroxidase 13  |
| <b>MNPs</b>                        | Magnetic nanoparticles   |
| <b>Ms</b>                          | Saturation magnetisation   |
| <b>MSCs</b>                        | Mesenchymal stem cells   |
| <b>MTC</b>                         | Magnetic twisting cytometry  |
| <b>N-Terminus</b>                  | Amino-terminus   |
| <b>NEAA</b>                        | Non-essential amino acids  |
| <b>NHS</b>                         | N-Hydroxysuccinimide   |
| <b>NO</b>                          | Nitric oxide   |
| <b>NOS2</b>                        | Nitric oxide synthase 2  |

|                                |  |
|--------------------------------|--|
| <b>NSAIDs</b>                  | Non-steroidal anti-inflammatory drugs                          |
| <b>OA</b>                      | Osteoarthritis   |
| <b>OARSI</b>                   | Osteoarthritis research society international                  |
| <b>PBS</b>                     | Phosphate buffered saline                                      |
| <b>PCNA</b>                    | Proliferating nuclear antigen                                  |
| <b>PdI</b>                     | Poly dispersity index  |
| <b>PG</b>                      | Proteoglycan   |
| <b>PGE2</b>                    | Prostaglandin E2   |
| <b>PLA2</b>                    | Phospholipase A2   |
| <b>qRT-PCR</b>                 | Quantitative polymerase chain reaction                         |
| <b>RGD</b>                     | Arg-Gly-Asp  |
| <b>ROS</b>                     | Reactive oxygen species  |
| <b>RunX</b>                    | Run-related transcription factor X                             |
| <b>sGAG</b>                    | Sulphated glycosaminoglycan                                    |
| <b>SOX9</b>                    | SRY (sex determining region Y)-box 9/transcription factor SOX9 |
| <b>SPIONs</b>                  | Superparamagnetic iron oxide nanoparticles                     |
| <b>TAE</b>                     | Tris acetate EDTA  |
| <b>TCP</b>                     | Tissue culture plastic   |
| <b>TEM</b>                     | Transmission electron microscopy                               |
| <b>TGF-<math>\beta</math></b>  | Transforming growth factor $\beta$                             |
| <b>TFN-<math>\gamma</math></b> | Interferon $\gamma$  |
| <b>TNF-<math>\alpha</math></b> | Tumour necrosis factor $\alpha$                                |
| <b>TREK-1</b>                  | Twin-related K <sup>+</sup> channel                            |
| <b>TRP motif</b>               | Tetratricopeptide motif  |
| <b>TRPV</b>                    | Transient receptor potential vanilloid                         |
| <b>UC-MSCs</b>                 | Umbilical cord-derived mesenchymal stem cells                  |
| <b>WJ-MSCs</b>                 | Warton jelly-derived mesenchymal stem cells                    |

## Publications and presentations

### **Associated publication**

Markides H, Foster NC, McLaren JS, Hopkins T, Black C, Oreffo ROC, Scammel B, White LJ, Echevarria I, El Haj A. Short-term evaluation of cellular fate in an ovine bone-formation model. *Cells*. 2021, 10 (7).

### **Oral presentations**

#### **WBC (World congress of biomechanics) Dublin 2018**

Echevarria I, Markides H, El Haj A. Mechano-activation of MSCs & chondrocytes with magnetic nanoparticles for chondrogenic differentiation.

#### **BioMedEng (Biomedical Engineering) London 2018**

Echevarria I, Markides H, El Haj A. Magnetic nanoparticle mediated activation for chondrogenic differentiation of MSCs.

#### **NALS (Nanomaterials applied to Life Science) Madrid 2020**

Echevarria I, Markides H, El Haj A. Remote control healing for OA repair. NALS Madrid meeting abstract, 2020, page 52.

### **Poster presentations**

#### **TCES (Tissue and Cell Engineering Society) Keele 2018**

Echevarria I, Catchpole B, Markides H, El Haj A. Remote magnetic activation of ovine MSCs and chondrocytes using MICA technology.

## Acknowledgments

I would like to thank my supervisor Alicia El Haj for the opportunity of taking part in this project and for introducing me into the research world, allowing me to learn by myself when required and guiding me when needed. I would also like to thank my co-supervisor Hari Markides for being an example to follow, for her endless patience and her though love that helped me in my professional and personal life, this experience wouldn't have been the same without her guidance.

Thank you also to Lucrezia Righelli, Nicky Foster, and Kiran Dhillon for their endless help. In addition to the lab support, they have been a key part of this PhD, making the experience very enjoyable even when times were rough with their sense of humour and the great support provided.

I would like to thank Anabel Palacios for the huge impact she has had during this year. For always making me feel supported and understood and for the invaluable lessons she's thought me. Thank you for making me not want to finish this PhD to enjoy longer this adventure, wouldn't have been the same without you.

I would also like to thank my family, for the constant support through the years, for always being there when I needed them and for their great faith on me, always pushing me to achieve what I aimed for. I would not be the person I am today without the wise advices of my father and without the strength learned from my mother. Thank you also to my political family for taking care of me as a member of their own during this lengthy journey. I would finally like to thank my partner, Ricardo, for being the key support during these years. Thank you for always believing in me when I doubted myself, for your positivity, for your so-needed contagious good mood and for being an example in life. I hope to I can give back even a little of what you have given me during these past years.

I would like to thank the collaborators Dr. Steven Woods and Prof. Sue Kimber (Manchester University), Dr. Claire Mennan and Prof. Sally Roberts (RJAH Oswestry) and Dr. Glyn D. Palmer for their implication in this project.

The work described in this thesis was funded by partially via the EPSRC as part of the Loughborough, Keele and Nottingham Universities' CDT and partially via the Institute for Science and Technology in Medicine at Keele University and the University of Birmingham.

---

# *Chapter 1*

---

## *Introduction*

## 1.1 Joints and Cartilage: Anatomical review

The key element for a fluid, painless and frictionless movement resides in the good health of the skeleton joints. The joints are the flexible connections between bones that allow for free movement. There are various types of joints in the body with different mechanical properties based on their function and they can be classified according to both the structure or the function.

The structural classification sets the difference based on the type of connection of the adjacent bones, being connected either by connective tissue or cartilage, and bone connected by a joint cavity filled with fluid (2).

Attending to the structural classification three joint types can be described:

- **Fibrous Joint:** the bones are joined by a fibrous connective tissue
- **Cartilaginous Joint:** bones are joined by hyaline cartilage or fibrocartilage
- **Synovial Joint:** the bones are not directly connected, and they make the connection within a joint cavity that contains a lubricant fluid. These synovial joints are the most common joints of the body

When classifying the joints according to the function they serve, the differences are set by the grade of mobility from the adjacent bones (3):

- Synarthrosis otherwise known as immobile joint
- Amphiarthrosis or slightly movable joint
- Diarthrosis or movable joint

All synovial joints are classified as diarthrosis however, depending on the location the fibrous joints and the cartilaginous can be allocated either into the synarthrosis or amphiarthrosis category. The synovial joints or diarthrosis are the most common in the human body and can be found in the knee, shoulders, hips, and elbows among other areas (Figure 1-1). They allow for the majority of the skeletal

movements. Under normal conditions they allow for a free and frictionless movement, however, the failure of these structures leads to arthritis development (4). Lining the diarthrodial joints two layers of synovium can be found: the intimal lining layer and the sublining layer. The intimal layer forms a barrier between the synovial fluid cavity and the sublining layer. Synovial fluid is secreted by the synovial membrane that lines the articular cartilage. The composition of the synovium and the extracellular matrix (ECM) is regulated by the fibroblast-like synoviocytes that reside in this space by their production of components such as hyaluronic acid and other joint lubricants (5).

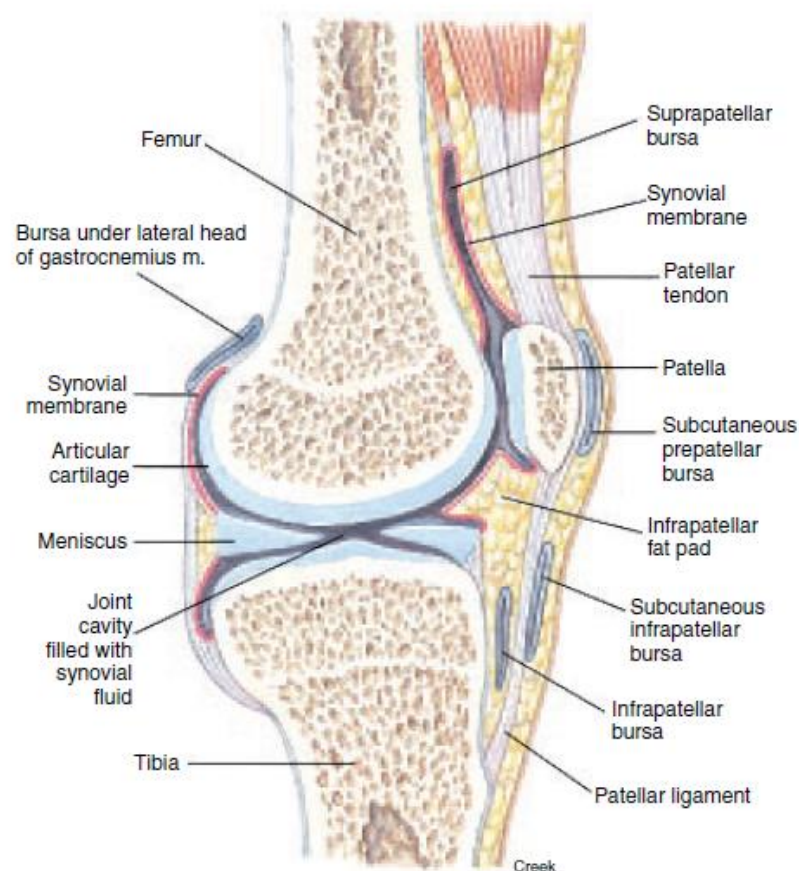


**Figure 1-1. Anatomical description of the knee joint in a sagittal view.** The elements surrounding the knee structure are key for bringing functional and anatomical support to the joints. The cartilage covering the surface of the femur and tibia protect from frictional forces and the space between them is filled with the synovial fluid (2).

## 1.2 Articular cartilage

The gliding surfaces of the synovial joints are covered by a specialised tissue known as articular cartilage (AC). The principal function is to provide frictionless and smooth movement of the joints and to facilitate the load transmission (6). According to the matrix composition, the cartilage can be classified into hyaline, elastic, fibro-elastic, and fibro-cartilage tissue. The articular cartilage classifies as hyaline cartilage. The majority of the skeleton is pre-formed by hyaline cartilage and prior to maturity, the hyaline cartilage content of the bones will partially determine their growth. However, some tissues will remain composed by hyaline cartilage and this is the case for the articular cartilage of the synovial joints (7). The hyaline cartilage structure responds to the load-bearing function of the joints, having low-friction and wear resistant properties that allow to bear, distribute and transmit the load to the underlying subchondral bone (8).

### 1.2.1 Structure of articular cartilage

The hyaline cartilage is aneural, avascular and alymphatic. It is composed of a highly organised matrix that responds to the function of the tissue. This tissue is formed by very specialised cells called chondrocytes embedded within a thick ECM that varies its composition with depth. The mature cartilage has a low cellularity, being <5% of wet weight corresponding to chondrocytes (9). Articular cartilage is usually 2-4 mm thick and covers the inner surface of the joints. The biomechanical properties of the AC are highly influenced by the solid phase of the tissue, comprised of the collagen network and the proteoglycans, and together with the ability of retaining water allows load distribution (10). A subdivision of the zones of the cartilage is formed by the variable distribution of the chondrocytes – the superficial zone, the middle zone, the deep zone, and the calcified zone (Figure 1-2). Each of the zones is composed by three regions – the pericellular region, the territorial region and the interterritorial region (6).

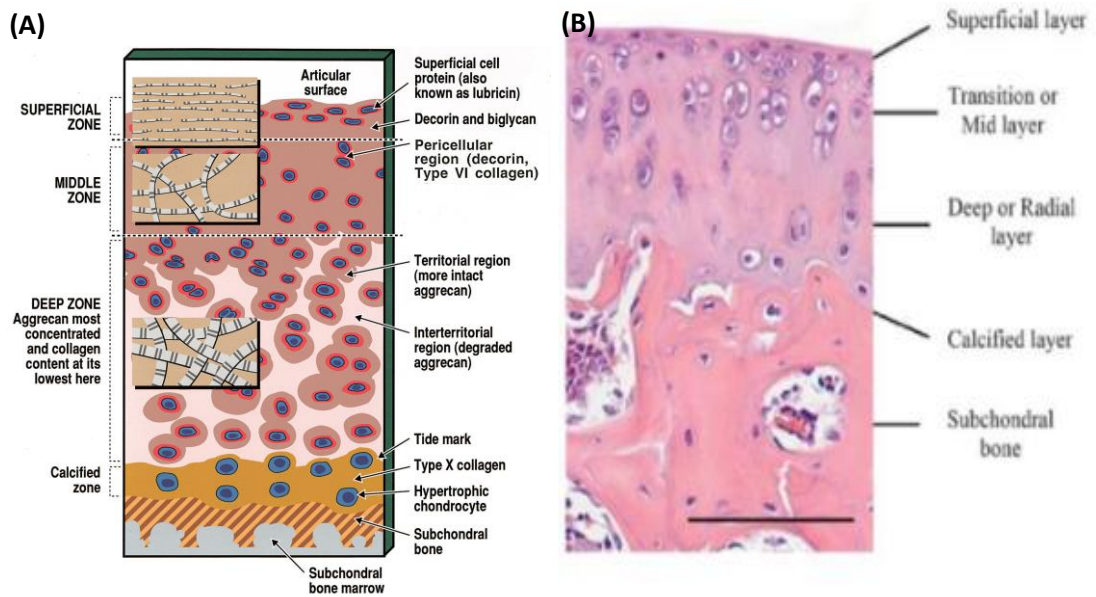


**Figure 1-2. Zonal organisation of articular cartilage.** (A) The structural arrangement of the collagen fibres orientation and the water and proteoglycan zonal distribution are the main contributors to the load bearing function of the cartilage. The zonal distribution allows for a rearrangement of the interstitial fluid volume that allows the tissue to withstand deformation under dynamic compression events (11). (B) Histological viewing of mice proximal tibia with a clear zonal distribution (12).

The thin superficial zone is characterised by the parallel arrangement of the collagen fibres, mainly collagen type II and IX. It is formed by dense layers of flattened chondrocytes that mainly synthesize proteins that have a lubricating and protective role (13). This layer represents 10-20% of the cartilage thickness. The outer layer of the cartilage is in contact with the synovial fluid and is covered by a thin layer called 'lamina splendens' (14) and protects the deeper layers, hence the importance of the preservation of the integrity of this layer. The water content is higher at this depth of the tissue, being also the lowest proportion of proteoglycans. The parallel arrangement of the collagen fibres allows for the great resistance to shear and tensile forces (15).

Following the superficial zone, the middle zone, also known as the 'transitional zone', has a more disorganised structure of thicker collagen fibres. The fibres are organised in a more oblique orientation, and there is an increase in proteoglycan content. The chondrocytes found in the middle zone are more spherical with a reduced density. It accounts for 40-60% of the volume of the tissue

and its main function is the resistance to forces, being the deep zone the principal defence against compressive forces.

The collagen fibres found in the deep zone are the thickest among the tissue, and the perpendicular distribution grants the load bearing function. The highest proportion of proteoglycans and lowest amount of water can be found in this layer. The cells are arranged in columns, parallel to the collagen fibres. The few cells residing in the deep zone have a hypertrophic phenotype. It represents 30% of the tissue volume and is followed by the tide mark. This area sets the limit with the calcified zone, which is mineralised ECM that acts as the binding region with the underlying bone. The calcified zone has a small volume of cells with low metabolic activity, and they express a hypertrophic phenotype. These chondrocytes synthesize collagen type X that provides structural integrity and absorbs the shock together with the subchondral bone (16).

A further organisation of the cartilage zones, based on the diameter and organisation of the collagen fibres, the cellular distribution, and the proteoglycan content, divides the ECM into three regions. The most external area surrounds the surface of cells and is known as the pericellular matrix. It is mainly composed of proteoglycans and other non-collagenous proteins. This region has been proposed to mediate the signal transduction within the cartilage. Surrounding the pericellular matrix, the territorial matrix surrounds individual chondrocytes and has been proposed to have a protective role against mechanical stresses given by the collagen fibre network around the cells. This area might be a key element to the load bearing role of the tissue. The final and largest region, the interterritorial matrix is responsible for the majority of the biomechanical properties attributed to cartilage. The collagen fibres found in this region are parallel to the surface of the most external zone of the cartilage and have a random orientation (6).

### 1.2.2 Extracellular matrix

The function of the articular cartilage is mainly determined by the structure, composition, and integrity of the ECM. The ECM together with cells and other elements composes a specialised connective tissue formed by a hydrated proteoglycan gel that withstands and distributes the external loads. The structure of the ECM is reinforced by the fibrillar network formed by the collagen fibres. The solid elements of the ECM, collagen and proteoglycans, represent about 70-75% of the dry fraction of the tissue against the 65-80% corresponding to fluid wet weight (4,11). The water content of the ECM highly varies across the tissue responding to the functionality. The majority of the fluid can be found within the space formed by the collagen fibres as a gel and lesser in the intracellular space. The water provides the essential lubrication for a frictionless movement and allows for the distribution of the nutrients to the chondrocytes. The fluid is key for the intrinsic ability of the cartilage to withstand load and can be displaced by the application of external forces.

The collagen network forms 10-20% of the wet weight of the tissue and is the most abundant macromolecule found in the ECM. Most specifically collagen II (90-95%) can be found among the ECM forming a fibril network together with the proteoglycans. Other collagen types that can be found in fewer amounts are collagen type I, IV, V, VI, IX and XI that help to stabilize the fibril network (17).

The second largest macromolecules present in the ECM are the proteoglycans that forms 10-20% of the wet weight. Proteoglycans are formed by a protein core with glycosaminoglycan (GAG) chains attached (Figure 1-3). GAGs are formed by the union of monosaccharides negatively charged forming two types of disaccharides, chondroitin sulphate or keratin sulphate. The two main groups of GAGs to be found within the cartilage are the large aggregating proteoglycan monomers, also known as aggrecans and the small proteoglycans biglycan, decorin and fibromodulin (16). Aggrecan is the most abundant and largest of the proteoglycans found among the ECM. It plays a crucial role on the

resistance of compressive loads due to the osmotic properties given by its structure. It forms large aggregates by linking to hyaluronan molecules via link proteins.

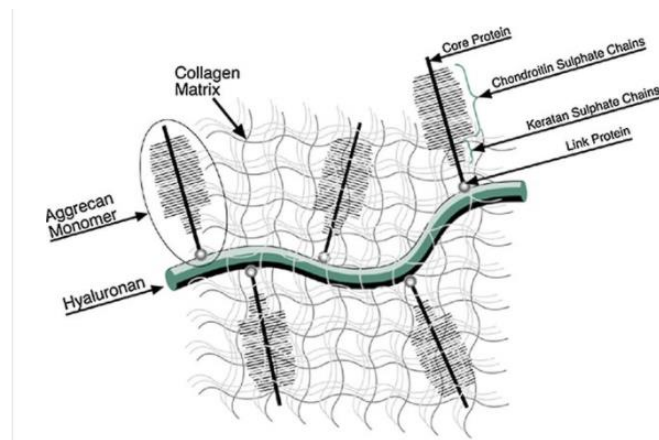


**Figure 1-3. Macromolecular structure of proteoglycans embedded on a collagen network.** Hyaluronan molecules act as a core region where the glycosaminoglycans are bound by a link protein. Aggrecan monomers bind to the core forming large GAGs chains that support the cartilage structure together with the collagen network (18).

Chondrocytes represent 1-5% of the entire volume and they are found in varying dispositions across the depth of the tissue. They are responsible for the synthesis of the matrix components and for maintenance and repair of the ECM. These highly specialised cells create a microenvironment within their vicinity and have the ability to effectively transduce biomechanical cues from the environment. The complex of the chondrocyte and its pericellular matrix is known as the chondron, considered as the structural, functional and metabolic unit of the articular cartilage (19). The replication capacity of these cells is low and together with the lack of vascularisation of the tissue, highly limits the regenerative capacity of the cartilage following an injury. The lack of vascularisation limits the nutrient supply that is performed by diffusion and thus, chondrocytes depend on anaerobic metabolism.

The chondrocytes are responsible for the maintenance and repair of the ECM. They can synthesize matrix components; however, their function can be altered by the signals received from the external

environment and the biochemical cues. These alterations lead to either enhancing the synthesis or the degradation of the proteoglycans of the surrounding matrix (20).

The ECM together with the chondrocytes plays a homeostatic role maintaining the composition and structure of the tissue. Chondrocytes are protected from the external forces by the ECM and they balance the degradation and synthesis of the matrix components by synthesizing new macromolecules. The complete renewal of the proteoglycans can take up to 25 years (21).

### 1.2.3 Function and Mechanical Properties

The hydrophilic nature of the cartilage with its tendency to embed water and electrolytes is responsible for the highly specified load-bearing function of the AC. The biomechanical properties are highly influenced by the integrity and structure of the tissue, with the loss of the native structure being precisely the main cause behind the onset of pathologies. Articular cartilage has unique viscoelastic properties, and provides a smooth, lubricated frictionless surface. The load bearing properties allow for the transmission of the load to the subchondral bone, necessary to withstand the high pressures that the tissue is subject to under normal daily activities (22).

The biphasic nature of the tissue allows for its unique biomechanical properties. During joint loading, the forces applied lead to an increase of the interstitial fluid pressure. This translates into fluid flowing out of the ECM into the permeable solid matrix which then deforms, modifying the hydrostatic pressure. The viscoelastic behaviour of the cartilage is given both by the frictional drag force of the interstitial fluid that flows into the matrix, and the time-dependent deformation of the matrix under compressive forces (23). The cartilage ECM solid fraction is mainly composed of a collagen network and negatively charged proteoglycans that attract a high cation concentration within the tissue. This results in a difference between the osmotic pressure between the ECM and the surrounding synovial fluid which leads to swelling of the tissue allowing it to withstand the compressive forces and the deformation (Figure 1-4) (24,25).

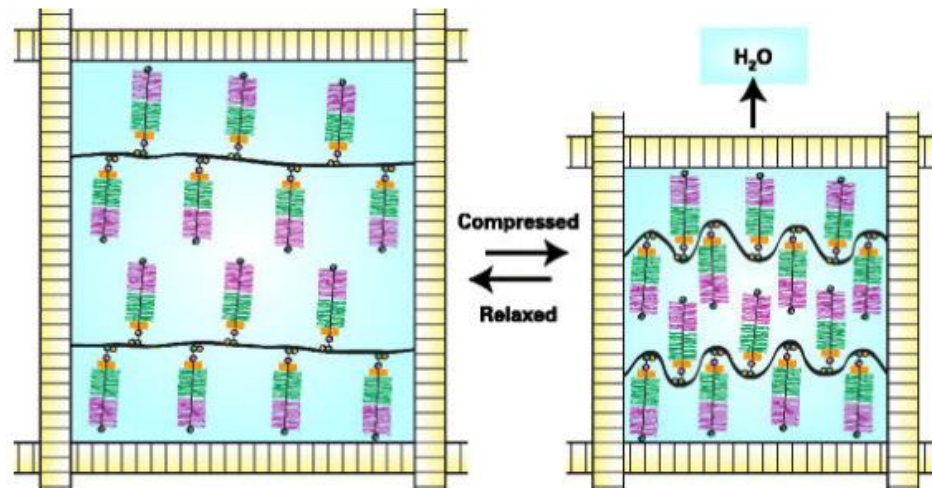


**Figure 1-4. Schematic representation of the role of proteoglycans in the cartilage under compressive load.** Under static conditions, the negatively charged proteoglycans attract a high concentration of cations, therefore increasing the interstitial osmolarity. The difference between the osmotic pressure with the surrounding leads to an increase of the water content in the cartilage ECM, and the volume increase is resisted by the collagen network. Following compression, the water is forced to exit the tissue in order to withstand the pressure, with the following increase of osmolarity within the tissue. (26).

### 1.3 Osteoarthritis and clinical approaches

It is well known that the articular cartilage has limited capacity for repair following a lesion due to its isolation from the systemic circulation. The constant use of the joints throughout life, and a combination of other factors that damage the layer of the articular cartilage, lead to a degenerative state of the tissue known as arthritis. Among this disease, osteoarthritis (OA) is the most common type of arthritis (27). OA is a complex multifactorial chronic degenerative disease characterised by the progressive loss of native cartilage structure, and the following thinning of the tissue with a final exposure of subchondral bone in advanced stages. OA symptoms vary from joint stiffness, pain, swelling, or limited and impaired movement amongst others. The disease begins with lesions on the articular surface associated to the disruption of the collagen network causing a collapse on the tissue structure with the subsequent loss of the innate ability of load-bearing (15).

The exact mechanisms of the pathology of OA remain under constant investigation however, some factors such as the sex, age, body mass index (BMI), inactivity, hereditary factors or dietary intake are known to have an impact on the onset of the disease (28). It has been proven that OA is more prevalent in women compared to men and symptomatic OA is more common among the 65-year-old and older population. In addition to the enormous impact that this disease has in the patient's life, hindering daily activities, it also has an impact on mental health (29). Moreover OA represents a major economic burden in the UK from the diagnosis to the treatment of the disease (30).

Articular cartilage injuries can be divided into partial or full thickness defects. Partial thickness defects do not reach the subchondral bone and do not have a spontaneous self-repair mechanism. Full thickness defects, however, reach the subchondral bone leading to the local influx of mesenchymal stem cells and blood from the breach. The chondrocytes have a limited repair capacity and despite the repair attempt, the newly formatted tissue does not match the same structural and functional characteristics as the native tissue. Chondrocytes response results in an increased matrix synthesis and undergo hypertrophic differentiation, expressing hypertrophy markers such as run related transcription factor X (RunX), collagen X (Col X) and manganese peroxidase 13 (Mnp13) (31). This scar tissue is known as fibrocartilage and is characterised by a collagen network composed of a higher collagen I to II ratio than native tissue (11). The damage of the articular cartilage leads to the activation of inflammatory signalling pathways with recruitment of proinflammatory cytokines such as interleukin-1 beta (IL- $\beta$ 1), tumour necrosis factor-alpha (TNF- $\alpha$ ) and matrix degrading proteins such as metalloproteases that damage the ECM (Figure 1-5) (32).

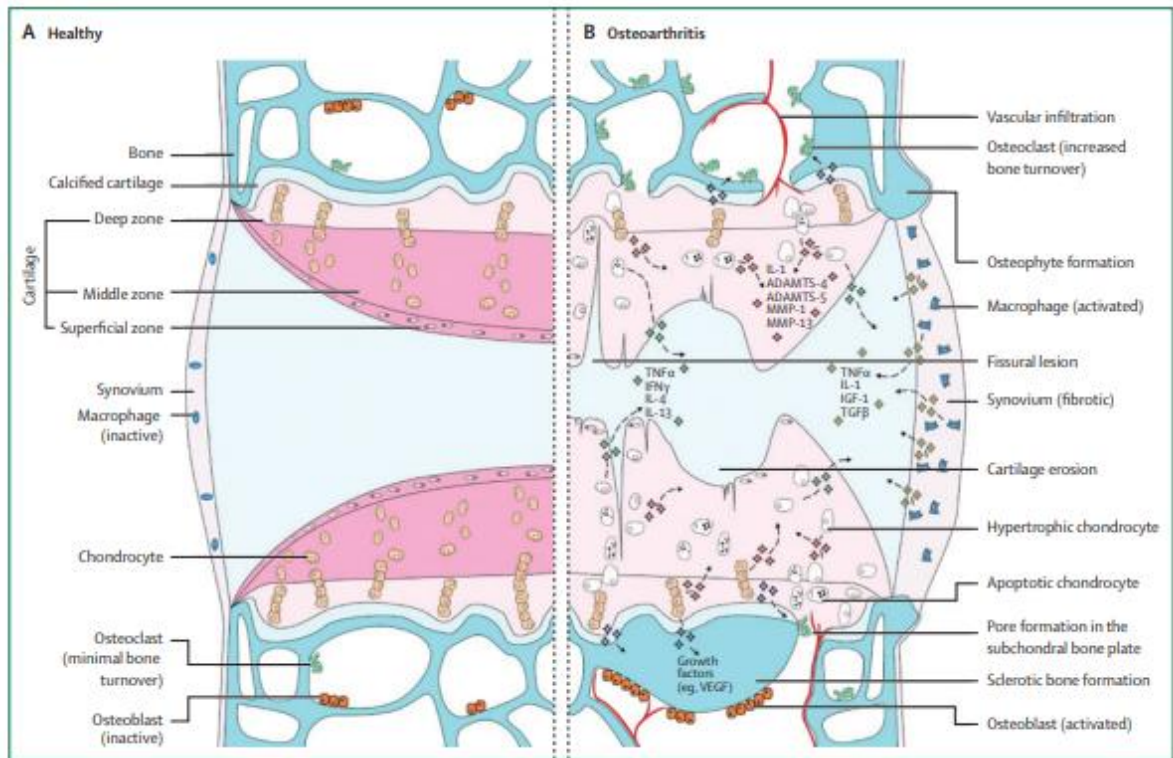


**Figure 1-5. Structural and molecular changes in OA.** Healthy joints show a smooth surface of the articular cartilage layer that allows for a painless and frictionless movement. OA commences with small lesions on the surface of the cartilage layer that progress into the depth of the tissue until the subchondral bone is exposed. The activation of the immune system triggers the infiltration of inflammation mediators such as TNF- $\alpha$ , interferon gamma (IFN- $\gamma$ ) or interleukin 4 (IL-4) that further damage the tissue with subsequent formation of bone osteophytes and vasculature infiltration (32).

Chondrocytes are subjected to extracellular stimuli that regulate their biosynthetic and catabolic activity. The imbalance of these regulatory events produced by factors such as aging, injury or disease may result in loss of tissue homeostasis hindering the limited repair ability of the cartilage. This set of events often result in changes in the gene expression pattern driving the alterations on the ECM composition that ultimately lead to OA (33). Under pathological conditions, the chondrocytes produce more catabolic factors that lead to the destruction of the tissue ending with chondrocytes apoptosis and subsequent complete loss of integrity. The destruction of the cartilage leaves the bone surface

exposed which turns into friction between surfaces with the development of the acute pain that characterises the disease (34).

Commonly, the severity of OA is evaluated by a histological grading of the tissue. The criteria established by the International Cartilage Research Society (ICRS) has been classically used in clinics to macroscopically classify the OA in four grades. This evaluation system is based on a 0-4 scoring system ranking the degree of defect repair, integration to border zone and macroscopic appearance (35). Histologically, OA is characterised by the formation of clefts and the incursion of capillaries into the calcified zone and progressive erosion until exposure of the subchondral bone (11). The water content of the tissue is observed to increase by 90% due to the progressive disruption of the matrix that creates an enhanced permeability (16). In addition to the macroscopic grading of the disease, the need for standardising the assessment of OA at the histopathological level allowed experts to generate a microscopic grading system. This grading system was published by the osteoarthritis research society international (OARSI) and sets a 0-6 severity grade of the disease attending to a scoring system from histological analysis based on structural observation of stained microscopy sections (36).

### 1.3.1 Pharmacological and surgical approaches

OA affects 7% of the population worldwide, with 500 million people affected by this disease. This represents a heavy economic burden to global healthcare systems (37). Most current treatments for OA are palliative, with exercise, weight loss or drug administration as the first line of treatment after the appearance of the first symptoms (38). Clinicians often prescribe non-steroidal anti-inflammatory drugs (NSAIDs) and corticosteroids injections to ease down the inflammation causing the pain (39). Despite the potential to improve the symptoms, this approach does not stop the progression of the disease and is not able to regenerate the damaged tissue. Ultimately, patients with OA tend to require a total joint arthroplasty. Surgical strategies aim to repair cartilage defects ( $<4 \text{ cm}^2$ ) (40). The most common treatment for end-stage OA of the knee lesion is the knee arthroplasty - this is total knee

replacement. However, this treatment is only indicated as a last resource for patients aged 60 or above (16). Less invasive techniques are currently performed with the aim of preventing further degeneration.

Bone marrow stimulation is commonly used for full thickness contained defects that reach the subchondral bone. This technique employs a drill to disrupt the blood vessels of the underlying bone, with the following formation of a fibrin clot in the chondral defect, and the migration of the mesenchymal stem cells which will differentiate and form the fibrocartilage. This technique has evolved from joint debridement first described by Magnuson to Steadman's microfracture technique (41). Currently debridement is usually performed in combination with other techniques. This method involved the drilling of the subchondral bone and the cleaning of the loose ends of cartilage. Most commonly, microfracture and debridement are used now in combination. A stable defect is created by eliminating the unhealthy tissue and performing multiple wholes perpendicular to the tissue that penetrate the subchondral bone. The drilling allows for a clot to be formed and for the recruitment of the stem cells around the defect area, aiming to attempt to repair the tissue. However, it has been reported that the newly formed tissue does not match the mechanical properties of the native cartilage (16,42).

With the aim of solving the mismatch on the structural and mechanical properties, approaches such as mosaicplasty use healthy tissue to replace the defects. Cylindrical osteochondral plugs are harvested for a minimal-load-bearing area from the knee and are used to fill in the previously cleaned defect. Despite the good outcomes reported by this technique, concerns arise regarding the donor site morbidity. This issue has been approached by limiting the defect area to 1-4 cm<sup>2</sup> (43). Nevertheless, further concerns on the potential instability caused by the fibrocartilage formed around the plugs and the difficulties for the plugs itself to integrate into the native tissue have disrupted the practice of this technique.

A promising line of treatment resides on cell-based techniques (Figure 1-6). These approaches have the advantage of customising the implant attending to the specific defect which allows for the treatment of bigger lesions (>3-4 cm<sup>2</sup>) (42). Among these techniques, autologous chondrocyte implantation (ACI) has become a popular approach in clinic. The first generation ACI described by Peterson et al. involved the harvesting of tissue from a low-bearing area of the knee, followed by culture of the chondrocytes for expansion in number. The cell suspension was then implanted under a periosteal patch. Now-a-days this technique has evolved involving the use of scaffolds and growth factors, being included among tissue engineering procedures (16). Matrix-induced ACI (MACI) introduces the seeding of the cells into a collagen scaffold prior to implantation. This eliminates the complications experienced with the graft hypertrophy reported with ACI. The third generation of ACI introduces the culture of the chondrocytes directly into a biodegradable membrane of collagen type I and III, that is secured into the defect with fibrin glue (44). Despite the promising outcomes, there are yet no long-term reports to assess the success of the procedure and the evaluation is limited to biopsies, hindering long term follow-up (45). Moreover, this technique still requires double arthrotomies and hence less invasive approaches are being sought.

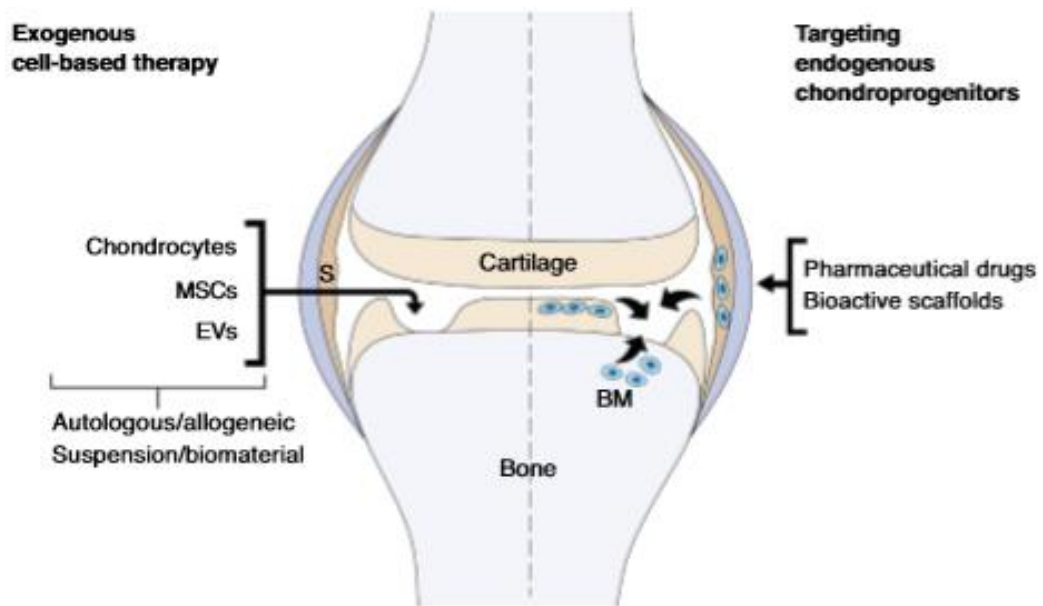


**Figure 1-6. Therapeutic strategies to address cartilage repair and regeneration.** Exogenous cell-based therapies aim to deliver autologous or allogenic chondrocytes, mesenchymal stem cells or extracellular vesicles directly to the injury site with the aim of providing aid to regenerate the damaged tissue. Other lines of treatment opt for delivering drugs to treat the symptoms and trigger the intrinsic regenerative response by recruiting endogenous chondroprogenitors to the injury site (46).

## 1.4 Cartilage tissue engineering

Despite the success rates reported for some of these approaches, common limitations are met such as donor site morbidity, the injury size, the invasiveness of the procedure, or the inadequate integration of the graft within the native tissue. The tissue formed by these techniques, fibrocartilage, has a different collagen composition and a limited durability, showing decline in clinical outcomes after a long term follow-up (47). These limitations raise the need for novel approaches that can overcome such difficulties.

The lack of long-term solutions for articular cartilage damage has pointed tissue engineering techniques as a promising strategy to face the difficulties encountered by clinicians. Tissue

engineering aims to regenerate or replace the native tissue involving the use of cells, growth factors, scaffolds, and bioreactors.

### 1.4.1 Cell sources

#### Chondrocytes

A big debate has been set amongst researchers over the last years concerning the source of cells for tissue engineering techniques for AC repair. Chondrocytes have always been an obvious choice and are currently being used for therapies such as ACI, obtaining enough cells to treat small defect sizes. However, the difficulty to culture and expand these cells while maintaining their phenotype is a major limitation. It has been observed that after 2D culture, chondrocytes have a tendency to de-differentiate showing higher levels of collagen type I and X expression and lower expression of collagen II and aggrecan (48,49). The phenotype has also been observed to vary from rounded-shaped cells to flattened cells. Moreover, the cell number and the responses achieved when expanding chondrocytes are limited by their low proliferative potential specially for older patients. Variability of response to growth factors on human articular chondrocytes from different donors with variable age has also been observed (50).

The limited proliferative potential of chondrocytes and the multiple complications associated with the use of these cells such as donor site morbidity or the phenotypic change following expansion, has addressed the need for alternative sources for cartilage tissue engineering.

#### Adult stem cells

The issues encountered with the use of chondrocytes for cartilage repair have drawn the attention into stem cells. Stem cells are undifferentiated cells with high proliferative potential, ability for self-renewal and capability of multilineage differentiation. These types of cells can be classified as Embryonic cells (ES Cells), Induced pluripotent stem cells (iPSCs) and foetal and adult stem cells (ASCs)

with the latter ones being proposed for tissue engineering applications (51). ES cells have an enormous potential due to their pluripotency nature, as they can generate any tissue from any of the three germ lines, however, they cannot give rise to the whole embryo (52). Nevertheless, the use of ESCs for regenerative medicine is restrained by the ethical concerns regarding the origin of these cells. In addition, concerns for the potential tumorigenic effect of the cells have made researchers focus on the use of multipotent stem cells (53).

Adult stem cells can be found in specific locations of adult tissues such as bone marrow, blood, muscle, adipose tissue, liver, skin or umbilical cord (54). Their differentiation capacity into several lineages is limited to their location in the adult body. It has been proposed that their potential is limited to maintain the integrity of each tissue. However, it now appears that some of these cells can transdifferentiate when moved from their original location giving rise to cells from any of the three germ layers (52). As opposed to ESCs neither adult or foetal mesenchymal stem cells (MSCs) have been observed to form teratomas *in vivo* and present a stable karyotype when cultured *in vitro* (55). An advantage presented by these cells is the proposed immunomodulatory role. MSCs have been classified by many authors as “immune privileged cells”. They are involved in the reduction of the inflammatory process by releasing anti-inflammatory factors such as interleukin 1 receptor antagonist (IL1RA) and by decreasing monocyte activation (56,57). Papadopoulou et al. suggested that MSCs were involved in the inhibition of T cell proliferation *in vitro* and *in vivo* via the inhibition of TNF- $\alpha$  and IFN- $\gamma$  leading to an increase of the anti-inflammatory cytokine IL-10 levels (58). MSCs have also been observed to suppress the formation of dendritic cells from monocytes as well as inhibiting their maturation and function through IL-6 expression (59).

The immune privileged condition of these cells opens the window for the use of allogenic sources of MSCs, this is, using cells from healthy donors and transplanting them into the patient. Being able to use an allogenic source of MSCs would overcome the issues related to the deficient functionality observed when isolated from patients with end stage OA (60). Despite studies like the one performed

by Chen et al. which reported similar results on the therapeutic effects of autologous versus allogenic MSCs, conclusions about the immunogenicity of allogenic MSCs should not be made without consideration of the specific experimental conditions (61). A review of studies comparing the immunogenicity of both autologous and allogenic MSCs addressed the fact that the immunological recognition might be subject to the delivery method or the time the cells survive post-implantation (62). Regardless of the need for further studies to assess the immunogenicity of allogenic MSCs, it is clear they are a promising source of cells for OA treatment. A multitude of studies have demonstrated the advantages of stem cell delivery for cartilage repair. Vega et al. proved that administration of allogenic MSCs in OA patients showed improved cartilage quality measured by magnetic resonance imaging (MRI) when compared to the group administered with hyaluronic acid injections (63). On another study, the efficacy and safety of intra-articular injection of allogenic bone marrow-derived MSCs in osteoarthritic knees showed improvements in pain and no sign of adverse effects was observed (64).

The mechanisms by which adult MSCs act still remain under investigation however, it has been proposed that MSCs therapeutic effect is not restricted to cell replacement but also mediated by the paracrine effects on tissue repair, inflammation and angiogenesis (65). Stem cells residing in their natural environment maintain an undifferentiated phenotype that is preserved by their niche. Following an injury, the signals released by the surrounding tissue invoke proliferation and differentiation of the stem cells to regenerate the damaged tissue (54). In addition, MSCs have been suggested to have antiapoptotic properties. Altogether these properties attributed to the secretome of MSCs might be of interest for joint tissue regeneration by stimulating the proliferation of endogenous cells, regulating the inflammation within the injury site and preventing the degeneration led by OA (66).

The best characterised source of MSCs are the ones obtained from the bone marrow (BM). BM-MSCs have a relatively easy extraction and isolation method, and they do not dedifferentiate when cultured

*in vitro* as opposed to chondrocytes. A good and easily accessible source of MSCs is also fat. Adipose tissue derived stem cells (ATMSCs) have also been proposed for cartilage repair strategies, however, several studies report the inferior chondrogenic potential when compared to bone marrow MSCs (53,67). BM-MSCs have been widely studied for clinical applications delivered via intra-articular injection or seeded into a biomaterial, with the aim of improving current surgical approaches. Saw et al. delivered intra-articular injections of marrow aspirate and hyaluronic acid (HA) after subchondral drilling in goats. After a 6 month follow-up they reported hyaline cartilage-like formation in the experimental groups compared to the control, with drilling alone or drilling and HA administration (68). Following the animal study, the same group performed a randomised controlled trial involving 50 patients comparing the effect of post-operative injections, after subchondral drilling, of HA to injections of HA in conjunction with injections of peripheral blood stem cells. Results showed a more consistent cartilage-like tissue and good filling of the defect for the intervention group with intense proteoglycan staining and type I and II collagen in superficial and deep layers correspondingly (69). In another study, a caprine model with a focal cartilage defect was used to compare the recovery after bone marrow stimulation with or without intra-articular injection of MSCs. A follow-up of 6 months was performed in which MSCs injection was found to improve the integration and filling, and the GAGs and collagen type II production of the newly formed tissue versus drilling alone (70). Despite BM-MSCs increasing popularity for therapeutic approaches, their use is limited due to their proliferation rate and the fact that the differentiation potential of the cells is directly correlated with the donor age (55).

## Foetal stem cells

An alternative source of stem cells is the use of foetal MSCs. Given the origin of these cells the proliferative potential and self-renewal capacity is much greater than adult MSCs. Foetal MSCs successfully meet the criteria for regenerative medicine applications: there are no ethical concerns associated with their use; they are also harvested painlessly; they are young and share some

embryonic features such as high cell proliferation, and have a great differentiation potential. In addition, they are immuno-privileged and have not been observed to be tumorigenic (71). Foetal MSCs can be isolated from the amniotic fluid, the umbilical cord and the placenta (72). These cells are capable of regenerating damaged tissue while secreting growth factors, cytokines and other molecules (73). Umbilical cord-derived MSCs (UC-MSCs) have become an interesting source of MSCs for clinical application given the fact that the tissue is discarded as waste material after delivery (74). UC-MSCs expression of major histocompatibility complex (MHC) class I molecule is very low and they do not express MHC class II, necessary for T cell activation, therefore a potential use as an allogenic source would be possible (75). In addition, they are able to be stored in liquid nitrogen for long periods of time with good recovery properties (76). Some studies have analysed the chondrogenic potential of umbilical cord-derived MSCs reporting promising results for orthopaedic applications. In a study, Reppel et al. compared the chondrogenic potential of BM-MSCs to Warton Jelly- derived MSCs (WJ-MSCs) (a connective tissue found in the umbilical cord) embedded in an alginate/ hyaluronic acid scaffold. Despite the lack of stimulation with growth factors, chondrogenesis was observed for the WJ-MSCs by enhanced expression of chondrogenic genes like Sox9 (SRY (sex related-Y)-type high mobility group box), in comparison to BM-MSCs. In addition, collagen type II synthesis was observed to be greater for WJ-MSCs, at both transcript and protein levels (77). The first human clinical study was performed by Park et al. where they aimed to investigate the safety and efficacy of Cartistem<sup>®</sup>, a novel medical product made of allogenic human UC-MSCs and HA, for cartilage regeneration in OA patients. After a 7-year follow-up no adverse effects were observed. In terms of efficacy, an arthroscopy performed 1-year post treatment revealed good integration of a hyaline-like tissue at the lesion site. These findings were reinforced by histological assessment and MRI imaging. In addition, the pain score improved from the first check up after implantation and was maintained up to 7 years (78). This study warranted the safety of human UC-MSCs for clinical applications and opened the door

for future studies to further assess the chondrogenic potency of foetal MSCs in contrast to currently used stem cells.

Previously it has been reported that autologous BM-MSCs or ATMSCs are negatively affected by increasing age (79). The proliferation, self-renewal and differentiation ability seems to be drastically reduced for patients aged over 60, or obese patients. A retrospective study on 128 patients treated with allogenic UC-MSCs implantation for OA repair, showed after a 2-year follow-up a significantly improved clinical outcome. In addition, the patients' characteristics such as age, lesion size and obesity were also analysed reporting no significant differences on the clinical outcome regardless of these aspects (80). These findings suggest that UC-MSCs might be a potential source of allogenic stem cells for those patients with an unviable source of autologous MSCs. A more recent study on the combined delivery of HA and human UC-MSCs on 29 subjects showed improvement in several clinical scores however, no significant improvements were seen on MRI (81). The mechanism of action by which UC-MSCs improve OA symptoms needs to yet be elucidated. It remains unclear if these MSCs undergo chondrogenic differentiation or if the improvement is due to the stimulation and proliferation of the resident progenitor cells by the paracrine effect of the MSCs (82). Hence further investigation needs to be done to determine the potential for clinical use in OA models of UC-MSCs.

#### 1.4.2 Bioreactors and biomaterials

Mimicking the native environment of the cartilage involves attempting to recreate also the biochemical and physical stimuli within the joint niche. Bioreactors have been widely used in the past to closely monitor and control biological and biochemical processes. In tissue engineering, bioreactors are defined as systems that use mechanical means to control mechanical processes (83). Bioreactors have been widely used to deliver and control both growth factors and mechanical signals in the form of compression, hydrostatic pressure, or shear with the aim of directing the differentiation towards a specific tissue. Many tissue engineering products have failed in the past due to the inability of the

construct to withstand *in vivo* the frequency of loading and the stresses that tissues are subjected to *in vivo* (84). This issue has been addressed with the introduction of bioreactors for construct culture.

Often bioreactors are used to stimulate cells seeded into specialised scaffolds. A broad range of synthetic and natural biomaterials have been studied with the aim of providing a scaffold to support and guide the cell growth and differentiation processes. Scaffolds introduce the advantage of incorporating growth factors generating a favourable niche for cells to grow at the same time as providing mechanical stability (85). One of the main focus on scaffold development for cartilage repair is the generation of materials that match the mechanical properties of the native tissue and are able to withstand the forces exerted by the bioreactors. Over the past years, clinicians have often resorted to the use of intra-articular injections of hyaluronic acid (HA) for OA treatment. HA has been observed to palliate some of the symptoms while being relatively free of side effects (68). HA can be found in native cartilage, and it has been observed to support and promote chondrogenesis of MSCs. In addition, the use of HA as a vehicle may ensure the delivery of MSCs to the injury site (86). Other scaffolds proposed for orthopaedic applications are decellularised tissues. Recent studies have proposed the use of decellularised tissues to produce ECM- derived scaffolds. Up till now several decellularised tissues have been approved for clinical use in patients, such as porcine heart valves, urinary bladder and small intestinal submucosa and human dermis (74) (87). However, when selecting a scaffold for cartilage tissue engineering, the ability to resist and transmit the external forces is a key factor to consider and this is one of the major limitations that scaffold selection currently encounters.

Tissue engineering approaches aim to optimise cell growth and guide the differentiation process by providing a regeneration template in the form of a scaffold and by adding growth factors. However, the static culture conditions are often a source of limitations for optimal cell growth, highlighting the importance for combining all three aspects of regenerative medicine: stem cells, scaffolds, and bioreactors. It has been observed that a heterogeneous cell growth on static culture hinders the 3D formation of the tissue. In addition, the difficulty for nutrients to reach the core of bigger scaffolds

generates necrosis within this area. The cells located at the periphery have more availability of nutrients and have an optimal growth and ECM production. Nevertheless, the ECM layer produced causes cells on the interior of the scaffold to often not obtain enough nutrients by diffusion, generating a tendency for the cells to move towards areas with more nutrient availability (88,89). This has specially been described for hard or mineralised tissues such as bone and cartilage where a strong ECM builds up on the outer layer of the construct. It was previously reported that when cultured in identical conditions in a 3 dimensional (3D) model, MSCs produced an inferior quality matrix and differential gene profile when compared to chondrocytes (90). However, later studies like the one performed by Farrel et al. attributed the inferior functional properties to the differential diffusional gradients across the constructs. MSCs cultured in agarose scaffolds were observed to produce a functional cartilage matrix in areas of optimal nutrient availability however, an inferior ECM deposition was observed within the inside of the construct. Moreover, when comparing the properties of the superficial region of MSCs against the chondrocyte construct, they matched or exceeded the ECM quality. Interestingly, the regional differences across the constructs were reduced or disappeared when cultured in dynamic conditions (91).

Among other purposes, bioreactors have been introduced as a solution to ensure the adequate diffusion of nutrients, oxygen, chemical signals and waste products by introducing flow systems (92). For this purpose, flow perfusion bioreactors have long proved their efficiency. Already in 1998, Glowacki et al. proved the efficacy of flow systems for high density culture conditions, by showing increased media diffusion and cell proliferation across the depth of the construct (93). However, this may not be of benefit for cartilage tissue engineering given the fact that oxygen tension is a regulator of MSCs fate. Lower oxygen tensions have been proposed to enhance chondrogenesis on MSCs (94,95). Dynamic culture systems have been shown to increase oxygen transport across the depth of the scaffold while suppressing chondrogenesis. On the contrary, static cultures manage to preserve the oxygen gradient observed in native tissue, leading to an enhanced matrix synthesis (96). Dali et al.

however, showed improved chondrogenesis and distribution of matrix components on scaffolds cultured dynamically when low oxygen tension (3%) was applied, when comparing to higher oxygen tension (20%) and static culture (97).

Despite the chondrogenic potential for MSCs being clearly established (98), it is proposed that the stimulation with differentiation factors such as transforming growth factor  $\beta$  (TGF- $\beta$ ) alone might not be enough for obtaining a mechanically viable scaffold. Hence, mechanical stimulation has been proposed as a strategy for optimising the construct functionality. This is of vital importance for cartilage applications given the key role of mechanical loading for development, remodelling and maintenance of healthy articular cartilage (99). Currently there are several types of bioreactors able to deliver mechanical stimuli by different means. For articular cartilage engineering, the most widely studied are the ones delivering dynamic compression or shear forces (100,101).

Recently a novel type of bioreactor is being used for orthopaedic applications: the magnetic force bioreactor. This technology is based on the use of magnetic nanoparticles to deliver localised forces directly to the cells. The specialisation of this method allows for a direct stimulation of the cells, eliminating the need for the scaffold to transmit the force to the cells. The magnetic force bioreactor is further discussed in the section 1.5.

Although it remains clear that the application of external forces is beneficial in order to improve the mechanical properties of the construct, it also highlights the need for a deeper study on the stimulation type, magnitude and duration needed for optimal tissue formation (102). In addition, the existence of opposing results regarding the stimulation regimes in order to induce chondrogenesis and achieve a fully functional tissue, evidence the need for a deeper understanding on the chondrogenic events occurring at the molecular level.

## 1.5 Mechanotransduction

While hydrostatic pressure or dynamic loading of chondrogenic constructs has been demonstrated to improve the mechanical and functional properties of the constructs and promote ECM deposition, it also delivers the risk of activating unspecific signalling pathways. Fine control of the mechano-responsive elements of the cells could potentially direct them towards a specific differentiation pathway.

It is well known the importance of mechanical stimuli for the healthy development and maintenance of bone and cartilage tissue. In cartilage, after load is applied, the collagen network of the ECM stretches by the osmotic force exerted by the hydration of the PGs. These forces are also transmitted to the cells residing in the tissue (103). At a cellular level, this is the result of small distortions exerted on the cell membranes that lead to the activation of specific ion channels that turn into a whole cellular response. Among other cells, chondrocytes and MSCs have reported to have responsive elements to external stimuli (104). The ability of the cells to translate an external signal into a cascade of internal messengers with the following gene activation is known as mechano-transduction. These external signals are often “sensed” by cell membrane receptors called integrins (Figure 1-7). These molecules form a molecular bridge that links the membrane to the cytoskeleton of the cell, through a molecular framework that gives structure to the cell formed by actin microfilaments, intermediate filaments, and microtubules. Integrins, amongst other specialised receptors can sense the external mechanical stimuli and transmit to the cell in form of chemical signals that lead ultimately to gene expression. Often this response is also mediated by the physical coupling of the receptors that are internally linked to acto-myosin filaments by altering the cytoskeleton tension (105,106). These unions are known as focal adhesions, and they are important connection points of the cytoskeleton with the ECM. When the focal adhesion sense an external stimuli, the signal transduction molecules change their activity with the following calcium influx through mechano-sensitive ion channels, and the subsequent protein phosphorylation and activation of second messengers (Figure 1-7) (106).

## Mechanotransduction through integrins

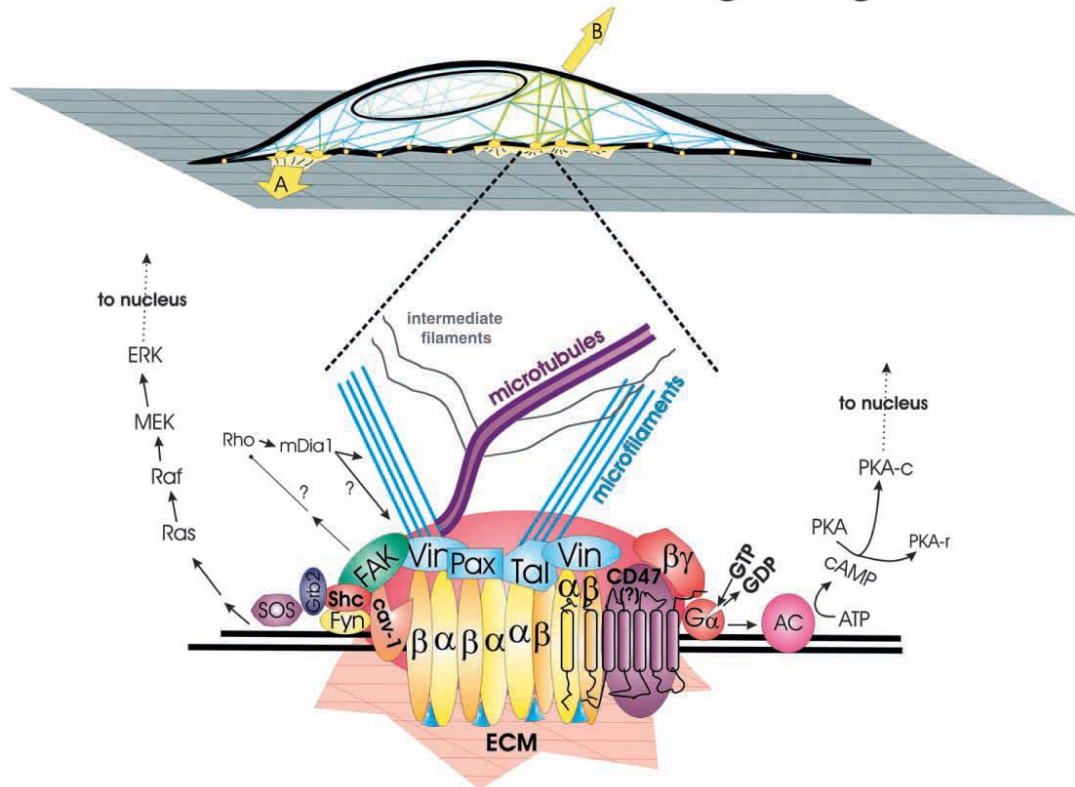


**Figure 1-7. Focal adhesion mediated mechanotransduction.** Mechanical stimuli coming from the exterior or interior of the cells travel through the anchoring points of the cells. The focal adhesion complexes transduce the signals bidirectionally through the inner microfilament network that is in a natural pre-stressed state. The stimuli detected by the integrins located in the focal adhesions can induce the clustering of the  $\alpha$  and  $\beta$  units with the following recruitment of the focal adhesion proteins. Stimuli are then translated into chemical signals that will mediate intracellular signalling cascades ultimately leading to gene expression and protein production (84).

The structural disposition of the cytoskeleton plays a crucial role in the cell fate by influencing viability and differentiation fate. Conservative models of cell mechanics describe the microfilament network connected to the cell membrane as the primary load-bearing structure of the cell. However, a novel model has emerged based on the tensegrity principle. This concept suggests that cells are tensegrity systems that stabilise their shape by the continuous tensions instead of by the constant exertion of compression forces (107). The tensional forces are generated by the cytoskeletal filament network and ECM adhesions that resist the compression, placing the cell in a pre-stressed state that stabilises

the same. The tensegrity model suggests that stresses applied to the cells are withstood by the molecular network and transmitted to the cell cytoplasm via the microfilament network, through mechanically sensitive transmembrane receptors such as integrins. This model differs to the established models in that it claims that the stresses are transmitted to the cells equally at all points on the cell membrane. With the aim of supporting the tensegrity model, Ingber and Wang, developed the magnetic twisting cytometry method. By using magnetic microbeads, they were able to manipulate specific cell surface receptors by delivering tensional stresses. With this technique, they were able to show that selectively stressing mechano-sensitive structures linked to the cytoskeleton, such as integrins had a higher degree of mechanical coupling than when other transmembrane molecules were manipulated (105,108). In addition, it has been previously demonstrated that the modification of location of the focal adhesions on the cells interferes with the viability by means of altering the cell shape. It has been previously observed that cell survival and growth increases with cell spreading (109).

It now remains clear that contrary to prior models, the mechanical forces exerted to the cells do not generally distort the whole structure. Instead, mechano-responsive elements such as integrins, linked to the internal microfilament network of the cell have been attributed the role to rapidly transduce the signal to the cytoplasmic compartment. However, integrins are not the exclusive mechano-transducer elements found in the cells. Other membrane molecules such as stretch-sensitive ion channels, extracellular signal-regulated protein kinase (ERK), focal adhesion kinase (FAK) or protein kinase C among others, have been attributed the role of signal transducers (110). It has been proposed that the stress-sensitive ion channels sense the mechanical signals through their cytosolic linkage molecules and these signals are translated into intracellular chemical signals (111). This model supports that there is a global structural alteration of the cytoskeleton. Davies demonstrated that when submitting endothelial cells to fluid shear stress, an intracellular signalling event was activated

however, after cells reorganised the cytoskeleton to be oriented in line with the fluid flow, these events were ceased (112).

Hence mechanical stress alters the whole cytoskeleton triggering the physiological response of the cells to stress. Nevertheless, some researchers disagree on this model claiming some mechanosensitive events happen independently of the focal adhesion union to the cytoskeleton (111). However, some studies show a link between these independent mechano-receptors and integrins. This was the case of the membrane transport vesicles, caveoles, that have been seen to elicit messenger recruitments and signalling cascades following mechanical stimulation by fluid flow. A study on this case of mechanotransduction revealed that an association between the caveoli and integrins was needed for recruitment of specific molecules required for ERK pathway activation (113). Although it remains controversial the specific mechanism by which cells transduce the stimuli into chemical signals, it is clear that cells have specific designated molecules capable of sensing and translating membrane alterations. Signals proceeding both from mechanical stress and specialised mechano-sensitive structures both converge into combined signalling pathways that ultimately affect gene expression (111). This leads to the idea that targeting specific molecules on the cell membrane may be of use for tissue engineering approaches in order to modify and guide the cell behaviour.

### 1.5.1 RGD

With the aim of further studying the effect of individual membrane receptors in the signal transducing process and the relation of these molecules and the cytoskeleton, research has focused on the selective stimulation of specific integrins. Wang et al, delivered shear stress to the fibronectin receptor integrin  $\alpha5\beta1$ , by attaching ferromagnetic microbeads coated with the receptor ligand Arg-Gly-Asp (RGD) peptide. By magnetising these beads and applying a magnetic field, they were able to twist the beads and exert a controlled stress. Stimulated cells were seen to become stiffer in culture and

increased resistance to mechanical stress was observed. This however, was not observed for cells that had attached beads coated with nonspecific ligands (114).

RGD is a cell adhesion sequence discovered for the first time in fibronectin 12 years ago and it has been observed to be the cell attachment site for a variety of adhesive proteins such as fibrinogen, vitronectin, osteopontin and some collagens (115,116). This adhesion peptide has been previously used in cartilage tissue engineering with the purpose of improving the adhesion of chondrocytes to the scaffold (117). The fibronectin receptor has been previously found among other cells in chondrocytes, the RGD ligand units  $\alpha 5\beta 1$  have been studied for its role in regulating the chondrocyte metabolism and ECM maintenance and repair (118). By submitting agarose seeded constructs to compression regimes and adding an integrin blocking agent to the medium, Mock et al, demonstrated the role of the RGD-dependent integrins on chondrocytes gene expression and matrix synthesis (119). More recent studies have focused on the potential use of mechanical stimulation of integrins using the RGD peptide for tissue engineering applications. Magnetic nanoparticles (MNPs) coated with RGD peptide were previously used for bone tissue engineering. By attaching the beads to the integrin receptor of osteoblasts and applying a cyclic magnetic force, the stimulated cells showed enhanced osteogenic markers via gene expression and histological staining (120). A similar study using the same methodology and by delivering a static magnetic field for 21 days, showed an increase on the intracellular calcium following mechanical stimulation. These events happened in a significantly lower proportion of cells without MNPs or cells labelled with MNPs that where not mechanically stimulated, supporting previous theories on the role of integrins in mechano-transduction (121).

In cartilage tissue engineering RGD has been merely used as a tool for improving cell attachment on several biomaterials with promising results (117,122). Some more novel applications for RGD had focused on the potential that brought the possibility of applying selective forces directly to specific structures of the cells. Scaffold design has been challenged by the need to withstand the external mechanical forces applied. Delivering the forces directly onto the cells highly reduces the limitations

to design the 3D structure specially for orthopaedic applications (120). Despite the applications reviewed for some fields of tissue engineering, there has not been associated a role of RGD mediated integrin activation on driving chondrogenesis. Hence further investigation is being actively performed with the aim of seeking specific targets that under stimulation will drive cells towards the desired differentiation pathway.

### 1.5.2 TREK

Despite integrins being studied as the main mechano-responsive elements of the cells, other membrane proteins and stretch ion channels have been proposed to be signal transducers. This is the case for the family of the potassium ( $K^+$ ) channels. The members of this family are divided into six subfamilies. Focusing on the “two-pore domain” ( $K_{2p}$ ) subfamily, TWIK-Related  $K^+$  channel (TREK) potassium channels are formed by 2 monomers containing each subunit two pore regions and four transmembrane segments. Three different splice variants have been identified and they vary among each other on the amino terminus (N-terminal) intracellular domain (123,124). The first member of the  $K_{2p}$  subfamily, TREK-1 has been described to be a mechano-sensitive channel regulated by several external stimuli such as voltage, membrane stretch, cell swelling, heat, intracellular acidosis, G-protein linked receptors, and polyunsaturated fatty acids such as arachidonic acid (Figure 1-8) (125,126). The domain affected by both mechanical and chemical signals is the cytoplasmic carboxyl-terminal (C-terminal) segment located next to the transmembrane domains. Deletion of the C-terminal domain leads to increased resistance of the channel to be activated following membrane stretch (127,128). It has been observed that the membrane tension regulates the activity of the channel, with opening induced by membrane stretch and cell swelling (129,130). Matching the principles of the tensegrity model, it was observed that disruption of the cytoskeleton, by addition of biochemical agents, controlled the mechano-gating of the potassium channel. This is indicative that the tension of the membrane regulates the channel activity and that the mechanical forces are transmitted to the channel through the lipid bilayer (131).

The mechanical activation of the channel leads to the activation of the phospholipase A2 (PLA2) pathway (127). TREK-1 was firstly described as a channel involved in neuronal processes, due to the voltage regulatory processes and the differences on the membrane charge generated following the channel activation. Expression of this channel has also been demonstrated for the heart, gastrointestinal tract, bladder and the uterine smooth muscles among other tissues (123). In addition, it has been implicated in mechanotransductive processes in several tissues such as bone or tendon.

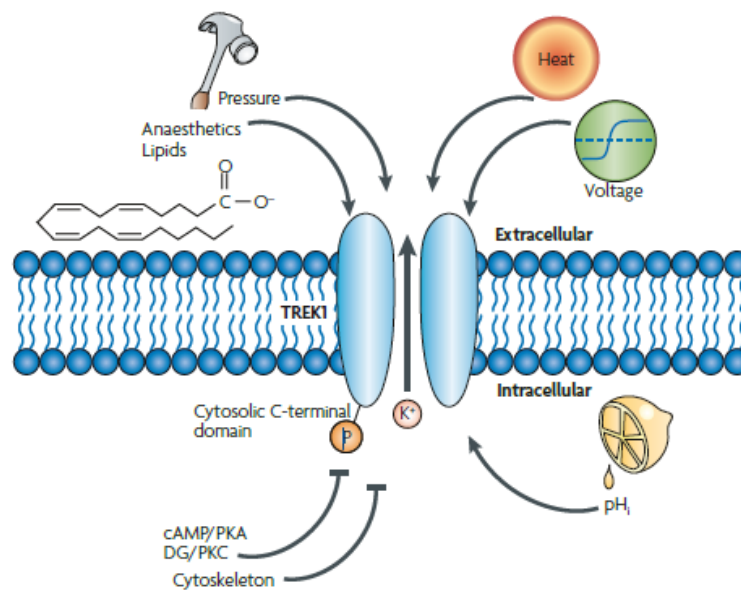


**Figure 1-8. Molecular structure of TREK-1 channel and the various stimuli triggering the channel activity.** External stimuli such as the variation on the membrane voltage, an increase of temperature, mechanical pressure as the one applied by shear forces or poly-unsaturated fatty acid trigger the activation of the channel with the following outward leak of  $K^+$  ions. Cytosolic changes of the acidity, as well as signalling mediated by G-protein receptors also control the gating of the channel, triggering the activation of intracellular second messengers (123).

Techniques that allow for a mechanical activation of single cells have focused on the stimulation of TREK-1 channel for tissue engineering purposes. Hughes et al. attempted for the first time to deliver localised forces directly to the TREK-1 ion channel by tagging MNPs to the channel. To enable the tagging of the MNPs they developed a mutant channel with a 6 Histidine repeat inserted into one of the extracellular loops, which is a high affinity binding site that allowed for optimal attachment.

Following MNPs attachment, a cyclic magnetic field was applied to deliver forces to the MNPs. By using whole-cell electrophysiology they were able to show in a proportion of cells activation of the channel tagged with MNPs following application of the magnetic field (132). In another study, encapsulated BM-MSCs labelled with either TREK-1 or RGD MNPs were implanted subcutaneously into a mouse model. Mice were exposed to a magnetic field during 1h daily to activate the MNPs. Parallel to this, an *in vitro* study on both monolayer and encapsulated pelleted BM-MSCs labelled with both TREK-1 and RGD MNPs was performed. Both forms of culture were submitted to 1h daily cyclic field to assess the osteogenic and chondrogenic potential of the TREK-1 channel and RGD receptor. Following a week of stimulation regimes, they were able to observe in the monolayer culture an increase in osteogenic and chondrogenic genes for TREK-1 stimulated labelled cells. For the encapsulated pellets, production of matrix elements was remarkably observed for the RGD-stimulated pellets. This event was also observed for the subcutaneous implants after 21 days of magnetic stimulation, that showed enhanced matrix production with elevated expression of proteoglycans and collagen for the TREK-1 labelled constructs and in less amount for the RGD group in contrast to the unlabelled controls. In addition, TREK-1 and RGD labelled groups showed a collagen type I and II elevated expression and large regions of ECM being produced, showing the potential of specific mechanical activation at a cellular level for cartilage and bone regeneration (133).

Despite several studies which report the activation of chondrogenic genes following selective activation of TREK-1 channel on stem cells and chondroprogenitors, there is little literature about the presence of this channel on chondrocytes and the applications for cartilage regenerative therapies (132). The potential observed for this channel for bone tissue engineering has led researchers to search for chondrogenic-specific mechano-transducers and translatable therapies for OA repair.

### 1.5.3 TRPV4

Transient potential ion channels (TRP) are a family of non-selective cation channels sensitive to a diverse range of stimuli such as mechanical stress, osmotic force, voltage, temperature, and some

small molecules. TRP channels have also been described to participate in sensory physiological events such as pain transduction, chemosensory transduction and touch and hearing in invertebrate models (134). The original member of the family was firstly discovered in *Drosophila* as a key element for response to light. There are seven subfamilies classified on the basis of sequence similarity with different gating and permeability properties (135,136). Structurally, they are composed of four subunits each formed of 6 transmembrane domains and a pore loop (137). The tetrameric assembly of the channel is consistent with the structure of the voltage-dependent K<sup>+</sup> channels. A division of 7 subfamilies has been established into 2 groups based on the sequence similarity on the transmembrane domain. Among the first group, the transient receptor potential vanilloid (TRPV) subfamily can be found. Mammals express six different forms of that subfamily, and they respond to a variety of stimuli. The first four members of the subfamily TRPV1-4 are activated by heat although the range of temperature sensitivities varies across channels (138). However, each sub member of the family is sensitive to other specific stresses, and the sub members TRPV5 and TRPV6 have been described to not require any external stimuli for activation and are controlled solely by the membrane potential (139).

Several members of the TRP family have been implicated in the regulation of both systemic and local responses to osmotic stimuli. Moreover, researchers have focused particularly on TRPV4 due to its attributed role on the mechanosensing ability of non-sensory tissues such as bone cartilage and muscle in addition to its participation in the skeletal development and homeostasis. TRPV4 mammalian homologues have a similar length and they share a high degree of sequence identity (~95-98%) (140). The presence of the cation channel has been reported in a broad range of tissues such as epithelial tissues, spleen, skin, lung, liver, kidney, sensory neurons, osteoblasts and chondrocytes (141). TRPV4 initial studies were mainly focused on mechano-osmosensitivity properties (142,143). However, later studies have proven TRPV4 to have a polymodal activation responding to cell swelling, chemicals, phorbol esters, temperature changes and others. Nevertheless, the activation of the channel occurs

through multiple different mechanisms (136,139). It seems that the mechanosensitive region of the channel is located in the N-terminal intracellular domain, formed by 6 ankyrin repeats. Deletion of the ankyrin repeat domain has been observed to impair TRPV4 sensitivity caused by the disruption with the cytoskeleton link (143,144). Although it seems that the gating response to stimuli might be located in the N-terminus, it has been hypothesised that there might be different mechanisms triggering the activation of the channel. However, the effects of mechanical stimuli on the gating mechanism of the channel need to be further investigated. The activation of the channel has been widely proven to cause calcium- Calmodulin mediated signalling and inositol triphosphate (IP<sub>3</sub>) signalling. This event is initiated in the cytoplasmatic C-terminus domain, where there has been described the presence of a binding site essential for the response of the channel to external stimuli (Figure 1-9) (145).

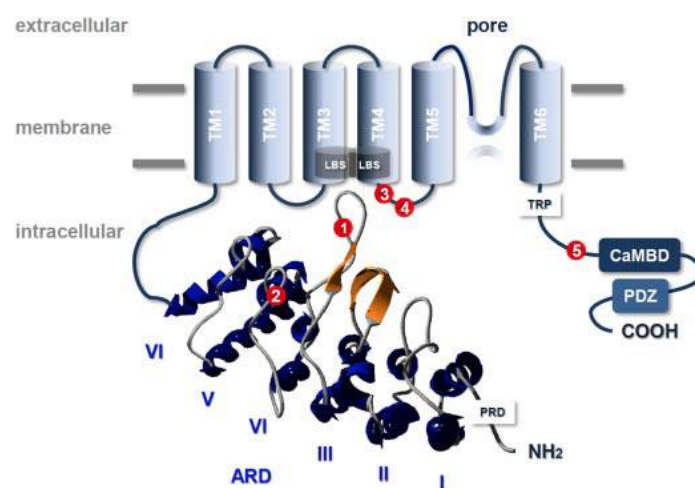


**Figure 1-9. Structural composition of the TRPV4 protein located in the membrane.** The channel is formed by 871 amino acids forming 6 transmembrane  $\alpha$ -helices and a cytosolic N-terminus domain with 6 ankyrin (ARD) repeats, and the C-terminus domain containing the Calcium-Calmodulin binding (CaMBD) region, the PDZ-like binding motif (PDZ) and the tetratricopeptide (TRP) motif, conserved among the channel family that gives the name to the channel. The pore of the channel is located between the fifth and the sixth transmembrane loops and the gating has been observed to be controlled by various mechanisms. The ligand binding site (LBS) that also controls the gating of the channel, has been located among the third and fourth transmembrane domains. Commonly observed mutation points causing skeletal dysplasias are indicated in red numbered circles (146).

TRPV4 has been implicated in the osmotic regulation of articular cartilage. The cartilage residing in the knees is highly subjected to dynamic osmotic and mechanical changes due to the load bearing function of the tissue and the structural properties within. The articular cartilage chondrocytes are often exposed to osmotic variations given by the changes of the water volume in the interstitial fluid due the native structure of the tissue with a high proportion of negatively charged proteoglycans in the ECM (147). The chondrocytes response to mechanic and osmotic changes has been associated to changes in the intracellular concentration of calcium ( $\text{Ca}^{+2}$ ) in the interstitial fluid, with a following increase in the interstitial osmotic pressure. Upon joint loading, the water leaves the tissue and is reabsorbed again once the loading ceases (148,149). Although the permeability of TRPV4 is similar for  $\text{Ca}^{+2}$ , strontium ( $\text{Sr}^{+2}$ ), magnesium ( $\text{Mg}^{+2}$ ) and barium ( $\text{Ba}^{+2}$ ), under physiological conditions, there is a modest preference for  $\text{Ca}^{+2}$  leading to set a relationship between TRPV4 activity and osmo- and mechano-regulation. Abundant expression of TRPV4 on porcine chondrocytes at both RNA and protein level was found by Phan et al. Moreover, they were able to demonstrate the role of TRPV4 on  $\text{Ca}^{+2}$  influx by activating the channel with the  $4\alpha$  12,13 phorbol didecanoate ( $4\alpha\text{PDD}$ ) agonist and inhibition of the channel using the antagonist N-[4-[2-[Methyl(phenylmethyl)amino]ethyl]phenyl]-5-(3-pyridinyl)-2-thiazolamine (GSK205), showing an activation and inhibition of  $\text{Ca}^{+2}$  influx respectively. In addition, they proved that in the presence of a stretch-activated channel blocker, gadolinium ( $\text{Gd}^{3+}$ ), the agonist response was attenuated. Importantly the  $\text{Ca}^{+2}$  signalling induced by  $4\alpha\text{PDD}$  was mostly dependant on extracellular  $\text{Ca}^{+2}$ , showing very low ion flux in cells in  $\text{Ca}^{+2}$  free media. The  $\text{Ca}^{+2}$  response was observed to be facilitated by intracellular stores of  $\text{Ca}^{+2}$ . The osmo-regulatory role of TRPV4 was demonstrated by observing increase in chondrocyte volume in iso-osmotic medium following  $4\alpha\text{PDD}$  administration that was reverted after blocking with GSK205. Furthermore, the inhibition by IL-1 of chondrocyte signalling and volume regulation was restored following channel activation with  $4\alpha\text{PDD}$

(150). All together, these and other similar studies largely confirmed the implication of TRPV4 regulating the osmotically mediated signal transduction in chondrocytes.

Given the structure of native cartilage, the mechanical loading directly translates into changes of the interstitial volume and osmolarity. Hence the demonstrated implication of TRPV4 as an osmo-regulatory receptor may also imply a role in the mechano-sensing of joint loading. Some other studies suggest that membrane stretch is the cause underlying the activation of the channel. As an example, it was observed that in patch clamp studies submitting the cells to both hypotonic media to the cell interior and to the extracellular compartment, avoided cell swelling and prevented the activation of the channel (151,152). However, direct membrane stretch experiments have not been performed as of yet.

The importance of TRPV4 in cartilage biology has been further investigated proposing a role of the cation channel in chondrogenesis. A study which performed a screening of the genes implicated in chondrogenesis identified among others, an increase of the expression of TRPV4 and *SOX9* genes. *SOX9* has been previously identified for playing a crucial role in chondrogenesis by regulating the transcription of cartilage-specific matrix components such as collagen II or aggrecan however, the activation mechanisms remain unclear (153–155). TRPV4 was observed to have a strong effect on Sox9 activation with increased mRNA and protein expression after stimulation of the channel with an agonist. TRPV4 gene was both identified in chondrogenic cell lines and cartilage tissue suggesting a definite implication in chondrogenesis. The activation of TRPV4 with the 4 $\alpha$ PDD in a collagen II reporter cell line, saw a dose dependant increase in the activity of the reporter. In addition, when stimulating cells with a chondrogenic chemical and 4 $\alpha$ PDD, a 2-fold increase on the collagen II and aggrecan gene expression was reported when compared to cells stimulated with the chondrogenic chemical alone. Moreover, and correlating to previous findings, the TRPV4-mediated activation of *SOX9* was observed to be Ca<sup>+2</sup>- Calmodulin dependent suggesting that the cation channel mediates the signal transduction through that signalling pathway (1). Adding to the increasing evidence of

TRPV4 implication in mechano-transduction, the channel has been located within the membrane and the primary cilium of chondrocytes. The primary cilia has been widely implicated in mediating chondrocyte signalling, responding to stimuli and inflammatory signalling, leading to the idea that TRPV4 might mediate some of these responses (150).

The implication of TRPV4 in skeletal development and homeostasis has been widely studied by analysing the effects of punctual mutations on the channel sequence (channelopathies) or by observing the effect of deletion of the protein in knockout animal models. Over 70 single amino acid mutations have already been described for TRPV4-caused diseases (146). The TRPV4 mutations can be separated in two groups attending to the type of diseases associated and the effect of the mutation. On one hand, the mutations causing skeletal dysplasia have been associated with gain-of-function mutations causing an increased activity of the channel or increased permeability. They are the most frequent ones and cover a wide range of skeletal malfunctions (156). On the other hand, the arthropathy-causing mutations are related to a decrease functionality of the channel and have been observed to develop over the life time course (157). In addition, TRPV4 mutations have been described as a major agent causing hereditary motor-sensory neuropathies (158). An example where a gain-of-function of the channel was seen to cause a skeletal dysplasia was found by Rock et al. A mutation on the fifth transmembrane region of the channel causing constitutive activity of the channel was found to be the cause of brachyolmia, a skeletal dysplasia affecting the spine. This data may suggest the key regulatory role of TRPV4 in the growth plate (159). The mechanisms behind the effect of the constitutive activation of the channel have been hypothesised to be linked to the increased regulation of *SOX9* following TRPV4 activation, which previous studies have reported to cause growth retardation in rats (160). On the contrary, reduced expression of *SOX9* has been observed to cause campomelic dysplasia, a severe disorder affecting the skeleton, amongst other tissues (161). The reduction of the activity of the channels has been related to maladaptation of the cartilage growth plate, hence targeting TRPV4 might be a potential therapeutic approach for this set of diseases. Moving to *in vivo*

studies, Clark et al. studied the role of TRPV4 deficient mice in OA. Following 9 and 12 months the TRPV4 knockout mice spontaneously developed a more severe OA and at a younger age than the control wild type group. In addition to erosion of the articular cartilage that penetrated the subchondral bone, the TRPV4 deficient mice also exhibited increased bone mass and calcified menisci. Matching other reports, they also observed a loss of  $\text{Ca}^{+2}$  signalling due to osmotic variations. A surprising finding of this investigation was the higher impact on OA degeneration in male mice compared to female which has been previously hypothesised (157,162).

The correlation between OA development and TRPV4 alterations has been clearly established (157). Despite the abundance of evidence brought by researchers, the mechanisms behind the pathogenesis remain uncertain. Studies on TRPV4 knockout animal models have showed that the loss of the channel activity correlated with an accelerated onset of the disease (163). However, TRPV4 expression is not limited to chondrocytes, being also present in other cell types within the joint niche such as osteoclasts, nerve cells, synoviocytes, MSCs and inflammatory cells, introducing the possibility of a global mechanism leading to OA (164). For this the study of the role of the channel in other cell types is becoming increasingly popular.

The role of TRPV4 in chondrocytes has been extensively studied for the better understanding of the molecular mechanisms to some skeletal disorders however, the functionality of the channel in MSCs is now beginning to be investigated. Corrigan et al. were able to demonstrate the presence of TRPV4 in MSCs with a preferential location for areas of high strain such as focal adhesions or cilium. They also demonstrated that the expression of the channel is mechano-regulated by observing a 1.53-fold increase in protein intensity staining following stimulation with fluid shear, in comparison with the static control. Matching with previous studies, they also observed for MSCs that  $\text{Ca}^{+2}$  signalling following fluid shear was decreased in the absence of TRPV4 functionality (165). Furthermore, during chondrogenesis the expression pattern of TRPV4 and the well-defined cartilage markers collagen II and aggrecan are observed to be similar (1). Altogether these data suggest the implication of TRPV4

in both MSC and chondrocyte mechanotransduction and opens the door to novel tissue engineering application at a cellular level. Moreover, TRPV4 has also been reported to be present in synoviocytes and to modulate with the inflammatory mediators such as IL-1 and IL-8 that drive the degrading and inflammatory process in OA (166). A study on bovine chondrocytes showed decreased nitric oxygen (NO) and prostaglandin E2 (PGE2) release in response to mechanical loading in the form of cyclic tensile strength, when treated with the pro-inflammatory mediator IL-1. However, this response was abolished when treating the loaded samples with the TRPV4 antagonist GSK205. When treating the cells with both IL-1 and the TRPV4 agonist (N-((1S)-1-[[4-((2S)-2-[[2,4-Dichlorophenyl)sulfonyl]amino]-3-Dic-3-hydroxypropanoyl)-1-piperazinyl]carbonyl]-3-methylbutyl-1-1-benzothiophene-2-carboxamide (GSK101), they observed that the addition of the channel activator abolished the pro-inflammatory response mediated by IL-1 (167). These data provided further evidence to the immunomodulation mediated by TRPV4, another potential mechanism by which the channel is involved in OA regulation and healthy cartilage homeostasis.

Given that the alterations on the normal functioning of TRPV4 have been described as the cause for several skeletal disorders, potential clinical approaches targeting the channel activity are slowly emerging. However, a big limitation in the therapy design is the broad role that TRPV4 plays in several tissues, thus, targeting the specific cells becomes crucial. Intra-articular administration of TRPV4 agonists and antagonists has been proposed to overcome systemic effects (157). Administration of channel activators could potentially both protect from further development of OA and have an anti-inflammatory effect in the synovium. More complex approaches propose the use of mediators that interact with the channel. Stanczyk et al. found that the MicroRNA-203 suppressed TRPV4 expression and observed upregulation of the MicroRNA in both OA and rheumatoid arthritis. Hence using anti-sense oligonucleotides blocking the MicroRNA activity could also be a potential target for arthritis disease (168,169).

Tissue engineering approaches have gathered efforts in developing cartilage constructs with an ECM that mimics the mechanical properties of the native tissue. To achieve this, researchers have resorted to the use of bioreactors to deliver physical stimuli to modulate the mechanical load that the tissue withstands *in vivo*. Unfortunately, despite the efforts of these approaches, the ECM formed has a bigger resemblance with fibrocartilage, failing to meet the criteria for clinical translation. The novel discovery of the TRPV4 implication in OA pathogenesis as a mechano-regulator, and the described role in cartilage ECM formation makes TRPV4 a promising candidate for not only pharmacological approaches, but also for cartilage tissue engineering. A first study proposing TRPV4 as a tissue engineering target for cartilage repair showed promising results after chondrocyte construct stimulation with 4 $\alpha$ PDD, showing after 28 days of culture, enhanced collagen production and tensile properties when compared to untreated controls. This study demonstrated that TRPV4 activation in cartilage constructs has the potential to produce tissue-level improvements (170). Following the steps of this initial study, O'Connor et al. evaluated the delivery of a physical stimuli to an agarose-embedded chondrocyte construct with the aim of activating TRPV4. After 2 weeks of culturing the constructs to allow for ECM formation, they delivered dynamic load for 3 hours on normal constructs and samples inhibited with GSK205. After 72 hours, an increase in transforming growth factor  $\beta$ 3 (TGF- $\beta$ 3) expression was observed for normal constructs that was completely inhibited under GSK205 presence. The antagonist presence was also noted to diminish the collagen II expression regardless of the loading regime. When stimulating the constructs for a period of 4 weeks, matrix accumulation was observed to increase with enhanced production of both GAGs and total collagen. This effect was attributed to indirect TRPV4 stimulation. Given that stimulated constructs cultured with GSK205 showed an attenuated response to load and prevented the increase of the specific matrix components, the treatment of the constructs with the TRPV4 agonist GSK101 had a similar response to dynamic loading attributing the observed effects directly to TRPV4 activity. Moreover, TRPV4 activation via dynamic load was shown to decrease a disintegrin and metalloproteinase with thrombospondin motifs

(*ADAMTS5*) and nitric oxide expression (*NOS2*), which are genes that are directly related to OA. The inhibition of the channel resulted in loss of the gene downregulation effect, bringing further evidence for the need of TRPV4 functioning for normal cartilage homeostasis (171). This study adds to the increasing evidence that TRPV4 plays a crucial role regulating chondrocyte mechano-transduction and physiological responses by activation of specific signalling pathways and gene expression.

The latest research on cartilage tissue engineering targeting TRPV4 has focused on engineering a “mechanically responsive bioartificial tissue construct for drug delivery”, that employs the signalling cascade that follows the  $Ca^{+2}$  channel activation. The aim of the study was to deliver the pharmaceutical agent anakinra, also known as interleukin-1 receptor antagonist (IL-1Ra), a drug that has been observed to attenuate OA progression in preclinical models. However, long-term delivery is suggested for an optimal effect in humans. They were able to successfully build chondrocyte constructs transfected with a cytomegalovirus enhancer, which, following the delivery of mechanical stimulation to the cells, resulted in a programmed production of the transduced genes. By later antagonising TRPV4 with GSK205 they observed an attenuation in the gene response, pointing to the need for TRPV4 activity for the system to work. However, they observed the activation of the channel was not restricted to mechanical load. While this novel technology promises a potential clinical application for OA management, many questions are yet to be solved in order to successfully treat a disease that has such a complex pathology (172). However, all these novel studies agree on the importance of designing therapies targeting TRPV4 activity. Moreover, it is becoming more evident that the key for a successful approach resides on the potential to specifically target the channel present in chondrocytes, without affecting its activity in the surrounding cells within the joint. Tissue engineering methods being able to selectively deliver mechanical activation of TRPV4 could potentially become the next generation of cartilage regenerative medicine approaches.

## 1.6 Magnetic nanoparticles

The popularity of MNPs is rapidly increasing among the scientific community. Magnetic nanoparticles can be commonly described as nanomaterials composed of a magnetic core formed of elements such as iron (Fe), Nickel (Ni) or Cobalt (Cu). Among the most popular particles for biomedical applications, iron oxide based particles such as magnetite ( $\text{Fe}_3\text{O}_4$ ) or maghemite ( $\text{Fe}_2\text{O}_3$ ) are currently being used due to the biocompatibility observed (173). Surrounding the core, there is typically an external protective shell and often with organic linkers to functionalise the MNPs for the specific purpose. The particle properties vary according to the synthesis method and can be easily modified according to the purpose of the particle. The modifiable parameters include particle size, shape, magnetic properties, density, mobility, ease of visibility and durability (174). In addition the surface coating allows for specific functionality such as targeting specific cell motifs, protection against oxidative damage or being immediately cleared by the reticuloendothelial system of the cell (175).

### 1.6.1 Magnetic nanoparticle design

The magnetic core of the nanoparticles provides them with magnetic properties, therefore MNPs obey Coulomb's law of electrostatic force interaction allowing the particles to be manipulated when submitted under the influence of a magnetic field (176). The properties of the nanoparticles are not the same as the ones on their bulk. The magnetic materials are composed of regions, also called magnetic domains, separated by domain walls that together form the bulk material. Each magnetic domain has aligned magnetic moments (dipoles), but this can be different in the other domains (177). According to the magnetic response of an external magnetic field, MNPs can be classified as diamagnetic, paramagnetic, ferromagnetic, ferromagnetic, and antiferromagnetic.

All materials react to a magnetic field to some extent, and the response to an external magnetic field depends on their remanent magnetisation value ( $\mu_r$ ), this is the capacity to retain magnetisation after the removal of the external magnetic field. The weakest response to an external magnetic field is

observed in diamagnetic materials. When a magnetic field is applied, the magnetic moment of these materials is opposed to the direction of the field and therefore the susceptibility (which indicates how much the material can be magnetised) is negative (178). The atoms of diamagnetic materials have no net magnetic moments hence displaying the weak response. Opposed to diamagnetic materials, ferromagnetic compounds exhibit a behaviour of a permanent magnet. In ferromagnets, the overall magnetisation can be separated into smaller domains, and the structure of the domains determines the size dependence on the materials behaviour. If the diameter is smaller than a critical value ( $D_c$ ), it becomes a single domain developing paramagnetic properties (179). Antiferromagnetic materials have magnetic moments of equal magnitude, but they are arranged in an antiparallel conformation. Therefore, they cancel each other, having a null magnetisation. Above certain temperature (Neel temperature), the magnetic moments fluctuate and materials show a paramagnetic behaviour (173). Ferrimagnetic materials are similar to the previous however, the magnetic moments are not equal in magnitude and are arranged in an antiparallel conformation and they exhibit a net spontaneous magnetisation below the critical temperature (180). As observed in antiferromagnetic materials, above the critical temperature they behave as paramagnetic materials. Paramagnetism is the magnetic state observed in materials with an unpaired electron. These materials also have domains, that in the presence of an external magnetic field they align in the same direction, however they are unable to perfectly align due to their random thermal motion (Figure 1-10) (181).

Most biomedical applications however, base their technology around materials with paramagnetic properties. For this state of the material, the size is a critical parameter to consider. Focusing on the magnetic domains, when the magnetic material diameter is lower than a critical value ( $D_c$ ), the domains commence to reduce until reaching a "single domain limit" (175). Below this limit, the material will behave as superparamagnetic. The single domain resulting from the sum of all the magnetic moments has two stable orientations with an anti-parallel conformation, and in specific conditions of thermal fluctuations, there can be a transition between both conformations with the

following reverse of the material's polarisation. These materials do not retain magnetisation once the external magnetic field is removed (176). Superparamagnetic materials have similar behaviour to paramagnetic objects however, they have slightly higher sensitivity to the external magnetic fields given their higher magnetic susceptibility (182).

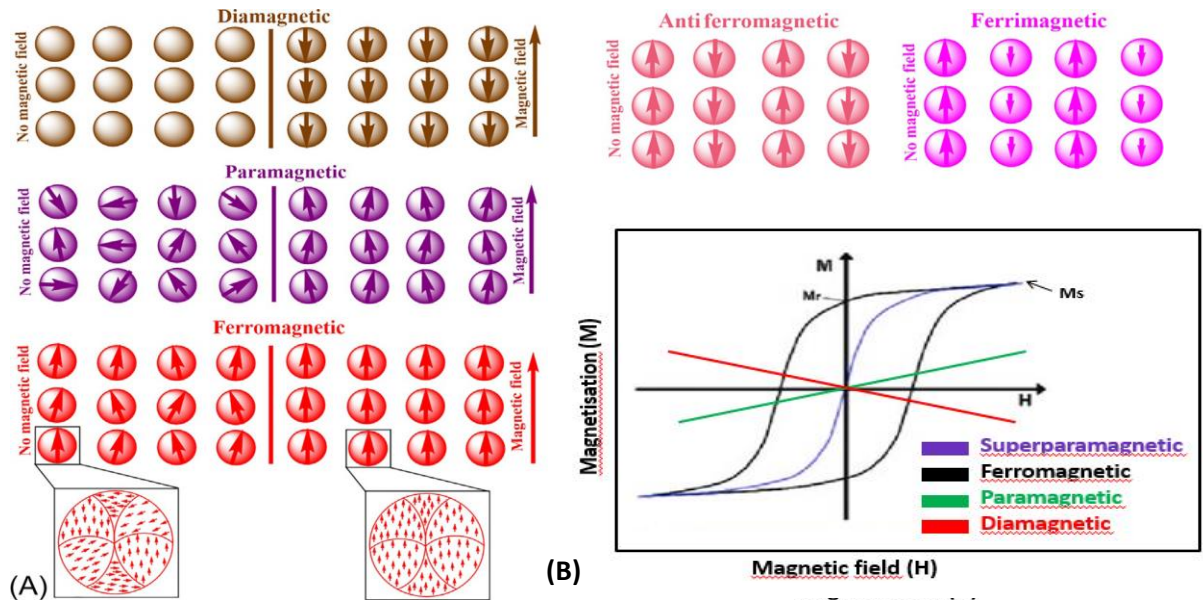


**Figure 1-10. Schematic representation of the different magnetic states of the materials without an external magnetic field and in the presence of the magnetic field.** A) Diamagnetic materials have no uncoupled electrons resulting in a lack of magnetisation without an external field. The presence of a magnetic field exerts a weak magnetisation. Paramagnetic materials exhibit random disposition of the spins without a field that attempt to align in the presence of it. Ferromagnetic materials present a certain kind of alignment in the natural state, and in the presence of an external field the moments of the different domains align parallel to the field. Both antiferromagnetic and ferromagnetic materials present opposing magnetic moments being compensated in the first and having different magnitudes in the latter. In the presence of an external field the magnetic behaviour resemblances to that of superparamagnetic materials. B) Diagram representing the hysteresis loop of the different magnetic behaviours in the presence of an external magnetic field. The remanent magnetisation ( $M_r$ ) represents the magnetisation left once the external field is removed and the saturation magnetisation ( $M_s$ ) is the state reached when an increase of intensity of the external field cannot induced higher magnetisation on the material (175).

Iron oxide particles made of magnetite or maghemite, also known as superparamagnetic iron oxide nanoparticles (SPIONs), have become attractive for biomedical applications given their biocompatibility and biodegradability and the reduced risk of agglutination. Superparamagnetic materials do not retain magnetisation following removal of the external field, hence making these nanoparticles interesting candidates for biological administration. The synthesis process of the nanoparticles must always reply to the purpose of the application: seeking for biocompatibility, durability of the particle until reaching the target or fulfilling the properties to work as a contrast agent. The biological response to foreign objects could hinder the therapy by restricting the nanoparticle free movement or altering the physical properties and even activating the immune system against the MNPs. Moreover, the MNPs must reach the target tissue, making the size a critical parameter to consider so that it can trespass the blood barriers (183,184). Other aspects found to be crucial in the nanoparticle design include the hydrodynamic size and the surface properties. To ensure the delivery of the MNPs to the target, these parameters need to be highly controlled when engineering the particles to avoid events such as MNP clustering, avoiding early clearance mechanisms and facilitating delivery to the tissue by avoiding early interactions with plasma proteins (185). There are several routes for the synthesis being classified as physical methods such as electron beam lithography, or gas-phase deposition, however, issues arise when trying to control the particle size. Wet chemical methods such as co-precipitation are popular due to its simplicity and high reproducibility. Lastly, microbial methods provide a simple route for MNPs synthesis with great control over the particle composition and geometry (186).

MNPs are often coated to ensure preservation of the properties of the particle once administrated and to avoid degradation or oxidation of the core and the subsequent loss of the magnetic properties. Moreover, the particle coating potentially prevents from agglomeration, provides stability, and improves biocompatibility. Several coatings can be used to stabilise the particles such as dextran, silica, or gold. However, it is important for the coating not to affect the properties of the particle (175).

Further modification of the MNPs is made with the aim of functionalising the particle for the specific functional goal. Often linkers or specific receptor ligands such as peptides, small molecules or antibodies have been linked to the MNPs to target the particles towards a specific cell or tissue. When adding the ligands, the multivalency phenomenon must be taken into consideration. The particle size, and the number of ligands attached per particle can potentially increase the adhesion to the target by binding to multiple receptors however, up to a maximum number of ligands the process is not favoured. For each synthetic state of the MNPs the properties such as size, charge shape or hydrophobicity can be altered. Hence it is important to always consider the application purpose and the required properties to meet the criteria for a therapeutic agent.

Biomedical applications need to take into account not only the adequate design of the particle for a specific purpose, but also the toxicity and biodegradation of the nanoparticles. Importantly, a MNP might not be toxic itself however, the elements released following degradation must also be considered. Moreover, accumulation of the particles when hindered the diffusion can also lead to toxicity by accumulation (186). A key element to consider is the type of metal that forms the nanoparticle core. For example, it has been observed that particles made of nickel or cobalt turn out to be toxic in contrast to iron-oxide particles (187). On the contrary, several toxicity studies have been performed for iron-cored superparamagnetic nanoparticles with no evidences of toxicity shown (188,189). As iron is naturally found in the human body, metabolising this metal is not a rare event. Nevertheless, toxicity depends not only on the nanoparticles composition but also on the administrated dose, method of administration, biodistribution, solubility and size (190). The surface area has been determined as one of the key factors to control toxicity. Particles with a higher surface area induce higher toxicity than smaller ones at same dosages (191). Another element observed to highly influence cytotoxicity is the particle size. Karlsson et al. evaluated in an epithelial cell line the cytotoxic effects of Fe<sub>2</sub>O<sub>3</sub> nano and micro particles showing that nano-sized particles caused more oxidative damage than micro-sized particles. However, at lower concentrations there were no signs

of toxicity for any of the sizes (192). This indicates that generalisation cannot be achieved for delimiting toxicity parameters for particles and the whole set of factors must be taken into consideration.

Regarding the degradation of the SPIONs upon cellular uptake, it is described that under normal conditions the nanoparticles enter the cells via receptor-mediated endocytosis, and are metabolised in the lysosomes (193). The iron metabolised then becomes part of the body iron stores and is eventually bounded to haemoglobin and transported by transferrin, prior to faecal elimination. Coatings such as dextran are mostly eliminated by urine (194). Oxidative stress is generated when there is an imbalance of reactive oxygen species (ROS) and is the main cause of cellular toxicity, caused by disruption of the cellular components and function impairment. The excess of free iron metabolised or the leaching of ions from the MNP core has been found to induce ROS production, inflammation and apoptosis (195,196). Therefore, unless abnormal amounts of iron are generated due to a high dose of administrated particles, the iron released should not cause harmful effects.

### 1.6.2 Current applications

The magnetic properties of the nanoparticles have made them excellent candidates for biomedical applications (Figure 1-11). The heat generated from the alignment of the magnetic moments to a magnetic field has been used for hyperthermia-mediated applications such as cancer therapy. In addition, MNPs are being studied for a wide range of applications such as treatment of infectious diseases, drug delivery, MRI contrast agents or biosensors.

A very extended use for MNPs has been magnetic hyperthermia. The concept is referred to the heat produced by MNPs in response to the application of an external alternating magnetic field. Cancer therapy has benefited from this application, which allows MNPs to specifically target cancer cells and induce apoptosis by overheating the cells to sensitive temperatures. This has been assessed in several tissues such as brain or prostate among others (197,198). The heating effect created by the activation

of the MNPs has also been used for the treatment of infectious diseases overcoming recurrent issues such as drug-resistance (199). Another potential application for MNPs being widely studied is the use of the nanoparticles as carrier vectors to efficiently deliver drugs, viral particles, nucleic acid fragments or proteins. This methods allows for a safer and more stable delivery, protecting the therapeutic load from immediate destruction by the immune system and improves the cellular uptake of the compound reducing the side effects so neighbouring tissues are not affected (200,201).

The field of medical diagnostics has found MNPs a useful contrast agent for MRI. SPIONs have been studied for producing an enhanced proton relaxation time when compared to other contrast agents (173). The food and drug administration (FDA) approved SPIONs are already being used for *in vivo* MRI diagnostics although some of the agents have been retired due to mild secondary effects driven by the metabolisation of the particles. The use of nanoparticles for imaging has allowed for *in vivo* imaging of molecular processes bringing enormous advantages for non-invasively study of diseases. By internalisation of the MNPs by the cells, the magnetic properties are transferred, allowing for *in vivo* tracking of the implanted cells. The MRI resolution (25-100  $\mu\text{m}$ ) allows for individual tracking of cells together with the surrounding tissue (202). Markides et al. studied the potential use of SPIONs for cell tracking in a rheumatoid arthritis murine model and showed the potential of stem cell labelled treatments for online monitoring of the therapy, in addition to optimise the protocol for optimal imaging (203). On the down side, the continuous cell proliferation following implantation hinders the localisation of the particles due to division of the nanoparticle load and therefore, long-term tracking is in some cases unavailable (177). Thus, some challenges remain unsolved for an improved use of MNPs in diagnostics.

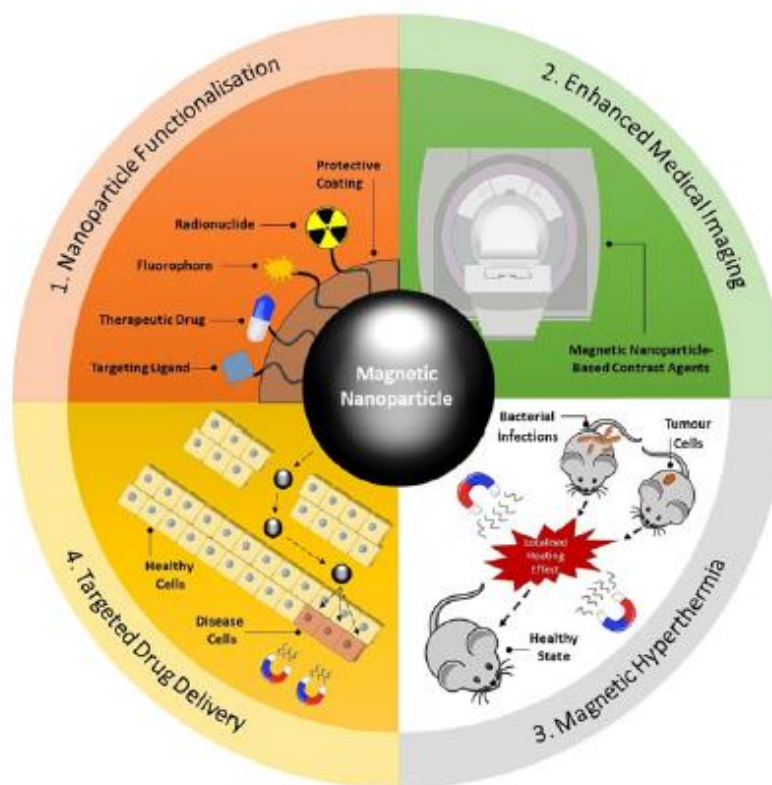


**Figure 1-11. Biomedical applications of MNPs.** (1) Functionalising the MNPs surface with different agents such as drugs or specific ligands introduces the possibility of using the nanoparticles as vehicle devices to deliver a compound or a specific effect. (2) SPIONs and other MNPs have been used to enhance the signal obtained from MRI signals or (3) to target the destruction of cancer cells through the heating generated by magnetisation through an external field. (4) MNPs are also studied for the potential to specifically deliver a drug to the target tissue or cellular group (176).

Tissue engineering researchers have also found nanoparticles a useful tool for clinical applications. MNPs introduce the possibility to selectively target small tissue components such as cells, proteins, or genes. In addition, cell therapies will also hugely benefit from labelling the cells with MNPs since it will allow monitoring the cellular distribution, localisation, and expansion post-administration. Previous studies have already proven that is possible to trap labelled cells into a specific site, opening the door for clinical applications that need to retain the stem cells at the injury site (204,205). Moreover, it has been demonstrated that administrated stem cells could be recovered from the tissues using magnetic separation columns, allowing for a thorough analysis of the treatment (206). One of the major

concerns on the use of MNPs has been the effect they exert on the stem cells following labelling. However, a combination of studies have reported that MNPs do not show a cytotoxic effect on stem cells and neither influence their proliferation and differentiation potential (207,208).

Among the variety of applications, the possibility of targeting a specific cell or tissue is being studied. MNPs introduce the possibility of directing the particles to specifically reach targets at a molecular level by making use of their magnetic properties. However, with the need for an external magnetic field, these applications are limited to tissues close to the body surface in order to be effective (209).

### 1.6.3 MNPs and Mechanotransduction: Applications in orthopaedics

Regenerative medicine has provided promising therapies for OA despite the lack of long-term results yet to be available. Nevertheless, the current approaches still have the need to overcome certain difficulties, one major concern being the lack of techniques for *in vivo* assessment. Procedures such as ACI, could benefit from the possibility of tracking the stem cell location post-transplantation and being able to track the number of viable cells or the repair rate of the injury site. For researchers, this often translates into the need to terminate the experiment for histological processing, being incompatible with a long-term follow up (202). Initial studies for orthopaedic applications have focused on improving current OA approaches by labelling MSCs with SPIONs aiming to retain the cells at the defect site. Kobayashi et al. labelled MSCs with ferumoxides particles and delivered the cells through an injection directly into an osteochondral defect. By placing *ex vivo* the joint next to an external magnetic device they observed accumulation of the labelled MSCs on the injury site, in contrast to the control without magnetic force (210). The same group also demonstrated following the same procedure, that cartilage could be regenerated *in vitro*. Human cartilage fragments from osteoarthritic patients were cultured in special flasks with chondrogenic differentiation media containing labelled MSCs. They were able to observe that under the influence of an external magnetic

force a cell layer was formed within the cartilage tissue. This layer showed to have native cartilage histological markers suggesting chondrogenic events taking place (211).

Several studies have confirmed that labelling MSCs with MNPs does not affect the ability of the cells to drive chondrogenesis or other types of differentiation processes (207,210). Despite the great advantages that the unspecific labelling of MSCs with SPIONs bring to current orthopaedic applications for cell retention and *in vivo* imaging, novel studies are now addressing the possibility of delivering specific external stimuli to the cells by improving the labelling techniques and taking advantage of the mechano-transductive potential of cells. These innovative approaches overcome some of the current problems for clinical translation, such as the incapacity of differentiating cells with chondrogenic media when delivered *in vivo*.

As previously documented, cells sense external stimuli through membrane alterations that lead to cytoskeletal rearrangement processes with the following signal transduction and gene expression events. Novel studies have addressed the possibility of delivering stimuli selectively to specific cells by targeting MNPs towards key elements on the cell membrane. The application of an external magnetic field with the following alignment of the MNPs can induce membrane alterations, leading to cytoskeletal rearrangements and transmembrane changes in ion influx (212). In addition, mechanical deformation can induce activation of mechano-sensitive ion channels through several mechanisms.

One of the major issues encountered for cell labelling for specific purposes is the optimal delivery of MNPs to the cells. The nature of the MNP coating defines the type of interaction given with the cells. FDA approved nanoparticles such as Feridex<sup>®</sup>, now taken off the market, are coated with molecules such as dextran, a negatively charged coating that confers the particles a hydrophilic character allowing for the prevention of MNP aggregation (213). Nevertheless, the negative nature of the coating hinders the delivery of the MNPs to the cells due to the negative nature of the cell membrane. To overcome this challenge, transfection reagents are often used although the protocol needs to be

carefully adjusted for each condition due to the toxicity of these agents (205). Other approaches such as the use of polycationic reagents or magnetofection are currently being used, however, issues such as the complexity of the method or particle aggregation should also be considered. A method with increasing popularity aims to coat the particles with antibodies targeting specific elements on the cell membrane. This approach allows for target-specific binding and opens the possibility to deliver stimulus directly to nano scaled-structures.

Two magnetic approaches have been studied to deliver stress to the cells (Figure 1-12); the first technique is based on using magnetic drag to translate the force and the second approach physically deforms the cell membrane by twisting the MNPs attached. Both techniques are based on the dragging effect of the attached MNPs in response to a high gradient magnetic field (212). For this principle to successfully work, the attachment of the MNP to the cell should be firm, and the external magnetic force exerted strong enough to deform the cell membrane, but without disrupting the membrane. Wang et al. initially developed this approach termed as magnetic twisting cytometry (MTC). They studied the effect on single cells of exerting a torque in MNP bound to cell membrane ligands by using nanoparticles with the ability to retain magnetisation following elimination of the external magnetic field. By applying two magnetic pulses in different directions, they were able to exert a twist in the particles that punctually deformed the cell membrane (114,214). Initial studies performed on a cell population rather than individual were performed on a population of osteoblasts by targeting the integrins of cells, a well-described mechano-responsive element. MNPs were coated with RGD peptides, that have affinity for the integrin receptor, and an external time-varying magnetic field was applied for 21 days. The mechanical activation of the cells led to an increase of mineralized bone matrix production (120). Despite the promising outcomes observed by the activation of integrin receptors, the events following activation might lead also to undesired effects, given the wide role that these molecules have on the intracellular signalling. Voltage-gated ion channels present in tissues such as bone cells or chondrocytes, has been previously reported to activate favourable routes for

bone engineering. Membrane stretching events have been described to activate the channel thus, directly targeting these channels with the MNPs technology has been studied for bone tissue engineering applications (215). Moreover, stem cells also require mechanical cues for differentiation hence, researchers have gathered their efforts designing an approach for bone and cartilage engineering including the use of MNPs, stem cells and bioreactors.

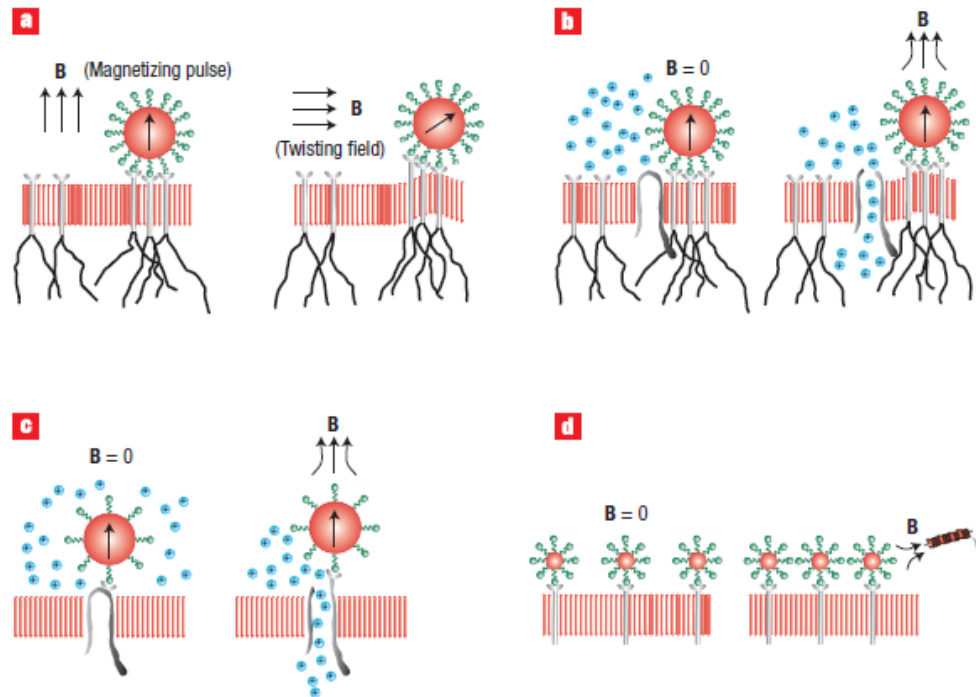


**Figure 1-12. Different methods for MNP actuation on cell mechanotransduction.** (B = magnetic field vector). (A) Magnetic twisting cytometry-based applications use MNPs of bigger sizes capable of retaining remanent magnetisation attached to membrane receptors such as integrins. Following a series of magnetic pulses, the torque exerted over the MNP deforms the membrane and the effect is transmitted via the integrin receptors bound to actin filaments linked to the cytoskeleton. (B) Larger MNPs are attached to integrins located near to ion channel. Following application of a magnetic field, the MNPs attracted to the field exert a pulling effect on the membrane activating the gating of the adjacent channels. (C) Superparamagnetic nanoparticles are directly attached to mechano-sensitive ion channels on the cell membrane, that following a magnetic pulse are forced open with the following exchange of ions. (D) Particles on the nanoscale range are bound to a complex of receptors. When a magnetic field is applied with a needle, the particles attracted to the field induce the receptor clustering and activation of downstream signalling (216).

The next step that followed this new concept was the design of a magnetic force bioreactor that could deliver an alternating external magnetic field, mimicking the mechanical activity that cells are subjected to under physiological conditions. Dobson et al. presented a model for a magnetic force bioreactor (MFB) capable of delivering forces in the scale of pico-newtons, sufficient enough to induce membrane deformation caused by the pulling effect of the MNPs attracted to an alternating magnetic field (216). The dragging or torque effect induced in the MNPs attached to elements of the cell membrane is directly transmitted to the actin cytoskeleton inducing the activation of secondary messengers. The magnetic stresses were designed to be applied with a frequency of 1-3 Hz, known to be optimal to mimic physiological stresses (217). The MFB allows for stimulation of cells seeded either in a 2D surface or onto a scaffold in an isolated sterile environment (209). In addition, this novel approach to bioreactor design eliminates some of the previously observed complications such as the inability of some bioreactors to successfully deliver a force to the scaffold that is equally translated to the cells, or the inability to preserve the construct constantly in a sterile environment. This system allows for a direct delivery of the force to the cell membrane, allowing for a close control of the mechanical stimuli.

Following the study of the response of a mechano-responsive ion channel, TREK-1, in osteoblasts and its contribution to bone proliferation (212), MNP-mediated activation of an ion channel embedded in the cell membrane was firstly attempted. By attaching MNPs to TREK-1 and following the application of a magnetic field they observed, through single cell electrophysiology, the activation of the channel activity for some of the cells (132). This novel concept is now known as magnetic ion channel activation (MICA) and has been further studied for tissue engineering applications (Figure 1-13) (Table 1-1). Kanczler et al. used this technology to activate TREK-1 in bone marrow MSCs implanted in mice, by activating the particles with the MFB previously described. After 21 day of magnetic stimulation observations seen induced enhanced matrix production and increased proteoglycan and collagen expression, suggesting a potential application of this technology for bone and cartilage differentiation

guidance of MSCs (133). Other receptors have been targeted by the MICA technology to induce osteogenic differentiation of MSCs with promising results for clinical applications (218).

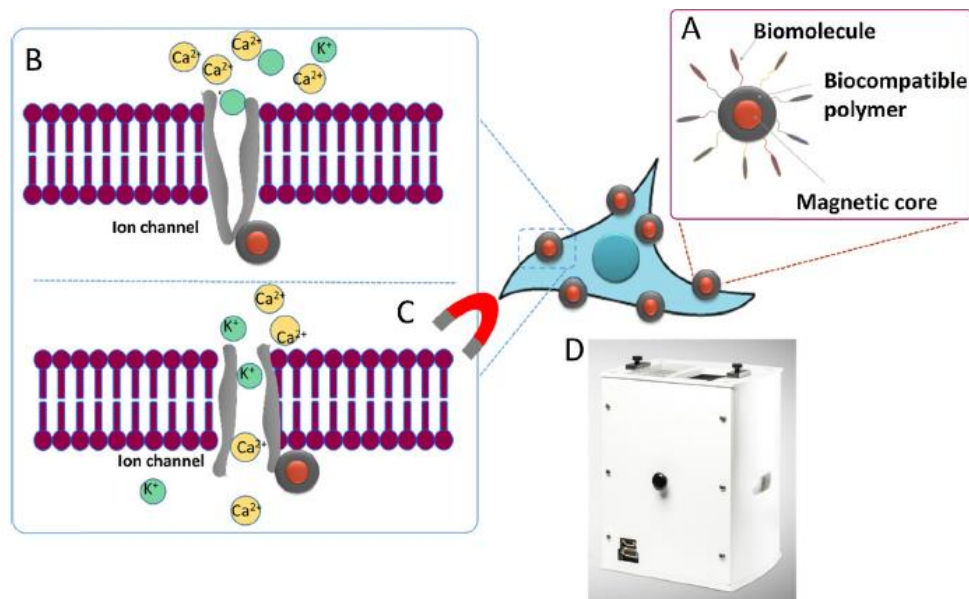


**Figure 1-13. Schematic representation of the magnetic ion channel activation (MICA) principle.** (A) Superparamagnetic nanoparticles coated with a biocompatible polymer and the specific antibodies, (B) are attached to the mechanotransductive domain of mechano-sensitive ion channels located in the cell membrane. Cells are placed inside the magnetic force bioreactor that applies an alternating magnetic field to the cells. Under the influence of the magnetic field, the MNPs magnetic moments align in the direction of the field, exerting a force directly onto the channel that activates the gating mechanism. The channel activation leads to a current of ions through the channel that translates into activation of secondary messengers and downstream signalling events (219).

**Table 1-1. Studies based on MICA technology and their application.**

| TE Application                         | Membrane Target       | Year | Study |
|--|-----------------------|------|-------|
| <b>Bone &amp; Vascular endothelium</b> | PDGFR $\alpha$        | 2013 | (218) |
| <b>Bone</b>                            | TREK-1 and RGD        | 2014 | (220) |
| <b>Bone &amp; Cartilage</b>            | Wnt Frizzled Receptor | 2015 | (221) |
| <b>Bone</b>                            | TREK-1                | 2018 | (222) |
| <b>Bone</b>                            | Wnt Frizzled Receptor | 2018 | (223) |
| <b>Bone</b>                            | TREK-1                | 2018 | (224) |
| <b>Tendon</b>                          | Activin Receptor      | 2018 | (225) |

In an attempt to move one step closer to clinical translation, an *ex vivo* chick foetal femur model was designed to study the remote activation of MSCs for bone regeneration. 14 days after injection of pre-labelled MSCs on a defect site and remote activation of TREK-1, they observed increased generalised mineralisation and a raise in alkaline phosphatase activity (220). MICA technology was firstly studied on a pre-clinical ovine model for bone tissue regeneration by Markides et al. where the *in vitro* role of the MFB was replicated and adapted to enable the cell activation *in vivo*. After 13 weeks, determined by micro-CT, MICA treated defects showed improved repair in the defect site when compared to the control limb from the same animal. Enhanced expression of bone markers was also found in the experimental groups and a recruitment of endogenous cells associated to bone remodelling was achieved (222). The promising results achieved by this study lead a great promise for a future development of an injectable therapy using the MICA technology for bone and cartilage clinical repair.

## 1.7 Concept approach and hypothesis

Current strategies for OA repair have shown promising results and continue to be studied and improved to address the clinical demands. Nevertheless, these approaches find common limitations hindering the optimal tissue repair and the ability to successfully track the treatment outcome. Often, the regenerated tissue has been observed to fail to fulfil the mechanical needs of the native tissue for developing a normal function. In addition, cell therapies have encountered difficulties retaining the implanted cells in the defect size, reducing the effectiveness of the treatment while also raising concerns on the possible activation of the immune system. Moreover, a follow-up on the treatment is restricted to MRI imaging of the tissue and invasive tissue biopsies.

The work described in this thesis gathers the bases for the development on an injectable stem cell therapy by applying the principles of the MICA technology. Based on previous research on the topic for bone tissue engineering strategies, this work proposes to apply the same principles for cartilage repair. TRPV4 has been widely demonstrated to be a mechano-inducible receptor closely related to

cartilage development. By targeting TRPV4 mechano-sensitive responsive domain in MSCs with MNPs and following activation using the MFB, the activation of the channel should trigger specific signalling pathways that will lead to chondrogenic gene transduction with increased production of cartilage-specific markers such as aggrecan, collagen II and Sox9. This approach could then potentially be translated for clinical applications into an injectable therapy of stem cells labelled with MNPs. The simplicity of this technique could reduce the invasiveness of current procedures by activating the chondrogenic response with an external magnet adapted to deliver the magnetic field externally through a bandage over the human knee. This work has been conducted using stem cells from different species and sources to support translation of the therapy through large animal pre-clinical trials into human. In addition, different sources of stem cells have been studied to assess the one with the highest chondrogenic potential for clinical translation.

In order to firstly study the suitability of the MNPs used during this work, Chapter 3 gathers the experiments concerning the magnetic properties of the MNPs and the efficiency of labelling process, the cell viability when cultured with MNPs, and the MNP ability to translate the external stimuli into the cells for driving chondrogenic differentiation via histological and gene expression analysis. Once the potential of the TRPV4- MNPs for driving chondrogenic differentiation was successfully assessed, equine MSCs were studied in Chapter 4, with the aim of analysing the best mechano-responsive target for driving chondrogenesis. This was done by measuring the collagen 2 production through a GFP-Col2 reporter, together with histological and biochemical analysis of chondrogenic markers. In addition, oMSCs were also used to test the effect of the MICA technology and understanding the role of TGF- $\beta$  in chondrogenesis. Finally, Chapter 5 was focused on studying the effects of TRPV4 activation with MNPs in hUC-MSCs as a potential cell type candidate for translating the technology into a large animal model. This was assessed following histological, biochemical and gene expression findings in order to allow comparison with the work performed in previous chapters.

The conducted work hypothesised:

- 1) Mechanical activation of TRPV4 delivered by magnetic actuation guides stem cell differentiation towards a chondrogenic lineage and aids chondrocytes to maintain the phenotype in 3D culture.
- 2) Selective activation of the TRPV4 receptor in combination with chondrogenic cues improves the histological properties of the formed cartilage in pellet culture and enhances cartilage-specific marker expression.

---

# *Chapter 2*

---

## *Materials and Methods*

## 2.1 Materials

Unless otherwise indicated materials were obtained from the manufacturer or their distributor within the United Kingdom.

**Table 2-1. List of reagents, catalogue number and suppliers.**

|   | Catalogue number | Supplier              |
|---|------------------|-----------------------|
| 1-ethyl-3-(3-dimethylaminopropyl) carbodiimide hydrochloride (EDAC) | E2247            | Life Technologies     |
| 2-Mercaptoethanol   | M6250            | Sigma-Aldrich         |
| 2-Methylbutane  | 78-78-4          | Sigma-Aldrich         |
| 2-Propanol  | I9516            | Sigma-Aldrich         |
| 3,3'-Diaminobenzidine (DAB)   | D8001            | Sigma-Aldrich         |
| 3-aminopropyltriethoxysilane (APES)                                 | A3648            | Sigma-Aldrich         |
| ABC Staining Kit Rabbit specific                                    | Ab64261          | Abcam                 |
| ACAN antibody   | Orb213537        | Biorbyt               |
| Acetic acid glacial, 99%  | A/0360/PB17      | Fisher Scientific     |
| Acetone   | A/0560/17        | Fisher Scientific     |
| Agarose   | BP1356-500       | Fisher Scientific     |
| Alcian Blue 8GX   | A3157            | Sigma-Aldrich         |
| Ammonium acetate (5M)   | AM9070G          | Invitrogen            |
| Anti-Aggrecan antibody  | Ab140707         | Abcam                 |
| Anti-Collagen II antibody   | Ab34712          | Abcam                 |
| Anti-Dextran Antibody, Clone DX1                                    | 60026FI          | Stemcell Technologies |
| Anti-KCNK2 (TREK-1) antibody  | APC-047          | Alomone Labs          |
| Anti-Ki67 antibody  | Ab15580          | Abcam                 |
| Anti-SOX9 antibody [3C10]   | Ab76997          | Abcam                 |

|   |            |                            |
|---|------------|----------------------------|
| Anti-TRPV4 antibody   | OSR00136W  | ThermoFisher               |
| Arg-Gly-Asp   | A8052      | Sigma-Aldrich              |
| Bovine Serum Albumin (BSA)  | 9998S      | Cell Signalling Technology |
| Calcium chloride  | 793639     | Sigma-Aldrich              |
| Cell Tracker™ CM-Dil Dye  | C7000      | ThermoFisher               |
| Chicken anti-Goat IgG H&L (Alexa Fluor™ 647)  | A21469     | Thermo Fisher              |
| Chondroitin Sulphate sodium salt  | C4384      | Sigma-Aldrich              |
| CO1A2 antibody  | Orb27313   | Biorbyt                    |
| Collagenase from <i>Clostridium Histolyticum</i>  | C6885      | Sigma-Aldrich              |
| Collagen X antibody   | Orb114057  | Biorbyt                    |
| DAPI  | D9542      | Sigma-Aldrich              |
| Dexamethasone   | D4902      | Sigma-Aldrich              |
| Dimethyl methylene blue (DMMB)  | 341088     | Sigma-Aldrich              |
| Dimethyl sulfoxide (DMSO)   | D5879      | Sigma-Aldrich              |
| DMEM/F-12, HEPES  | 31330-038  | Gibco                      |
| DNA AWAY™   | 10223471   | Thermo Fisher              |
| DNA Oligos Customised Equine Primers: <i>Acan</i><br><i>Col2a1</i><br><i>S18</i><br><i>Sox9</i> | 4157405    | Thermo Fisher              |
| Donkey anti-Goat IgG H&L (Alexa Fluor® 488)   | A11058     | Thermo Fisher              |
| DOTAP Liposomal Transfection Reagent  | 11202375   | Roche                      |
| DPX Mountant for Histology  | 06522      | Sigma-Aldrich              |
| Dulbecco's Modified Eagle's Medium (DMEM)   | 10-013-CVR | Corning                    |
| Dulbecco's phosphate buffered saline without calcium and magnesium (DPBS)                       | 14190094   | Gibco                      |
| EDTA (0.5M), pH 8.0   | AM9260G    | Invitrogen                 |

|  |                         |                      |
|--|-------------------------|----------------------|
| Eosin Y solution                                 | HT110216                | Sigma-Aldrich        |
| Ethanol (absolute)                               | E0650/17                | Fisher Scientific    |
| Ethidium bromide                                 | E1510                   | Sigma-Aldrich        |
| Fast Green FCF                                   | F7252                   | Sigma-Aldrich        |
| Foetal Bovine Serum (FBS)                        | FBS-70831-<br>EPS117650 | LabTech              |
| Fibronectin human plasma                         | F0895                   | Sigma-Aldrich        |
| Fluoromount™ Aqueous Mounting Medium             | F4680                   | Sigma-Aldrich        |
| FM1-43 FX  | F35355                  | Life Technologies    |
| Formol 4%, buffered                              | 11699404                | QPath Labs           |
| Gel loading buffer                               | G2526                   | Sigma-Aldrich        |
| GeneRuler 100bp DNA Ladder                       | SM0321                  | Thermo Fisher        |
| Glycine  | 50046                   | Sigma-Aldrich        |
| Goat anti-Mouse IgG Fc                           | Ab97261                 | Abcam                |
| Goat anti-Mouse IgG H&L (Alexa Fluor® 647)       | A21236                  | Invitrogen           |
| Goat anti-Rabbit IgG Fc                          | Ab97197                 | Abcam                |
| Goat anti-Rabbit IgG FITC                        | 10006588                | Bertin Bioreagent    |
| Goat anti-Rabbit IgG H&L (Alexa Fluor® Plus 647) | A32733                  | Invitrogen           |
| GSK1016790A                                      | G0798                   | Sigma-Aldrich        |
| GSK2193874                                       | SML0942                 | Sigma-Aldrich        |
| Guanidine Hydrochloride                          | G3272                   | Sigma-Aldrich        |
| Hematoxylin Solution, Harris Modified            | HH16                    | Sigma-Aldrich        |
| High Capacity cDNA Reverse Transcription Kit     | 4368814                 | Fisher Scientific    |
| Histo-Clear                                      | HS2001GLL               | National Diagnostics |
| Histoplast Paraffin                              | 6774060                 | Thermo Fisher        |

|  |             |                      |
|--|-------------|----------------------|
| Hydrochloric Acid (5M)                                     | 10605882    | Fisher Scientific    |
| Hydrogen peroxide  | BPE2633-500 | Fisher Scientific    |
| IMS  | M/4400/17   | Fisher Scientific    |
| Insulin-Transferrin- Selenium-Sodium Pyruvate (ITS) (100X) | I3146       | Sigma-Aldrich        |
| L-Ascorbic Acid  | A4544       | Sigma-Aldrich        |
| L-Glutamine (200mM)  | 25030-081   | Gibco                |
| L-Proline  | 81709       | Sigma-Aldrich        |
| Live/Dead™ Fixable Blue Dead Cell Stain Kit                | L34962      | Invitrogen           |
| Linolenic Acid water-soluble                               | L5900       | Sigma-Aldrich        |
| Magnesium sulphate   | M5921       | Sigma-Aldrich        |
| MEM Non-Essential Amino Acid Solution (100X)               | M7145       | Sigma-Aldrich        |
| MES  | M3671       | Sigma-Aldrich        |
| Methanol   | M/3900/17   | Fisher Scientific    |
| Molecular Water  | W4502       | Sigma-Aldrich        |
| Nanomag® -D 250 nm COOH                                    | 09-02-252   | Micromod             |
| N-Hydroxysuccinimide (NHS)                                 | 130672      | Sigma                |
| PCNA antibody  | MCA1558     | Biorad               |
| Penicillin-Streptomycin (5000 U/mL)                        | 15070-063   | Gibco                |
| Phalloidin CF(R)488A                                       | BT00042-T   | Cambridge Bioscience |
| PicroGreen™ ds Assay Kit (Quant-IT™)                       | P7589       | Invitrogen           |
| Picric Acid  | P6744       | Sigma-Aldrich        |
| Pierce™ BCA Protein Assay Kit                              | 23225       | Thermo Fisher        |
| Poly(ethylene glycol) diacrylate                           | 475629      | Sigma-Aldrich        |
| Potassium ferrocyanide                                     | P3289       | Sigma-Aldrich        |

|  |  |                      |
|--|--|----------------------|
| Presto Blue™ Cell Viability Reagent  | A13261   | Invitrogen           |
| ProFreeze™ CDM Nao (2X)  | BEBP12-769   | Lonza                |
| Proteinase K   | 25530015   | Sigma-Aldrich        |
| QuantiTect Primer Assays:<br><i>ACAN</i><br><i>BTG2</i><br><i>COL2A1</i><br><i>COL10A1</i><br><i>GAPDH</i><br><i>JUN</i><br><i>MAFF</i><br><i>NFATC2</i><br><i>RCAN1</i><br><i>SOX9</i><br><i>SPP1</i> | QT00001365<br>QT00240247<br>QT00049518<br>QT00096348<br>QT00079247<br>QT00242956<br>QT00094507<br>QT00053599<br>QT00029428<br>QT00001498<br>QT01008798 | Qiagen               |
| Ready-To-Glow™ Secreted Luciferase Reporter Assay  | 631726   | Takara Bio           |
| Recombinant human TGF-β1   | 100-21   | Preprotech           |
| Recombinant human TGF-β3   | 100-36E  | Preprotech           |
| RNeasy Mini Kit  | 74106  | Qiagen               |
| RT <sup>2</sup> qPCR Primer Assay for Horse Sox9   | PPE00130A-200  | Qiagen               |
| Safranin-O   | S2255  | Sigma-Aldrich        |
| Sirius Red/ Direct red 80  | 365548   | Sigma-Aldrich        |
| Sodium bicarbonate   | S5761  | Sigma-Aldrich        |
| Sodium chloride  | S7653  | Sigma-Aldrich        |
| Sodium hydroxide   | S8045  | Honeywell            |
| Sodium Pyruvate Solution   | S8636  | Sigma-Aldrich        |
| SYBR® Green PCR Master Mix   | 4309155  | Fisher Scientific    |
| Toluidine Blue   | T3260  | Sigma-Aldrich        |
| TRI Reagent  | 93289  | Sigma-Aldrich        |
| Tris-Acetate-EDTA (TAE) buffer (50X) (2 M Tris Acetate, 100 mM Na <sub>2</sub> EDTA)   | EC-872   | National Diagnostics |
| Triton™ X-100  | T8787  | Sigma-Aldrich        |

|                      |           |                   |
|----------------------|-----------|-------------------|
| Trypan Blue Solution | T8154     | Sigma-Aldrich     |
| Trypsin-EDTA (0.5%)  | 15400-054 | Gibco             |
| Tween® 20            | P1379     | Sigma-Aldrich     |
| Xylene               | X/0250/17 | Fisher Scientific |

**Table 2-2. List of equipment and suppliers/ manufacturers.**

|                                      |               |                      |
|--------------------------------------|---------------|----------------------|
| AriaMx Tube Strips 8                 | 401493        | Agilent Technologies |
| Counting slides                      | 145-0011      | BioRad               |
| Mx3000P Optical Strip Caps 8         | 401425        | Agilent Technologies |
| Polypropylene pestle                 | Z359947-100EA | Sigma-Aldrich        |
| Thin-walled 0.5 mL PCR tube (Ambion) | AM12275       | Fisher Scientific    |
| Superfrost glass microscope slides   | 10150061      | Fisher Scientific    |

## 2.2 General cell culture techniques

To maintain sterility, all cell culture procedures were performed in a class II microbiological safety cabinet and disposable plastic consumables were employed. All cells and pellets were cultured in humidified, tri-gas controlled incubators with 21% oxygen, 5% carbon dioxide and 93% nitrogen. Pellets were cultured for all experiment in 1.5 mL sterile microcentrifuge tubes.

### 2.2.1 Coating tissue culture plastic with fibronectin

Prior to seeding the isolated human mesenchymal stem cells from a bone marrow aspirate, it was necessary to coat the tissue culture flasks with 10 ng/mL of fibronectin diluted in DPBS, in an amount sufficient to cover the bottom surface of the flask. Flasks were then incubated at room temperature for 1 hour. After coating, the fibronectin solution was removed and discarded.

### 2.2.2 Resuscitation and seeding of frozen cells

Frozen cryovials of transfected adipose-derived equine MSCs (dTomato and GFP-Col2) and (CMV-Luciferase and Col2-Luciferase) were cultured immediately upon arrival for expansion purposes. Ovine MSCs previously obtained by Dr. Hareklea Markides were stored in liquid nitrogen. Following removal from the liquid nitrogen dewar, frozen vials were transported in dry ice. Upon arrival to the laboratory, the frozen vials were left at room temperature until 90% of the content was defrosted. The cryovials were then sprayed for disinfection with 70% industrial methylated spirits (IMS) and transferred into a class II microbiological safety cabinet. The content of the cryovial was then transferred to a T75 cm<sup>2</sup> sterile flask containing 15 mL of basal expansion medium (DMEM 4.5 g/L glucose supplemented with 10% foetal bovine serum (FBS), 1% L-Glutamine and 1% Penicillin/Streptomycin solution). Flasks were then stored in an incubator and media was changed every 2-3 days.

### 2.2.3 Passaging cells

Cells were cultured until reached 80% confluence. When reached a confluent state, media from the flasks was discarded and DBPS was added to the flasks to eliminate any media residues. To cleavage the union of the cells to the tissue culture plastic (TCP), 1:10 Trypsin-EDTA (0.5%) solution diluted in DPBS was added to the flasks and incubated at 37 °C for 5 minutes or until detachment of the cells. An equivalent volume of culture media containing 10% FBS was added to the flasks to quench the trypsin effect. Following re-suspension, the content of the flask was transferred into a 50 cm<sup>3</sup> sterile centrifuge tube. The cell suspension was then centrifuged for 5 minutes at 1200 r.p.m. The supernatant was then discarded, and the remaining pellet was re-suspended and consistently mixed in the desired volume of media prior to seeding in flasks. The number of cells seeded, and size of flask selected according to the purpose of the specific experiment.

### 2.2.4 Cryopreservation of cells

For long term storage, cells were detached from TCP following the above mentioned method and following centrifugation, the cell pellet was re-suspended in 10 mL of basal medium (supplemented with 50% Profreeze with 15% DMSO) and transferred into cryovials (1.5 mL of the cell solution per vial), containing approximately  $2 \times 10^6$  to  $3 \times 10^6$  cells, depending on the cell type. Cryovials were then placed in a 2-propanol-filled Mr. Frosty freezing container and stored in a  $-80^\circ\text{C}$  freezer before transferring the vials to the liquid nitrogen dewar.

### 2.2.5 Manual cell counting

Following detachment of cells as described in 2.2.3, the cell suspension was homogeneously re-suspended in the desired media. If viability was to be assessed, a small volume of the cell suspension was separated and mixed 1:1 with trypan blue. The Neubauer haemocytometer was previously prepared by exhaling on the surface and placing a haemocytometer coverslip by gently pressing to cover the chamber. 10  $\mu\text{L}$  of the cell solution was then introduced by capillary action underneath the coverslip. Cells were then counted under the microscope. A mean count was performed from the 4  $1\text{mm}^2$  corner regions to give the number of cells per 0.1  $\mu\text{L}$ . To determine the total number of cells, the mean was multiplied by  $1 \times 10^4$  and the total mL of suspension media containing the cells. If trypan blue was used, this was also taken into account when calculating the amount of cells.

### 2.2.6 Automated cell counting

The BioRad TC20™ automated cell counter uses the imaged acquired from the best focal plane to identify the cells and exclude the debris. To count cells, the cell pellet generated after centrifugation was diluted in media. A small amount of the cell suspension was separated and mixed in a 1:1 proportion with trypan blue. From the mixture, 10  $\mu\text{L}$  were inserted into the slide chamber that was then placed in the automated cell counter. The cell counter performs accurate readings within the

$5 \times 10^4$  and  $1 \times 10^7$  cells/mL range and for cells within the 6-50  $\mu\text{m}$  diameter range. It automatically accounts for the trypan blue dilution giving a reading of cell/mL.

## 2.3 Isolation and culture of cells

### 2.3.1 Isolation and culture of bone marrow mesenchymal stem cells from bone marrow aspirate

Human MSCs were isolated from a bone marrow (BM) aspirate commercially obtained from Lonza USA from 3 different donors (21-year-old male, 19-year-old female and 21-year-old female). Each aspirate (containing  $19.6 \times 10^6$ ,  $16.3 \times 10^6$  and  $15.6 \times 10^6$  cells) was then seeded in 30 T75 culture flasks coated with fibronectin as described in section 2.2.1, at the mononuclear density of  $1.5 \times 10^3$  cells/cm<sup>2</sup>, in 15 mL of isolation media (DMEM 4,5 g/L of glucose supplemented with 5% FBS, 1% L-Glutamine, 1% Penicillin/Streptomycin). Cells were cultured in the isolation media for a week. Following 7 days, 50% media change was performed with isolation media and after 14 days a complete media change to proliferation media (10% FBS) was done, removing the majority of the non-adherent cells. After 21 days, adherent cells were cryopreserved using cryopreservation media (90% DMSO, 10% FBS) at an approximate density of  $5 \times 10^5$  cells/mL or expanded until passage 3 for specific purposes.

### 2.3.2 Isolation and culture of ovine chondrocytes from lamb knee

Chondrocytes were isolated from ovine articular knee cartilage (Staffordshire Meat Packers, Stoke-on-Trent, UK), two hours post slaughtering. The isolation method used was a modification from Hayman et al. (226). The cartilage tissue was gently removed from the upper condyles of the knee in small sections, and then rinsed 3 times in a DPBS solution supplemented with 2% Penicillin/Streptomycin. The ECM was digested overnight in an incubator at 37°C, in isolation media consisting of DMEM HAMS F12, 2% Penicillin-Streptomycin, 1 mg/mL clostridial collagenase and 50  $\mu\text{g}/\text{mL}$  sterilised ascorbate. The solution containing the tissue was under constant agitation using a magnetic

stirrer for improved digestion. On the following day, the digested cartilage solution was filtered and washed with media through 100 µm cell strainers to eliminate the debris. The remaining supernatant was centrifuged at 600 g for 10 minutes. Cells were then counted with trypan blue for viability assessment and seeded at a density of  $2 \times 10^4$  cells/cm<sup>2</sup> with basal expansion media consisting of DMEM 4,5 g/L of glucose (supplemented with 10% FBS, 1% L-Glutamine and 1% Penicillin-Streptomycin). Chondrocytes were then incubated and expanded up to a maximum of passage 3 for de-differentiation purposes. Some of the chondrocytes were cryopreserved at passage 0 for future experiments.

### 2.3.3 Lentiviral transfection and culture of adipose-derived equine

#### mesenchymal stem cells

Equine adipose-derived transfected MSCs (eMSCs) were provided in separated occasions by Dr. Glyn D. Palmer (University of Florida). The collagen II-GFP reporter cells were designed by cloning the cDNA of dTomato into multiple cloning sites of the lentiviral expression system, generating a pc-DH-CMV-tom / EF-1-GFP plasmid. For generating a dual expression cassette. The EF-1-GFP cassette was replaced by a Col2-GFP expression cassette, generating a dual lentiviral expression plasmid. The luciferase expressing-cell line was generated following the same procedure for dual expression. The lentiviral expression system was used for the generation of independent expression cassettes under the divided regulation of chondrogenic (Col2) and constitutive (CMV) promoters. The *Metridia* luciferase cDNA was copied into the plasmid generating the pd-DH-CMV-mLuc / EF1-GFP construct (227).

Cells cultured for expansion purposes with basal media (DMEM 4,5 g/L of glucose supplemented with 10% FBS, 1% L-Glutamine and 1% Penicillin-Streptomycin). Cells were normally seeded at a density of  $2 \times 10^4$  cells/cm<sup>2</sup> and expanded until reaching 80 % confluence. Equine MSCs cell line nature allowed for multiple division and higher passage number.

### 2.3.4 Isolation and culture of ovine MSCs

Ovine MSCs (oMSCs) were isolated and provided by Dr. Hareklea Markides. Cells were isolated from female English Mule sheep (2 – 4 years). The isolation was conducted in accordance to the UK Home Office Regulations and protocols approved by the University of Nottingham Animal Welfare and Ethical Review Body. Sheep were delivered fentanyl patches (Durogesic® Janssen-Cilag) 12-24 hours before the surgery for analgesic purposes. The wool was sheared from the desired areas prior to disinfection of the surgical area with chlorhexidine and isopropyl alcohol. Animals were then injected intra-muscularly with 2% xylazine (0.1 mg /kg body weight) followed by intravenous administration of Ketamine (2mg/kg body weight) and Midazolam (0.25-0.3 mg/kg body weight) and oxygen was supplied during the surgery. The bone marrow was aspirated from the sternum bone and transferred into 50 mL centrifuge tubes containing media. Cells were then isolated from the bone marrow aspirate by initial filtration with a cell strainer followed by centrifugation in serum free media of the filtrated solution at 220 g for 30 minutes. The supernatant was then discarded followed by addition of 3 mL of red blood cells lysing buffer. The lysis of the red cells was aid by addition of ice-cold DPBS followed by centrifugation at 220 g for 30 minutes or until visually observation of the white cells fraction pellet. Next the supernatant was removed followed by addition of 3 mL of sterile blocking buffer for pellet resuspension. Cells were seeded in T25 cell culture flasks containing expansion media with 20% FBS. Following expansion some cells were frozen for future use. The cells used for this experiment were thawed and cultured on basal media (DMEM 4,5 g/L of glucose supplemented with 10% FBS, 1% L-Glutamine and 1% Penicillin-Streptomycin). Cells were normally seeded at a density of  $2 \times 10^4$  cells/cm<sup>2</sup> and expanded until reaching 80 % confluence.

### 2.3.5 Culture of human umbilical cord-derived mesenchymal stem cells

Human umbilical cord-derived mesenchymal stem cells from three different donors were kindly supplied by Dr. Claire Mennan (RJA Orthopaedic Hospital) obtained under the REC ID number 10/H1013/62. Following isolation of the cells from the cord, they were cultured in TCP and at passage 1 they were expanded with the Quantum® bioreactor for one passage before testing the CD profile of the cells (228), and being frozen. Prior to collection cells were resuscitated, and expanded in TCP at passage 3 at a density of  $4.8 \times 10^3$  cells/cm<sup>2</sup>. Cells were collected and transported in tissue culture flasks maintaining a warm temperature during the transportation time. Upon arrival cells were examined under the microscope to evaluate viability and stored in the incubator at 37°C (Figure 2-1). On the following day, a complete media change was performed using DMEM/F12 (1:1) supplemented with 10% FBS and 1% Penicillin-Streptomycin. Cells were then expanded until passage 4-5 yielding approximately a total of 30 million of cells for the specific experimental purposes. Some early passages of the cells were cryopreserved for further experiments. Three experiment replicates were performed using single donors, and a fourth experiment was done combining the cells from all 3 donors.

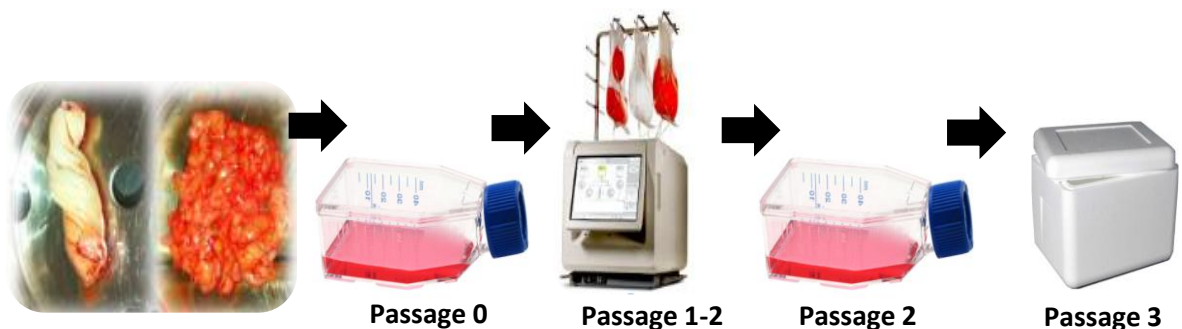


**Figure 2-1. Schematic diagram of the expansion process of the umbilical cord-derived stem cells.** Cells were dissected and digested from fresh umbilical cord tissue and seeded for expansion. Following the first passage, 5 million cells were injected in the cell Quantum® bioreactor. Approximately 200 million cells were harvested and seeded as passage 2 for further expansion. A further passage was made before transportation where 5 million cells were distributed across 6 T175 culture flasks.

### 2.3.6 Monolayers and micromasses formation and culture

For the formation of monolayers, cells were trypsinised following the usual procedure, re-suspended in the desired media, and counted. After counting, cells were seeded at a density of  $5 \times 10^3$  per well in variable sizes of well-plates according to the specific experiment requirements. Equine MSCs were used for micromass setting. After cell counting,  $5 \times 10^4$  cells were diluted in 50  $\mu$ L of the desired media and carefully seeded as a droplet in the middle of the well and kept overnight in the incubator. On the following day, the wells were topped-up with the relevant media and stored in the incubator. Samples identified as day 0 were left in the incubator overnight for optimal attachment of the cells prior to digestion or fixation of the samples for further analysis. Media changes were performed twice a week with special attention to the micromasses that had a tendency to de-attach due to overgrowth from day 10 of culture. The study of the chondrogenic differentiation of the equine MSC micromasses was performed by fluorescent imaging of the Col2-GFP reporter promoter activation. d-Tomato constitutive reporter was used as an indicative of the transfection rate. Cells were monitored firstly using the Nikon Eclipse Ti-S inverted microscope and then the automated Cytation™ 5 microscope.

### 2.3.7 Pellet formation and culture

Following detachment of the cells from tissue culture plastic, and resuspension in media, cells were counted in order to form a homogeneous set of pellets containing each the same cell number. Cells were then diluted in a proportion of  $2 \times 10^5$  cells/mL for human MSCs and human UC-MSCs and  $4 \times 10^5$  cells per mL for ovine MSCs, ovine chondrocytes and equine MSCs. While continuously mixing, 1 mL of the suspension containing the cells was added per each 1.5 mL microcentrifuge tube and quickly centrifuged at 500 g for 5 minutes. Following formation of the pellet, the microcentrifuge tubes were carefully transferred into the incubator at 37 °C. Samples corresponding to day 0 time points were left 24 hours in the incubator to allow the formation of the cell pellet. On the next day, the specific method for preservation was used, or the digestion solution was supplied to the samples. Three media changes

were performed weekly, being two of them complete and half a media change for the remaining one, with the purpose of allowing endogenous produced molecules to act on the cells.

## 2.4 Chondrogenic differentiation induction media

The chondrogenic potential of the protocols selected for this study were previously assessed for equine MSCs, ovine MSCs and human MSCs during my master project. The selection was made based on the culture of the mentioned cell types with 3 different differentiation protocols, and the evaluation of the viability of the cells and chondrogenic differentiation under the different protocols. This was assessed by presto blue, histological and gene expression analysis. Except for hUC-MSCs, DMEM 4.5 g/L of glucose was used. For hUC-MSCs DMEM F12 was used for both expansion and differentiation as stated by the followed protocol. The differentiation protocol was a modification from Mennan et al. following protocol development (228) (Table 2-3). For specific experimental groups, TGF- $\beta$  was eliminated from the differentiation mixture for some of the samples. This will be indicated for each specific case. Two complete and one half a media change were performed on a weekly basis

**Table 2-3. Supplements for chondrogenic induction media for each cell type.**

| Supplements             | oMSC and eMSC (229) | hMSC (230)    | hUC-MSC (228)     |
|-------------------------|---------------------|---------------|-------------------|
| L-Glutamine             | 1% v/v              | 1% v/v        | 1% v/v            |
| Penicillin/Streptomycin | 1% v/v              | 1% v/v        | 1% v/v            |
| FBS                     | 10% v/v             | 1% v/v        | 1% v/v or 10% v/v |
| ITS                     | 1% v/v              | 1% v/v        | 1% v/v            |
| Ascorbic acid           | 50 $\mu$ g/mL       | 50 $\mu$ M    | 0.1 nM            |
| Dexamethasone           | 0.1 $\mu$ M         | 0.1 $\mu$ M   | 10 nM             |
| TGF- $\beta$ 3          | 10 ng/mL            | 10 ng/mL      | 10 ng/mL          |
| NEEA                    | 1% v/v              | -             | -                 |
| Sodium Pyruvate         | -                   | 1% v/v        | 1% v/v            |
| L-Proline               | -                   | 40 $\mu$ g/mL | -                 |
| Linolenic Acid          | -                   | -             | 20 $\mu$ M        |

### 2.4.1 Biochemical activation of TRPV4

With the aim of setting a positive control, the well-characterised TRPV4 agonist (231), GSK1016790A, was supplemented to the media. The agonist was used when indicated, as a media supplement in a concentration of 10 nM (165). The chemical agonist was added to the media for every media change performed.

## 2.5 Particle labelling

### 2.5.1 Magnetic nanoparticle activation

Magnetic nanoparticles of 250 nm composed of an iron oxide core, coated with dextran, and modified with COOH were firstly activated. The activation of the MNPs allows for the COOH groups to react with primary amines via de formation of the amide bond. This is performed in order to covalently attach peptides such as the antibodies. For this purpose, 20  $\mu$ L of a solution containing 12 mg of EDAC, and 24 mg of NHS dissolved in sterile 0.5 MES buffer were added to a 100  $\mu$ L aliquot of the commercially available particles. The acidic pH of the buffer allows for the carbodiimide reaction to take place. The solution with the MNPs was then left to incubate for 1 hour at room temperature in a rotator device to allow mixing, before washing the excess of chemicals twice with 100  $\mu$ L of 0.1 MES buffer in a permanent magnet.

### 2.5.2 Magnetic nanoparticle coating with TRPV4, TREK-1 and RGD

Following MNP carbodiimide reaction for activation, MNPs were re-suspended in 100  $\mu$ L of 0.1 MES buffer and 20  $\mu$ g of the secondary antibody was added for the TRPV4 and TREK-1 labelling protocols. The solution of the MNPs and the antibody was incubated for 3 hours at room temperature or overnight at 4 °C with continuous mixing. Next, two washes with 0.1 MES buffer were done at a permanent magnet and particles were re-suspended in 100  $\mu$ L of MES buffer. The specific primary antibody was then added (TRPV4 or TREK-1) at a concentration of 10  $\mu$ g per mg of MNPs and incubated

for 3 hours at room temperature or overnight at 4 °C with continuous mixing. Following this step, 10 µL of 25 mM of glycine was added prior to 30-minute incubation at room temperature with continuous mixing. Lastly MNPs were washed with a 0.1% BSA solution at a permanent magnet and diluted to a final volume of 1 ml in the same solution. For RGD labelling, 25 µg of the RGD peptide were added straight after the carbodiimide reaction and the labelling protocol continued as for the antibody labelling following the addition of the primary antibody. The activated MNPs were stored at 4 °C up to a maximum of 3 months' post-activation.

### 2.5.3 Magnetic nanoparticle labelling of monolayers

TC-28 cells were labelled in monolayer for channel activation prior to RNA extraction. Human UC-MSCs were labelled in monolayer for transmission electron microscopy visualisation of the localisation of the MNPs following 1 hour and 48-hour post labelling. In addition, the different cell types were labelled in monolayer for histological characterisation. For labelling in monolayer, cells were counted and seeded at the specific density in well-plates with expansion media and stored in the incubator at 37 °C overnight. On the next day, media was discarded prior to washing with DPBS to eliminate FBS residues and replaced with serum free (SF) expansion media. For internalisation of MNPs labelled with internal-binding antibodies (TRPV4 and TREK-1), 1 µL of 1 mg/mL of the liposomal transfection reagent DOTAP was added per 25 µL of the MNPs solution for 5 minutes and incubated at room temperature. Next 25 µL of MNPs per every  $1 \times 10^5$  cells was added into the wells and mixed carefully. Plates were then left in the incubator at 37 °C during 3 hours for optimal uptake of the MNPs. After incubation media was removed and 3 washes with DPBS were done in order to eliminate the excess of MNPs not attached to the surface of the cells. Wells were topped-up with the desired media and stored in the incubator.

#### 2.5.4 Magnetic nanoparticle labelling of micromasses and pellets

Equine MSCs were cultured and labelled as micromasses with the aim of visually monitoring the differentiation process of the cells and microscopically visualising the fluorescent marker GFP associated with collagen 2 expression. Ovine MSCs, equine MSC, human MSC and human UC-MSC were labelled and cultured as pellets to assess the chondrogenic potential of different experimental conditions in a 3D environment. After re-suspending cells in expansion SF media and counting, cells were transferred into sterile centrifuge tubes at the desired amounts. If labelling with MNPs targeting an internal antibody, 1  $\mu\text{L}$  of 1 mg/mL of reagent DOTAP was added per 25  $\mu\text{L}$  of the MNPs solution for 5 minutes and incubated at room temperature. Then 25  $\mu\text{L}$  of MNPs per  $1 \times 10^6$  cells was added to the cell suspension, thoroughly mixed, and left to incubate for 3 hours at 37 °C with loose caps to allow for oxygen exchange. Following incubation, cells were centrifuged at 1200 r.p.m for 5 minutes and the media was discarded. Cells were then re-suspended into the desired media and plated if culturing micromasses or added into microcentrifuge tubes prior to a second centrifugation at 500 g for 5 minutes if making pellets. Cells were then stored in the incubator. Micromasses and pellets set as a control without MNPs went under the same conditions until pellet or micromass formation for homogeneity on the sample formation.

#### 2.6 Magnetic activation

A magnetic force bioreactor (MICA Biosystems Ltd) was used for activation of the magnetic nanoparticles (Figure 2-2) (220,223). The device working principle is based on the delivery of an alternating magnetic field. This is achieved by the movable magnetic arrays. When the arrays get the closest to the samples, the magnetic field exerted causes the alignment of the MNPs towards the magnetic field. Once the magnetic field is removed by the downwards movement of the arrays, the MNPs lose the magnetisation and return to their natural state given the superparamagnetic nature of the MNPs. This translates into the MNPs exerting a pulling effect on the receptor that they

are attached to. The mechanical effect causes the channel to open by deformation or by activation of the mechanosensitive domain.

Cells in well plates were placed inside the bioreactor, located inside an incubator at 37°C. The same was done for cells cultured as pellets, a 24-well plate with carved holes in the wells was used as an adaptor for the microcentrifuge tubes. The bioreactor can be defined in set programmes which alters time or number of cycles, frequency and height of the magnets. For all experiments, the frequency was set at 1 Hz and 3600 cycles, corresponding to 1 hour of stimulation (217). The computer sends the signal to the bioreactor that has 2 magnetic arrays (different sizes corresponding each size to well plates), and the magnetic arrays move towards the bottom of the well plate and away in a cyclical movement. As the magnet moves towards the particle there is a translational horizontal force applied to the particles corresponding to defined levels of stress delivered to the cell receptor (216). The setting of the displacement was variable across different units of the MICA bioreactor but was kept in accordance with the possible minimum distance to the samples, being 3 mm from the cells (1.5 mm distance of the array from the plate and 1.5 mm thickness of the well plate). A cooling system connected to the water tap allowed for the heating effect generated by the bioreactor to dissipate, ensuring the maintenance of the culture temperature during the stimulation. When the bioreactor cycle was completed, samples were transferred back into the culture incubator. Unless stated otherwise, samples were stimulated on a 5/7 regime day for 1 hour for 7, 10, 14 and 21 days.

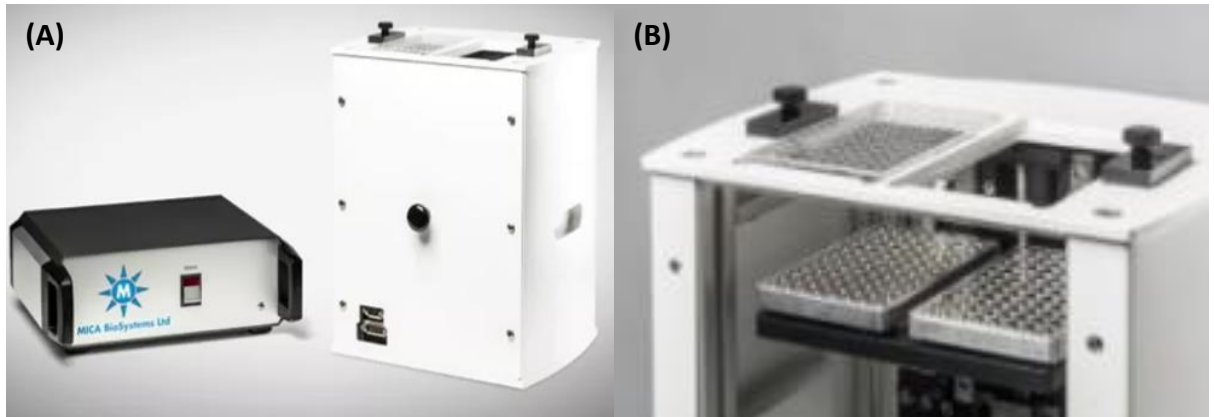


**Figure 2-2. MICA Magnetic Bioreactor and control unit.** A) The bioreactor is placed inside an incubator during stimulation periods and is connected to the control unit. B) The arrays are designed for the different well plates with pre-set measurements for distance from the bottom of the plate.

## 2.7 Histological staining of pellets and tissue section

On the termination of the experiment pellets in microcentrifuge tubes were washed with DPBS to eliminate media residues and fixed with 10% formalin. Samples were fixed for 1 hour after which they were washed and stored in DPBS at 4 °C. Human cartilage sections were kindly provided by Dr. Claire Mennan for gold-standard histology controls.

### 2.7.1 Pellet size

Prior to dehydration of the pellets, the whole pellet area size was measured using the EVOS M5000 fluorescent microscope. The pellets were transferred from the microcentrifuge tubes with tweezers into a petri dish and the area was manually drawn around each of the pellets using the microscope tools. The same magnification and settings were kept for all the measured samples. Pellets were then transferred back to the microcentrifuge tubes and continued with the dehydration protocol.

### 2.7.2 Sample dehydration and paraffin embedding

To eliminate the water of the cell pellet to allow paraffin to enter the tissue, samples were firstly dehydrated with increasing alcoholic concentrations, for 1 hour each, with 70% IMS, 90% isopropanol, and 2 changes of 100% isopropanol. Following dehydration, samples were transferred to melted paraffin wax at 60 °C in the HistoStar paraffin embedder (Thermo Fisher). Samples were left overnight for optimal embedding, after which they were transferred to fresh paraffin in an embedding mould, added a labelled cassette and left to solidify in the cold plate.

### 2.7.3 APES Coating of slides

Superfrost glass microscope slides were coated with APES for improved adherence of the sectioned samples. To coat the slides, they were immersed in acetone for 2 minutes to remove any trace residues and then air dried. Slides were next transferred into freshly prepared 2% (v/v) APES in acetone for another 2 minutes and lastly washed for 2 minutes in distilled water (dH<sub>2</sub>O). Slides were then transferred to an oven and dried at 60 °C before using or storing them.

### 2.7.4 Sample sectioning and deparaffinisation

Prior to sectioning, sample blocks were trimmed to remove excess of paraffin. Samples were then positioned in the HistoCore Biocut rotary microtome (Leica) and sectioned at 7 µm. 2-3 discontinuous sections were taken from each pellet for each slide, approximately 70 µm apart, to allow visualisation of different depths of the pellet. Sections were then transferred into a water bath with dH<sub>2</sub>O at 40 °C and collected onto APES-coated slides. Slides were then left in the oven overnight at 60 °C to improve adherence of the sections and stored in slide boxes at room temperature until needed. Before staining, samples were deparaffinised by soaking into 2 changes of histo-clear for 5 minutes each, followed by 2 minutes' immersion in decreasing alcoholic concentrations (100% IMS, 90% IMS, 80% IMS, 75% IMS, 50% IMS) and re-hydrated in dH<sub>2</sub>O for another 2 minutes before staining immediately.

### 2.7.5 Haematoxylin and eosin staining

This stain was used for observation of the general structure of the constructs. The affinity of the basic dye, haematoxylin, for acid components such as nucleic acids allows for visualisation of the nuclei stained in a purple-blue coloration. In contrast, the acidic nature of eosin stains the basic components such as the cytoplasm or collagen fibres in a light pink colour. Deparaffinised and rehydrated tissue sections were soaked in Harri's haematoxylin solution for 5 minutes, then rinsed in running tap water, and dipped twice in 0.3% acid alcohol (70% ethanol with 0.3% concentrated HCl). Slides were then rinsed with running tap water and rinsed in Scott's tap water substitute (0.2% (w/v) sodium bicarbonate, 2% magnesium sulphate (w/v) in dH<sub>2</sub>O), rinsed with running tap water and soaked in Eosin Y aqueous solution for 90 seconds. Sections were then de-hydrated by soaking 2 minutes in 95% IMS, and 2 changes of 100% IMS and cleared in 2 changes of xylene for 5 minutes each. Slides were then mounted in DPX mounting medium and imaged in the EVOS Core XL microscope.

### 2.7.6 Toluidine blue staining

Toluidine blue was used for visualisation of the acidic sulphated mucopolysaccharides present in hyaline cartilage. Both toluidine blue dye and cartilage exhibit metachromasia, a property that shows in the sections different colour than the one from the dye (232). Deparaffinised and rehydrated tissue sections were immersed in 0.04% toluidine blue in a sodium chloride buffer solution for 3 minutes followed by 3 washes in dH<sub>2</sub>O. Sections were then dehydrated by soaking 10 times in 95% ethanol and 2 changes of 100% ethanol and cleared in 2 changes of xylene for 3 minutes each. Slides were then mounted in DPX mounting medium and imaged in the EVOS Core XL microscope.

### 2.7.7 Alcian blue staining

Alcian blue was used with the purpose of highlighting the sulphated proteoglycans present in the native tissue, as an indicator for chondrogenesis. This stain allows for visualisation of structures such as dermatan sulphate, heparin sulphate, chondroitin sulphate and hyaluronic acid (233).

Deparaffinised and rehydrated tissue sections were soaked for 30 minutes in 1% alcian blue solution prepared with 3% acetic acid solution in dH<sub>2</sub>O at pH 1. The acidic pH allows staining weakly and strongly sulphated acid mucins. Sections were then washed in running tap water for 2 minutes, rinsed in dH<sub>2</sub>O and dehydrated through immersion in 95% IMS and 2 changes of 100% IMS for 3 minutes each, followed by 2 changes of xylene of 3 minutes each. Slides were mounted in DPX mounting medium and imaged in the EVOS Core XL microscope.

### 2.7.8 Picrosirius red staining

Collagen deposition was visualised with picrosirius red stain. The stain is composed by Sirius red, and azo dye that stains all type of collagen fibres in a red-orange colour, and picric acid that stains the cytoplasm in yellow. Moreover, the birefringence nature of the collagen fibres stained in red allowed for observation of the fibres thickness and alignment (234). Deparaffinised and rehydrated tissue sections were immersed in 0.1% picrosirius red in saturated aqueous picric acid for 1 hour at room temperature. Sections were then washed in 2 changes of acidified water, dehydrated in 3 changes of 100% ethanol, and cleared in 2 changes of xylene for 2 minutes each. Slides were mounted with DPX mounting medium and imaged in the EVOS Core XL microscope and in the cross-polarised light microscope.

### 2.7.9 Prussian blue staining

Prussian blue stain allowed for visualisation of the MNPs present in the samples. This was possible due to the reaction of the oxidation of the acidic solution of the ferrocyanide salts. Any ferric ion present in the sample combines with the salts forming the blue pigment allowing to visualise the MNPs (235). Deparaffinised and rehydrated tissue sections were immersed in a mixture of equal parts of 20% aqueous solution of HCl and 10% aqueous solution of potassium ferrocyanide for 20 minutes. The staining solution was prepared immediately before use. This solution involves the reaction of the ferrocyanide with the iron of the particles allowing for their visualisation. Sections were then carefully

washed with DPBS, mounted with DPX mounting medium and imaged with the EVOS Core XL microscope.

### 2.7.10 Safranin O staining

Safranin O is a basic dye classically used for articular cartilage histology. The dye stains for the acidic proteoglycans in a red to orange colour, being the intensity of the stain proportional to the presence of the marker (236). Deparaffinised and rehydrated sections were immersed in 0.1% (w/v) safranin O solution for 5 minutes and dehydrated by soaking into 95% ethanol, 100% ethanol and cleared in 2 changes of xylene for 2 minutes each. Sections were then mounted in DPX mounting medium and imaged in the EVOS Core XL microscope. A modification of the original protocol was used to enable the visualisation of the cell's nucleus. Following rehydration of the samples, the slides were soaked in Harri's haematoxylin solution for 5 minutes, then rinsed in running tap water, and dipped twice in 0.3% acid, rinsed with running tap water, and rinsed in Scott's tap water substitute, rinsed with running tap water and stained with safranin O solution for 5 minutes and followed with the protocol as usual. For human cartilage tissue samples, a third variation of the original protocol was used introducing the staining with 0.05% Fast Green for 5 minutes as an initial step and continuing with the safranin O staining and the following steps as firstly described.

## 2.8 Histological assessment of monolayers and micromasses

### 2.8.1 Sample preservation

On the termination of the experiment, culture media was removed from the wells and samples were carefully washed with DPBS 2 times, fixed with 95% methanol for 10-20 minutes and stored in DPBS at 4°C until used.

## 2.8.2 Sample histological staining

Monolayer and micromasses were stained with toluidine blue, alcian blue, picosirius red, safranin O and prussian blue stains following the steps on section 2.7.6, 2.7.7, 2.7.8, 2.7.9. and 2.7.10. Samples did not undergo the dehydration or dehydration processes, and stains were directly applied to the well plates, followed by DPBS washes until removal of residual stain for all cases. Following staining, samples were preserved in DPBS and imaged with the EVOS Core XL microscope.

## 2.9 Immunohistochemistry

### 2.9.1 Antigen retrieval, permeabilisation and blocking

Deparaffinised and rehydrated slides were soaked in a solution of 0.1% trypsin in 1% calcium chloride and incubated at 37 °C for 10 minutes, to enable the reveal of the masked epitope in order to allow for antibody binding. Samples were then rinsed with DPBS and if the epitopes were found in the intracellular compartment, permeabilisation with 0.1% Triton X—100 was performed during 10 minutes at room temperature, followed by a DPBS rinse of the samples. Then samples were blocked with 3% BSA for 1 hour at room temperature and washed with DPBS. For well plates the same procedure was followed excepting for the dehydration process that was not required.

### 2.9.2 Primary antibody staining

The primary antibody (Collagen II, Collagen X, Sox9, PCNA, Ki67, Aggrecan, TRPV4 and Dextran) was added in a concentration specified by the manufacturer by dilution in 1% BSA and incubated overnight at 4 °C in a humidification chamber to avoid the slides from drying. On the next day 3 DPBS washes of 5 minutes each were carefully performed to remove the excess of antibody. A negative control without primary antibody was performed for every batch of stained slides or well plates.

### 2.9.3 Secondary antibody and DAPI staining

After performing the DPBS washes, the appropriate secondary antibody diluted in DPBS at the working concentration indicated by the manufacturer was carefully added to the samples in a dark environment. Slides were then incubated for 1 hour at room temperature in the humidification chamber and protected from light. Samples were then washed 3 times with DPBS for 5 minutes carefully protecting the samples for the exposure of light. DAPI was then added to the samples at a concentration of 1 µg/mL and incubated in the dark for 15 minutes at room temperature, followed by 5 washes of DPBS of 3 minutes each. Slides were then mounted with fluoromount aqueous mounting solution and left to dry in the dark. Well plates were preserved with DPBS at 4 °C in the dark. Samples were imaged using the automated microscope Cytation™ 5 (Biotek). Due to the need of imaging different batches of samples for the same parameter, all microscope settings were kept the same to ensure the comparability of the images.

### 2.9.4 Pellet immunohistochemistry

Due to the difficulties encountered for imaging fluorescently stained pellet sections with the available microscope, ovine MSCs and chondrocytes pellets were stained using the streptavidin-biotin (ABC) Kit. Rehydrated slides were covered in 0.1% trypsin and 1% calcium chloride solution prior to incubation at 37 °C for 10 minutes for antigen retrieval and then washed with DPBS. Endogenous peroxidase was quenched by covering the slides with a solution of 3% hydrogen peroxide in 50% methanol and incubated for 5 minutes at room temperature, followed by a DPBS wash, and blocking with 3% BSA for 1 hour at room temperature and a DPBS wash. The specific primary antibody (collagen II and aggrecan) was added onto the slides diluted in a 1% BSA solution at the concentration stated by the manufacturer and incubated in a wet chamber at 4 °C overnight. On the following day, slides were washed 3 times with DPBS for 5 minutes and the biotinylated anti-rabbit ABC system staining kit, diluted following manufacturer's indications, was added to the slides and incubated for 10 minutes at

room temperature, followed by 3 DPBS washes of 2 minutes each. Next the streptavidin peroxide plus from the ABC kit was added and incubated another 10 minutes at room temperature and 3 washes of 0.01% Tween 20 were performed. The 3,3'-diaminobenzidine (DAB) was prepared combining the chromogen and the substrate in a 1:50 proportion and applied to the tissue sections and left to incubate at room temperature until signal appeared first (2 minutes), then immediately washed with dH<sub>2</sub>O, mounted with aqueous hydromount mounting media and imaged using the EVOS Core XL microscope.

### 2.9.5 Fluorescence quantification

The quantification of the fluorescence intensity was performed by image J. Firstly a freehand selection of the fluorescent area was drawn. Using the software tools, the analysis of the area, integrated density and mean grey value were obtained. A small area of every images was selected (n=3) as the background measurement and the mean fluorescent of the background was calculated. Next the total fluorescence was calculated, normalising to the area selected to remove differences from samples size. The corrected total cell fluorescence (CTCF) was then calculated following the formula:

$$\text{CTCF} = \text{Integrated Density} - (\text{Area of Selected Cell} \times \text{Mean Fluorescence of Background readings})$$

## 2.10 Cell viability and proliferation

Several methods were used in order to assess the viability and the proliferation of the cells according to the nature of the experiment.

### 2.10.1 Presto™ blue

The viability of micromasses and pellets was assessed using the Presto™ blue reagent that measures the metabolic activity of the cells through monitoring of the reducing power of the cells. This method uses a resazuring-based reagent, a non-toxic cell-permeable reagent that enters the living cells and on reducing environment the reagent reduces to resorufin, increasing the blue colouring of the media

that can be measured with a spectrophotometer. For micromasses and monolayers, media was removed from the wells, followed by a DPBS wash and the Presto blue 10X reagents was diluted to 1X in culture medium and added to the wells with a variable volume according to the well size. Plates were then protected from light and left in the incubator at 37 °C for 30 minutes. After incubation, triplicates of 100 µL of volume was taken from each well and pipetted into a 96-well plate before measuring the fluorescence in the plate reader at 560 nm for the excitation and 615 nm emission parameters. For cell pellet samples, the media was removed from the microcentrifuge tubes and a DPBS wash was performed. 10% Presto blue diluted in media was added into the microcentrifuge tubes that were immediately protected from light. After optimisation, it was decided to add 160 µL of the 1X presto blue solution to each microcentrifuge tube to avoid longer incubation times. Samples were then transferred to an incubator at 37 °C and incubated for 5 hours. Next, triplicates of 50 µL were taken from each microcentrifuge tube and transferred into a 96-well plate for fluorescent measurement in the Spark<sup>®</sup> (Tecan) plate reader. Same excitation and emission parameters were used as the previous case. Controls containing media without cells were used for basal level references.

### 2.10.2 Live / Dead assay

Human UC-MSC pellets were fixed and processed as indicated in section 2.7. Rehydrated samples were then treated for antigen retrieval, permeabilisation and blocking (section 2.9.1). Live/Dead<sup>™</sup> staining kit was then used. The blue dye from the kit was reconstituted 1:50 in DMSO and slides were covered in a 1:100 dilution of the blue dye. Samples were then incubated in the humidified chamber at 4 °C overnight, and then washed 3 times for 5 minutes with DPBS. Samples were then covered with Ki67 primary antibody, in a dilution according to the manufacturer's instructions, in order to have another viability parameter. Samples were incubated for 1 hour at room temperature and washed 3 times with DPBS for 5 minutes. The specific secondary antibody was then added to the sections and incubated for 1 hour at room temperature protected from light before washing 3 times with DPBS for 5 minutes.

FM1-43 FX membrane dye was then added onto the slides, following manufacturer's recommendation, and incubated for 20 minutes at room temperature protected from light, then washed 3 times with DPBS for 5 minutes and mounted in hydromount aqueous mounting media. Slides were left to dry and imaged with the Cytation™ 5 automated microscope system keeping all settings equal for picture comparison.

## 2.11 CM-Dil labelling of pellets

Human UC-MSC pellets samples made of the combination from 3 different donors were labelled with a cell tracker prior to pellet formation to assess the effect of the dye on the pellet proliferation and differentiation processes, and the duration of the dye on the samples before a potential *in vivo* study. For this purpose, cells were labelled with MNPs as per indicated in section 2.5.4 and following the 3-hour incubation with MNPs, samples were centrifuged at 1200 r.p.m for 5 minutes, media was discarded, and the cell pellet was diluted in 1 mL of DPBS. Next CM-Dil working solution (2.5 µL of stock per 1 ml of DPBS) was added to the cell suspension and incubated for 5 minutes at 37 °C, followed by 15 minutes of incubation in the dark at 4 °C. Cells were then centrifuged at 1200 r.p.m for 5 minutes and re-suspended in the desired media before continuing with the normal pellet formation in 1.5 mL microcentrifuge tubes.

## 2.12 Proteinase K digestion of pellets

Chondrogenic differentiation and magnetic activation was induced as indicated in sections 2.4 and 2.6. On the termination of the experiment, media was discarded, and cell pellets were washed with DPBS and samples stored in empty microcentrifuge tubes at -80 °C until used. For pellets digestion, samples were covered with 250 µL of proteinase K per pellet (1 mg/mL dissolved in 100 mM ammonium acetate, pH 7.0), and incubated at 60 °C for 2 hours with vortex agitation every 30 minutes until cell pellets looked visually dissociated. Proteinase K was inactivated by heating the samples at 100 °C for 5 minutes in a heat block. Samples were then stored at -20 °C until used.

## 2.13 DMMB sulphated GAGs assay

Dimethyl methylene blue (DMMB) is a reagent commonly used for the detection of sulphated GAGs. The colour change that the reagent undergoes when read in a spectrophotometer gives a proportional measure of the sGAGs present in the sample. From the samples digested as in section 2.12, 50  $\mu\text{L}$  was used for this assay

### 2.13.1 Preparation of DMMB solution

DMMB working solution was prepared by dissolving 0.008 g of DMMB into 2 mL of 100% ethanol, before adding 1.52 g of glycine and 1.185 g of sodium chloride dissolved in 500 mL of  $\text{dH}_2\text{O}$ . The mixture was protected from light and mixed for 2 hours with a magnetic stirrer. pH was adjusted to 3.0 with hydrochloric acid and stored in the dark at room temperature until used.

### 2.13.2 Preparation of samples

Firstly, a standard assay was performed using chondroitin sulphate. A standard curve with concentrations of 50, 25, 12.5, 6.25, 3.125, 1.5625 and 0.78125  $\mu\text{g}/\text{mL}$  was prepared in 100 mM ammonium acetate. From each standard curve controls, 50  $\mu\text{L}$  were transferred into a 96-well plate in triplicates. From the digested cell pellet samples, 50  $\mu\text{L}$  were transferred in triplicates into the 96-well plate. A multichannel pipette was used to quickly add 200  $\mu\text{L}$  of DMMB working solution per well, trying to minimise the pipetting time across wells due to the fast reaction of the reagent. The plate was then transferred into the Spark<sup>®</sup> (Tecan) plate reader and absorption at 530 nm was determined.

## 2.14 PicoGreen<sup>™</sup> double stranded DNA assay

Following optimisation of the protocol for the specific purpose, 30  $\mu\text{L}$  of proteinase K digest (2.12) was used for this assay in a 1:10 dilution in 1x tris-EDTA (TE) buffer. The Quant-IT<sup>™</sup> double stranded DNA assay was performed as per the manufacturer's instructions. A standard curve of  $\lambda$  DNA was prepared at concentrations of 2, 1, 0.5, 0.25, 0.125, 0.0625, 0.03125 and 0.0156  $\mu\text{g}/\text{mL}$  in 100 mM ammonium

acetate. For the blank control of 0 µg/mL, 10 mM ammonium acetate in 1x TE buffer was used. Aliquots of 50 µL of the standard curve were added in triplicates to a 96-well plate and the same was done for the experimental samples. PicoGreen™ stock solution was diluted 1:200 in 1x TE buffer immediately prior to use. Next, 50 µL of working solution was added to each well and incubated for 2 minutes in the dark before the reading in the Spark® (Tecan) plate reader (excitation 480 nm, emission 520 nm). DNA concentrations were determined using a calibration curve of standards with linear regression.

## 2.15 RNA isolation from pellets

### 2.15.1 Cell lysis and homogenisation

For all procedures related with RNA isolation, surfaces were decontaminated with DNA AWAY™. On the termination of the experiment, media was discarded, and pellets were washed with PBS. Next 350 µL of RLT buffer was added per sample directly into the microcentrifuge tube and transferred immediately to store at -80 °C and left up to a maximum of 7 days. If predicted a hard digestion (for experiments with longer duration) 1% 2-mercaptoethanol was added into the RLT buffer and after addition of the digestion buffer to the samples, they were placed in the sonicator with iced water for 2 hours until disruption of the pellet. When this step was not sufficient to dissociate the pellet, manual disruption of the sample using a pestle was attempted.

### 2.15.2 Isolation of RNA using the RNeasy mini kit

The RNA extraction was carried out following the manufacturer's instructions of the RNeasy mini kit. Frozen samples were left to defrost on ice and all procedures performed during this protocol were done on ice. Samples were initially centrifuged at full speed for 3 minutes and the supernatant was carefully transferred into a new microcentrifuge to eliminate the cell membrane leftovers from the digestion. Next 350 µL of 70% ethanol were added to the lysate and mixed well by pipetting. The

resulting 700  $\mu\text{L}$  solution was then transferred into a RNeasy mini spin column and centrifuged at 8,000 g for 15 seconds. The flow-through was discarded and RNA was left bound to the column membrane. The membrane was then washed with 700  $\mu\text{L}$  of RW1 buffer, and twice with 500  $\mu\text{L}$  of RPE buffer with centrifugation of 15 seconds at 8,000 g between washes and a 2-minute centrifugation for the last wash. The flow-through was discarded after each centrifugation cycle. The collection tube was then discarded and replaced with a new one after which the tubes were centrifuged 1 minute at full speed to dry the membrane. The collection tube was discarded, and the mini column was finally transferred into a new 1.5 microcentrifuge tube. To elute the RNA from the membrane, 30  $\mu\text{L}$  of RNase free water was added directly into the membrane and allowed to soak for 1 minute. Next the columns were centrifuged for 1 minute at 8,000 g and the resulting elute was re-pipetted directly into the membrane and centrifuged a final time for 1 minute at 8,000 g. The extracted RNA was quantified with the NanoDrop and stored at  $-80\text{ }^{\circ}\text{C}$  or directly used for reverse transcription.

## 2.16 Reverse transcription

After extraction of the RNA from the pellets, the RNA was converted into cDNA using the High-Capacity Reverse Transcription Kit following the manufacturer's instructions. Firstly, a reverse transcription master mix was prepared by mixing 0.2  $\mu\text{L}$  RNase free water, 0.8  $\mu\text{L}$  25x dNTP Mix, 1  $\mu\text{L}$  MultiScribe™ Reverse Transcriptase, 2  $\mu\text{L}$  random primers and 2  $\mu\text{L}$  10x RT Buffer per sample. Following centrifugation of the master mix, 6  $\mu\text{L}$  were used per sample and transferred into a 0.5 mL thin-walled PCR tube. Another 14  $\mu\text{L}$  of the RNA sample were transferred to the tube. Samples were centrifuged and placed into the SimpliAmp Thermal Cycler (Thermo Fisher). The thermal cycler was set as follows:

- Step 1: 25  $^{\circ}\text{C}$  for 10 minutes
- Step 2: 37  $^{\circ}\text{C}$  for 120 minutes
- Step 3: 85  $^{\circ}\text{C}$  for 5 minutes
- Step 4: Hold at 4  $^{\circ}\text{C}$  until samples collected

Samples were then stored at -20 °C or kept in ice for gene analysis.

## 2.17 Quantitative real-time polymerase chain reaction

The amplification of the gene expression was performed using SYBR® Green fluorescent DNA-intercalating dye for real-time polymerase chain reaction (qRT-PCR). Primers used were obtained commercially pre-optimised (QuantiTect primer assays) for human cells and customised from Thermo Fisher and PrimerDesign for equine and ovine cells. The intercalating stain binds preferentially to double stranded-DNA and is detected by the fluorescent signal allowing to quantify the number of amplified copies of the gene product. The intensity of the dye is measured at the end of each PCR cycle on a total of 40 cycles-time. The thermal cycler device sets an arbitrary threshold that once surpassed by the sample fluorescent intensity, is logged into the programme as a  $C_T$  value. The number of the cycle where the  $C_T$  value of each sample is reached determines the level of expression of each gene. With the intention of setting a normalisation, genes constitutively expressed by the cells were used as controls, the ribosomal protein *S18* and gene glyceraldehyde 3-phosphate dehydrogenase (*GAPDH*). Relative expression was calculated by using  $2^{-\Delta CT}$  or  $2^{-\Delta\Delta CT}$  as appropriate.

### 2.17.1 Preparation of the samples

If previously stored, samples were defrosted on ice and diluted in RNase free water. Equine and ovine MSCs samples were diluted to 7.5 ng of cDNA per reaction (0.75 ng/ $\mu$ L) due to the limited amount of sample. For human MSCs and UC-MSCs 15 ng per reaction (1.5 ng/ $\mu$ L). A master mix was prepared with 0.5  $\mu$ L of RNase free water, 2  $\mu$ L of 10x primer mix (or 1  $\mu$ L of the forward primer and 1  $\mu$ L of the reverse primer) and 7.5  $\mu$ L of SYBR™ Green Master Mix per each sample. From the master mix, 10  $\mu$ L were transferred into each well of PCR tube strips, together with 5  $\mu$ L of the diluted cDNA per sample in triplicates. Master mix and RNase free water alone was added in triplicates for control readings. The tubes were sealed and centrifuged until bubbles completely disappeared to avoid alterations on the readings, and they were placed in the AriaMx Real-Time PCR System (Agilent Technologies).

## 2.17.2 Gene amplification

The thermal cycler programme was set as follows (Figure 2-3):

- One cycle of 95 °C for 10 minutes (DNA denature hot start and DNA polymerase activation)
- 40 cycles of:
  - 95 °C for 15 seconds (DNA melting)
  - 60 °C for 1 minute (DNA extension) (Temperature dependent upon primer pair)
    - Fluorescence determination
- One cycle of pre-programmed melt curve
  - 95 °C for 1 minute
  - 55 °C for 30 seconds
  - 95 °C for 30 seconds
    - Fluorescent determined while temperature increases gradually from 55 °C to 95 °C

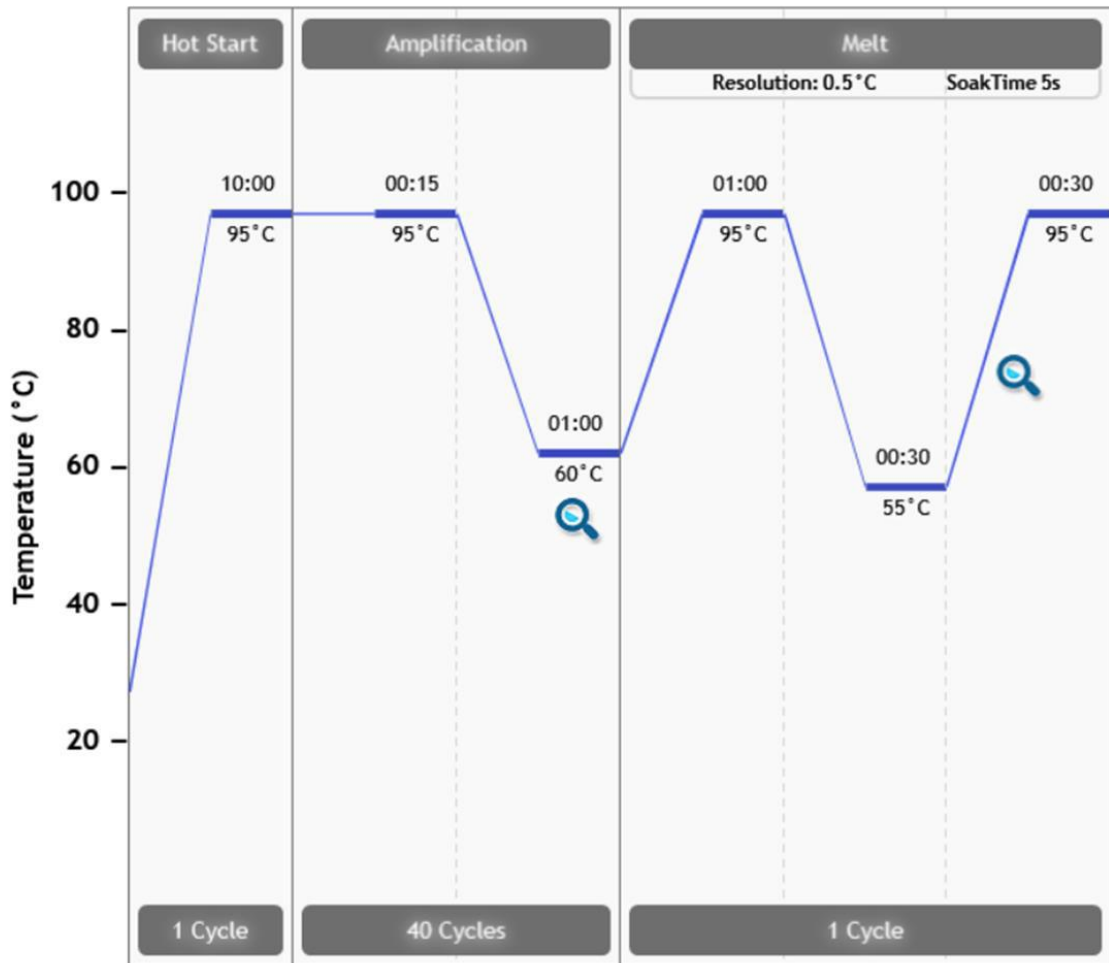


**Figure 2-3. qRT-PCR Thermal cycler programme.** Initial single cycle for DNA denature, followed by 40 cycles of product amplification ending with 1 cycle of melt curve formation.

### 2.17.3 qRT-PCR data analysis

Relative gene expressions in the form  $2^{-\Delta CT}$  were calculated using Microsoft Excel. The housekeeping gene values were used to normalise the expression of the examined genes.

### 2.17.4 qRT-PCR Primer design

Equine and ovine primers were custom-made by Thermo Fisher (Table 2-4) and Qiagen (Table 2-5) respectively. Primers were not previously tested by the company for optimal DNA extension temperature hence before use, qRT-PCR and agarose gel electrophoresis was done using the primers

until the optimisation of the products. Primer design was ensured to correspond to exon regions avoiding sequence introns.

**Table 2-4. qRT-PCR equine primer sequences.**

| Gene name<br>(Protein product)                                 | Forward primer<br>(5' to 3') | Reverse primer<br>(3' to 5') | Annealing temperature<br>(°C) |
|--|------------------------------|------------------------------|-------------------------------|
| <b>S18</b><br>(Ribosomal protein S18)                          | CGGCTTTGGTGACTCTAGATAACC     | CCATGGTAGGCACAGCGACTA        | 60                            |
| <b>Acan</b><br>(Aggrecan core protein)                         | CTTAGAAGGACAGAAAGCGAC        | ACTTTGGGCGGAAGAAGG           | 60                            |
| <b>Col2a1</b><br>(Collagen alpha-1(II) chain)                  | CTGGCTTCAAAGGCGAACAAG        | GCACCTCTTTTGCCTTCTTCAC       | 60                            |
| <b>Sox9</b><br>( <i>SRY (Sex Determining Region Y)-Box 9</i> ) | CAGGTGCTCAAGGGCTACGA         | GACGTGAGGCTTGTCTTGCT         | 60                            |

**Table 2-5. qRT-PCR ovine primer sequences.**

| Gene name<br>(Protein product)                                 | Forward primer<br>(5' to 3') | Reverse primer<br>(3' to 5') | Annealing temperature<br>(°C) |
|--|------------------------------|------------------------------|-------------------------------|
| <b>Gapdh</b><br>(Glyceraldehyde 3-phosphate dehydrogenase)     | CTGGTGCTGAGTACGTGGTG         | CGTCAGGAGAAGGTGCAGAG         | 59                            |
| <b>Acan</b><br>(Aggrecan core protein)                         | TAGGTGGCGAGGAAGACATC         | AAACGTGAAAGGCTCCTCAG         | 57                            |
| <b>Col2a1</b><br>(Collagen alpha-1(II) chain)                  | CCTCAAGAAGGCTCTGCTCA         | ATGTCAATGATGGGGAGACG         | 57                            |
| <b>Sox9</b><br>( <i>SRY (Sex Determining Region Y)-Box 9</i> ) | TGAATCTCCTGGACCCCTTC         | CTTGCCTCCTCGCTCTCCT          | 62                            |

## 2.18 Agarose gel electrophoresis

Customised ovine and equine primers were pre-optimised by qRT-PCR and fractionated by gel electrophoresis with the aim of optimizing the annealing temperature and confirming the presence of a single product per primer pair. Gels were made with a 2% (w/v) agarose solution in 100 mL 1X TAE buffer in a 250 mL glass bottle. The cap of the bottle was loosened, and the bottle was then placed in a microwave and heated intermittently for 2- 4 minutes, until the solution was dissolved, in 30 seconds intervals and periodically removing the content of the bottle. Next 5  $\mu$ L of ethidium bromide (10 mg/mL) was added to the mixture; the bottle was then swirled for distribution of the reagent and poured into a gel setting chamber. Combs were then inserted on the chamber and the solution was left to solidify for 1 hour. Ethidium bromide is a fluorescent DNA dye that intercalates with the DNA double-stranded helix and undergoes enhanced fluorescence after UV exposure, allowing for visualisation of the DNA bands within the gel. After gel was set, the combs were carefully removed, and the clear chamber was then transferred into a Bio-Rad electrophoresis chamber that was previously filled with 1x TAE buffer (pH 8). Next 2.5  $\mu$ L of gel loading buffer was added to each PCR amplified sample and 8  $\mu$ L from each sample were then loaded into each well of the gel. 5  $\mu$ L of the DNA ladder was loaded into 2 wells, usually located at the extremes of the gel, to allow for better visualisation. Gels were run during 1 hour at 100 V and then visualised in a UV Transilluminator (Synergene) chamber at 254 nm. Images of the gels were taken with the Synergene Genesnap software.

## 2.19 Flow cytometry characterisation

Human UC-MSCs labelled with MNPs on the previous day as described in section 2.5.4, and unlabelled cells were trypsinised, counted and fixed by re-suspending the cells in 10% (v/v) formalin and incubated at room temperature for 20 minutes. Cells were next centrifuged at 1,200 r.p.m, the liquid was discarded, and cells were re-suspended to wash in FACS buffer consisting of DPBS with 0.5% (w/v)

BSA and 2 mM EDTA and centrifuged again. Samples were re-suspended in 5 mL of 0.1% Tryton X-100 and incubated at room temperature for 10 minutes, followed by centrifugation, re-suspension in FACS buffer and centrifugation. Cells were then re-suspended in 5 mL of 2% (w/v) BSA and incubated at room temperature for 30 minutes and separated into equal volumes in 1.5 mL microcentrifuge tubes, being approximately  $2 \times 10^5$  cells per studied group in duplicates. Tubes were centrifuged at 500 g for 3 minutes, the liquid was discarded, and samples re-suspended in a dilution of the appropriate primary antibody (Dextran-FTCI, TRPV4 and IgG) according to manufacturer's instructions, or in 500  $\mu$ L FACS buffers for the controls, and incubated for 30 minutes at room temperature. Next samples were washed 3 times with FACS buffer by centrifugation and re-suspension and the secondary antibody was added (Alexa Fluor 647) according to recommended dilution, or 500  $\mu$ L FACS buffer was added to the control samples and incubated 30 minutes at room temperature in the dark, prior to centrifugation and 3 washes with FACS buffer. The samples were finally re-suspended in 300  $\mu$ L of FACS buffer and protected from light. The measurements were performed by Dr. Nicola Foster due to limitation of the equipment access, using the Beckman Coulter Cytotflex. Analysis was done using the CytExpert software.

## 2.20 Magnetic nanoparticle characterisation

### 2.20.1 Particle size

To determine the hydrodynamic particle, size a Malvern ZetaSizer instrument was used. The instrument is based on the use of dynamic light scattering to measure the size and the size distribution of particles in a suspension. This measurement is key to study the properties if the MNPs since the hydrodynamic size highly influences the properties exhibited by the nanoparticles (237). From the 250 nm Nanomag stock (1 mg/mL), 50  $\mu$ L was diluted in 3 mL dH<sub>2</sub>O in the cuvette, vortexed and placed in the instrument. The working volume made a count rate of 300-400, enough to select a good range of

MNPs for the measurement. 3 measurements of the Z-Size were taken from each sample made in triplicates.

### 2.20.2 Particle surface charge

The Z-potential of the nanoparticles was measured using the Malvern Zetasizer, giving a measurement of the particle stability in suspension. 250 nm Nanomag stock particles were diluted to the previous concentration (2.20.1) in MiliQ water and injected into the Malvern capillary cuvette by using a syringe, avoiding the formation of air bubbles. The cuvette was then placed in the instrument and the software run 120 readings in triplicates for each sample.

### 2.20.3 Total protein determination

In order to determine the amount of antibody bound to the MNPs, the Micro™ BCA Protein Assay Kit was used. This method is based on the reduction of  $\text{Cu}^{+2}$  to  $\text{Cu}^{+1}$  reaction in the presence of proteins in an alkaline medium that is detected by colorimetric detection of the reduced element by the bicinchoninic acid (BCA). The colour change is the measured by absorbance reading with a spectrophotometer. A standard curve was prepared using serial dilutions of BSA of 200, 40, 20, 10, 5, 2.5, 1 and 0.5  $\mu\text{g}/\text{mL}$  using DPBS as diluent. A sample containing only the diluent was also prepared. MNPs labelled with RGD, TREK-1, TRPV4 and particles labelled with the secondary antibody and unlabelled as described in section 2.5.1 and 2.5.2, were washed with DPBS twice in a permanent magnet and re-suspended in 1 mL in DPBS to eliminate reading errors induced by the presence of protein in the nanoparticle's diluent solution. The working reagent was then prepared by mixing the reagents A, B and C provided by the kit according to the manufacturer's instructions. The working solution was vortexed and mixed in a 1:1 proportion with each of the samples to be studied, and incubated for 1 hour at 60 °C. Next 150  $\mu\text{L}$  of each standard and sample solution was transferred into a 96-well plate in triplicates and 150  $\mu\text{L}$  of the working solution was added to each well before mixing

for 30 seconds and allowing for the plate to cool. The absorbance was read at 562 nm using the Tecan Spark® plate reader.

## 2.21 Transmission electron microscopy (TEM)

Human UC-MSCs labelled with magnetic nanoparticles were used to examine the close behaviour of the MNPs within the cells and proving the presence of the same inside the cells. Cells were firstly seeded in UV-sterilised coverslips placed in a 6-well plate (200.000 cells per well) and allowed to attach for 24 hours before labelling as per indicated in section 2.5.3 and left in the incubator for 48 hours before fixation. Cells were also labelled and immediately fixated after 3 hour-incubation with the MNPs. Cells were washed with DPBS and fixed with 2 mL of Cacodylate fixative (provided by the TEM service) for 1 hour at 4 °C, then DPBS was added into the wells and the plates were transferred to TEM facilities where they were processed. This experiment was performed with the collaboration of Kiran Dhillon.

## 2.22 Luciferase measurement

The metridia luciferase secreted by the CMV-Luc and Col2-Luc was measured with the Takara Ready-To-Glow™ kit following the manufacturer instructions. 24 hours before measurement, media was changed for all the groups. For the measuring 100 µL of media were collected from the cells and diluted in DPBS 1:100 for the Col2-Luc cells and 1:1000 for the CMV-Luc cells. 50 ml from each dilution were mixed with the substrate buffer from the kit and a reading was performed with the luminometer.

## 2.23 RNA sequencing

For further assessment of the MICA potential in chondrogenesis, human TC28 chondrocyte cell line was used, kindly provided by Dr. Steven Woods and Prof. Sue Kimber (Manchester University). This experiment was performed with the help of Kiran Dhillon. Cells were cultured in monolayer for expansion purposes in basal media, labelled with TRPV4-MNPs in monolayer and 24 hours after

labelling cells were submitted for 1 hour of MICA activation, added GSK101 (100 nM) or left in the incubator for 4 hours before RNA extraction. All samples were treated equally with removal of media and addition of fresh media prior to the 4-hour incubation time to avoid variation among experiments. RNA was extracted on the same day and qRT-PCR on *JUN*, *MAFF*, *RCAN1*, *NFATC2*, *SPP1* and *BTG2* transcription factors was performed on the following day after preserving the samples at -80 °C. The experiment was repeated 4 times and one sample per group per experiment was sent for RNAseq analysis by our collaborators in Manchester University (Supplementary figures 1 and 2).

## 2.24 Statistical analysis

Statistical analysis was conducted using the GraphPad Prism V7 software. Differences with a p value lower than 0.05 ( $p < 0.05$ ) were considered significant. For experiments with more than 3 technical repeats of gene expression or sGAGs, DNA and sGAGs/DNA were compared across groups performing a two-way ANOVA with Tukey comparison of column means. When the number of repeats varied slightly for each group, an ordinary one-way ANOVA was performed instead, with Tukey correction and comparison of column means. For comparison of paired samples, a two-tailed paired T-test was performed.

Unless otherwise stated all values quoted in the results are mean  $\pm$  standard deviation.

---

# *Chapter 3*

---

## Cells and MNPs characterisation

### 3.1 Introduction

Magnetic nanoparticles have been widely studied in the biomedical field for several applications such as contrast agents for MRI, cell labelling and tracking and magnetic hyperthermia for cancer therapy or drug delivery (238). The use of magnetic nanoparticles for injectable cell therapies has introduced the possibility of controlling the stem cell behaviour *in vivo* and localising the cells following implantation via MRI tracking of the MNPs, removing the need for contrast agents (239,240). Despite the great advantages for *in vivo* applications the functional properties of the MNPs need to be assessed prior to every individual experiment. Moreover, the particle design is a key element for the purpose of the application and needs to be closely aligned to the magnetic properties desired (241).

The MNPs properties such as size, coating and functionalisation, can affect the biocompatibility, biodistribution, uptake and toxicity of the particles. Moreover, the internalisation of the MNPs can also be affected by the cell type and the proliferation rate of the cells while at the same time, labelling the cells with MNPs can alter the proliferative properties of the culture (212). The fabrication of MNPs is a complex process that often leads to batch-to-batch variability and it can also be found variability among the same batch. This issue is often avoided when using commercially available particles (242). Nevertheless, it may also occur that the commercially available MNPs do not meet the stated specifications. Hence, it is of great importance to characterise the MNPs used to ensure the efficiency of the experiment (243). This is of special importance if there is an aim for translating the therapy into the clinic, being a requirement that the MNPs match the accepting validation criteria to ensure firstly, the safety, followed by the effectiveness of the treatment (244).

The biodistribution of the MNPs is determined by the nanoparticle coating and the surface chemistry. Biocompatible coatings can reduce the immune response(245). This is key to allow for the nanoparticles to remain longer in circulation before being detected and engulfed by the macrophages. Coating particles with dextran has been demonstrated to prolong the presence of MNPs in systemic

circulation(246). The coating of the MNPs also influence the magnetic behaviour by decreasing the magnetic properties of small particles such as iron oxide when compared to the bulk properties or by modifying the anisotropy or the magnetic moment (247). Moreover, surface modifications such as antibody coating, can play an elemental role in the interaction of the MNPs with the cellular components.

Among the variety of proposed strategies for the use of MNPs for cell therapy, a novel application based on the remote activation of stem cells with MNPs has been studied for several tissues such as bone, brain and cartilage (220,221). This approach is based on the mechano-transduction concept, aiming to selectively activate mechano-sensitive structures on the cells to guide the differentiation process.

For the MICA technology to adequately function, several approaches can be addressed. The magnetic activation of the channel can be achieved either by direct deformation of the membrane, or by exerting a mechanical force that changes the channel conformation with the following activation (216). Nevertheless, a more specific way to apply the MICA technology is by directly targeting the mechano-sensitive domain of the channel. Hence, it is key to both successfully coat the MNPs with a high affinity antibody and to be able to target the desired mechano-sensitive structure. The process of labelling the MNPs with antibodies for directing the particles towards specific elements of the cells is known as active targeting (248). The use of functional groups for targeting intra- or extracellular elements provides an efficient bonding for nanoparticles that aids prolonging the time that the MNPs reside in the tissue, in addition to introducing the advantage of selectively targeting small elements of the cells, which is the case for the magnetic ion channel activation approach.

MNPs ranging from 250 nm can be engulfed by the cells event if not labelled with any specific antibody (196,249). For this reason, the effective nanoparticle coating and labelling efficiency are two essential parameters that should be characterised for these types of approaches. Nevertheless, the

demonstration of the MNPs binding to the receptor, can be a complex matter to demonstrate given the often transient presence of the MNPs bound to the membrane. This is the case for the TRPV4 channel that has been described to rapidly internalise following activation (250).

In addition to guaranteeing the effective labelling, the MNPs are required to reach their target externally or internally. The majority of mechano-transductive elements are located at both the internal and the external side of the cytoplasmic membrane connected by transmembrane domains. This is so that the external stimuli can be sensed by the outer part of the receptor, and translated into the cytoplasm by the transmembrane and internal domains of the channel linked to the cytoskeleton elements (251,252). For both TRPV4 and TREK-1, this mechano-sensitive domain is located in the internal side of the membrane (141,253). To ensure the uptake of the particles, transfection agents can be used such as the cationic lipid DOTAP. The supplementation of the cells with these agents aid for the particle internalisation by the formation of a liposomal complex that fuses with the cell membrane (254). However, these agents are often related with toxicity and impaired biological function and hence, when used, it is of great importance to ensure cell viability and that the differentiation potential of the cells has not been affected (255).

The work in this chapter aims to characterise the MNPs used for all experiments conducted for this thesis, by measuring the size of the particles and proving the effective coating and labelling of the MNPs with the specific agents. A study was also performed to test the hypothesis that iron oxide cored-MNPs coated with dextran do not induce cytotoxicity and neither the transfection agent used. The chondrogenic potential of MSCs was also assessed *in vitro* with a preliminary study of the MICA technology that was executed for histological observation of the cartilage constructs formed under mechanical stimulation.

## 3.2 Aims

The aims of this chapter were:

- To characterise the MNPs properties used for all labelling experiments
- To characterise the MSCs and the labelling efficiency
- To study the effect of MICA technology on chondrogenic differentiation of human MSCs

## 3.3 Methods

### 3.3.1 Magnetic nanoparticle characterisation

Commercially available MNPs were activated, coated, and labelled with the antibodies used for this thesis as explained in section 2.5. The hydrodynamic size and particle surface charge (Z potential) was measured using a Malvern ZetaSizer instrument following the procedure explained in sections 2.20.1 and 2.20.2. For control purposes, characterisation experiments of MNPs were performed also in uncoated MNPs. All measurements were performed in replicates of 3 for higher accuracy.

For quantification of the total amount of protein/ antibody bound to the MNPs after labelling, a Micro BCA™ assay was performed according to procedure described in section 2.20.4. This measurement was performed for all types of proteins used for the experiments for the duration of this work.

### 3.3.2 Cytotoxicity study of MNPs

The study of the effect of MNPs labelling on cell pellets and micromasses was performed using hUC-MSCs for the pellet determination and equine MSCs for the micromasses. Presto blue™ reagent was used, as explained in section 20.10.1 for measuring the metabolic activity of the cells that directly correlates to cell viability. For each cell type, 3 replicate measurements of 3 different samples from each group were taken at days 1, 7, 10, 14 and 21 of culture for the pellets, and days 1, 3, 5 and 7 for

the micromasses, adjusting to each experimental condition. For immunohistochemical assessment of the viability, 1 pellet per group of hUC-MSCs was processed and 3-4 sections of each pellet were stained with Ki67 and Live/ Dead™ stain (section 2.9 and 2.10.2). The Live / Dead™ dye reacts with the free amine groups from the inside of the cells and from the cell surface producing a bright blue immunofluorescence signal in the presence of dead cells. The samples stained with this dye emitted fluorescence regardless of the presence of living cells. For an accurate analysis, pellets formed with the same cell source were cultured with PEGDA for inducing apoptosis. Pellets were then sectioned and stained with Live / Dead™ and Ki67 as the studied samples. The images were processed with Image J software and the quantified fluorescent intensity values from the studied group were normalised to the values from the sections of the samples that were induced to apoptosis and hence, considered as a positive control for the marker.

### 3.3.3 Characterisation of MSCs

MNPs presence on the cells was studied by transmission electron microscopy as described in section 2.21. This study was performed in hUC-MSCs fixed after labelling for 3 hours with MNPs following the protocol described in section 2.5.3. Subsequently, these cells were fixed 48 hours after labelling with the aim of studying the fate of the MNPs post-labelling.

The presence of TRPV4 was detected in human, ovine and equine MSCs and in human UC-MSCs prior to initiating any experiments activating the channel. PCNA antibody was also tested on monolayer to prove effectiveness on detecting proliferating cells for those cells that required viability study of pellet sections. For this purpose, cells were stained in monolayers following the description in sections 2.8 and 2.9. Different magnifications were used with the aim of improved visualisation given the unexpected high cell density unexpectedly achieved for some cultures, that hindered the use of a higher magnification. For these cultures, DAPI staining was also used for allowing to distinguish between individual cells.

Flow cytometry was used to characterise the cells and demonstrate the presence of the TRPV4 channel expression on the cell membrane of human UC-MSCs and equine MSCs as explained in section 2.19. Isotype controls were performed to eliminate any signal due to unspecific binding of the secondary antibody.

### 3.3.4 Magnetic activation of MSCs for chondrogenic differentiation

Human BM-MSCs isolated from a commercially available aspirate following the protocol in section 2.3.1, were used to test the chondrogenic potential of the cells with the aid of biochemical cues and with MICA activation. Cells were expanded until the desired number of cells and pellets were formed as described in section 2.3.7. All groups were cultured in the chondrogenic media detailed in section 2.4. Unless otherwise stated, samples were cultured with 10% FBS. With the purpose of comparing the effects of mechanical activation of TRPV4 with the MICA technology and direct biochemical activation, some pellets were cultured with the TRPV4 agonist GSK101 as indicated in section 2.4.1. The experimental groups for this experiment are detailed in the Table 3-1. The specific groups were submitted to MICA stimulation for 1 hour in a 5/2 regime as specified in section 2.6 and were also compared to labelled groups under static conditions.

**Table 3-1. Human MSCs experimental groups tested for chondrogenic differentiation.**

| Experimental groups                |
|------------------------------------|
| Cells                              |
| Cells + GSK101                     |
| Cells + TRPV4 MNPs Static          |
| Cells + TRPV4 MNPs + MICA          |
| Cells + TRPV4 MNPs + MICA (1% FBS) |

Pellet size was measured prior to fixation of the sample using the EVOS M5000 microscope by placing the pellet in a petri dish and manually delimitating the contour of the pellet to measure size of the total area. Samples were analysed at days 0 (24 hours after pellet formation), day 7, 10, 14 and 21. The analysis was based on the determination of cartilage markers production by histological processing as detailed in sections 2.7.2 and 2.7.4, by staining for collagen with picosirius red (section 2.7.8), GAGs with toluidine blue and alcian blue (sections 2.7.6 and 2.7.7), and MNPs iron content detection by prussian blue staining (section 2.7.9). Immunohistochemical detection of collagen II was performed according to the protocol indicated in section 2.9. The histological and immunohistochemical analysis was performed in 1 pellet per group and 3 sections of different depths of the pellet. The fluorescence signal from the immunohistochemical analysis was quantified using the Image J software as per detailed in section 2.9.5.

### 3.3.5 Gene expression analysis of TC28 cells

The chondrocyte human cell line TC28 was cultured for expansion purposes before monolayer formation as per stated in section 2.3.6. Samples were then labelled with TRPV4-MNPs in monolayer (section 2.5.3) and activated with the MICA bioreactor for 1 hour (section 2.6). The chemically activated group had the TRPV4 agonist added as detailed in section 2.23. All samples were kept in the incubator for 4 hours before processing following TRPV4 activation. Samples were then digested and RNA was isolated (section 2.15) and converted into cDNA (section 2.16). qRT-PCR was performed following the protocol indicated in section 2.17. This experiment was repeated 4 times for all groups studied, with the exception of experiment 4 that lacks the group of unlabelled cells MICA stimulated due to a constrain in the cell number.

### 3.3.6 Statistical analysis

Statistical analysis was performed as indicated in section 2.24.

## 3.4 Results

### 3.4.1 Determination of MNPs hydrodynamic size and charge

The properties of the particles (Nanomag COOH) were studied for size and charge given the importance these parameters have in the effective uptake of MNPs by the cells. The nanoparticle fabrication can be a highly variable process and often the commercially acquired particles of a defined size and charge can also vary. With the aim of comparing the particles to the manufacturer's indications, particle characterisation was performed. In addition, the particle properties were also measured after surface modification by functionalising the particles and coating with TRPV4, with the aim of understanding the changes exerted in the particles properties.

The hydrodynamic size of the commercially available MNPs was measured by dynamic light scattering principle that provided the hydrodynamic diameter (HD) of the MNPs. The particles were expected to have a diameter of 250 nm as stated per the manufacturer. Particles were characterised in dH<sub>2</sub>O at a concentration of 15 µg/mL directly from the stock or after surface modification and coating with TRPV4 antibody. Unlabelled particles exhibited an average size of 256.2 nm ± 7.45 as expected for the indications of the manufacturer's data (Figure 3-1). Surface modification with TRPV4 coating of the particles resulted in an increase of the hydrodynamic size being 380 nm ± 21 evidencing that the presence of the antibody in the surface membrane had an effect on the particle size.

The zeta potential ( $\zeta$ ) is a measurement of the electrokinetic potential in colloidal systems and is an indicator of the aggregation or repulsion between the particles in suspension. High values of z potential for the same sign in a particle suspension generate forces that prevent from particle aggregation due to the generation of repulsion forces. Unlabelled particles charge was significantly higher ( $p < 0.05$ ) than the charge observed for MNPs labelled with TRPV4 indicating the higher stability of TRPV4-MNPs in suspension when compared to plain particles (Figure 3-1).

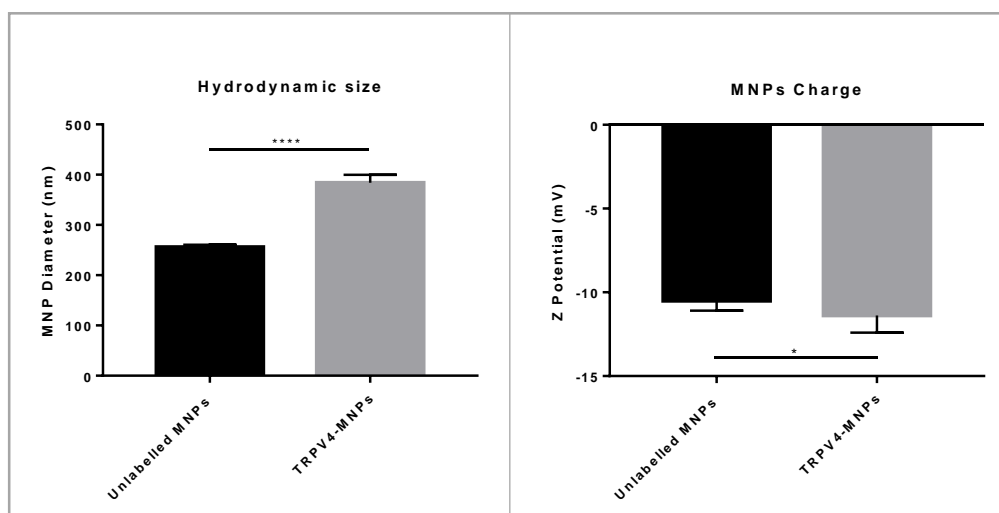


**Figure 3-1. Surface modification of 250 nm Nanomag particles increases the hydrodynamic size and results in a more stable solution than plain particles.** Hydrodynamic size and z potential was determined for commercially available particles alone and particles after surface functionalisation with TRPV4 in dH<sub>2</sub>O. Data are expressed as mean  $\pm$  standard deviation, n=3 (technical repeats), \*p<0.05, \*\*\*\*p<0.0001.

The poly dispersity index (Pdl) measures the distribution of particle size in the solution. This is, the heterogeneity of the MNPs samples based on the measurement of the size. Being commercially available MNPs, the variability of the size distribution can be due to agglomeration of the MNPs in the solution. The agglomeration of the particles can occur if the charges of the MNPs are not strong enough to generate the electrostatic repulsion that stabilised the particles against aggregation (256). The Pdl was obtained from the Malvern zetasizer instrument, and the values provided a range between 0-1, where lower values represent monodispersed solutions and higher values are indicative of agglomerations. Values lower than 0.05 are found in monodispersed samples and values higher than 0.7 are indicative of a broad size distribution in the sample (256). Table 3-2 indicates the Pdl of plain particles being lower than coated particles, however, both index values are found in the range of normal size distribution values.

**Table 3-2. Polydispersity values of Nanomag particles unlabelled and labelled with TRPV4.**

| Particle        | Pdl             |
|-----------------|-----------------|
| Unlabelled MNPs | 0.15 $\pm$ 0.04 |
| TRPV4-MNPs      | 0.36 $\pm$ 0.06 |

### 3.4.2 MNPs protein determination

The surface modification process is a key element required for many approaches based on *the in vivo* delivery of MNPs. MICA technology requires the effective targeting of the MNPs towards specific membrane channels or proteins. This event is achieved via the linkage of antibodies with high binding affinity for the membrane targets and hence, the surface modification of the MNPs with antibodies is key for the technology to effectively work. The quantification of the bound protein was studied by Micro BCA™ assay. The protein quantification method is based on the reduction of  $\text{Cu}^{2+}$  to  $\text{Cu}^{+}$  by the presence of proteins in an alkaline medium producing a light blue-to-violet complex after detection of the  $\text{Cu}^{+}$  ions by the bicinchoninic acid. The colour change that is detected by the spectrofluorometer and the intensity is proportional to the amount of protein present in the solution. Functionalised and activated particles showed some levels of protein presence (Figure 3-2). MNPs activated and coated with the secondary antibody alone, had higher presence of protein and samples fully functionalised and coated with both primary (TRPV4) and secondary antibodies showed 0.9-fold when compared to the functionalised, MNPs, demonstrating the presence of antibody in the samples.

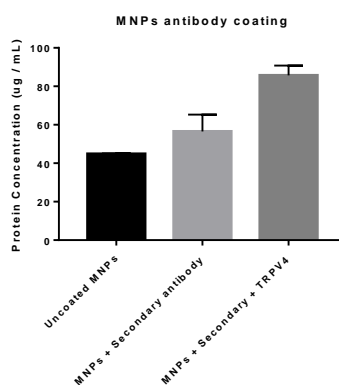


**Figure 3-2. MNPs antibody coating was successfully performed.** Protein quantified in MNPs activated with EDAC and NHS, activated MNPs coated with the secondary antibody and activated MNPs coated with secondary and primary antibody (n=3). Data are expressed as mean  $\pm$  standard deviation.

### 3.4.3 Study of the cytotoxic effect of the MNPs

The effect of MNPs on cell pellets was performed using hUC-MSCs labelled with TRPV4-MNPs, samples labelled with activated MNPs and compared to the viability of unlabelled cell pellets. The viability was measured using the PrestoBlue™ reagent that when added to the medium, is rapidly taken by the cells and the reducing environment of the metabolically active or living cells, converts the reagent into a red fluorescent dye that is measured by the spectrophotometer. The colour change is proportional to the amount of metabolic activity. Samples were analysed 24 hours after pellet formation and at 7, 10, 14 and 21 days of culture (Figure 3-3). No statistical differences were found among compared groups or time points. All 3 groups studied followed a similar tendency over culture time with an initial decrease of the metabolic activity followed by an increase after 10 days of culture that was maintained until the termination of the experiment.

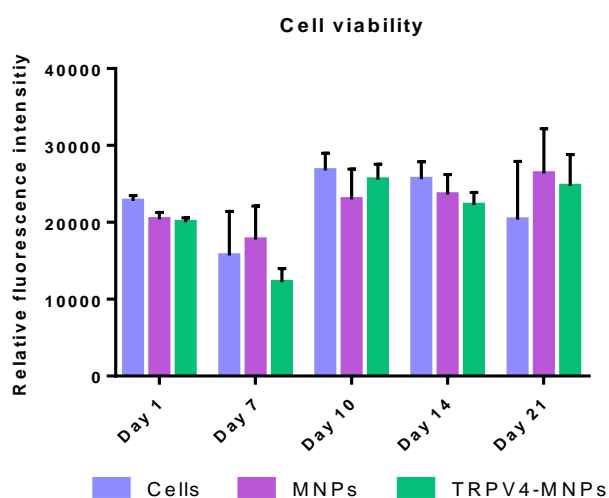


**Figure 3-3. Cell viability is not affected by the presence of MNPs.** The metabolic activity was measured through the course of 21 days for every time point in n=3 samples per group. Data are expressed as mean  $\pm$  standard deviation, n=3 (technical repeats and samples per group).

The assessment of the viability on cultured 3D pellets can be hindered due to the dense nature of the samples and the impossibility for the reagent to reach the core. With the aim of analysing the viability

in the centre of the samples, sections of hUC-MSCs pellets were stained with Live / Dead™ assay and the proliferative marker Ki67. A positive control for the stain was generated with sacrificed pellets and was considered as 100% dead cells for quantification purposes (Figure 3-4).

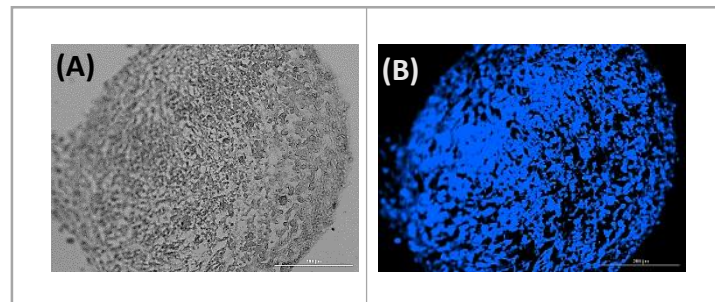


**Figure 3-4. Representative images of dead cells cultured in pellets.** Bright field images of apoptosis-induced pellet sections in A) bright field and B) sections stained with Live / Dead™ reagent showing saturation of the fluorescence signal. Higher intensity of the stain is an indicator of presence of dead cells. Scale bar = 200  $\mu\text{m}$ .

The combination of the Live / Dead™ stain together with the Ki67 proliferation marker allows for further understanding on the viability of the pellets constructs. This allows to visualise the commonly-occurring cell death events occurring in the centre of the pellets, while at the same time visualising where the proliferations events are given on the constructs. Samples stained with Live / Dead™ showed less stain intensity on day 1 of culture, indicator of a lower presence of dead cells. Over culture time all groups were observed to have increased the population of dead cells with a clear tendency to locate in the centre of the sections (Figure 3-5). A notable difference was observed between day 1 samples, showing small areas of dead cells in the most central regions that extended towards the periphery over the course of the experiment. The control group with cells only and pellets labelled with MNPs showed a small area of accumulation of dead cells towards the centre region of the pellet at day 14. Matching with the dead cells' analysis, the location of the proliferation marker Ki67 was observed to be mainly in the periphery of the samples. The highest intensity of the stain was observed at day 1 of culture for control samples and samples labelled with MNPs, and was drastically reduced after 1 week until the termination of the experiment. Pellets labelled with TRPV4-MNPs showed higher

presence of the marker at days 7 and 14 of culture with nucleus of proliferative cells located in internal regions of the sections. Despite showing higher presence of the Ki67 marker than the other groups, the intensity of the marker also decreased with culture time showing similar levels than the studied groups by day 21.

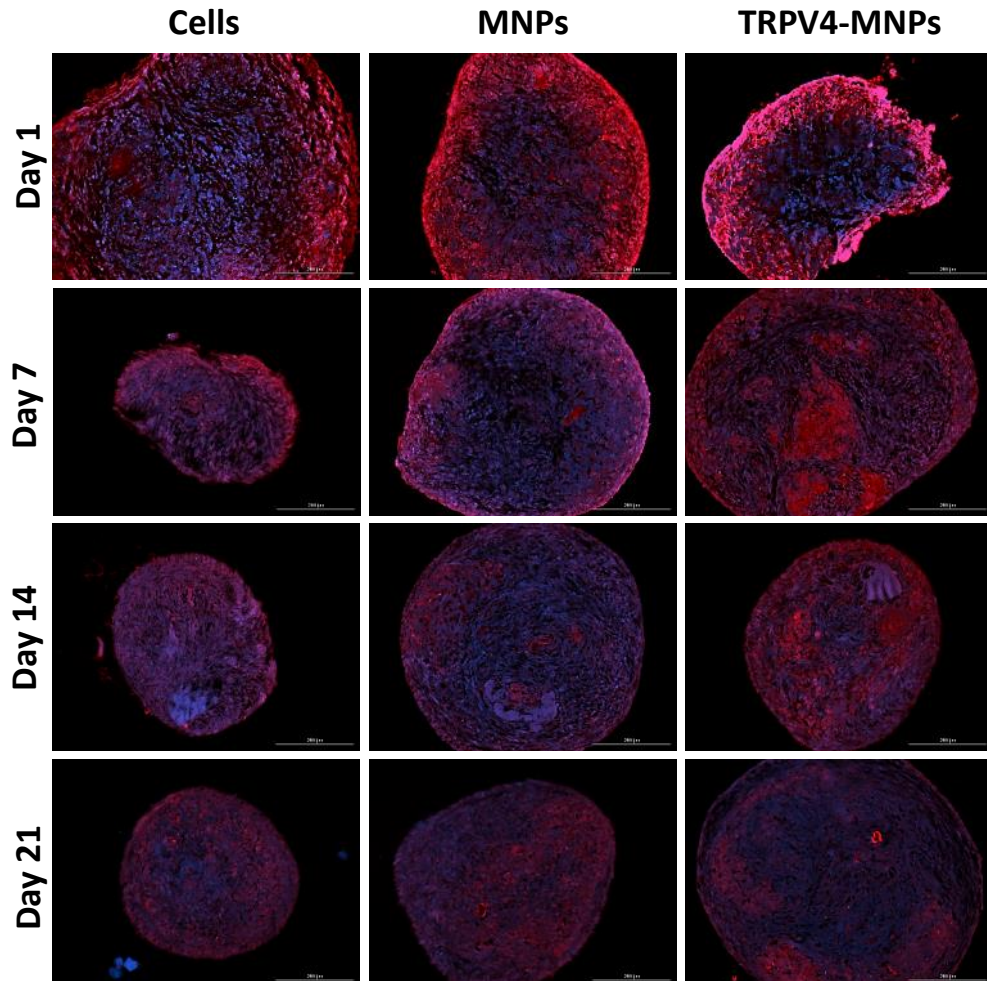


**Figure 3-5. Decreased proliferation over culture time.** Representative immunohistochemical fluorescence images of 7  $\mu\text{m}$  hUC-MSC pellets at days 1, 7, 14 and 21 of culture. Live / Dead™ stain is shown as blue and Ki67 as red.

Live / Dead™ stain was quantified by Image J using the values obtained from dead pellets images as gold-standard positive controls (100% cell death). Quantification of the fluorescence images showed similar results to those visually observed with the exception of the cells only control, which showed a slight decrease of cell death over culture time. Nevertheless, great variation was found among samples from the same group (Figure 3-6). No statistical significance was found when comparing the different

studied groups, however, samples labelled with unspecific MNPs reached 39% cell death on the first week of culture, and moderately decreased with culture time. Samples labelled with TRPV4-MNPs showed similar percentages of cell death over the duration of the experiment.

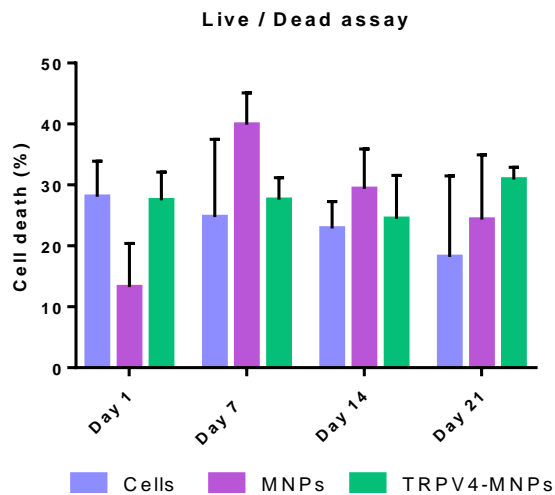


**Figure 3-6. Quantification of the cell death showed similar levels for all groups and time points.** Quantification based on the immunohistochemical fluorescence images of Live / Dead™ stained pellet sections contrasted to positive controls. Data are expressed as mean ± standard deviation n=3 sections.

The viability of MNPs was assessed on micromass culture of equine MSCs by the quantification of the metabolic activity with PrestoBlue™ reagent. For this study, different MNPs surface protein coatings used in Chapter 4 (TRPV4, TREK-1 and RGD), were used to examine the effect on cell viability. Given the duration of the micromass culture experiments, the time points measured were adjusted to days 1, 3, 5 and 7. Initially all groups showed similar levels of activity that were slightly increased by day 3 of culture and maintained for the following measurements (Figure 3-7). Significant differences were found among groups, with higher activity found for cells labelled with TRPV4-MNPs when compared to the control with cells only, for days 3, 5 and 7. Micromasses cultured with cells alone also showed significant lower metabolic activity than groups labelled with TREK-1 and RGD-MNPs.

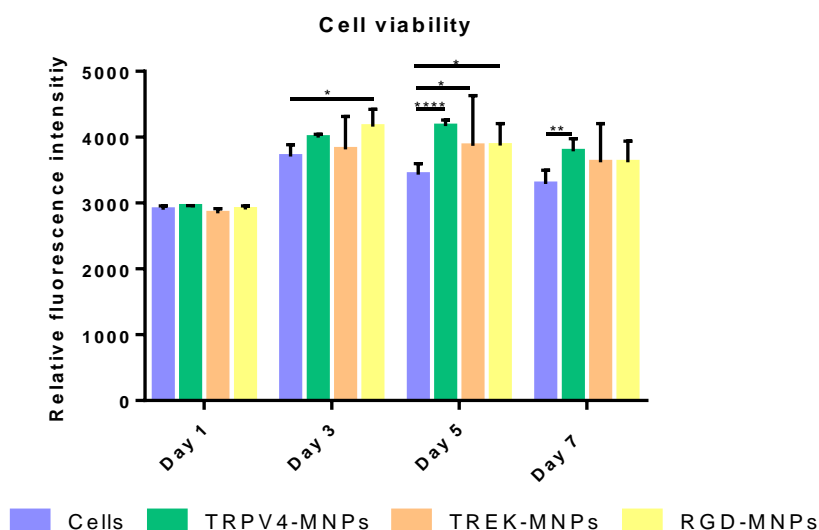


**Figure 3-7. No toxic effects found when labelling cells with MNPs regardless of the protein functionalisation.** The metabolic activity was measured through the course of 1 week for every time point. Data are expressed as mean  $\pm$  standard deviation n=3 samples per group (3 technical repeats).

#### 3.4.4 TRPV4-MNPs labelling efficiency

High resolution microscopy was used to study the fate of the TRPV4-MNPs after labelling cells in monolayer (3 hours) and 48 hours post-labelling. Electron transmission microscopy images revealed MNP uptake for both time points, demonstrating the effective labelling of the cells (Figure 3-8). Samples imaged after labelling had initiated the internalisation process of the MNPs, however, some MNPs were observed to be located next to the cell membrane. Samples imaged 48 hours after labelling showed a clear process of vesicle formation with MNPs inside, apparently attached to the vesicle membrane. For the samples studied, 1-3 vesicles were able to be observed with internalised particles. These data were supported by prussian blue staining of MNPs iron shown in later sections.

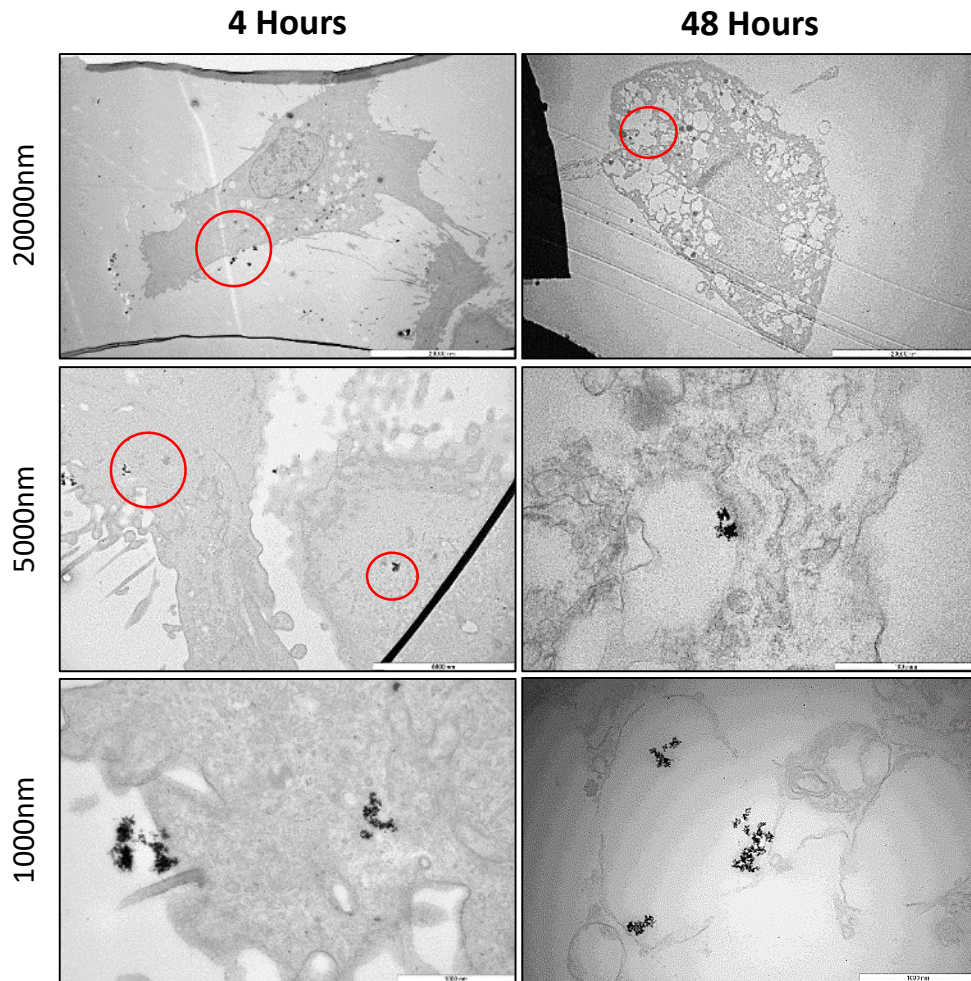


**Figure 3-8. Internalisation of MNPs observed immediately after cell labelling.** Representative images of TEM hUC-MSCs labelled in monolayer with TRPV4-MNPs after labelling (3 H) and fixation and after labelling, culture for 48 hours and fixation. Different magnifications are stated in the left axis.

### 3.4.5 MSCs characterisation

The presence of the TRPV4 channel in human, equine and ovine MSCs and in human UC-MSCs was determined prior to initiation of activation experiments. TRPV4 expression was demonstrated by immunohistochemical staining of all the cell types seeded in monolayer for an improved visualisation of the marker (Figures 3-9, 3-10, 3-11 and 3-12). PCNA immunostaining was performed to ensure the adequate staining of the desired cell types prior to testing in pellet culture. DAPI was also use to better distinguish individual cells given the high confluence achieved for human and ovine MSCs. This was not necessary for equine MSCs and human UC-MSCs given the lower confluence.

The presence of the TRPV4 channel was evident for all cell types. The presence of the proliferation marker PCNA was also visualised for all samples imaged with an enhanced intensity of the stain gathered around the nucleus.

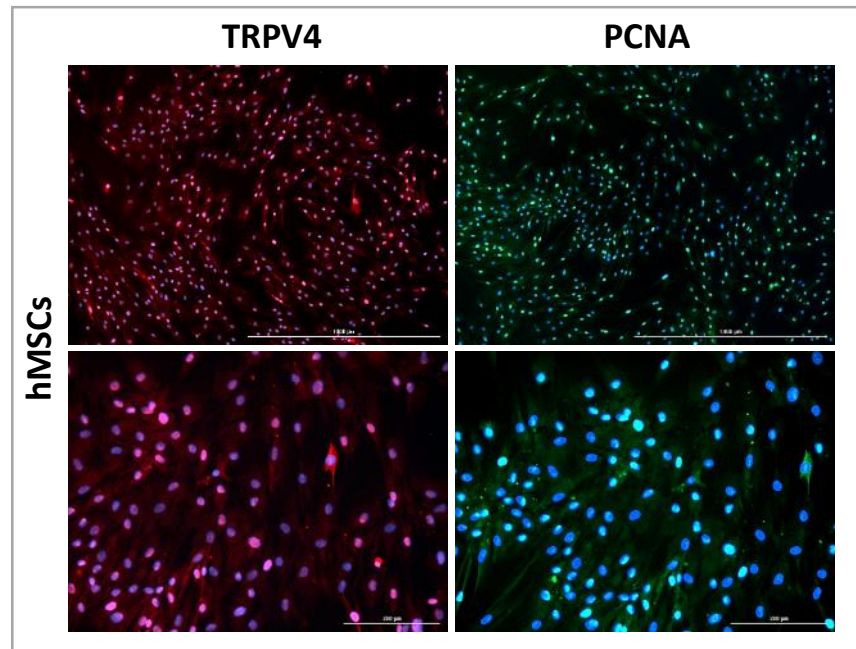


**Figure 3-9. TRPV4 channel is found among hMSCs.** Representative images of immunohistochemical staining of TRPV4 channel (shown in red), PCNA (green) and DAPI (blue) on hMSCs seeded in monolayer. Scale bars = 1000  $\mu\text{m}$  and 200  $\mu\text{m}$ .

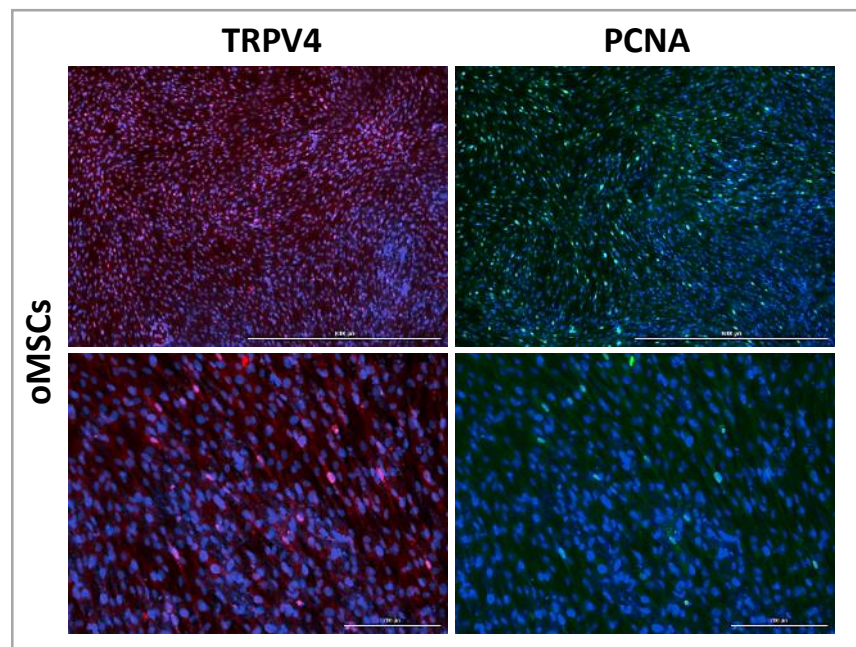


**Figure 3-10. TRPV4 channel is present in ovine MSCs.** Representative images of immunohistochemical staining of TRPV4 channel (shown in red), PCNA (green) and DAPI (blue) on oMSCs seeded in monolayer. Scale bars = 1000  $\mu\text{m}$  and 200  $\mu\text{m}$ .

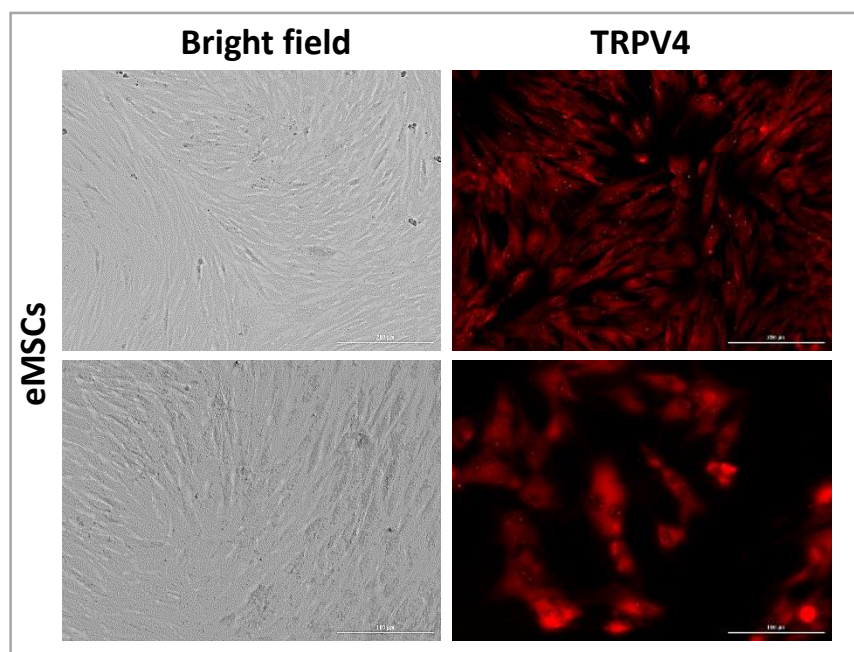


**Figure 3-11. TRPV4 channel is found among eMSCs.** Representative images of bright field and immunohistochemical staining TRPV4 channel (shown in red) on eMSCs seeded in monolayer. Scale bars = 200  $\mu\text{m}$  and 100  $\mu\text{m}$ .

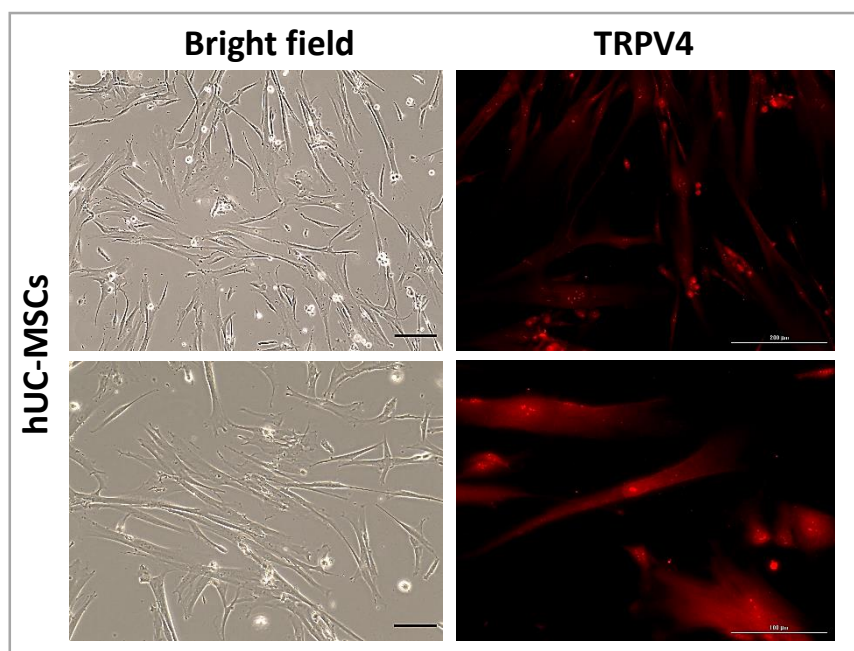


**Figure 3-12. TRPV4 channel is found among hUC-MSCs being present for all visualised cells.** Representative images of bright field and immunohistochemical staining TRPV4 channel (shown in red) on eMSCs seeded in monolayer. Scale bars = 200  $\mu\text{m}$  and 100  $\mu\text{m}$ .

The presence of the TRPV4 channel was also assessed by flow cytometry analysis for human UC-MSCs and equine MSCs. As a control, the analysis was performed on a blank sample containing cells alone and an isotype control was used for the secondary antibody. Both human and equine samples presented some levels of auto-fluorescence for the secondary antibody Alexa Fluor 647 (Figure 3-13). For the determination of cells positive for the TRPV4 channel, a shortage was made in attempt to exclude those cells considered as positive due to the unspecific binding of the secondary antibody. For human UC-MSCs 85.94% of the cells tested positive for TRPV4 and in the case of the equine MSCs the positive fraction consisted of 77.25%.

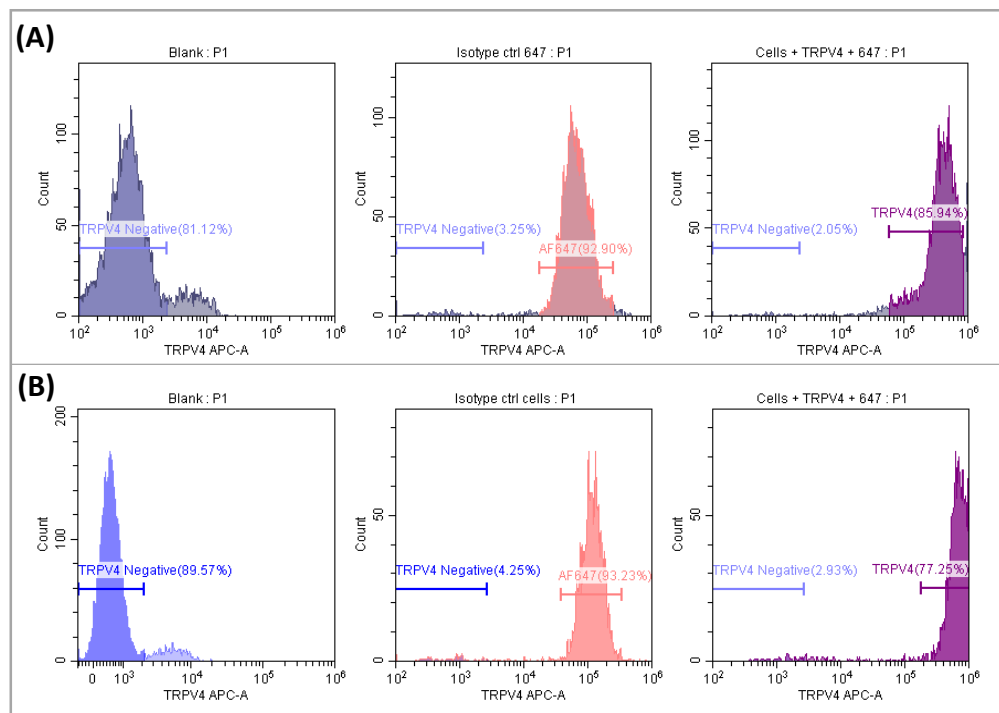


**Figure 3-13. TRPV4 channel is expressed in both human UC-MSCs and equine MSCs.** FACS analysis of the TRPV4 marker in A) human UC-MSCs and B) equine MSCs. Results from unlabelled cells are referred as blank. The secondary antibody Alexa Fluor 647 is referred as isotype control and cells positive for the isotype control were attempted to be excluded for the TRPV4 positive population.

### 3.4.6 Human MSCs chondrogenic potential following MICA induction

MICA technology was studied on human MSCs given their well-defined chondrogenic potential. The study was performed in 3D pellets containing cells and cell pellets labelled with TRPV4-MNPs cultured in high and low serum media with the aim of making a preliminary study for driving MSC chondrogenesis. For comparative purposes pellets were also cultured with the TRPV4 chemical agonist GSK101. The chondrogenic potential of the pellets was determined by histological staining of the samples for collagen and GAGs reveal. Immunohistochemical detection of collagen II was performed followed by quantification of the marker by Image J.

The pellet size was analysed by manually measuring the pellet prior to fixation (Figure 3-14). Sample size was observed to decrease over culture time; with the exception of MICA activated samples in 10% FBS that showed a growth peak at day 10. All groups had similar sizes of the samples, with the exception of MICA activated samples cultured in 10% FBS that showed a discrete tendency of increased pellet growth. However, the opposite was observed for MICA activated samples in 1% FBS.

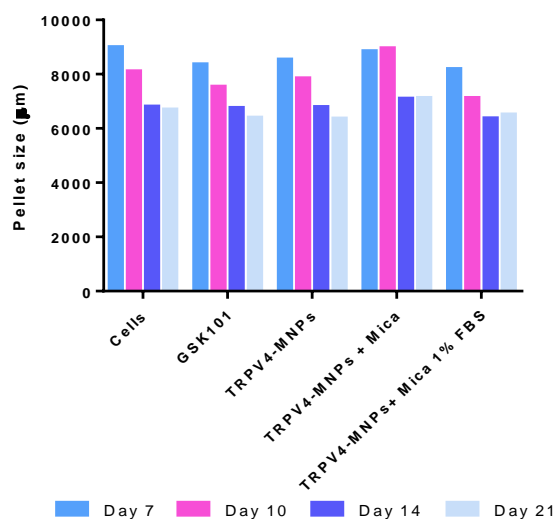


**Figure 3-14. Pellet size decreased over culture time being higher for MICA activated samples in 10% FBS.** Total area of the pellets manually delimited for all groups from donor 1 samples at all culture time points, n=1.

### 3.4.6.1 Prussian blue – MNPs detection

The iron content of the MNPs was determined by prussian blue staining. Samples not labelled with MNPs did not show presence of the particles (Figure 3-15). All labelled groups exhibited presence of MNPs from initial days of culture until day 21 with no sign of loss or dilution of the MNPs. Samples cultured with 10% FBS showed some levels of MNPs agglomeration visualised as blue stained areas. This was not observed for the group cultured in 1% FBS, that showed a more homogeneous distribution of nanoparticles, which is visualised as a lower presence of blue areas given the spread disposition of the MNPs. There was a mild tendency of the clusters of particles to be located in the periphery of the sample for all groups studied. Despite the presence of MNPs aggregated in TRPV4-MNPs samples cultured in 10% FBS, higher magnification pictures (results not shown) showed an evident spread distribution of the particles among the surface of the sections.

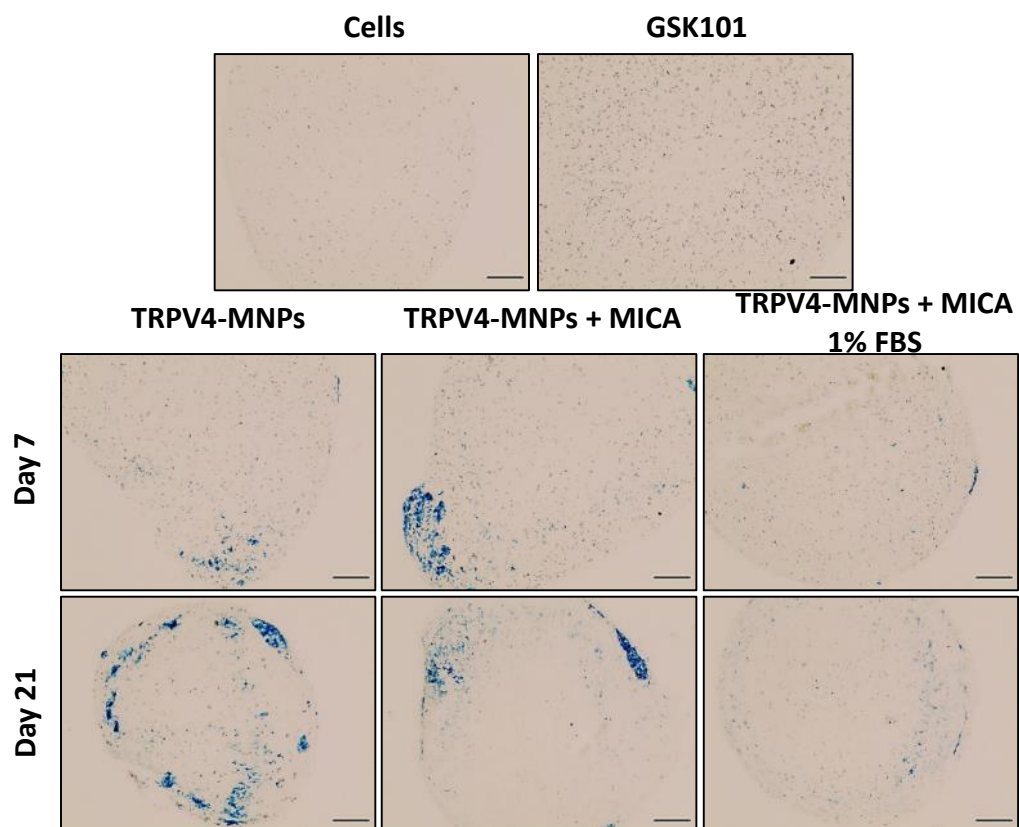


**Figure 3-15. MNPs remain present after 21 days of culture.** Representative images of Nanomag 250 nm on 7  $\mu\text{m}$  pellet sections from hMSCs of at days 7 and 21 of cultured on A) samples not labelled with MNPs and B) samples labelled with TRPV4-MNPs. The iron content of the MNPs is stained in blue by using prussian blue. Scale bar = 100  $\mu\text{m}$ .

### 3.4.6.2 Alcian blue – sGAGs analysis

The presence of sulphated GAGs was revealed by alcian blue staining of pellet sections from all groups. A low intensity of the stain indicated low production of sGAGs in the samples (Figure 3-16). Day 7 sections showed a very discrete production of sGAGs. Control samples showed even lower production of the marker than all the compared groups. After 21 days of culture, the production of sGAGs increased for all groups with a higher evident production in samples stimulated with the TRPV4 agonist GSK101, and samples labelled with TRPV4-MNPs both in static and activated conditions, when cultured in 10% FBS. The stain was not homogeneously distributed on the surface of the sections, with lower sGAGs deposition on the central area of the pellets as appreciated for both time points studied. The pellet sections for samples cultured with TRPV4-MNPs and cultured in 1% FBS was damaged and hence part of the middle section was folded on the right corner showing a higher intensity of the dye due to the layering of the sample.

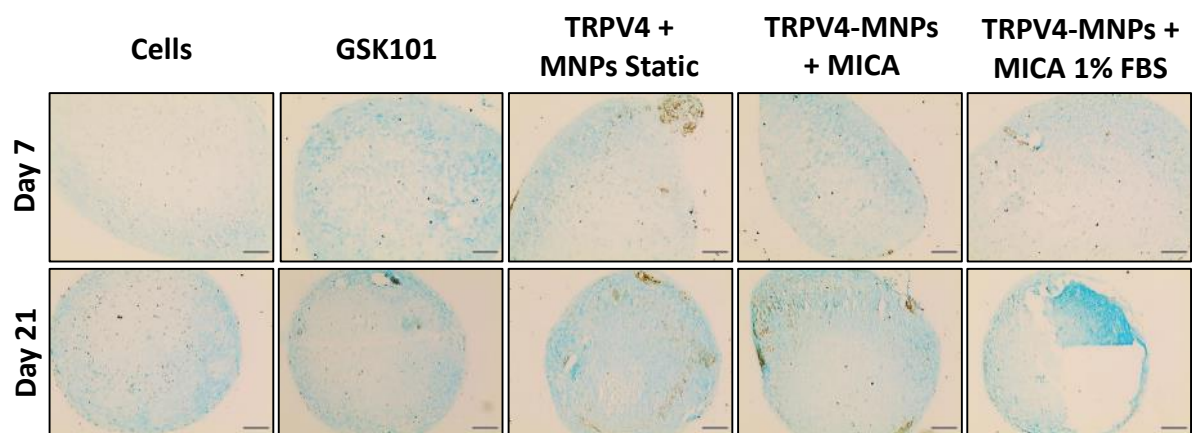


**Figure 3-16. Moderately higher deposition of sGAGs in TRPV4 activated samples cultured in 10% FBS.** Representative images of 7  $\mu$ m pellet sections of hMSCs cultured in 10% FBS and 1% FBS and stained with alcian blue for sulphated GAGs reveal at days 7 and 21 of culture. The higher intensity of the colour of the stain reveals the presence of GAGs in the sections. Scale bar = 100  $\mu$ m.

### 3.4.6.3 Toluidine blue – proteoglycan detection

Samples from all groups were stained with toluidine blue for evaluation of proteoglycan production at days 7 and 21 of culture. The presence of the chondrogenic marker is visualised by the appearance of a metachromatic purple coloration on the samples, while the cytoplasm is visualised as blue. A moderate production of proteoglycans after 7 days of culture was observed for all groups except the control group with cells only (Figure 3-17). The marker was mostly exhibited on the periphery of the samples and the distribution was not observed to be homogenous. After 21 days of culture the production of proteoglycans had increased for all groups with lower amount of metachromatic stain observed for the control. The distribution of the stain followed the same pattern as day 7, with the difference of increased areas on the periphery of the samples that showed proteoglycan deposition. TRPV4-MICA and GSK101 activated samples showed slightly enhanced production of the marker than all the compared groups.

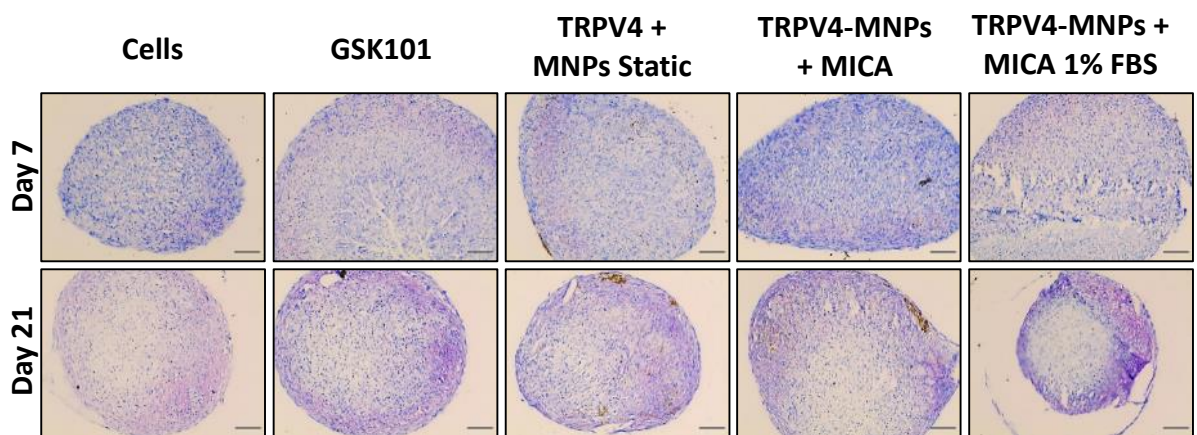


**Figure 3-17. Mechanically and chemically TRPV4 activated samples showed enhanced proteoglycan production.** Representative images of 7  $\mu\text{m}$  pellet sections from hMSCs cultured in 10% FBS and 1% FBS and stained with toluidine blue for GAGs detection at days 7 and 21 of culture. The stain shows a purple colouring when bound to GAGs and a blue tone for the rest of the structures. Scale bar = 100  $\mu\text{m}$ .

### 3.4.6.4 Collagen study

The total collagen deposition in pellets was studied by picosirius red staining. Collagen fibres are stained in red and the cytoplasm stains in yellow. Collagen production was clearly visualised from early time points for all sample groups with the exception of the control and TRPV4 MICA-activated samples cultured in 1% FBS (Figure 3-18). Both TRPV4 chemically and mechanically activated samples showed an enhanced deposition of collagen at day 7, with a homogeneous distribution among the surface of the section. An increased production of the marker was observed after 21 days of culture; however, MICA activated samples cultured in 10% FBS showed apparent lower production of the marker than observed for earlier time points. Samples labelled with TRPV4-MNPs under static conditions, and samples with GSK101, had enhanced collagen deposition when compared to any of the studied groups. The deposition of collagen was only observed to be moderately homogeneous for unstimulated TRPV4-MNPs labelled samples, however, lower production of the marker was observed on the centre of the section. The remaining experimental groups presented collagen stain localised mainly in the periphery of the sections.

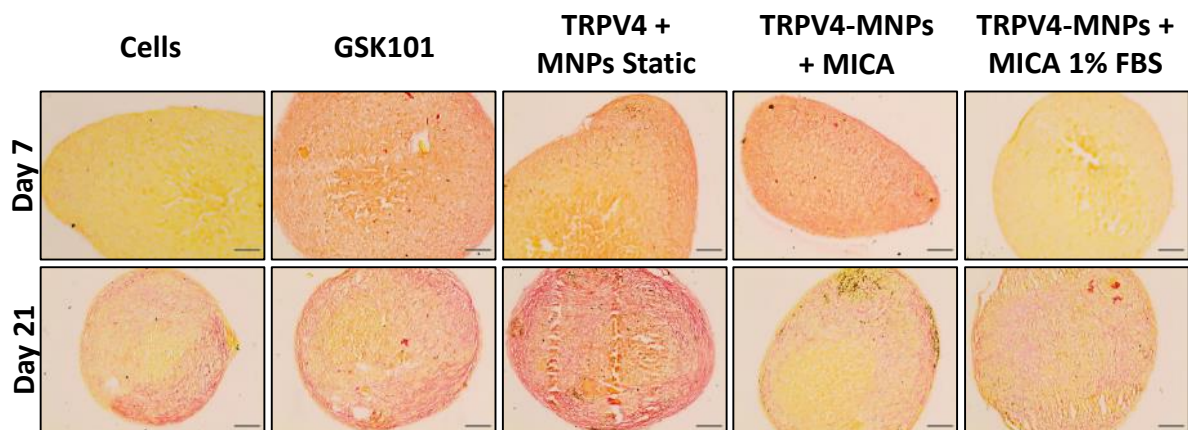


**Figure 3-18. Higher collagen deposition for TRPV4 static samples.** Representative images of 7  $\mu\text{m}$  pellet sections from hMSCs samples cultured in 10% FBS and 1% FBS were stained with picosirius red for collagen reveal at day 7 and day 21 of culture. Collagen fibres are shown in a red colour and the background in yellow. Scale bar = 100  $\mu\text{m}$ .

The production of the cartilage-specific marker collagen II was revealed by immunohistochemical staining of pellet sections. The presence of the marker was detected at early time points for all studied groups, with a discrete production for control and MICA-activated pellets cultured in 1% FBS (Figure 3-19). In contrast, MICA-activated samples cultured in 10% FBS showed an enhanced production of collagen II when compared to all groups. The distribution of the marker was moderately even on the pellet sections; however, all groups had small spots of higher deposition of the marker. The presence of the marker appeared to be reduced after 21 days of culture for all groups, being barely observable in the cells only control group either by a remodelling of the ECM of the samples or most likely due to a technical issue with the antibody used or the staining technique. The collagen II deposition for the remaining groups was observed to be discrete and had a less homogeneous distribution than observed for previous time points.

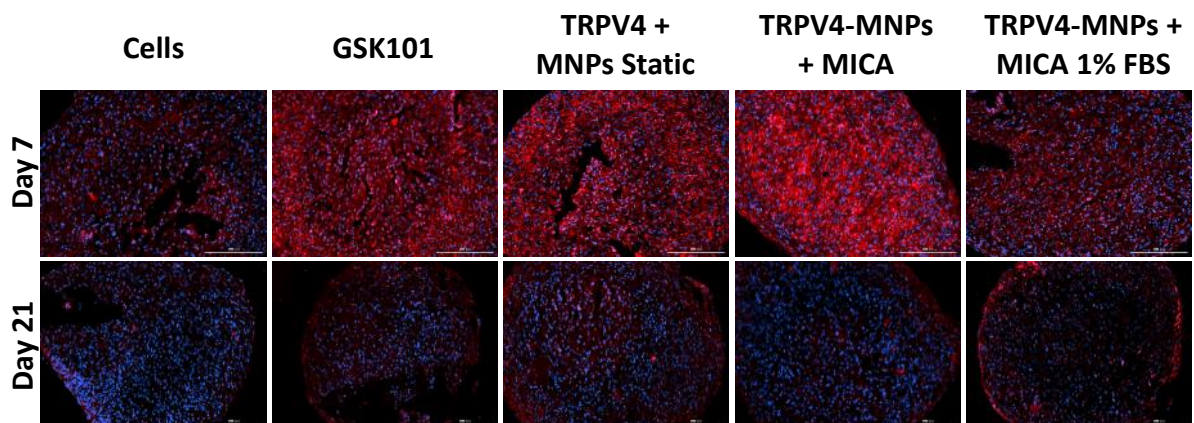


**Figure 3-19. Enhanced collagen II production for MICA activated samples in 10% FBS at early time points.** Representative immunohistochemical fluorescence images of 7  $\mu\text{m}$  pellet sections of hMSCs at day 7 and day 21 for all groups cultured in 10% FBS and 1% FBS. Collagen II is shown red and DAPI stains nuclei in blue. Scale bar = 200  $\mu\text{m}$ .

The fluorescence from images from immunohistochemical analysis of collagen II was quantified by Image J. The quantification of the images matched visual observation of the samples with a decrease of collagen II with culture time. Control samples with cells, showed significantly lower deposition of the marker for all time points when compared to other groups (Figure 3-20). Higher levels of collagen II deposition were found among cells cultured with GSK101 and TRPV4-MNPs labelled cells (static and

MICA activated) cultured in 10% FBS. However, variation of the expression was found among these groups for several time points, with no clear trend being observed. MICA activated samples cultured in 10% and 1% FBS followed a similar expression pattern, with decrease of the marker deposition after 14 days of culture, being higher the expression for samples cultured in 10% FBS.

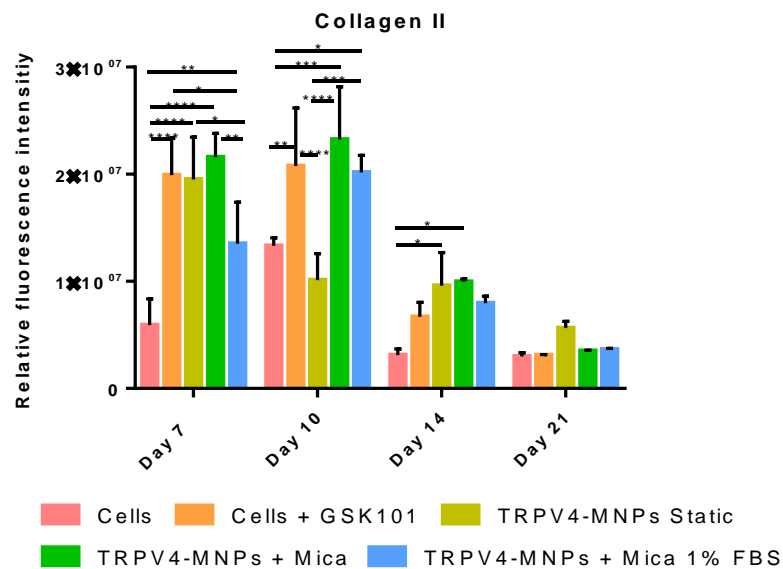


**Figure 3-20. Decrease of collagen II signal with culture time.** Collagen II quantified data was obtained from 3 images of each group and quantified by Image J. Data is expressed as the mean  $\pm$  standard deviation, \* $p < 0.05$ , \*\* $p < 0.01$ , \*\*\* $p < 0.001$  and \*\*\*\* $p < 0.0001$ .

### 3.4.7 Chondrogenic early transcription factor study

The effects of TRPV4 mechanical (MICA) and biochemical (TRPV4 agonist) activation were studied on the chondrocyte human cell line TC28. The early expression transcription factors known to be related with chondrogenesis were measured 4 hours after TRPV4 stimulation or 4 hours' post-incubation, for labelled and unlabelled samples under static and dynamic conditions. The transcription factors studied were selected according to a previous study by our collaborators Dr. Steven Woods and Prof. Sue Kimber, where *JUN*, *MAFF*, *NFATC2* and *RCAN1* showed a high response following GSK101 activation, and *SPP1* and *BTG2* reported to have a low activity.

The gene expression analysis revealed as expected higher expression of *JUN*, *MAFF* and *RCAN1* for the TRPV4 activated samples with shared results for experiments 1 and 2 (Figure 3-21). Despite the same trend was observed for experiments 3 and 4, some variability was observed on the expression response with an increased expression for the control group. *NFATC2* and *SPP1* expression showed lower activation of the transcription factors for all groups, with an increased activation in experiment 4, for both cases. *BTG2* expression was statistically higher for MICA activated samples for experiments 1 and 2 and differences were reduced in experiments 3 and 4, which were observed to present some variability.

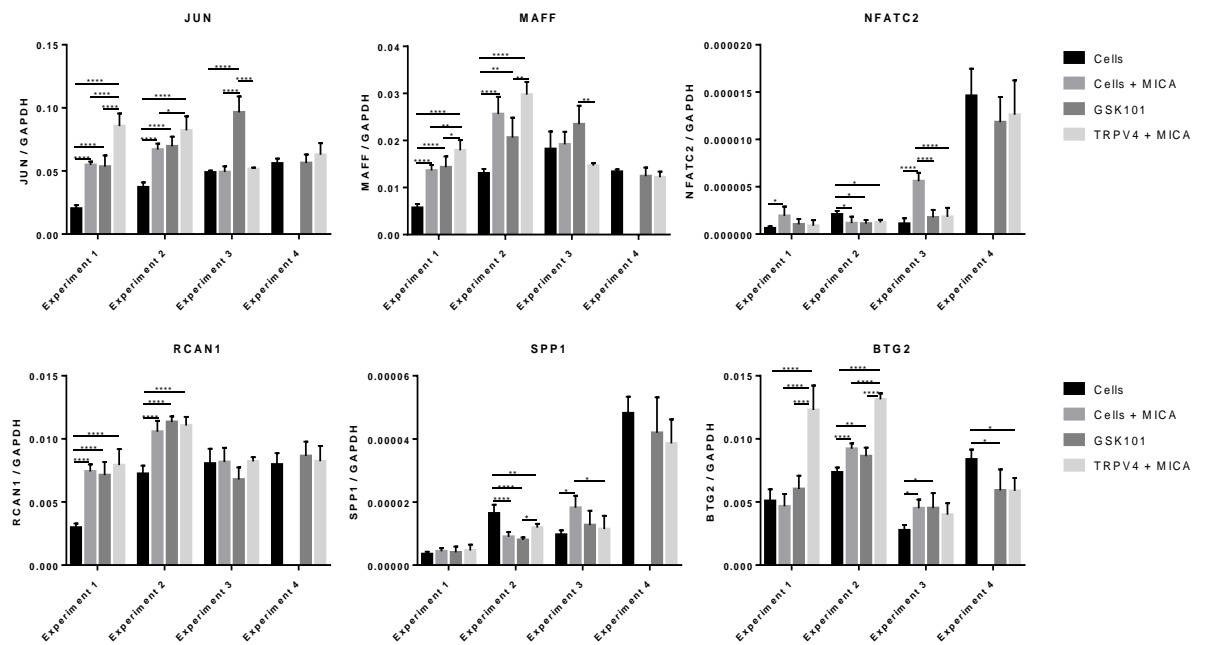


**Figure 3-21. Chondrogenic transcription factors were activated for TRPV4 activated samples with GSK101 or MICA stimulation, with little variation across experiments.** qRT-PCR performed on monolayers of TC28 cells 4 hours after activation. Experiments were replicated 4 times with one group missing for experiment 4. Results expressed as relative expression to *GAPDH*. Data are expressed as mean  $\pm$  standard deviation, n=5 (n=3 technical repeats), \*p<0.05, \*\*p<0.01, \*\*\*p<0.001, \*\*\*\*p<0.0001.

### 3.5 Discussion

Particle design and surface modification highly influence the properties of the MNPs (175). This is of special importance when using the particles for clinical therapies due to the contact of cells with systemic circulation and the targeted tissues. More specifically, the particle size impacts the magnetic properties, key for some applications such as magnetic hyperthermia, MRI or magnetic activation (257). Commercially available 250 nm Nanomag MNPs were used for all experiments during this work to ensure the homogeneity of the particle sizes and the superparamagnetic properties required for the magnetic activation conducted for this work. Regardless of the specified manufacturer information it is important to characterise the particle properties prior to initiation of any experiments. The dynamic light scattering measurement of the hydrodynamic size was in accordance with the manufacturer's specifications. Surface modification of the particles also introduces changes in the particles properties by the formation of a "corona" of antibodies, as demonstrated by changes in the hydrodynamic size following the coating of the particles with TRPV4 antibody (258). A further study on the particle size under the influence of FBS, that is reported to form a corona and increase the particle size, would have been beneficial for the understanding of the differential effect of MNPs on samples cultured in high and low concentration of FBS (259).

The size and the bioactivity properties of the MNPs can also change due to particle aggregation (260). Aggregation events often occur due to the lack of electrostatic charge that maintains particles separated due to repulsion forces, or by covalent binding of the coating biomolecules. Moreover, particle aggregation can affect the uptake efficiency by the cells. Despite the surface modification of the coated antibody, the charge of the particles was not reduced, but on the contrary, slightly increased giving the solution a higher stability. This effect was attributed to the stability brought by the carbodiimide chemistry coating of the particles that produces stable antibody-MNPs conjugate complexes.

Surface characterisation of the particles plays a crucial role for *in vivo* delivery of MNPs. Particles exceeding the 200 nm size are often phagocytised by the macrophages hence, modification of the surface properties can achieve for the particles to remain longer time in systemic circulation until reached the target tissue (261). Surface modification of the particles requires for a series of reactions that initiate with the activation of the particles by carbodiimide coating followed by antibody binding. The surface functionalisation generates specific antibody orientation due to the packing density, leading to the antigen binding domain of the antibodies to be oriented away from the particles increasing the probability of binding the antigen (262). Particles were coated with an excess of antibody in order to ensure the saturation of the MNPs surface with the antibody. Protein quantification demonstrated the presence of the protein in the samples, measured in accordance with the amount of antibody supplied to samples labelled alone with the secondary antibody, and samples labelled with both the primary and secondary antibody. The discrete difference of the protein found among coated samples, compared to the total amount of antibody used for the coating was hence a result of the excess of protein supplied to the particles, to ensure all available surface was covered. Protein levels found among uncoated samples were attributed to the reagents used during the activation of the particles interfering in the assay.

Despite the abundance of studies performed on toxicity of MNPs for biomedical applications, the high amount of factors influencing the toxicity makes it essential to assess the cytotoxicity for every individual study (263). Iron oxide particles have been reported to be non-toxic for injectable therapies, however, the biodegradation of the particles generates metal ions that can generate toxicity events such as oxidative stress or inflammation (245,264). Moreover, the MNPs could potentially lead to the generation of reactive oxygen species (ROS) that generate DNA damage and toxic effects on the cells affecting the metabolic activity and the proliferation of the cells (265). The toxicity of the MNPs used for this work was tested for all different forms of culture by measuring the metabolic activity. An initial lower activity was observed by the first week of culture, followed by a tendency towards an increased

metabolic activity after day 7 of culture. The observed data would match with current literature reporting a decrease of the proliferative and metabolic activity of cells when undergoing differentiation events (266,267). Nevertheless, the reagent used for the metabolic assay was thought to only be able to penetrate into the pellets for early time points, given the solid and compact structure obtained due to matrix deposition. The evaluation of the proliferation in pellet sections allowed for the examination of the complete depth of the pellets with a suspected higher tendency for dead cells to locate in the deeper areas of the pellet. Necrosis in the centre of the pellet has been widely reported in the scientific community specially for larger pellets (268–270). Moreover, the proportion of dead cells on each group indicated a similar ratio of dead cells after the first week of culture, which was attributed to difficulties for nutrient and oxygen to reach the core of the samples. Nevertheless, proliferative events were continued along the culture time for cells labelled with TRPV4-MNPs following MICA activation. Hence, it was hypothesised that cell death was not due to the MNPs presence and MICA activation can positively influence cell proliferation.

Internalisation of MNPs occurred within 3 hours of labelling the cells with MNPs. Reduced metabolic activity over the first day of culture would also be a direct consequence of the reduced activity of the cells due to the phagocytosis events. The regulation of the channel trafficking is key for the regulation of the channel activity and the mechano-sensitive role. Mechanical stress is a regulator of TRPV4 activity known to trigger the rapid exocytosis of the receptor (271). Moreover, activation of TRPV4 with the agonist GSK101 has been reported to increase the  $[Ca^{+2}]_i$  within the first-minute after activation due to channel transport to the membrane. After 30 minutes the channel is known to recycle and internalise, a process required for the downstream signalling events (250). The formation of vesicles was observed in both TEM images taken 3 hours and 48 hours after MNP incubation. The internalised particles were observed to be attached to the vesicle membrane. This could potentially be due to particles tagged to the TRPV4 channel being internalised together with the receptor, following the activation exerted by the specific tagging of the particles to the mechanotransductive

domain of the channel. A further study fluorescently labelling the channel would allow for a better understanding of the channel trafficking. Nevertheless, the visualisation of MNPs taken by the cells was able to be demonstrated by TEM images.

The TRPV4 channel has been described to be present in a variety of tissues such as cartilage, heart, kidney, sensory neurons or liver (135). Regardless of the broad evidence of TRPV4 presence and role in MSCs mechanotransduction, immunohistochemical detection of the channel was performed to determine the presence of TRPV4 for all cell types used for this work (165,272). TRPV4 was effectively detected in human, equine and ovine MSCs and in human UC-MSCs. This data was also supported by flow cytometry analysis in hUC-MSCs and equine MSCs with a high proportion of the population expressing the channel, satisfying the needs for the TRPV4 targeting work.

Human MSCs potential for chondrogenic differentiation has been the focus of many studies for cartilage regeneration tissue engineering approaches (55,70,273,274). The *in vitro* study of chondrogenesis is often performed in 3D culture. This protocol began to be performed after demonstration that chondrocytes were not able to retain the phenotype in 2D culture (275,276). 3D culture of dedifferentiated chondrocytes or MSCs has been observed to form constructs that resemble more to *in vivo* chondrocyte phenotype due to the formation of a micro-niche within the cell pellet (277). Human MSCs chondrogenic potential was assessed hence, using a 3D pellet culture model. The addition to culture media of chondrogenic-inductive factors successfully guides cells towards chondrocyte differentiation nevertheless, many authors expose the need for additional stimulation for an adequate chondrogenic differentiation (278). This work aimed to test the potential of the MICA technology to achieve a construct with a quality resembling to that of native tissue. The preliminary study conducted on human MSCs showed that culturing the cells with chondrogenic media alone was not sufficient to achieve a satisfactory level of chondrogenesis. Histological analysis of the samples evidenced the low deposition of cartilage-like markers. The stimulation of the TRPV4 channel, biochemically with GSK101 or mechanically with TRPV4-MNPs resulted in an improved chondrogenic

response with higher deposition for all examined markers. More interestingly, it was also observed an early production of the marker deposition if compared to those samples cultured in chondrogenic media. Samples containing unstimulated TRPV4 MNPs-labelled cells also showed an improved chondrogenesis than control samples. This was attributed to the side effect caused by targeting the MNPs into the mechano-sensitive domain of the channel. The collagen II analysis showed an enhanced production of the marker for the TRPV4-stimulated samples that was dramatically reduced after 2 weeks of culture. As only 1 pellet was available for this test, the analysis could not be repeated and hence it was hypothesised to be an isolated issue generated by either remodelling of the pellet structure or a user-related error.

The initial study of the MICA effect on chondrogenic transcription factor activation revealed elevated expression for TRPV4 activated samples for those transcription factors related to chondrogenesis. *JUN* has been described to have a role in the signalling pathway of chondrocytes following mechanical activation (279) and *MAFF* has been involved in chondrocyte differentiation (280). *RCAN1* was also observed to be elevated for TRPV4 activated samples matching previous literature (281), however, the expression of *NFATC2* was expected to follow a similar trend due to the tight relation of both factors. *RCAN1* and *NFATC2* act together regulating the calcineurin synthesis required for IL-2 activation (282). The expression of the anti-proliferation factor *BTG2*, was down-regulated together with the expression of *SPP1*, a transcription factor controlling bone osteopontin activity. This results were in line with our collaborators expression panel observed following TRPV4 activation with GSK101 (281). Nevertheless, a further study of the transcription factors expression time lines and activated signalling pathways, and the relation to chondrogenic events could throw some light into this preliminary results. RNAseq was performed on these samples with the aim better understanding the events following TRPV4 mechanical and chemical activation (Supplementary figures 1 and 2).

### 3.6 Conclusions

The experiments conducted for this work required an initial characterisation of the MNPs and the stem cells studied. Commercially obtained 250 nm Nanomag particles met manufacturer's specifications. The surface modification of the particles with antibody coating, had an impact on the particles properties. Despite the increase observed in the hydrodynamic size, the particle suspension was found to be slightly more stable than plain particles, being beneficial for this work's application. The cytotoxicity study of the MNPs was performed for all forms of culture with no observed effects on the metabolic activity of the cells. Nevertheless, the proliferation of the cells was reduced with culture time and a longer study would be required to assess if the reduction was due to differentiation events or was a temporary effect. However, it is safe to conclude that the MNPs used for this study did not interfere with the proliferation or differentiation of the cells.

The MICA technology that will be used during this work, required the presence of the TRPV4 channel in the cell membrane of several cell types. TRPV4 was successfully demonstrated to be expressed in the cells employed during this work. In addition, the chondrogenic potential of hMSCs was tested for comparative purposes with other cell types. The culture of cells with chondrogenic media alone was not sufficient to induce cartilage-markers adequate production. Further experiments will focus on enhancing the chondrogenic differentiation by using the MICA activation of the cells.

---

# *Chapter 4*

---

## *Assessment of MICA potential for in vitro chondrogenic induction in animal cells*

## 4.1 Introduction

Cartilage repair has often been the target of stem cell-based therapeutic approaches. The selection of MSCs as a cell source for tissue engineering applications, is based on the immunomodulatory potential of the cells and the chondrogenic ability widely demonstrated *in vitro* and *in vivo* (283,284). Nevertheless, *in vivo* studies often encounter difficulties in achieving regenerated tissue with the structural and functional demands of healthy tissue (285). In addition, the tissue formed is often classified as fibrocartilage and has a tendency to degrade over time, introducing the need for a second follow-up procedure (286).

The lack of vascularisation hinders the systemic repair of the tissue, which is exposed only to the niche microenvironment. Current available approaches focus on the symptom relieve until the level of degeneration hinders the autonomy of the patient, or until they reach the appropriate age for knee replacement. Although surgical joint replacement often reports good outcomes, the implants usually last around 15 years, introducing the need for a second surgery (287,288). The lack of long term and non-invasive treatments has led a gap for the scientific community to investigate for an approach that can fulfil the current medical needs.

Despite most current novel approaches point towards the use of stem cells for cartilage repair, none of this approaches has seen the approval of the European Medicines Agency (EMA). Regardless of the potential of these approaches, broad evidence of safety and efficacy needs to be delivered in order to obtain either a use or commercialisation authorisation. Moreover, and despite the great amount of ongoing clinical trials based on intra-articular injection of MSCs, an innovative idea is also essential for approval of the treatment (289,290). These requirements, in addition to the need for the novel approach to be able to demonstrate higher benefits than current approaches, greatly hinder the development on novel treatments for OA repair. With this in mind, our group has developed a novel strategy for remote repair of the cartilage focused on the mechano-transductive potential of MSCs.

Previous studies have used targets such as Wnt, TREK-1 or RGD mostly for bone repair, with exciting results at promoting the successful differentiation towards the osteogenic lineage (220,224). The potassium channel TREK-1 controls the cell excitability and membrane potential and, therefore, has been widely studied for its role in the central nervous system (291). The RGD peptide has also been used to activate the receptor ligand of the integrin receptor  $\alpha 5\beta 1$ . This receptor has been identified as a cell adhesion site, and has been targeted for activation for several applications such as improving cell adhesion into scaffolds for osteogenic differentiation, or enhancing proliferation and tissue growth on scaffolds (292,293). Regardless of the evidence suggesting the role of these receptors in mechanotransduction, the effects on driving MSCs chondrogenic differentiation have not been yet examined.

Unlike RGD and TREK-1, the non-selective cation channel TRPV4 has been widely described to play an essential part in chondrogenesis (1,171). The channel is expressed in chondrocytes and has been described as a regulator of the chondrogenesis and also has a role in the maintenance of healthy adult cartilage (281). TRPV4 activation induces the activation of downstream signalling events that trigger *SOX9* expression that controls the expression of collagen II and aggrecan. *In vitro* activation of the receptor has been achieved by delivery of mechanical forces, such as low ultrasound or tensile strength, and by chemical activation with the TRPV4 agonist GSK101 resulting in *SOX9* expression (165,294,295). Given the implication of TRPV4 in the formation and the maintenance of the healthy tissue, the increased expression of the channel observed in OA patients is surprising (296), however, it has been hypothesised that other pathways are involved in this process (164). The activation of *SOX9* expression by TRPV4 is mediated by the  $Ca^{+2}$  / calmodulin signalling pathway, which commences with the C-terminal domain of the ion channel, and is directly responsible of the alterations of the intracellular  $[Ca^{+2}]$  that lead to intracellular signalling pathways (145).

The TRPV4 signalling pathway has also been studied in relation to TGF- $\beta$  pathway. TGF- $\beta$  is a growth factor known to play an essential role in the cartilage formation, and is also related to mechanical

loading and calcium signalling (297,298). This growth factor is secreted as an inactive protein that binds the type I and type II TGF- $\beta$  cell surface receptor, with the subsequent formation of an active complex that leads to the phosphorylation of the transcription factors SMAD2/3, which in turn interact with SMAD4. The formation of the SMAD2/3-4 complex triggers the decondensation of the chromatin with subsequent gene transcription activation (281,299). TRPV4 and TGF- $\beta$  have been associated by the enhancement of the TGF- $\beta$  signalling pathway following the activation of the ion channel (281). Nevertheless, the activation of the TRPV4 channel is subject to tight control and small alterations in the channel activation, resulting in repression of the TGF- $\beta$  signalling pathway, are needed for initial chondrogenic differentiation and avoidance of the hypertrophic phenotype (300).

Several studies have focused on the mechanical activation of the channel by delivering mechanical stresses to the cells, and observed an increased chondrogenic activity with enhanced matrix deposition, increased cartilage-like gene expression, in addition to anti-inflammatory effects (167,301,302). Nevertheless, delivery of mechanical stresses at a tissue or cellular level, can potentially lead to activation of unspecific receptors with unknown effects on the cells. Moreover, often the mechanical activation is delivered directly to a scaffold, and difficulties have been encountered when aiming to translate the mechanical forces to a cellular level. The MICA technology allows for specific activation of the cell elements, being able to individually target the desired receptor. Introducing the selective activation of TRPV4 with MNPs, could enhance the chondrogenic differentiation of cells, without introducing the risk for unspecific target activation.

Cartilage tissue engineering approaches aim to generate tissue constructs that match the functional and anatomical structure of the native cartilage. Despite the advances achieved by introducing the use of scaffolds and mechanical stimulation into these applications, researchers often find that newly formed tissue does not fulfil the load-bearing requirements of the original tissue, and fails to meet the criteria for being considered functional cartilage. One of the fundamental elements to achieve the required mechanical functionality is the development of the ECM. Cartilage ECM is primarily

composed of collagen type II and a proteoglycan network containing GAGs among others and is under constant renewal by degradation of the matrix with metalloproteinases and regeneration by the resident chondrocytes. Moreover, the ECM plays a role regulating the chondrocytes' functions by the signalling events promoted by the cell-matrix interaction (303). The loss of the ECM native structure results in a loss of the functionality as observed with the progression of OA (304). Hence, the difficulty of the cartilage tissue engineering resides on the adequate fabrication of a stiff matrix, that gathers the load distribution and compression resistance qualities present in the native tissue.

With the aim of analysing the quality of the cartilage matrix achieved through tissue engineering applications, many studies base the classification of the cartilage ECM properties in the histological analysis of the constructs. The histological assessment of the tissue and the grading of the construct anatomical aspects, is broadly used as a scoring system of the cartilage quality allowing for comparison among different studies (36,305). Despite the constant improvement of the scoring matrix and the advantages brought by visual observation of the tissue structure, the possibility of quantifying the chondrogenic activity could improve the inter-study comparison of the chondrogenic potential. During the progress of this work, histological analysis of the samples has been used as the main method for visualisation of the ECM components for most of the studied cells. Nevertheless, the possibility of using collagen II reporter eMSCs by the expression of the GFP-Col2 and the Luciferase-Col2 promoter, introduced the possibility of using an additional method to measure and quantify the chondrogenic activity of MSCs under different experimental conditions.

The work conducted in this chapter is an initial approach to the MICA technology. With the objective of establishing novel targets for the remote magnetic activation of MSCs for guiding chondrogenic differentiation, several membrane proteins were tested under different culture conditions. The work of this chapter is divided into two parts. Firstly, an initial study of the pharmacological targets for MICA technology was performed using the reporter eMSCs to measure the chondrogenic activity. The second part of this chapter was focused on responding to the questions raised by the initial work, with

the aim of optimising the MICA technology for future work. For this part of the work oMSCs were used as a tool for comparative purposes with previous work performed by our group in bone regeneration in a pre-clinical animal model.

## 4.2 Aims

The aims of this chapter were:

- To assess the best therapeutic target for driving chondrogenic differentiation with the MICA technology
- To examine the effect of TGF- $\beta$  in the TRPV4 transduction pathway
- To quantify the level of chondrogenesis induced by the MICA technology with a cell reporter system and through in-depth histological analysis
- To optimise the MICA technology for future work in human cells

## 4.3 Methods

### 4.3.1 Experimental design: Part I

The work of this chapter is divided in 2 sections. For the part 1 of the chapter, adipose-derived reporter equine MSCs were used, kindly gifted from Dr. Glyn D. Palmer (University of Florida). Two different cell lines were used, a GFP-Col2 reporter cell line constitutively transfected with d-Tomato, and Col2-Luciferase cells with a control cell line referred as cytomegalovirus (CMV)-Luciferase, with constitutive expression of luciferase.

Cells were cultured and expanded as explained in section 2.3.3, labelled and cultured as micromasses in 12 well-culture plates (sections 2.5 and 2.3.6). The fluorescence emitted by the cells was directly proportional to the collagen II expression and was closely monitored by fluorescent microscopy on a daily basis, and imaged after micromass formation and at days 7, 10, 14 and 21. Micromasses often showed accelerated growth and cell detachment from the well plate and hence, some experiments

were terminated after 14 days of culture. Cells were also cultured as 3D pellets following the protocol in section 2.3.7 and samples were cultured for 21 days with the exception of experiment 2, which aimed to analyse the effect on chondrogenesis over longer culture periods (28 days). Labelled samples received stimulation as per indicated in section 2.6. The metabolic activity measurement was performed following the protocol in section 2.10.1.

The experiments performed during this chapter were adapted and optimised according to the initial experimental findings. The layout of the design for each experiment is indicated in table 4.1. Each experiment is referred to both micromass and 3D pellet culture, however, the analysis was divided between both forms of culture according to the test requirements.

**Table 4-1. Experimental conditions of the eMSC study performed in pellets and micromasses.**

|           | Experiment 1                             | Experiment 2  | Experiment 3  |
|-----------|--|---|---|
| Aim       | MNPs target assessment                   | MICA and TRPV4 effects in chondrogenesis                      | Collagen II production quantification                               |
| Cell type | GFP-Col2                                 | GFP-Col2  | Col2-Luciferase   |
| Analysis  | Fluorescence imaging<br>Histology<br>PCR | Fluorescence imaging<br>Histology<br>PCR<br>DMMB / Pico Green | Luciferase detection<br>Histology (Not shown)<br>Metabolic activity |

### 4.3.2 Collagen II tracking

The Col2-GFP follow-up was performed using the Nikon Eclipse Ti-S for experiment 1 and the Cytation 5 microscope for experiment 2. Images were taken when visual changes were observed. Samples from experiment 1 were cultured in chondrogenic media, detailed in section 2.4, with and without TGF- $\beta$  in order to assess the effect of MICA on a less chondro-inductive environment. For experiments 2 and 3 the same chondrogenic media was used with all the differentiation factors added. For experimental purposes, samples were studied with and without magnetic field.

### 4.3.3 Histological and immunohistochemical analysis

Histological processing of the micromasses and pellets was carried as indicated in sections 2.7 and 2.8. Samples were stained with alcian blue for sGAG reveal (section and 2.7.7), picosirius red for collagen detection (section 2.7.8), safranin O as a cartilage stain (section 2.7.10) and prussian blue for MNPs visualisation (section 2.7.9). Samples were imaged using the EVOS XL microscope.

Pellets were sectioned and processed (section 2.7) and immunohistochemical analysis of the proliferation marker PCNA and the presence of TRPV4 were evaluated following indications in section 2.9. Samples were imaged using the Cytation 5 microscope.

### 4.3.4 Primer optimisation and gene expression

Gene expression analysis was performed on pellets from experiments 1 and 2 following the protocol detailed in sections 2.15, 2.16 and 2.17. Pellets were collected at days 0, 7, 10 and 21 and digested and stored at -80 °C until the termination of the experiment. As primers were customised, optimisation was made prior to use in order to find the adequate melting temperature and ensure the lack of dimers presence. This was done by running the amplified products in an agarose gel as explained in section 2.18 (results not shown). Samples were found difficult to digest for time points later than day 7 and were manually disaggregated with the aid of a pestle prior to RNA extraction. For the gene expression analysis 4-5 samples from each group were measured in triplicates.

### 4.3.5 DNA and sGAG analysis

The determination of the total amount of DNA present in the pellets from experiment 2 was quantified by Pico Green<sup>TM</sup> assay following the protocol on section 2.14. Total sGAGs present in the pellets were quantified by DMMB as detailed in section 2.13. Both assays were performed in triplicates with 3 technical repeats. The sGAGs were normalised to each sample's DNA amount.

#### 4.3.6 Luciferase detection

For experiment 3, cells transfected with a luciferase reporter linked to collagen II expression were used. The cultured samples received a media change 24 hours prior to obtaining the sample for the quantification. A control group with the CMV/ Luciferase cell was cultured and treated in the same conditions. The secreted metridia luciferase was measured on days 7 and 14 of culture in 3 samples per group and 3 technical repeats, and results were normalised to the CMV-Luc constitutive expression reporter cells. The secreted metridia luciferase was measured with the Takara Ready-To-Glow™ kit as described in section 2.22.

#### 4.3.7 Experimental design: Part II

The second part of this chapter was performed as an optimisation study after the chondrogenic evaluation of the first part of the chapter. For those question left unsolved, further experiments were designed. During this work, the cells used were ovine MSCs supplied by Dr. Hareklea Markides and chondrocytes isolated from ovine knees as per detailed in section 2.3.2. Chondrocytes were used directly following cell seeding for expansion after extraction, and also in a dedifferentiated state at passage 4-5. The chondrogenesis was studied in a 3D pellet culture system, following the protocol on section 2.3.6. Cells were studied alone or labelled with MNPs coated with TREK-1 and TRPV4 antibodies (section 2.5). The samples were cultured in chondrogenic media detailed in section 2.4., and some groups were cultured in chondrogenic media without TGF- $\beta$ . Samples were cultured for a duration of 21 days and pellets were collected after 1, 7, 10, 14 and 21 days of culture. The samples containing MNPs were stimulated 1 hour per day and 5 days a week as per detailed in section 2.6.

#### 4.3.8 Histological and immunohistochemical assessment

The chondrogenic performance was mainly evaluated by conventional histological staining of the sectioned pellets following the protocol in section 2.7. Samples were stained for collagen detection with picosirius red (section 2.7.8), safranin O (section 2.7.10), proteoglycan detection with toluidine

blue and alcian blue (sections 2.7.6 and 2.7.7) and iron detection of the MNPs with prussian blue (section 2.7.9). The sections stained with picosirius red were imaged under a polarised microscope to evaluate the collagen alignment. Samples were imaged using the EVOS XL microscope.

Immunohistochemical analysis was performed following the protocol in section 2.9, using the DAB kit according to the manufacturer instructions for collagen II and aggrecan reveal, and the corresponding antibodies for PCNA evaluation of the proliferative state of the samples (results not shown). Samples were imaged using the Nikon Eclipse Ti-S microscope.

#### 4.3.9 Molecular analysis of chondrogenesis

Pellets were digested at the mentioned time points following the protocol in section 2.15. Samples were left in a sonicator with iced water for 2 hours and then manual mechanical disruption was performed due to the difficulties encountered digesting the samples. Gene expression of *Acan*, *Col2a1* and *Sox9*, was evaluated by qRT-PCR (section 2.17).

#### 4.3.10 Statistical analysis

Statistical analysis was performed as indicated in section 2.24.

## 4.4 Results

### PART 1

#### 4.4.1 Determination of possible chondro-inductive targets for the MICA technology

The MICA potential for guiding chondrogenic differentiation was assessed for 3 pharmacological targets: RGD, TREK-1 and TRPV4. The chondrogenesis was studied in collagen II-reporter eMSCs cultured as micromasses and assessed by visual observation of the fluorescence emitted for each of the groups, which is directly proportional to the collagen II expression. The cells were constitutively transfected with a dTomato dye and imaged at early time points to ensure the adequate transfection of the cells (Figure 4.1).

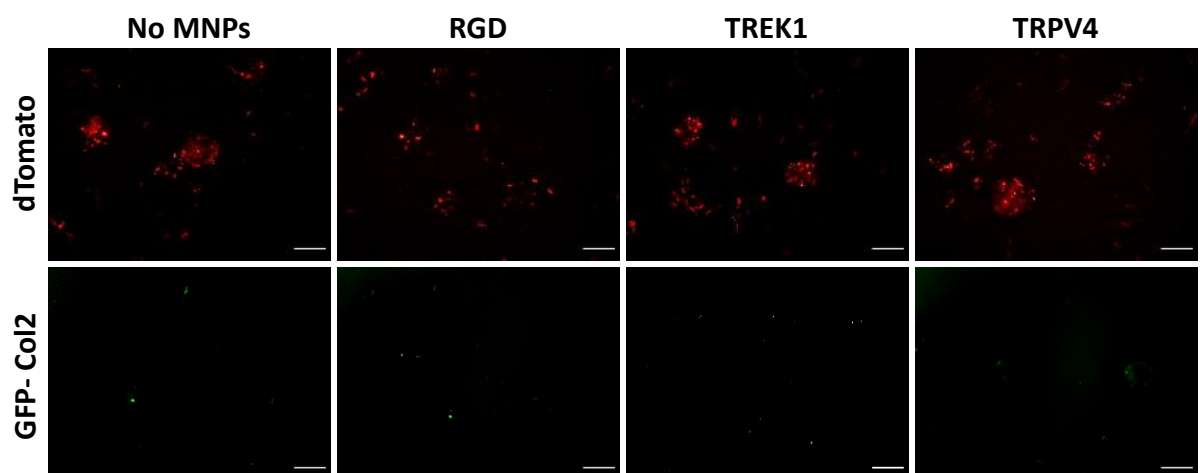


**Figure 4-1. dTomato markers observed in eMSCs indicate successful transfection of the GFP-Col2 reporter.** Representative images of eMSCs cultured in chondrogenic media at day 2 of culture. The visualisation in the micromasses of the dTomato marker (red), and the lack of GFP (green), indicate that cells were transfected correctly and GFP expression is solely controlled by the collagen 2 promoter. Scale bar = 300  $\mu$ m.

With the aim of initially assessing the effects of MICA activation on different receptor tags, cells were cultured in basic media for 21 days. Magnetic stimulation was only applied to the samples labelled

with MNPs. Culture of the micromasses without the presence of biochemical cues was observed to be insufficient for relevant collagen II production for any of the studied groups (Figure 4-2). Micromasses labelled with TRPV4-MNPs showed slightly higher fluorescence than the other groups, however, none of the groups showed chondrocyte-like cell morphology at higher magnifications (results not shown). Regarding the disposition of the micromasses, only TRPV4 activated samples showed small formation of pellets. The remaining experimental groups formed sheets of cells that lost partial attachment to the well plate.

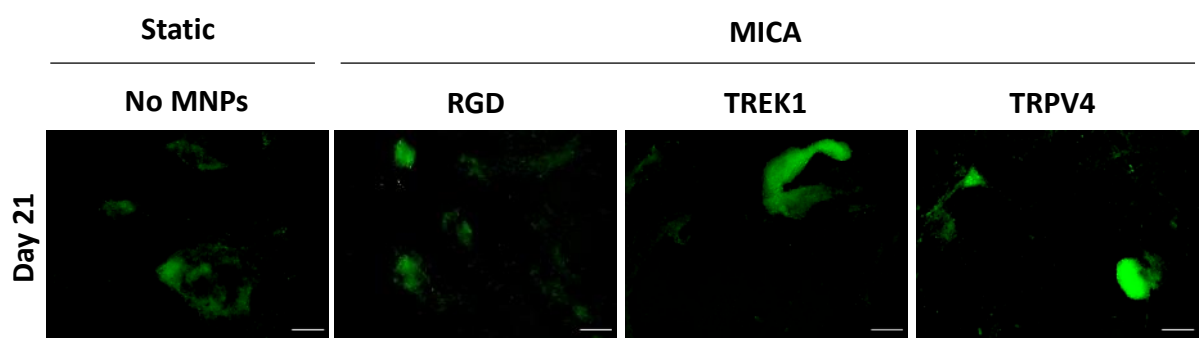


**Figure 4-2. Culture of samples in basic media is not sufficient for chondrogenic induction after 21 days of culture regardless the magnetic activation.** Representative images of eMSCs micromasses viewed as aggregated cell structures, cultured for 21 days in expansion media. Scale bar = 300  $\mu\text{m}$ .

Micromasses were also cultured in chondrogenic media without one of the key differentiation factors, TGF- $\beta$ 3, in order to see the potential of MICA activation. Samples were imaged at several time points, with changes being clearly appreciated every 7 days. Micromasses cultured with no MNPs showed lower collagen II production than all compared groups, however, some signal was detected after 3 weeks of culture (Figure 4-3). MNPs-labelled samples showed a moderate amount of collagen II expression with earlier and higher detection of the marker for TRPV4 activated cells, for all time points compared. TREK-1 activated samples showed similar results to those observed for TRPV4, with slightly lower fluorescence intensity, and RGD-labelled micromasses showed collagen II production levels more akin to those of the static control. For all groups, the micromasses appeared to have formed

smaller forms of cell aggregates similar to pellet formation, being observable the GFP signal for the mentioned pellets and not the individual cells in monolayer.

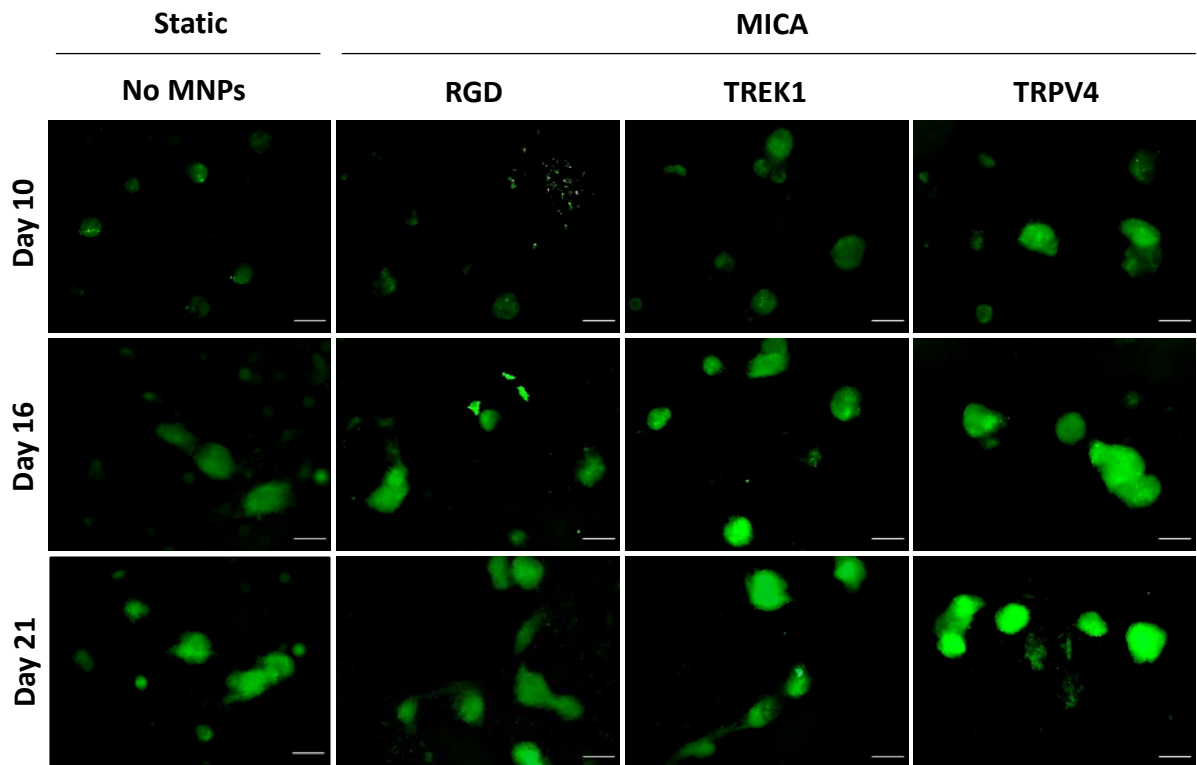


**Figure 4-3.** Regardless of the lack of TGF- $\beta$ , TRPV4-labelled samples showed early expression of collagen II at day 10. Representative images of eMSCs micromasses at days 10, 16 and 21 of culture. Samples were cultured in chondrogenic media without TGF- $\beta$ . Scale bar = 300  $\mu$ m.

The same groups were cultured in chondrogenic media under static conditions (control group with no MNPs), and MICA activation for those samples containing particles. The control static sample showed little signs of collagen II expression for all time points with similar levels of fluorescence after 21 days, to those observed for samples cultured in basic media (Figure 4-4). Interestingly, the expression of collagen II was detected at later time points than observed for the incomplete chondrogenic media, with fluorescence signal beginning to show by day 14. Nevertheless, the collagen II expression peaked by day 21, with higher expression than previously observed for all groups labelled with MNPs. Matching previous findings, samples labelled with TRPV4-MNPs showed enhanced collagen production when compared to other groups, followed in intensity signal by cells labelled with TREK-1.

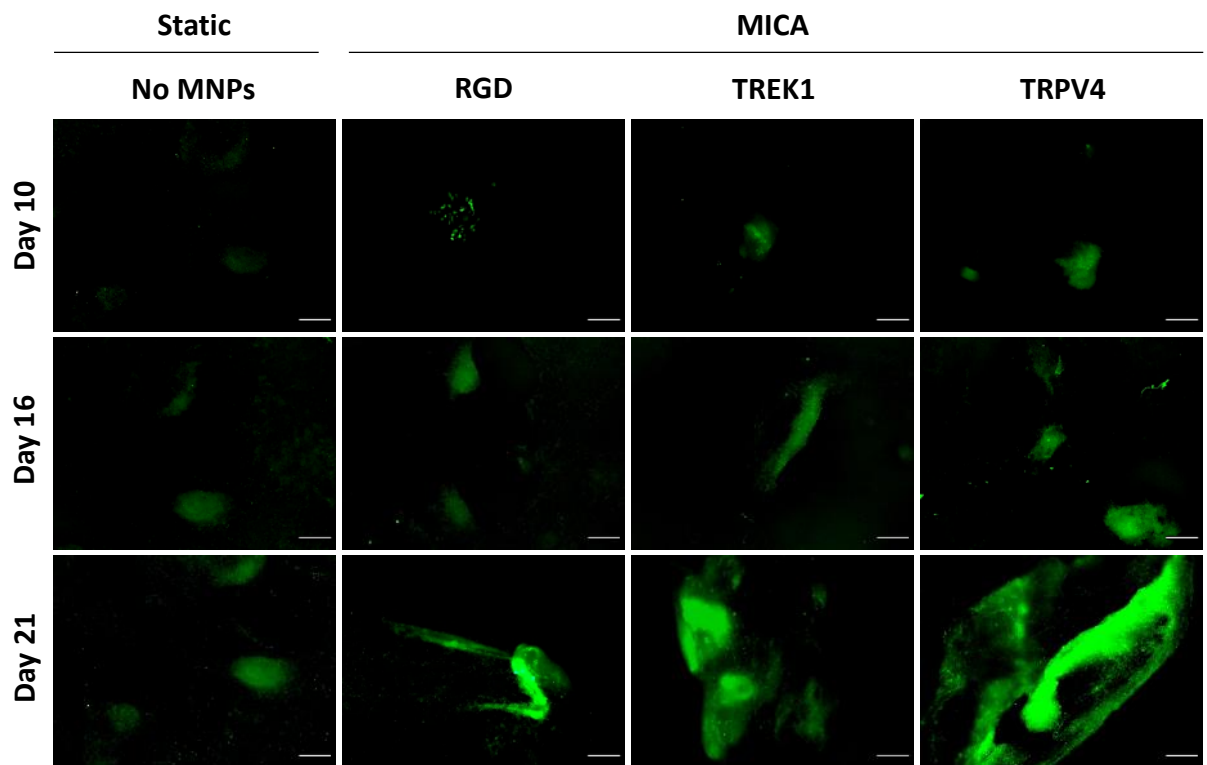


**Figure 4-4. TRPV4 labelled samples showed enhanced collagen II production at day 21 of culture.** Representative images of eMSCs micromasses at days 10, 16 and 21 of culture. Samples were cultured in complete chondrogenic media. Scale bar = 300  $\mu$ m.

The levels of collagen production were also assessed in pellet sections in an experiment replicating the same culture and experimental conditions but using picrosirius red. Sections corresponding to day 2 of culture did not show collagen production for any of the groups, with the exception of TREK-1, which showed a small area with a red coloration (Figure 4-5). After 16 days of culture, all samples labelled with MNPs cultured in both complete chondrogenic media and media without TGF- $\beta$ , showed an irregular collagen deposition. Among the MICA activated groups, RGD produced the lowest amount of collagen, as previously observed in the fluorescence analysis. Similar results were observed between TREK-1 and TRPV4 activated samples for both culture conditions. Interestingly, with the

exception of the control, samples cultured without TGF- $\beta$  had slightly higher collagen production than samples cultured with the complete media.

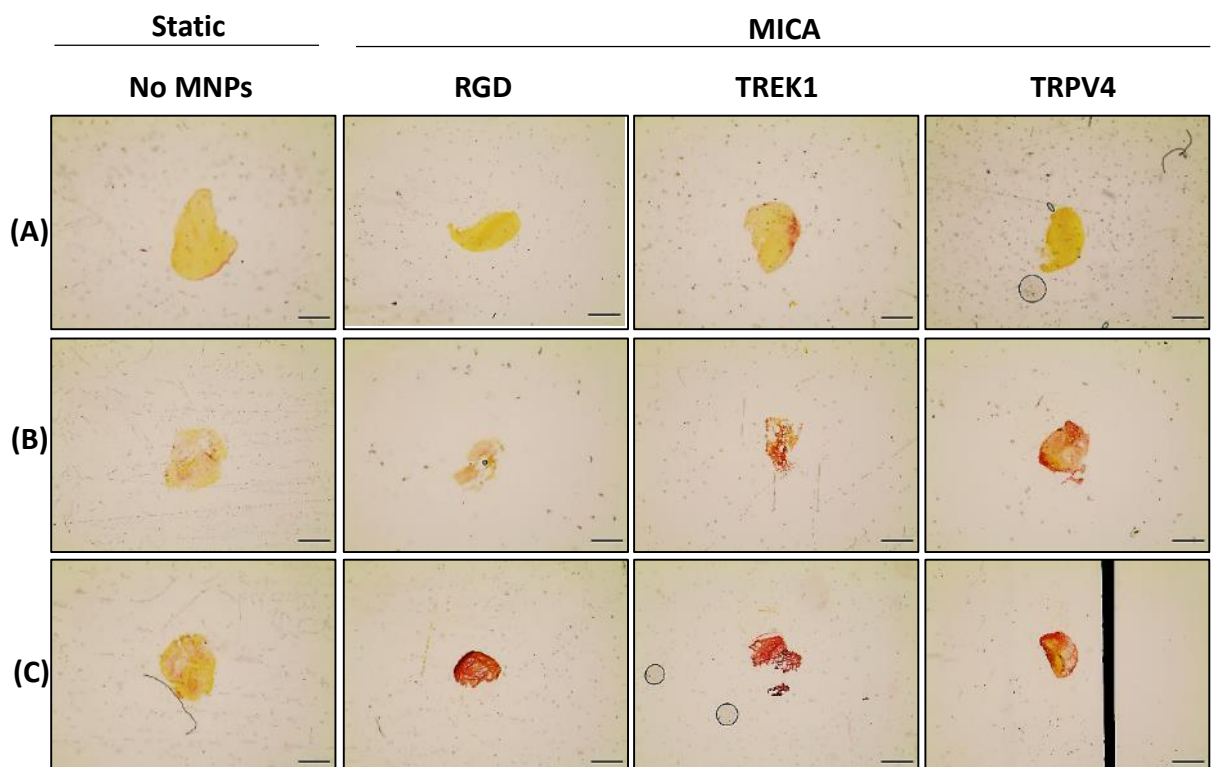


**Figure 4-5. Collagen fibres were observed in all MICA activated samples regardless of the presence of TGF- $\beta$  in the culture medium.** Representative images of 7  $\mu$ m pellet sections from samples A) cultured in chondrogenic media after 2 days of culture, B) samples cultured for 16 days in complete chondrogenic media and C) samples cultured for 16 days in chondrogenic media lacking TGF- $\beta$ . Collagen fibres are visualised in red and the cytoplasm in yellow. Scale bar = 500  $\mu$ m.

Gene expression analysis of the cartilage ECM markers, *Col2a1* and *Acan*, was measured on pellets after 2 and 16 days of culture. The expression of both markers was relatively low, so results are expressed in fold change relative to a control sample cultured in basic media. The analysis revealed significantly higher expression in TRPV4 activated samples cultured in chondrogenic media without TGF- $\beta$ , for all time points and genes measured except for the aggrecan analysis on day 2 (Figure 4-6). TRPV4 activated samples cultured without TGF- $\beta$  after 2 days of culture, showed 760-fold expression to that measured in the basic control. The expression of collagen was low for the remaining measured

groups for both time points. The expression of aggrecan at day 2 of culture was similar for all compared groups, with a tendency for higher expression for samples labelled with MNPs cultured without TGF- $\beta$ . After 16 days of culture however, the differences were increased with higher expression observed for both TRPV4 labelled samples being only significantly different for the pellets cultured without TGF- $\beta$ .

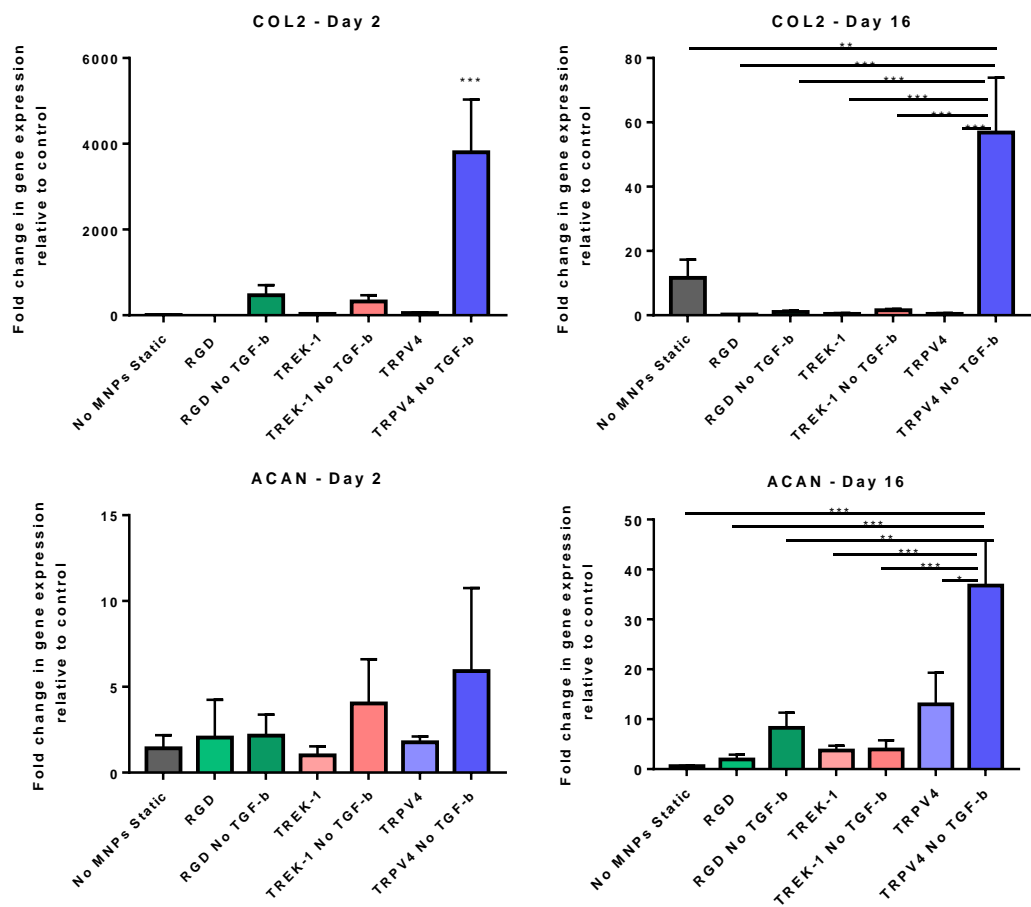


**Figure 4-6. TRPV4 activated samples cultured with TGF- $\beta$  showed enhanced gene expression for all genes and when compared to all groups.** qRT-PCR performed on pellets from experiment 1, after 2 and 16 days of culture. Results expressed as fold change relative to the control samples cultured in basic media and normalised to S18. Data are expressed as mean  $\pm$  standard error, n=4 and 2 technical repeats, \*p<0.05, \*\*p<0.01, \*\*\*p<0.001.

#### 4.4.2 MICA activation of TRPV4 channel

After results obtained from experiment 1, TRPV4 was further studied as a potential chondro-inductive target, and an additional study was performed on the activation of the mechano-sensitive ion channel with and without the effect of a magnetic field. Equine MSCs were cultured as micromasses and a follow-up on the GFP-Col2 fluorescence signal was performed. With the aim of observing the transfection state of the cell line, images were taken on the first day of culture before any stimulation was applied. No signs of GFP signal were observed, however, dTomato constitutive marker was observed in the cells (Figure 4-7). In addition, a bright field image of the cells demonstrated the classical spindle-like morphology of equine MSCs.

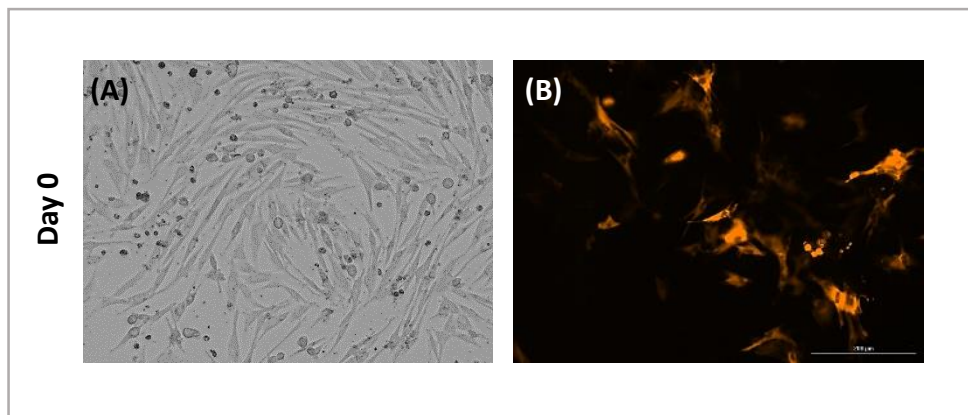


**Figure 4-7. The constitutively expressed dTomato fluorescence was visualised from the initiation of culture with no signs of a GFP-Collagen II signal.** Representative images of eMSCs cultured as micromasses on day 1. A) Bright field image of the spindle-like morphology of the cells. B) Fluorescence images of dTomato fluorescence. Scale bar = 200  $\mu\text{m}$ .

The collagen II production analysis performed by imaging of the GFP transfected cells, showed similar results to those observed in the previous experiment. TRPV4 MICA-activated samples showed presence of collagen II expression from day 7 of culture (Figure 4-8). Samples labelled with TRPV4 that were not magnetically activated, showed signs of initial expression of collagen II, nevertheless, the GFP signal was almost negligible. Control samples without MNPs showed no collagen II expression until the 10th day of culture. Both samples without MNPs appeared to have formed 2 pellets in the

well-plates, and no sign of individual cells was detected. For this reason, the fluorescence observed in the images was a result of all the grouped cells and hence, the images were considered to be partially the result of auto-fluorescence from accumulated cells. TRPV4-MNPs labelled samples formed multiple smaller pellets with individual cells still being able to be visualised. The brighter spots of fluorescence were considered as cells expressing collagen II, with higher expression than observed for the initial time point. After 16 days of culture both samples without MNPs showed similar levels of fluorescence to those seen at day 10, and some single cells seemed to have detached from the pellet. TRPV4-MNPs labelled cells showed a clear increase in fluorescence intensity, being higher for the MICA activated samples. Both TRPV4 groups were observed to have multiple cell pellets among the wells, and the GFP marker was also observed in single cells for the MICA activated group.

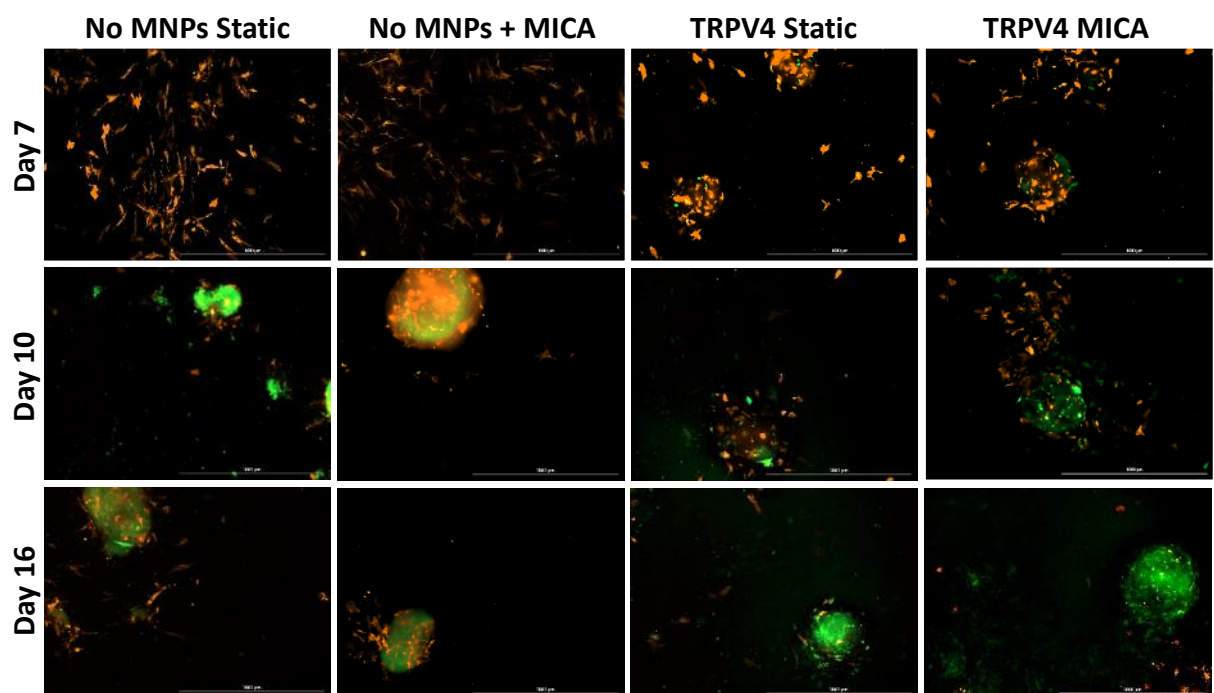


**Figure 4-8. TRPV4 MICA-activated samples showed early expression of collagen II that increased for the duration of the culture time.** Representative images of eMSCs micromasses cultured in chondrogenic media at days 7, 10 and 14 of culture. Cells expressed constitutively the dTomato fluorescence (red) and GFP was linked to collagen II expression (green). Scale bar = 1000  $\mu$ m.

Analysis of the variation in cell phenotype was done by bright field imaging. A magnified view of dTomato fluorescence images was added for improved visualisation of the cell phenotype (Figure 4-9). As observed previously in Figure 4-7, cells initially had an elongated shape that changed throughout the culture period for all groups. Unlabelled samples under both static and MICA activation conditions showed elongated cells until day 14, when a mixed population with more squared-like looking cells and elongated cells was observed. Samples labelled with TRPV4-MNPs under static conditions began to show altered morphology of the cells by day 10 of culture, finding a mixed population that after 14 days of culture acquired an almost homogeneous population of chondrocyte-looking cells, with some individual spindle-like cells. MICA activated samples labelled with TRPV4 had more rounded cells already from day 7 of culture and after 10 days of culture the majority of the population had a clear chondrocyte phenotype. This was maintained after 14 days of culture with proliferation of the chondrocyte-like cells.

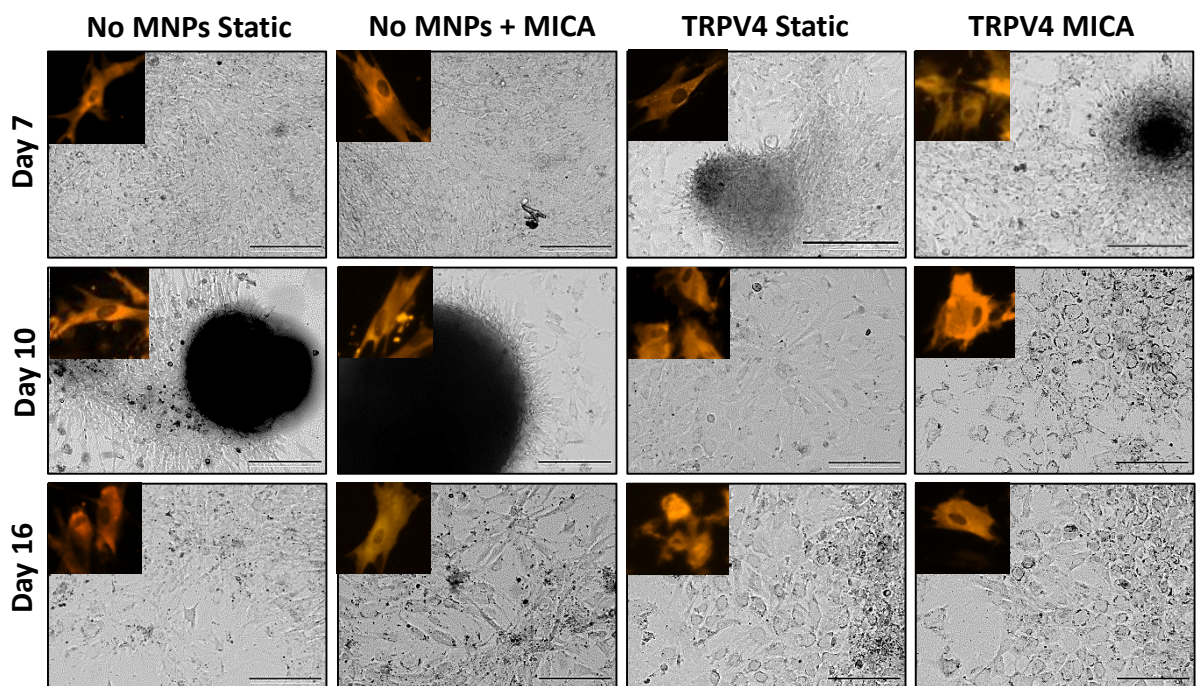


**Figure 4-9. TRPV4 MICA-activated cells beginning to acquire a chondrocyte-like phenotype from early culture time points.** Representative bright field of eMSCs micromasses cultured in chondrogenic media at days 7, 10 and 14 of culture. A closer view of the cells showing dTomato fluorescence is displayed on the top corner. Scale bar = 200  $\mu\text{m}$ .

In order to further assess the chondrogenic potential of MICA technology, histological analysis was performed for total collagen and sGAGs detection on samples cultured with complete chondrogenic media. Picrosirius red stain was used in order to detect the collagen production after 16 days of culture. Matching with the GFP-Col2 reporter fluorescence results, samples not labelled with MNPs showed less collagen produced, that was mostly deposited in the single big pellet of cells that was created from the micromass (Figure 4-10). The only difference among static and MICA activated unlabelled samples was the bigger size of the pellet for the MICA activated group. TRPV4-MNPs labelled cells showed enhanced collagen production, with deposition in the pellets and observable collagen production on single cells. Similar stain intensity was found among the static and the activated groups, however, single cells showed higher stain intensity in the MICA activated samples.

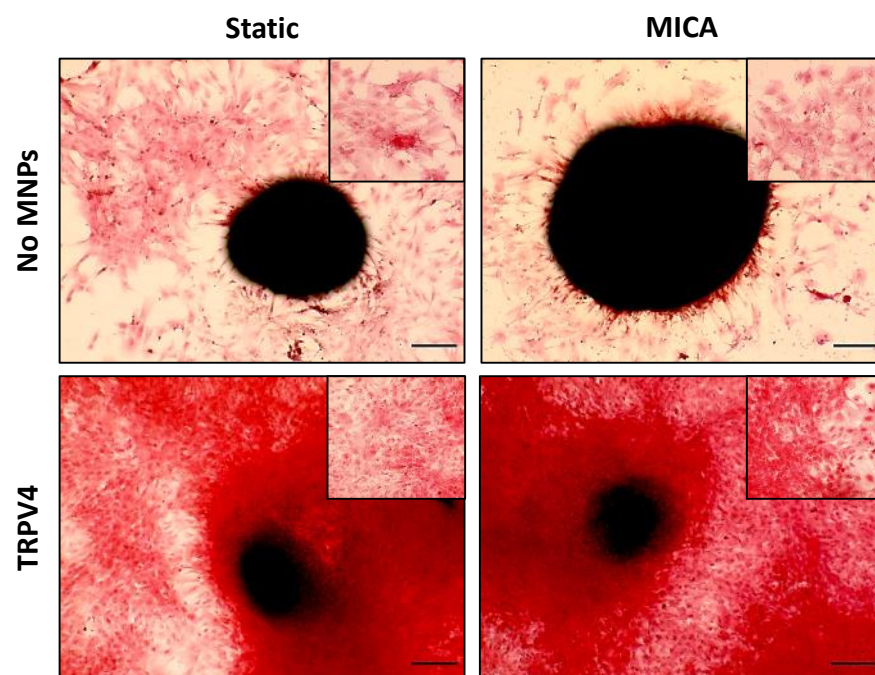


**Figure 4-10. TRPV4-MNPs labelled samples showed higher collagen production than unlabelled samples.** Representative images of day 16 cultured micromasses. A closer view of the micromasses spread cells is displayed on the top corner. Collagen presence is detected as a bright red colour. Scale bar = 200  $\mu\text{m}$ .

The presence of sGAGs was revealed by alcian blue staining of the micromasses cultured in complete chondrogenic media. Samples not labelled with MNPs under dynamic or static conditions showed a very discrete production of sGAGs (Figure 4- 11). The stain appeared to have been unwashed from the big pellets formed, and the cells that were isolated from the pellet showed a very mild blue stain presence. TRPV4-MNPs labelled samples showed sGAGs production as observed in the spread cells surrounding the pellets. Nevertheless, MICA activated micromasses showed enhanced production of the marker with an evident higher intensity of the stain and a higher density area evidencing sGAGs presence.

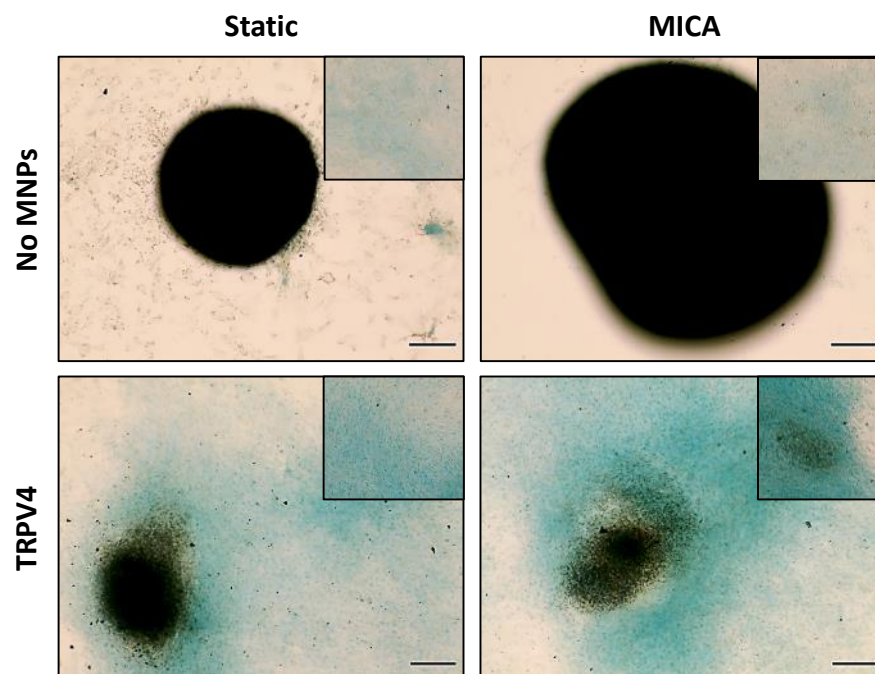


**Figure 4-11. Enhanced sGAGs deposition in TRPV4-MNPs labelled samples with a higher density observed for MICA activated micromasses.** Representative images of micromasses at day 16 of culture. Closer images of cells outside the pellet formation are shown in the top corner. The sGAGs are visualised as a stronger light blue colour. Scale bar = 200  $\mu$ m.

Safranin O is a dye commonly used for cartilage staining, particularly to reveal the presence of proteoglycans. The intensity of the stain is proportional to the proteoglycan produced in the matrix. Micromasses stained with safranin O showed similar results to previous histological assessment of the

ECM (Figure 4-12). All groups were cultured in complete chondrogenic media. Samples not containing MNPs showed a light stain tone, mostly trapped in the pellet formed. The spread cells did not show a strong intensity of the stain, in contrast to those cells imaged from TRPV4-MNPs labelled cells. Both labelled samples showed enhanced proteoglycan production being also slightly higher for MICA activated samples as appreciated both in the pellet formation area of the micromasses and the closer image of the spread cells forming monolayers. These results, together with the previous histological analysis, revealed an improved matrix deposition for cells cultured in chondrogenic media when labelled with TRPV4-MNPs, and a matrix with higher collagen and GAGs content when samples received MICA stimulation compared to static conditions.

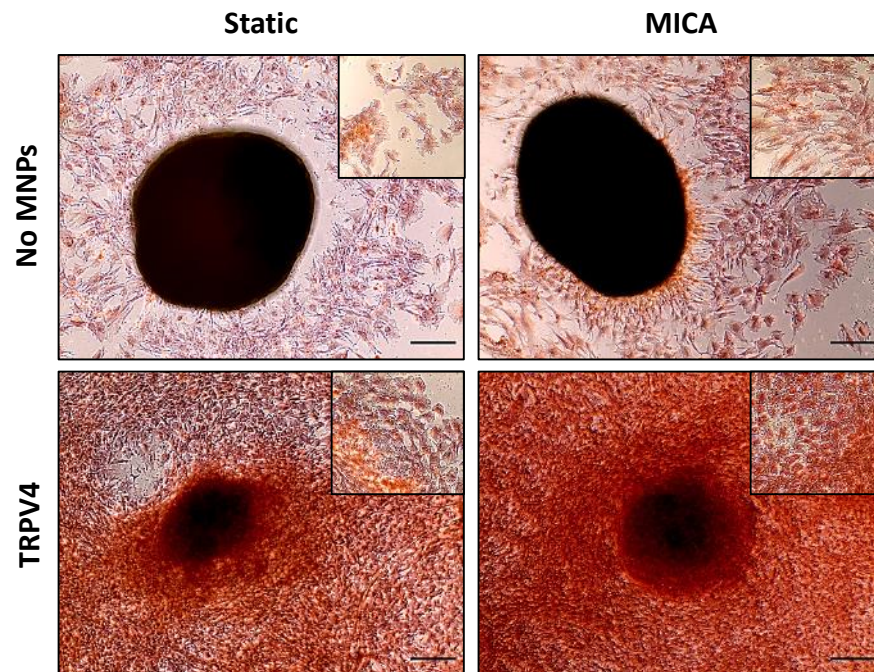


**Figure 4-12. Enhanced cartilage ECM deposition on TRPV4 MICA-activated samples.** Representative images of micromasses after 16 days of culture. Closer images of the cells in a monolayer are displayed on the top corner. The intensity of the stain is proportional to the ECM formation. Scale bar = 200  $\mu\text{m}$ .

The presence of the MNPs in the micromasses was demonstrated by prussian blue staining that reveals the presence of iron. Samples not containing MNPs did not show iron presence and samples labelled with TRPV4-MNPs showed that most of the MNPs were located in the pellets formed in the micromasses with few particles in the newly formed cells surrounding the pellet area (Figure 4-13).

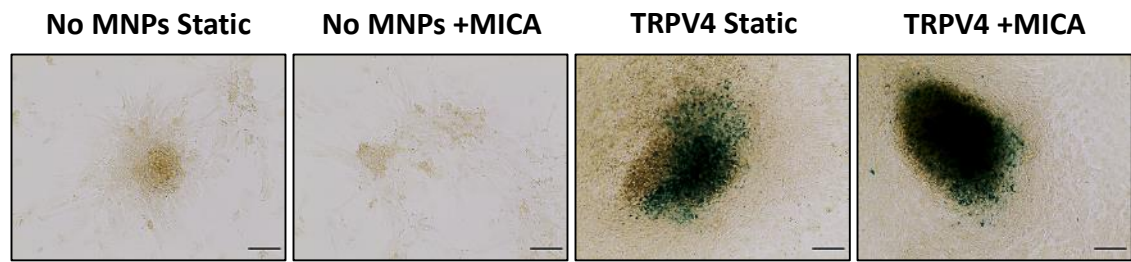


**Figure 4-13. MNPs of the labelled micromasses were found mostly on the pellets formed by the cells.**

Representative images of day 16 cultured micromasses. The iron of the particles is visualised in blue.

Scale bar = 100  $\mu$ m.

A proliferation analysis was performed in the micromasses by immunohistochemical staining with PCNA. Regardless of the lower amount of cells appreciated in the imaged micromasses, the intensity of the stain was also evidently lower for samples cultured without MNPs (Figure 4-14). Samples without MNPs and submitted to MICA stimulation had an apparent higher intensity of the dye that could be attributed to the higher proliferation of cells. TRPV4-MNPs labelled samples showed an evident higher presence of the proliferation marker, being evidently higher the fluorescence signal for MICA activated samples. The presence of the targeted channel, TRPV4, was also demonstrated by immunohistochemical analysis, with the aim of observing the effects of MICA activation on the channel presence on the cells. Regardless of the cell density, all samples excepting for the TRPV4-MNPs static group, showed a high fluorescence signal revealing the presence of the channel. The micromasses labelled with TRPV4 and cultured under static condition had a less intense stain, however, the channel presence was still detected. The TRPV4 MICA-activated group showed, however, areas with high expression of the marker and overall high fluorescence levels.

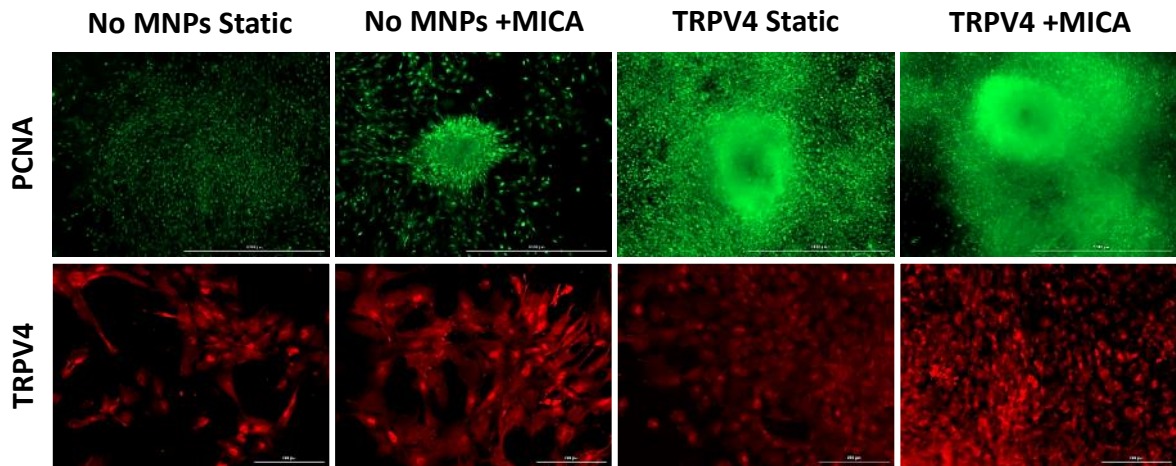


**Figure 4-14. TRPV4 MICA-activated samples showed enhanced proliferation and the TRPV4 channel was present for all treated conditions.** Representative images of micromasses after 16 days of culture. Top images represent PCNA staining (scale bar = 1000  $\mu\text{m}$ ) and lower row images are stained with TRPV4. Scale bar = 200  $\mu\text{m}$ .

Pellets were cultured in parallel to experiment 2, in a simplified version of the micromasses experiment, with the aim of further analysing the effects of TRPV4 MICA-activation on chondrogenesis. Samples were cultured for a longer period of time (28 days) to allow for observation of further changes past the usual 21 days of culture for chondrogenic induction. The concentration of sGAGs and DNA was quantified following the spectrophotometric DMMB and PicoGreen™ assays for days 1, 10, 14, 21 and 28 (Figure 4-15). The PicoGreen™ analysis was performed with the aim of normalising the presence of sGAGs in the sample, according to the cell density present in the sample. The normalisation allows quantifying the chondrogenic potential of each sample regardless of the size. In addition, it also provided an insight on the proliferative effect of the studied conditions. Samples cultured in basic media showed significantly lower production of sGAGs and lower DNA was found among the pellets when compared to the other conditions for most time points studied (Table 4-2). The differences were observed to increase with culture time. Unexpectedly, samples cultured with chondrogenic media alone showed a trend for slightly higher sGAGs produced for all time points excepting for day 28, when compared to MICA activated samples. Nevertheless, when normalised to

the DNA amount, significant difference was only found on day 21 of culture, being observed high variability among the samples cultured in chondrogenic media. As expected, day 1 samples showed higher DNA amount due to the initial state of pellet formation. This matches with Chapter 3 results on metabolic activity assays of the pellets. Overall, low levels of sGAGs were detected for all groups analysed.

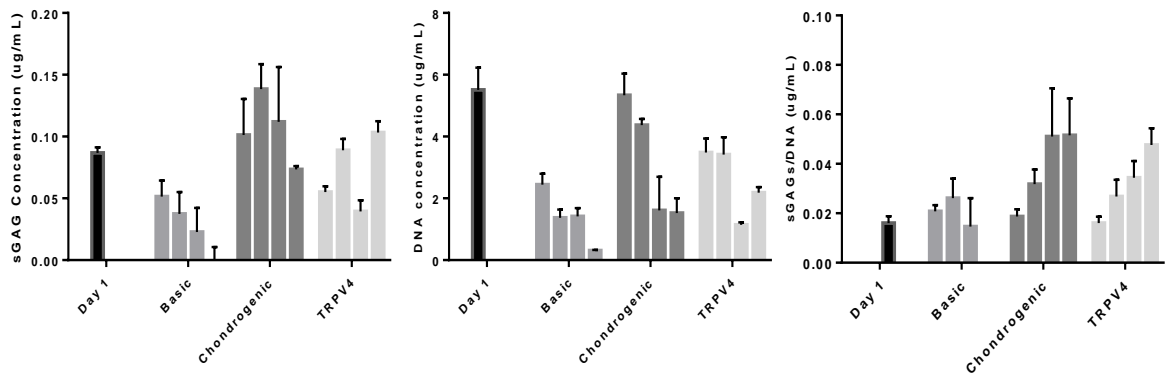


**Figure 4-15. Few differences were found between samples cultured in chondro-inductive media unstimulated and TRPV4 MICA-activated groups for sGAGs production.** SGAGs and DNA were quantified at days 1, 10, 14, 21 and 28 of culture for pellets formed of cells from eMSCs cultured in basic (expansion) media, chondrogenic media, and samples labelled with TRPV4-MNPs MICA-activated also cultured in chondrogenic media. Normalised data are expressed as a ratio sGAGs/DNA. Data is expressed as the mean  $\pm$  standard deviation in n=2-3 repeats for 3 different samples per group.

**Table 4-2. Statistical analysis of Figure 4-14.**

| sGAGs concentration ( $\mu\text{g}/\text{mL}$ )       |              |              |              |              |
|---|--------------|--------------|--------------|--------------|
| Group   | Day 10<br>P< | Day 14<br>P< | Day 21<br>P< | Day 28<br>P< |
| Day 1 vs. Basic                                       |              | **           | ***          | ****         |
| Day 1 vs. Chondrogenic                                |              | **           |              |              |
| Day 1 vs. TRPV4                                       |              |              | **           |              |
| Basic vs. Chondrogenic                                | **           | ****         | ****         | ****         |
| Basic vs. TRPV4                                       |              | **           |              | ****         |
| Chondrogenic vs. TRPV4                                | **           | **           | ****         |              |
| DNA concentration ( $\mu\text{g}/\text{mL}$ )         |              |              |              |              |
| Group   | Day 10<br>P< | Day 14<br>P< | Day 21<br>P< | Day 28<br>P< |
| Day 1 vs. Basic                                       | ****         | ****         | ****         | ****         |
| Day 1 vs. Chondrogenic                                |              | *            | ****         | ****         |
| Day 1 vs. TRPV4                                       | ****         | ****         | ****         | ****         |
| Basic vs. Chondrogenic                                | ****         | ****         |              | *            |
| Basic vs. TRPV4                                       |              | ****         |              | ****         |
| Chondrogenic vs. TRPV4                                | ***          |              |              |              |
| SGAGs / DNA concentration ( $\mu\text{g}/\text{mL}$ ) |              |              |              |              |
| Group   | Day 10<br>P< | Day 14<br>P< | Day 21<br>P< | Day 28<br>P< |
| Day 1 vs. Basic                                       |              |              |              | *            |
| Day 1 vs. Chondrogenic                                |              | *            | ****         | ****         |
| Day 1 vs. TRPV4                                       |              |              | *            | ****         |
| Basic vs. Chondrogenic                                |              |              | ****         | ****         |
| Basic vs. TRPV4                                       |              |              | **           | ****         |
| Chondrogenic vs. TRPV4                                |              |              | *            |              |

The gene expression analysis of the ECM markers *Col2a1* and *Acan*, was performed on eMSCs pellets in order to further evaluate the chondrogenic potential of MICA activation. In contrast to the results observed for the micromasses GFP-Col2 reporter analysis, gene expression analysis revealed low levels of collagen expression for all groups until 21 days of culture, where an expression increase was observed which continued until the termination of the experiment (Figure 4-16). TRPV4 MICA activated samples showed significantly higher expression of *Col2a1* than the other compared groups from day 21 of culture. Moreover, samples cultured in chondrogenic media also showed significantly higher expression of *Col2a1* when compared to those samples cultured in basic media, which

presented negligible levels of collagen production for all time points analysed. The aggrecan gene expression analysis, however, showed similar expression levels for all groups compared, following a similar expression pattern to that observed for the sGAGs DMMB analysis. A tendency for higher expression was observed for TRPV4-MICA activated samples, nevertheless, statistical differences were only seen at day 10 of culture with samples cultured in chondrogenic media. The expression of aggrecan was observed to decrease with culture time, as opposed to the collagen II expression.

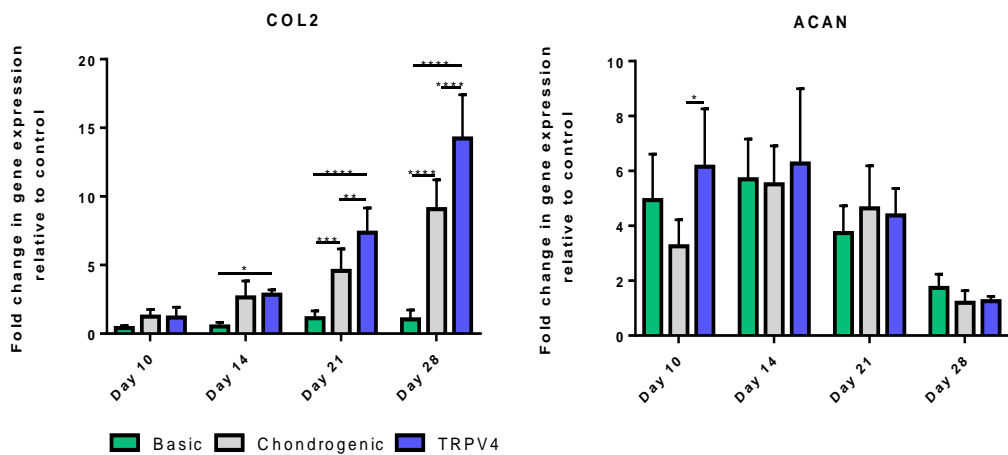


**Figure 4-16. Higher *Col2a1* expression was observed for TRPV4 MICA-activated samples, and no differences were found among groups for *Acan* expression analysis.** qRT-PCR performed on pellets 2 at days 10, 14, 21 and 28 of culture for samples cultured in basic (expansion media), chondrogenic media and pellets cultured in chondrogenic media labelled with TRPV4-MNPs. Results expressed as fold change relative to control samples from day 1 and normalised to *S18*. Data are expressed as mean  $\pm$  standard deviation, n=4 and 3 technical repeats, \*p<0.05, \*\*p<0.01, \*\*\*p<0.001, \*\*\*\*p<0.0001.

#### 4.4.3 Collagen II expression analysis: Luciferase – Col 2 Reporter

For this study, eMSCs labelled with luciferase/GFP dual constructs were employed. Two cell lines were used, both with GFP under constitutive control (EF1) promoter, while the luciferase is controlled either under the Col2 promoter (Col2-Luc) or under the CMV promoter (CMV-Luc). With the aim of proving the efficiency of the transfection, cells were imaged with fluorescence microscopy for all experimental conditions. The presence of the GFP reporter was taken as an indicator of a successful transfection (Figure 4-17).

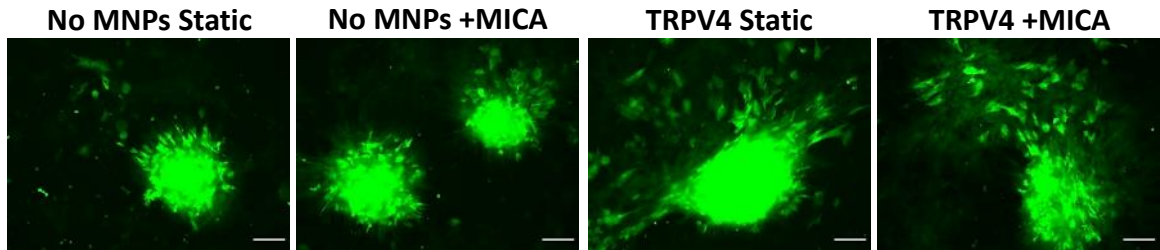


**Figure 4-17. Cells were successfully transfected with the GFP reporter.** Representative images of micromasses cultured in chondrogenic media and different experimental conditions at day 16. Scale bar = 200  $\mu\text{m}$ .

The collagen II expression was measured through the Col2-Luciferase reporter cell line in micromasses cultured in chondrogenic media on unlabelled samples and samples labelled with TRPV4-MNPs under static and MICA activation conditions (Figure 4-18). The CMV-Luc reporter cell line was used to normalise the results and obtain the relative chondrogenic activity. No statistical differences were found among the experimental conditions for any of the time points compared. All samples except for TRPV4 MICA-activated samples showed a tendency to decrease the luciferase activity with culture time. MICA activated samples with and without MNPs had a higher chondrogenic activity than the static groups, with the exception of day 7 comparison of the TRPV4-MNPs labelled samples, however, great variability was found among the samples from the same groups.

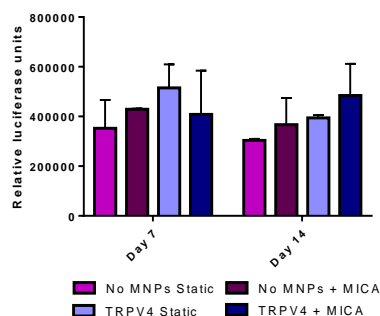


**Figure 4-18. No statistical differences were found among experimental groups for Col2-Luc reporter cell line.** Micromasses production of metridia luciferase was quantified and normalised to CMV-Luc production for each studied condition. All samples were cultured in chondrogenic media and measurements were taken after 7 and 14 days of culture. N= 3 technical repeats. Data are expressed as mean  $\pm$  standard deviation.

In order to understand if the results obtained from the Col2-Luciferase analysis were due to any effects of the cell population due to the addition of MNPs, a viability assay was performed in the samples. The cell viability was measured with Presto Blue™ reagent for both cell types Col2-Luc and CMV-Luc, cultured in chondrogenic media and in plain and labelled cells with TRPV4-MNPs. No negative effects due to the addition of MNPs were observed in the metabolic activity of the cells (Figure 4-19). CMV-Luc cells, both labelled with TRPV4-MNPs and unlabelled, showed statistically lower levels of metabolic activity when compared with the Col2-Luc, possibly as a results of differential growth pattern. Little differences were found when comparing MNPs labelled groups with unlabelled samples from the same cell type hence, indicating that the addition of MNPs was not reducing cell proliferation.

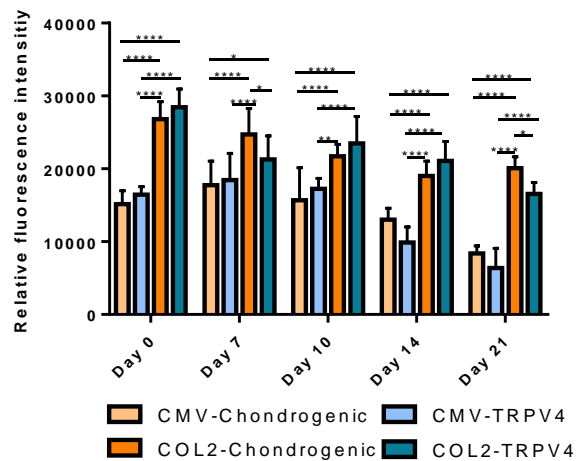


**Figure 4-19. No toxic effects found when labelling cells with MNPs for any of the cell types.** The metabolic activity was measured through the course of 21 days at days 0, 7, 10, 14 and 21 of culture. Data are expressed as mean  $\pm$  standard deviation n=3 samples per group (3 technical repeats).

## PART 2

### 4.4.4 Effect of TGF- $\beta$ presence in the culture medium following MICA activation

For the second part of this work, ovine MSCs, chondrocytes (passage 0-1) and de-differentiated chondrocytes (passage 4-5) were used to further study the best target for MICA activation. In addition, the potential implications of the TGF- $\beta$  effect in the downstream signalling following MICA activation were also analysed.

Histological assessment of 3D pellets was performed for the studied groups, however, chondrocytes on a passage 0-1 state did not show evidence of the presence of any of the cartilage ECM markers for any of the experimental groups after 21 days of culture (Supplementary figure 3). Samples stained with toluidine blue for proteoglycan reveal showed different patterns of behaviour between the MSCs and the de-differentiated chondrocytes, with an evident difference of the pellet size, being bigger for de-differentiated chondrocytes. MSCs showed a much lower staining intensity than the de-differentiated chondrocytes for all time points (Figure 4-20). All samples cultured with TGF- $\beta$  showed the formation of an outer ring stained with a higher intensity. Differences between compared groups for MSCs were not evident for some cases, with slightly higher GAG deposition for the no-MNP control cultured in chondrogenic media and TRPV4-MICA activated samples cultured with TGF- $\beta$ . Similar GAG deposition was observed at both measured time points. On the contrary, de-differentiated chondrocytes showed a great production of proteoglycans already from day 16 of culture. TRPV4 and TRPV4 activated samples showed enhanced GAGs production when compared to the control. Nevertheless, the purple metachromatic stain was clearly more intense for TRPV4 activated samples cultured with and without TGF- $\beta$ . The differences were reduced after 21 days of culture, especially for TRPV4 samples cultured in complete media, which appeared to have lost some of the intensity of the stain. However, the same pattern of differences observed for day 16 was also true for day 21 samples. As observed for the MSCs pellets, samples cultured with TGF- $\beta$  had formed an outer ring that stained in blue indicating the lack of proteoglycans. The GAGs were more present in the centre of the samples

for all cases. Interestingly, samples cultured without TGF- $\beta$  showed a more homogeneous distribution of the marker, when compared to the other groups that appeared to have nucleus of higher proteoglycan deposition.

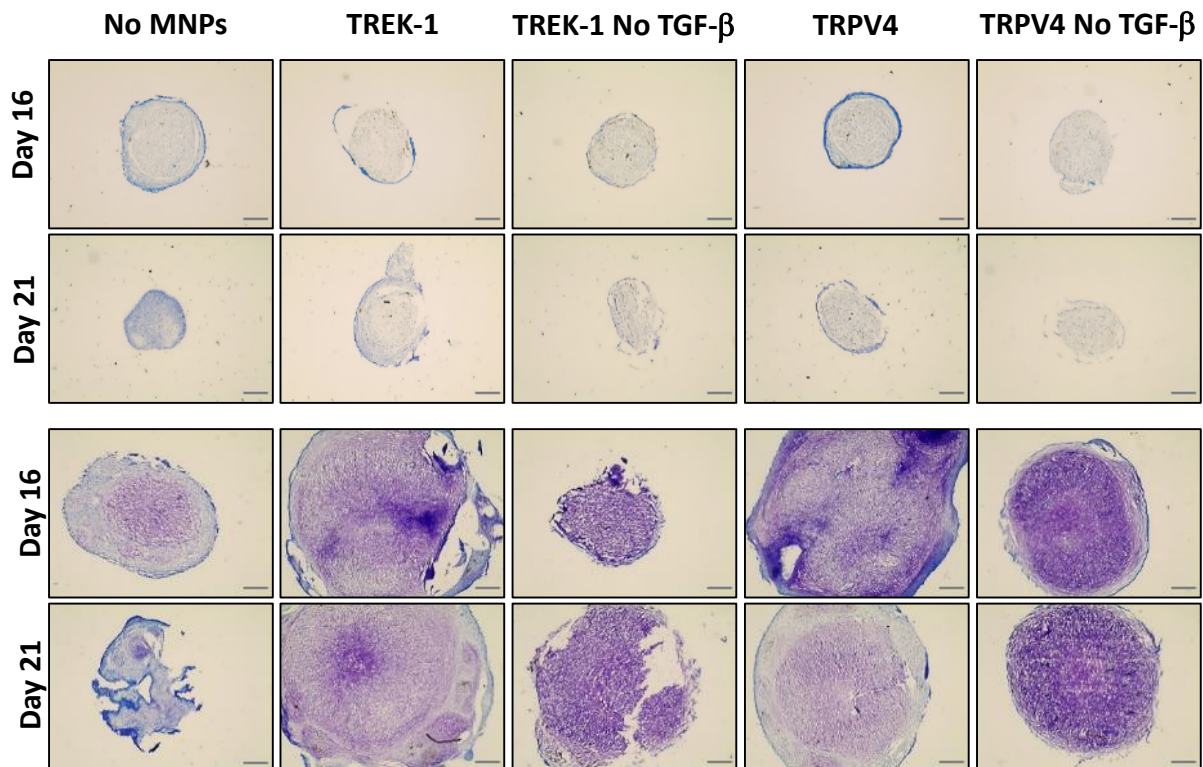


**Figure 4-20. Increased pellet size and GAGs deposition for de-differentiated chondrocytes pellets with elevated matrix formation in TREK-1 and TRPV4 activated samples.** Representative images of 7  $\mu\text{m}$  pellet sections from oMSCs at days 16 and 21 of culture (top rows) and de-differentiated chondrocytes at days 16 and 21 of culture (bottom rows) stained with toluidine blue for GAGs detection. The stain shows a purple colouring when bound to GAGs and a blue tone for the rest of the structures. Scale bar = 200  $\mu\text{m}$ .

The total collagen production was also determined by picosirius red staining. As observed previously for the GAGs deposition, oMSCs pellets showed a very discrete production of collagen when compared to de-differentiated chondrocytes (Figure 4-21). Little to no collagen was observed for the MSCs after 16 days of culture with the only appreciable fibres present in TRPV4-labelled samples cultured without TGF- $\beta$ . After 21 days of culture the production of collagen was increased for all studied groups. Samples cultured with TGF- $\beta$  were observed to have acquired an outer ring formed of collagen fibres.

Interestingly, the control samples and TREK-1 labelled pellets showed very thick rings with no collagen present in the centre of the samples and small nucleus of higher collagen deposition within the external rings. Contradictory to these findings, de-differentiated chondrocytes showed a high production of collagen by day 16 for all experimental groups. This was moderately higher for TREK-1 and TRPV4-labelled samples cultured with TGF- $\beta$ . This hierarchy of expression was continued after 21 days of culture. The control sample appeared to have a high collagen deposition, however, this was associated with the initial sectioned part of the pellet always showing a higher collagen production. As observed for the MSCs, an outer ring was observed for samples cultured in complete chondrogenic media with an apparent organised matrix observed in TREK-1 and TRPV4 samples, showing a gradient of collagen deposition with lower concentrations in the inside increasing to the outside part, that is finished by a thin layer of yellow stain corresponding to the cytoplasm of the cells.

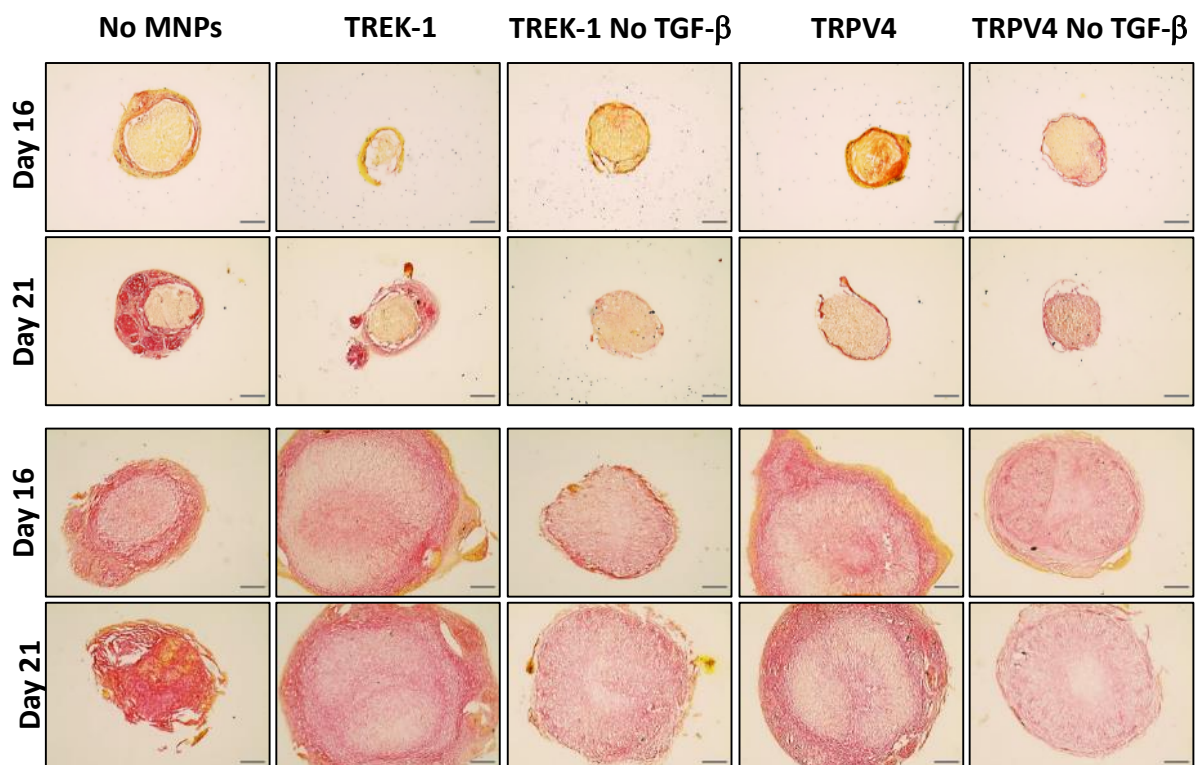


**Figure 4-21. Enhanced collagen production on de-differentiated chondrocytes over MSCs, with higher deposition for TREK-1 and TRPV4 MICA-activated samples in complete media.** Representative images 7  $\mu$ m pellet sections from oMSCs (top rows) and de-differentiated chondrocytes (bottom rows) stained with picrosirius red for collagen visualisation at days 16 and 21 of culture. Collagen fibres are shown in a red colour and the background in yellow. Scale bar = 200

Sections stained with picosirius red were imaged with a polarised microscope for further understanding the arrangement of the ECM fibres and the thickness of the collagen produced (Figure 4-22). The collagen fibres are visualised due to their birefringent nature, and the size and level of organisation can be determined according to the visualised colour. In decreasing range of size and organisation fibres are visualised as red/orange, yellow, green, and blue. MSCs showed an outer collagen ring with medium thickness fibres, that encapsulated the pellet which showed little birefringence, and when existing birefringence, it was showing a medium level of thickness and organisation. TRPV4-MICA samples cultured in complete chondrogenic media showed presence of more organised fibres in the inner part of the section. De-differentiated chondrocytes did not form such thick outer rings, that were mostly observed for samples labelled with MNPs cultured with TGF- $\beta$ , however, some of the ring is not visualised in the image due to the magnification. The majority of the surface of the pellets was observed to have medium to high organised fibres, being more obvious for TREK-1 and TRPV4 samples cultured in complete chondrogenic media after 21 days of culture.

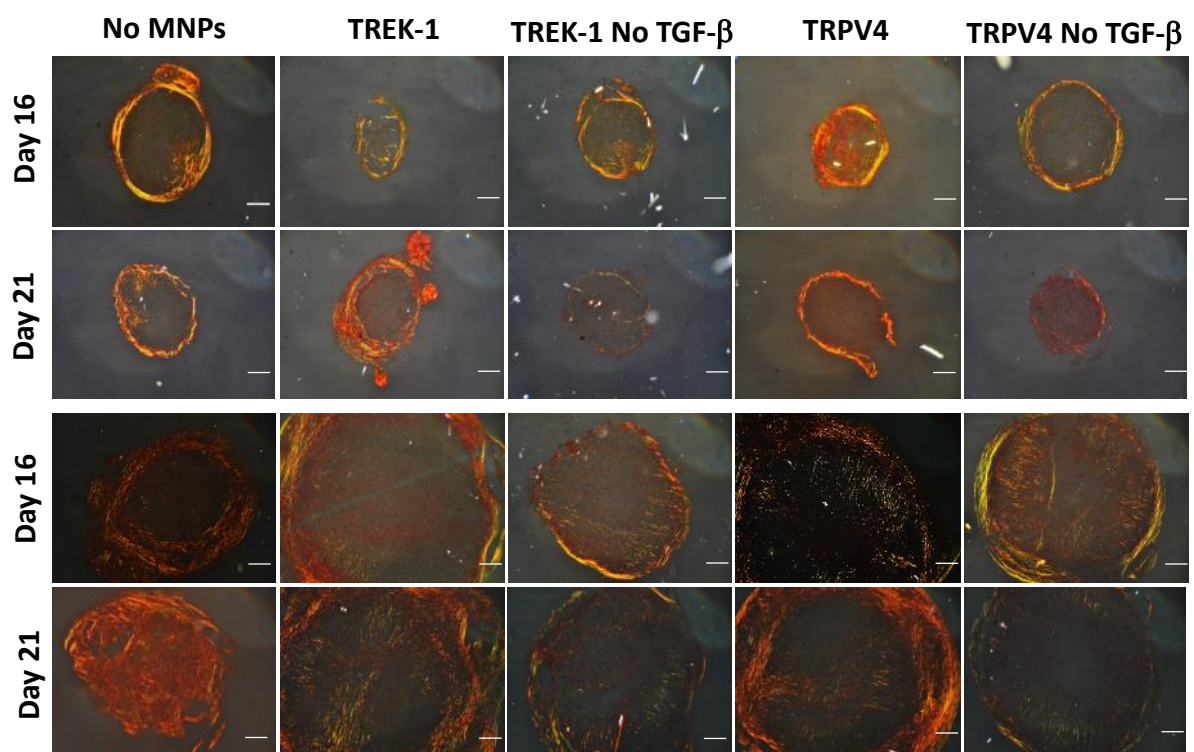


**Figure 4-22. Medium organised fibres for all samples with an outer ring formation.** Representative images of cross-polarised micrographs of 7 mm pellets sections of oMSCs (top) and de-differentiated chondrocytes (bottom) stained with picosirius red at days 16 and 21 of culture. Scale bar = 200  $\mu$ m.

Immunohistochemical analysis of collagen II was performed with immunoperoxidase of oMSCs and de-differentiated chondrocytes pellet sections. A negative control was performed without primary antibody, showing no signs of unspecific binding for the secondary antibody (results not shown). Unlike previously observed with picosirius red staining, MSCs showed collagen deposition by day 16 of culture being enhanced for TREK-1 and TRPV4 MICA-activated samples when cultured without TGF- $\beta$  (Figure 4-23). The differences were reduced after 21 days of culture, however, samples cultured without TGF- $\beta$  presented a higher deposition of the marker. The collagen II deposition was observed to be fairly homogeneous with exception of the control sample, unlike the zonal distribution observed for de-differentiated chondrocytes. For these samples opposing results were found, with higher collagen II staining for TREK-1 and TRPV4 labelled samples cultured in complete chondrogenic medium. For the de-differentiated chondrocytes, a slightly higher deposition of collagen II was observed for both TRPV4-labelled samples in both culture conditions tested.

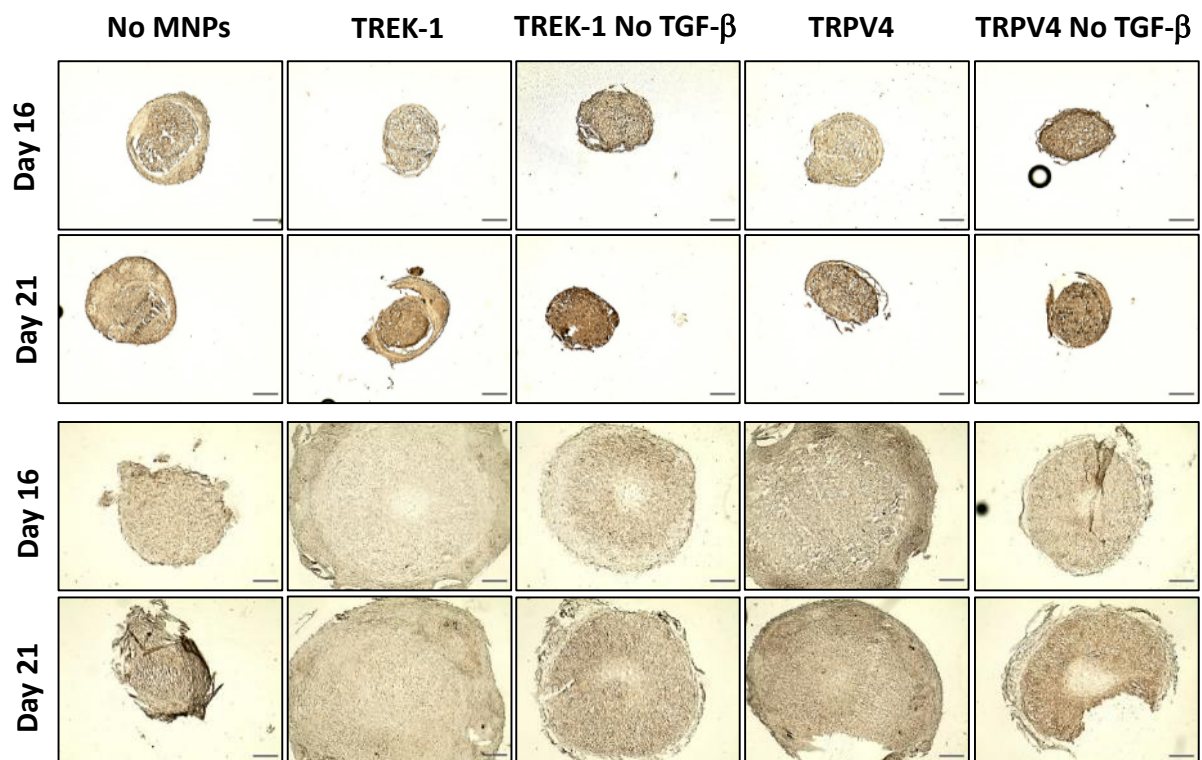


**Figure 4-23. Higher production of collagen II for both cell types in TREK-1 and TRPV4 activated samples cultured with or without TGF- $\beta$ .** Representative images of collagen II immunoperoxidase staining of 7  $\mu$ m pellet sections of MSCs (top) and de-differentiated chondrocytes (bottom) after 16 and 21 days of culture. More intense colour represents higher deposition. Scale bar = 200  $\mu$ m.

Aggrecan production was also studied by immunoperoxidase staining for both cell types (Figure 4-24). Contrary to the GAGs production results obtained with toluidine blue staining, MSCs did show deposition of the marker from the 16th day of culture for all groups, especially for TREK-1 and TRPV4 labelled samples. The production was increased after 21 days of culture for all groups with the exception of TRPV4 MICA-activated pellets cultured without TGF- $\beta$ , which presented a peak of expression at day 16. The distribution of the marker was mildly homogeneous, excepting for the control samples and TREK-1 labelled samples cultured in complete chondrogenic media, where the stain was deposited in the centre. De-differentiated chondrocytes showed a more discrete staining intensity for all samples with higher aggrecan production for MICA activated samples, especially for those samples labelled with TRPV4. A mild increase of the stain intensity was observed after 21 days of culture for all samples excepting for the control. The stain had a zonal distribution with low intensity in the more central and outer regions.

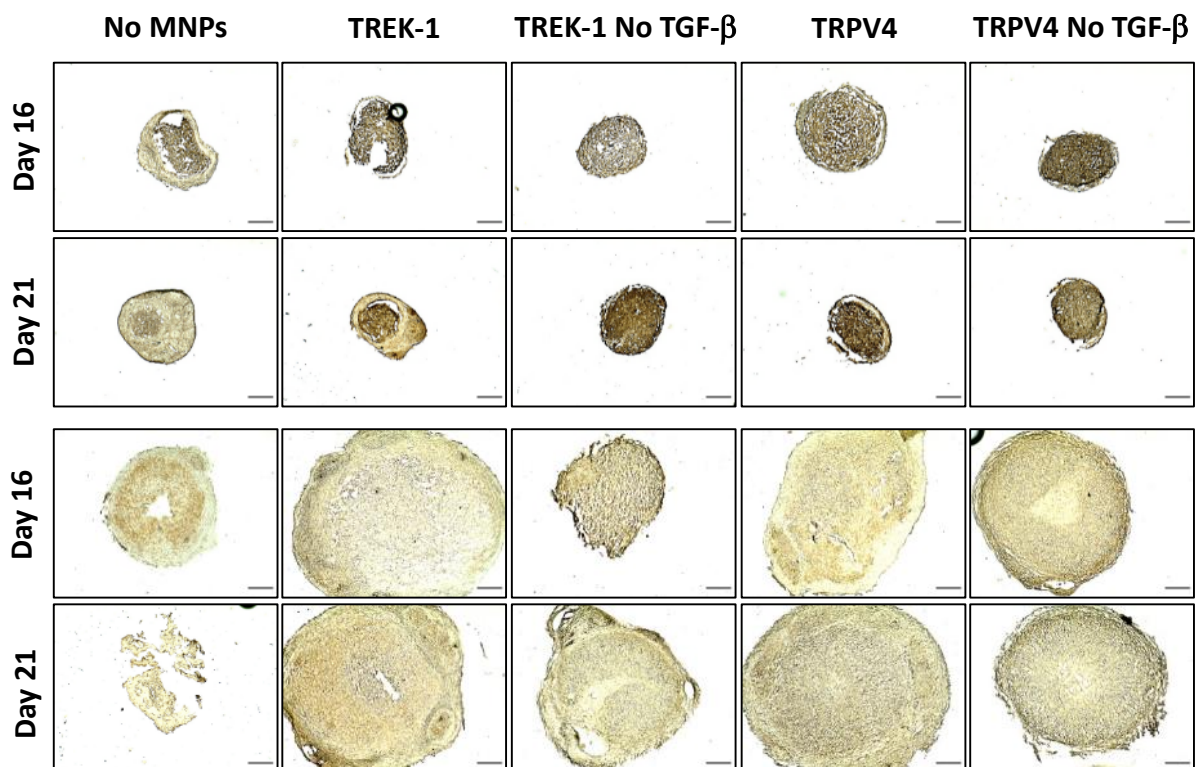


**Figure 4-24. Enhanced production of aggrecan for MSCs and TREK-1 and TRPV4-MICA activated samples.** Representative images of aggrecan immunoperoxidase staining of 7  $\mu$ m pellet sections of MSCs (top) and de-differentiated chondrocytes (bottom) after 16 and 21 days of culture. More intense colour represents higher deposition. Scale bar = 200  $\mu$ m.

The presence of MNPs in the labelled samples was histologically evaluated by staining the iron content with prussian blue. Control unlabelled samples did not exhibit the presence of MNPs (Figure 4-25). Certain aggregation of MNPs could be appreciated for MSCs labelled with TREK-1 in both media conditions however, this was attributed to the small size of the pellets. TRPV4-labelled MSCs showed a more spread disposition of the MNPs. De-differentiated chondrocytes showed a spread distribution of the MNPs for all labelled samples.

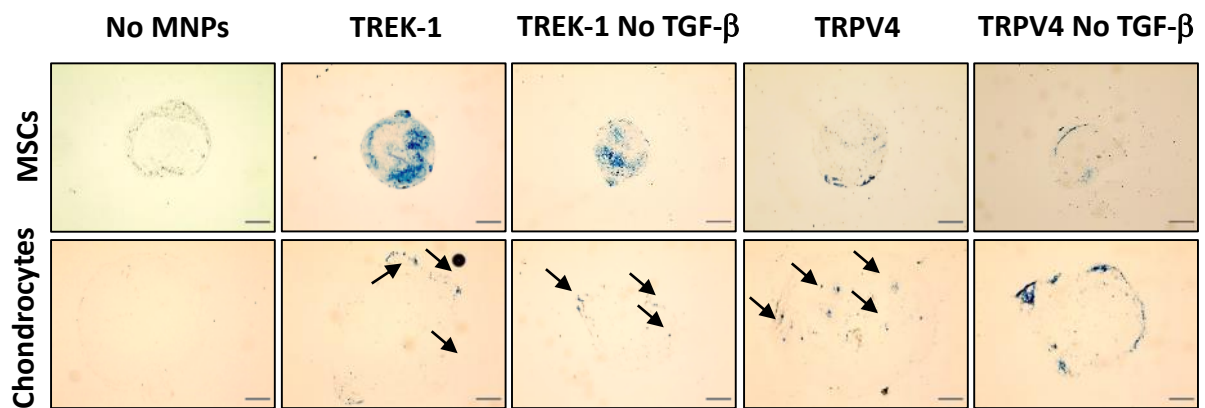


**Figure 4-25. MNPs were present in labelled samples for both cell types.** Representative images of 7  $\mu\text{m}$  pellet sections of oMSCs and de-differentiated chondrocytes after 21 days of culture and stained with prussian blue. The iron content of the MNPs is visualised in blue. Black arrows point the presence of MNPs were spread in the sample. Scale bar = 200  $\mu\text{m}$ .

The ECM markers were additionally studied by gene expression analysis with qRT-PCR. The expression of *Sox9*, *Col2a1* and *Acan* was studied for MSCs, and de-differentiated pellet samples collected after 21 days of culture. The gene expression analysis presented some variation among cell types studied (Figure 4-26). The expression of *Sox9* was observed to be similar for all groups compared on MSCs, with the exception of TRPV4 samples cultured in complete media that showed the highest expression. Expression of the same gene in de-differentiated chondrocytes showed more variability among groups, with higher expression found for the samples cultured without TGF- $\beta$ . The expression of collagen II followed a similar pattern between cell types with the highest expression found for the control and TREK-1 labelled samples cultured in complete chondrogenic media. De-differentiated chondrocytes followed this pattern with the exception of TRPV4-labelled samples, also cultured in

complete medium, which showed the highest expression with statistical differences compared to all groups except for the control. These results would match the immunostaining observation if the control did not show the high levels of gene expression. The aggrecan expression pattern was also relatively similar, however, statistical differences were only found among MSCs with an evident lowest expression found in TREK-1 samples cultured without TGF- $\beta$ .

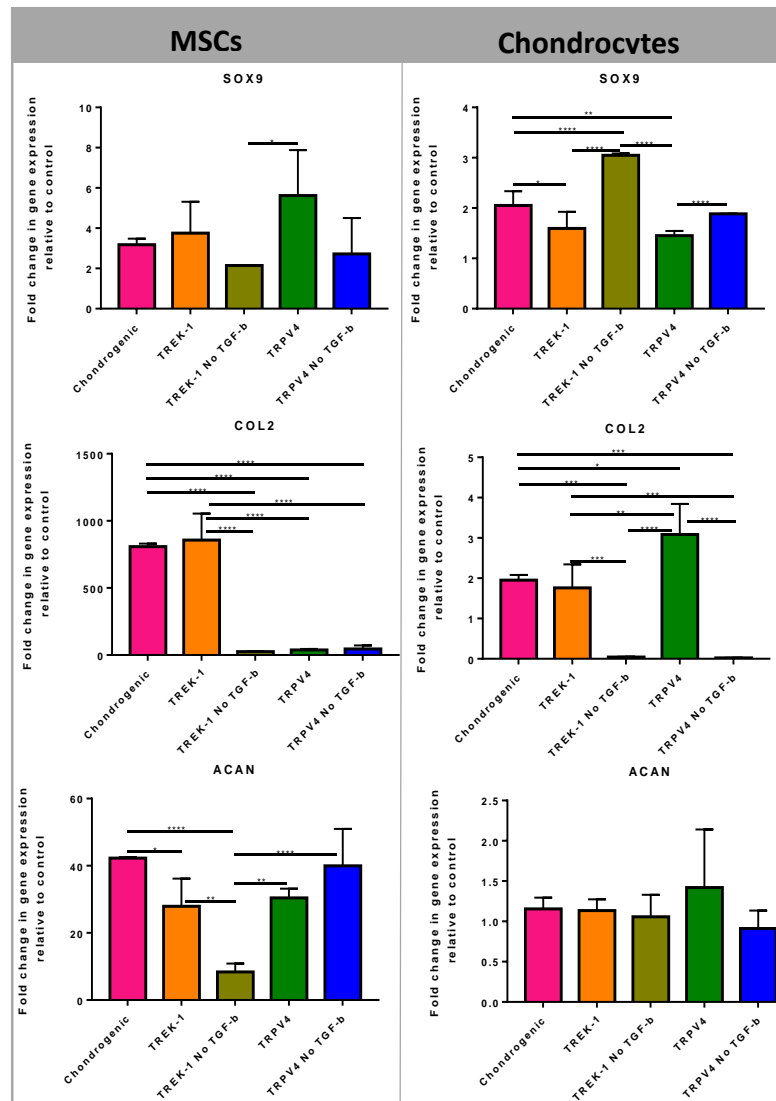


**Figure 4-26. Variable gene expression pattern with overall higher expression found among samples cultured with TGF- $\beta$  for both cell types.** qRT-PCR performed on pellets from MSCs and de-differentiated chondrocytes on day 21 day of culture. Results expressed as fold change relative to day 0 and normalised to GAPDH. Data are expressed as mean  $\pm$  standard deviation, n=4 (n=2 technical repeats), \*p<0.05, \*\*p<0.01, \*\*\*p<0.001, \*\*\*\*p<0.0001.

#### 4.4.5 Histological determination of TRPV4-MICA activation for chondrogenic differentiation

Ovine de-differentiated chondrocytes on passage 4-5 were expanded prior to studying the chondrogenic activity of TRPV4, the selected target for MICA technology. The study was performed on 3D pellets cultured in chondrogenic media. Samples were analysed with histological staining for the main ECM components, with the aim of comparing to previous experiments. Chondrocytes were imaged after dissection at passage 0, to visually ensure the presence of chondrocyte-like cells (Figure 2-27). Pellets were sectioned after 24 hours in culture with chondrogenic media for comparative purposes. No signs of ECM markers were detected for the samples after 1 day of culture.

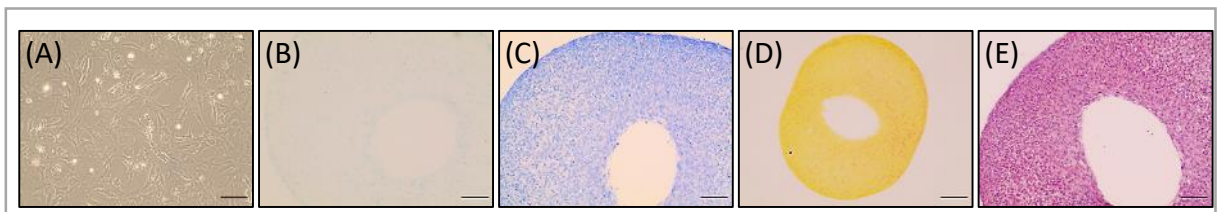


**Figure 4-32. Day 1 images.** Representative images of A) bright field-imaged chondrocytes after dissection and initial expansion, and 7  $\mu\text{m}$  sections of pellets stained with B) alcian blue, C) toluidine blue, D) picrosirius red and E) safranin O. Scale bar = 100  $\mu\text{m}$ .

The production of sGAGs was evaluated with alcian blue staining. Both compared groups showed low overall levels of sGAGs production, for all time points analysed (Figure 4-28). Samples with no MNPs showed some levels of the marker after 14 days of culture. TRPV4 MICA-activated samples presented some signs of sGAGs presence by day 10 of culture, that increased by day 14. The marker was mainly observed in the more central region of the samples, and in the outer limit of the pellet, as opposed to samples cultured with no MNPs that showed higher production only for the outer part to the pellet section.

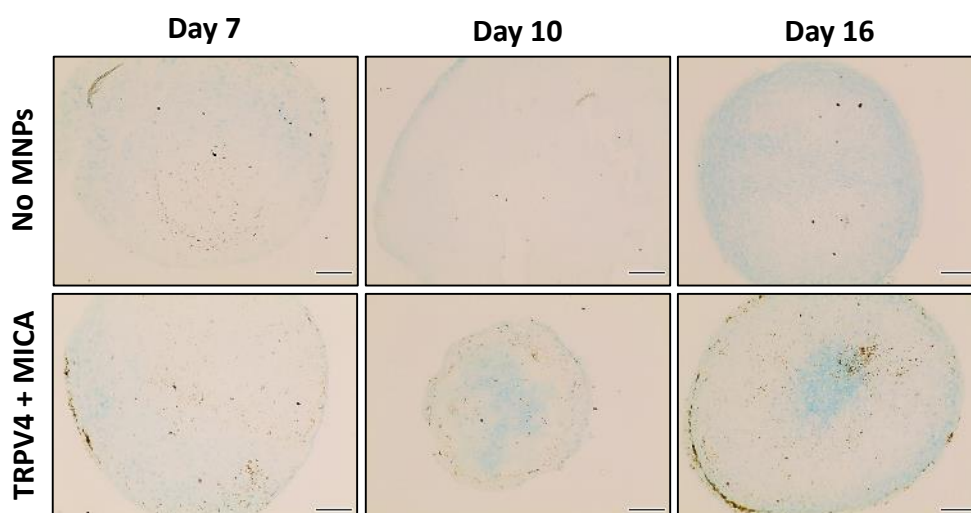


**Figure 4-33. Low levels of sGAGs were found for all compared groups.** Representative images of 7  $\mu\text{m}$  pellet sections from de-differentiated chondrocytes stained with alcian blue for sulphated GAGs reveal. Samples were cultured for 7, 10 and 16 days in chondrogenic media without MNPs and with TRPV4 MICA-activated MNPs. The higher intensity of the colour of the stain reveals the presence of GAGs in the sections. Scale bar = 100  $\mu\text{m}$ .

The production of proteoglycans was also measured by toluidine blue staining. In line with the results obtained from alcian blue staining, the proteoglycan production was discrete for both groups and for all time points (Figure 4-29). Pellets cultured without MNPs showed very mild production of proteoglycans, visualised as a purple metachromatic stain, which was able to be visualised mildly at days 7 and 10 of culture, but no after 14 days. TRPV4 MICA-activated samples showed a moderate production of the marker on the external region of the section by day 7 of culture and continued to be observed in the periphery of the sections for all the duration of the culture time. Nevertheless, the production of the marker did not increase greatly by day 14 of culture. However, the lack of samples examined after 21 days of culture did not allow to further study the production of this marker, which often greatly increases from the second to the third week of culture. The marker deposition was not uniform, with one side of the samples clearly showing higher proteoglycan deposition. These results do not match the previous findings of de-differentiated chondrocytes, showing an enhanced production of the marker with a tendency for deposition in the central regions of the pellets.

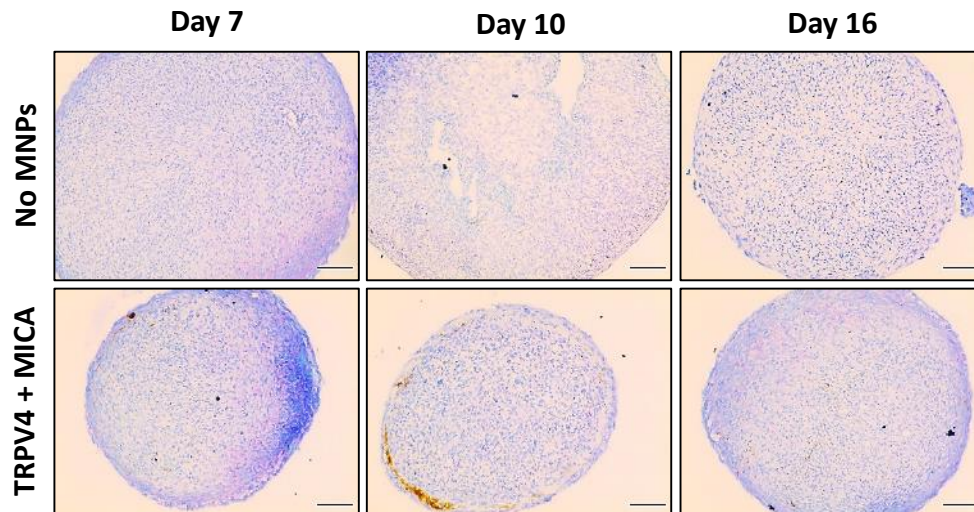


**Figure 4-34. Enhanced deposition found among TRPV4 MICA-activated samples with proteoglycans deposited in the periphery.** Representative images of 7 µm pellet sections from de-differentiated chondrocytes at days 7, 10 and 16 of culture, stained with toluidine blue for GAGs detection. The stain shows a purple colouring when bound to GAGs and a blue tone for the rest of the structures. Scale bar = 100 µm.

Collagen production was evidenced by picosirius red staining of the sections. This study showed more similarity to the previous analysis on de-differentiated chondrocytes, with greater production of collagen observed for TRPV4 MICA-activated samples (Figure 4-30). The collagen fibres were evident in both groups from day 7 of culture, being denser for MICA-activated pellets. After 10 days of culture, both compared groups showed a mild increase of fibre presence with a more uniform distribution, however, MICA activated samples showed increased deposition also in the form of an outer ring of collagen. The marker deposition greatly increased for both groups after 2 weeks of culture. Samples cultured without MNPs showed fibres present across all the surface of the sections however, the stain showed a more intense colour for the external regions of the samples. TRPV4 MICA-activated pellets, showed enhanced production of collagen when compared with the unlabelled samples. The collagen distribution was mildly homogeneous with some areas of lower deposition in the most external part of the section, as observed in the previous experiment with de-differentiated chondrocytes.

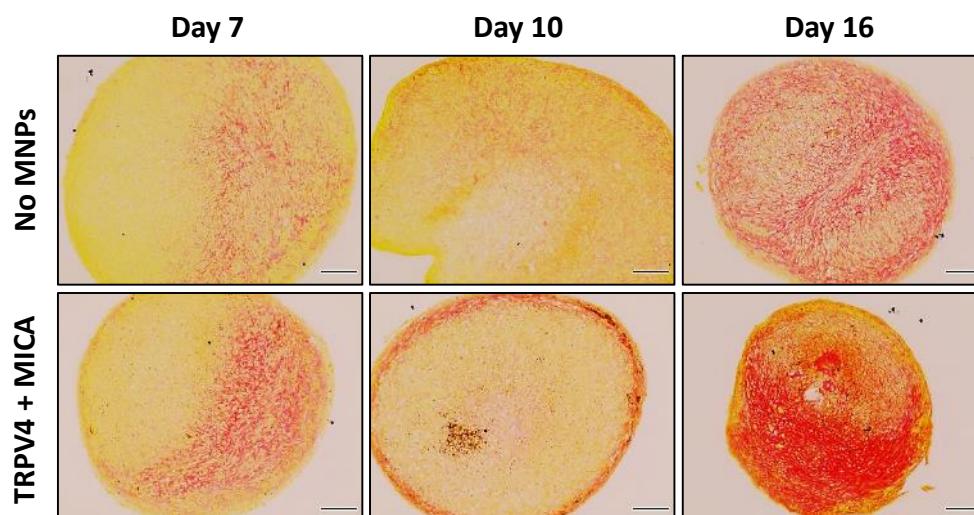


**Figure 4-35. Enhanced collagen production for TRPV4 MICA-activated samples from initial culture time points.** Representative images 7  $\mu\text{m}$  pellet sections from de-differentiated chondrocytes stained with picosirius red for collagen visualisation at days 7, 10 and 16 of culture. Collagen fibres are shown in a red colour and the background in yellow. Scale bar = 100  $\mu\text{m}$ .

Lastly, samples were stained with safranin O, a dye classically used for cartilage staining and haematoxylin for nucleus visualisation. The higher intensity of the stain represents higher cartilage matrix production. Samples cultured with no MNPs, showed an initial appearance of moderate production of ECM, localised not uniformly in a peripheral area of the samples (Figure 4-31). Nevertheless, the staining intensity decreased for the following time points analysed, as observed for the toluidine blue staining of the samples. Day 16 sections showed the higher intensity of the stain also in the periphery of the samples, despite not being homogeneous for all the sample's periphery area. Cells were spotted to be uniformly distributed among the section. TRPV4 MICA-activated samples showed a great intensity of the stain from the first week of culture, which was maintained or moderately increased, over the course of the experiment. The stain distribution was moderately homogeneous in the sections' surface for all time points analysed, with a tendency for higher intensity in the outer border of the samples, and the most central regions. Cells were also homogeneously

distributed among the surface of the section with a slight decrease of nucleus visualised in the central region of the samples at day 16 of culture.

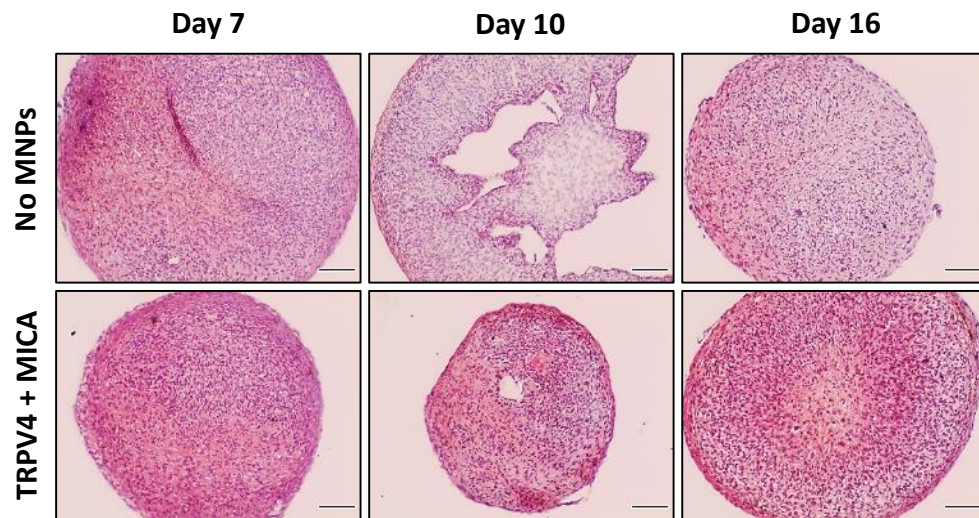


**Figure 4-36. Higher intensity of the stain observed in TRPV4 MICA-activated samples from day 7 of culture.** Representative images of 7  $\mu\text{m}$  pellet sections of de-differentiated chondrocytes at days 7, 10 and 14 of culture stained with safranin O. Higher intensity of the stain indicated higher matrix formation. Scale bar = 100  $\mu\text{m}$ .

## 4.5 Discussion

The success following an *in vivo* study of remote control healing for bone repair adapting the MICA technology to an animal study (222), led to the development of the present chapter. The regeneration of the bone tissue following stimulation of the TREK-1 channel opened the possibility of targeting specific mechano-sensitive proteins that controlled the chondrogenic response. After thorough study of the literature (1,157,164,171), TRPV4 was proposed as a mechanical target to induce chondrogenic differentiation of stem cells. During this chapter, an initial study evaluating the potential of MICA activation of mechano-sensitive elements on the cell membrane was performed in collagen II transfected eMSCs, to enable a comparison of different receptor targets and ease of the measuring impact. Collagen II is one of the key elements of the cartilage ECM and a chondrocyte specific marker (306) and hence, the chondrogenic activity of the mechano-inducible targets was assessed partially by the expression of the marker. TREK-1 and RGD are well-defined mechano-sensitive structures previously targeted by the MICA technology for bone healing. No direct correlation has been described in the literature for any of the chondrogenic events and therefore, an initial assessment of the effect on chondrogenic induction was carried aiming to establish a target for cartilage repair.

The expression pattern of collagen II was analysed over a time course, with initial expression observed on the first week of culture, mostly for those samples where TRPV4 was targeted. This was considered an effect enhanced by the mechanic stimulation of the channel, given that the expression of the marker is often observed to peak from day 14 to day 21 of culture (306,307). Activation of both RGD and TREK-1, also induced a higher expression of the marker when compared to those samples cultured in chondrogenic media alone without MNPs. Nevertheless, higher signal of expression was observed for all cases for TRPV4 stimulated samples. This was supported by the gene expression analysis with evident enhancement of the chondrogenic response in TRPV4 activated samples. For this reason, and based on the multiple studies showing a chondrogenic response following chemical or mechanical activation of TRPV4 (167,301,302), this was proposed as the main target of the current work, however,

given the similarity on the chondrogenic response observed with TREK-1 activation, further study was performed using other cell type, for the second part of this chapter.

The collagen production was also studied by histological staining of pellets with picosirius red. Despite the evidence of collagen production for all 3 tested targets, an in-depth analysis was unable to be performed due to the issues encountered with sample processing. The ECM formed specially for those samples labelled with TREK-1 and TRPV4, acquired a dense status that hindered the sectioning of the samples and the digestion for gene expression analysis. The potential of adipose-derived MSCs has been questioned due to the native origin of these cells. Despite observation that under conventional culture conditions AD-MSCs often transdifferentiate towards osteogenic and adipogenic lines, the culture in chondrogenic media has been reported to successfully induce chondrogenesis and ECM formation (308–310). In this study, AD-MSCs were able to undergo chondrogenesis when cultured with biochemical factors. The collagen production was indeed observed for the samples under static conditions cultured in chondrogenic media however, there was an enhanced and earlier production of ECM for those samples labelled with MNPs. Therefore, the collagen observed for the mechanically activated samples was attributed to the effect of mechanical stimulation. The delivery of mechanical stimulus to MSCs has been widely studied to promote chondrogenesis with upregulated ECM-protein production (104,311,312).

The addition of TGF- $\beta$  in the culture medium is often key for chondrogenic differentiation. TGF- $\beta$  acts by binding the type I receptor (ALK5), which leads to phosphorylation of the SMAD2/3 complex. However, TGF- $\beta$  can also find ALK1 activating alternative SMAD pathways that lead to hypertrophy states (278). The removal of the TGF- $\beta$  from the chondrogenic culture medium was planned with the aim of analysing the scope of the MICA activation. Although the collagen II expression was observed to be enhanced for those samples cultured with TGF- $\beta$  in the reporter cell fluorescence analysis, the expression of the marker was observed at earlier time points when lacking the growth factor. Moreover, gene expression analysis revealed enhanced expression of both *Col2a1* and *Acan* for those

groups cultured without TGF- $\beta$ , in contrast to the same groups cultured in complete media. This was hypothesised to be due to a later activation of the expression of some ECM markers, given that MICA treatment enhances the early expression of the matrix components. Moreover, some studies suggest the role of TGF- $\beta$  in hypertrophy development of cartilage (313), and given that is not clear when the growth factor switches from the protective role to cause a hypertrophy state, additional studies would be required to elucidate the exact role of TGF- $\beta$ . Further analysis on the effect of TGF- $\beta$  on the cartilage formation was assessed for the second part of this chapter.

Assessment of the *in vitro* chondrogenic potential is often based on histological scoring, however, there is a lack of universal consensus for a method of assessment that would allow for a more precise comparison among different studies. The use of a reporter cell line that allows to measure the chondrogenesis by visualising the collagen II expression, or quantification of the marker, by the measuring a secreted reporter, introduces the possibility of standardising chondrogenesis evaluation methods. The cells used for this study were provided by Dr. Glyn D. Palmer, and previously used as a successful transcriptional reporter system to measure chondrogenic activity (227). This study used the reporter system to support the histological and gene expression analysis, performed to measure the chondrogenic potential of the TRPV4 activation with the MICA technology. Our findings suggest that the combined effect of culturing cells in chondrogenic media, in addition to mechanically stimulating the mechano-sensitive ion channel TRPV4, results in an enhanced matrix deposition with increased production of the ECM markers collagen II and aggrecan. In addition, a morphological change in the cell phenotype was observed, whereby they acquired a square chondrocyte-like phenotype from the early days of culture. These observations are in line with the existing literature, attributing to TRPV4 a key role in cartilage development by the activation of *Sox9* transcription factor, responsible for the downstream production of collagen II and aggrecan proteins among others (1). TRPV4 has been defined as a key channel during the embryonic development of the skeleton, and the mutation of the channel is related to multiple skeletal dysplasias (157,231). Several studies have activated the channel

either with biochemical ligands or by delivery of mechanical forces nevertheless, the forces are delivered to a construct of cells, and other mechano-sensitive elements might be indirectly activating (170,171,295).

MICA technology principle is based on the delivery of an alternating external magnetic field which generates forces strong enough to pull the superparamagnetic MNPs tagged to the cell membrane, causing them to align with the external magnetic field (212,215). Once the magnetic field is removed, or the magnets stop exerting an effect due to the lack of proximity with the samples, the MNPs lose the magnetisation and return to their natural state (176). This aligning effect results in the delivery of selective forces to the mechano-inductive region of the channel, where the MNPs are directly targeted. The sum of the direct activation of the mechano-sensitive domain, and the “pulling” effect of the MNPs over the channel, induces the activation with the following ion exchange and downstream signalling activation. In this study, samples labelled with TRPV4-MNPs cultured without the external delivery of magnetic forces, showed similar results to those observed for magnetically activated samples. Although the chondrogenic effect was not as intense as the MICA activated samples, a clear enhancement was observed when compared to the control, cultured in chondrogenic media without MNPs. This was hypothesised to be an effect caused by the indirect activation of the mechano-sensitive ion channel, exerted by the MNPs being attached directly in the mechano-responsive region of the channel that controls the gating process. This was proposed to be an effect of the gravity of the MNPs affected and the usual movement of the culture plates. It may be a possibility that the channel indirectly activates under these events causing the channel to transiently activate showing a mild chondrogenic enhancement but not as strong as the magnetically stimulated groups. In line with these findings, previous studies have reported spontaneous calcium events on cells labelled with MNPs, without delivery of a magnetic field (121).

Despite the favourable results suggesting the improved chondrogenesis after MICA activation of TRPV4, the collagen II reporter luciferase system did not show statistical differences among MNP

labelled and unlabelled groups. Although a tendency towards higher collagen II expression was observed for TRPV4-MNPs labelled samples, there were no statistical differences among groups. Despite using the control cells constitutively expressing luciferase controlled by the CMV promoter, only 2 groups of these cells were studied; CMV-Luciferase cells cultured in chondrogenic media and labelled with TRPV4-MNPs. The addition of the static and MICA-activated conditions would have allowed for a more precise normalisation. This could potentially explain the low differences found among studied groups, since as observed in Chapter 3, TRPV4 MICA-activated samples often undergo a reduction on the metabolic activity of the cells over the initial 14 days of culture, while undergoing differentiation. The proliferative activity often resumes after the second week of culture, however, the luciferase readings were only performed up to 14 days of culture due to the fragile nature of the micromass culture. The metabolic activity measured for this study, only allowed to elucidate that the presence of the MNPs on the samples was not affecting cell viability however, this study was performed under static conditions and hence the effects of MICA activation over culture time remain unknown.

The presence of TRPV4 channel was successfully demonstrated for all studied conditions. A notable increased presence of the channel was observed for those samples mechanically activated. The trafficking of the channel is a highly controlled process. Some studies suggest that the activation of the channel with the agonist GSK101 does not affect the trafficking of the channel (314). Nevertheless, opposing research suggests that following activation of the channel with GSK101, newly recruited channels are expressed in the membrane, followed by internalisation of the channel that is observed within 20 minutes after activation (250). The lack of literature available for the control of the channel trafficking after mechanical stimulation led to the preliminary study in Chapter 3 of the fate of the channel following activation. Despite the observation of the internalisation of particles by the invagination of the cell membrane, the limitations accessing a high-power microscopy hindered the

in-depth analysis. Further studies could elucidate the causes behind the increased presence of the channel on the cell membrane following MICA activation.

Protocols for chondrogenic differentiation often culture cells for a standard period of 21 days (315–317). However, other studies use longer periods of culture time, usually consisting of 28 days of culture (318,319). The longer culture of chondrogenic constructs under biochemical or mechanical stimulation, may enhance the development of hypertrophic constructs and reduce the mechanical properties of the tissue (320). With the aim of better understanding the gene expression pattern on the chondrogenic constructs, samples were cultured for 28 days. Collagen II expression was observed to be increased with culture time until termination of the experiment, however, this was not the case for aggrecan. The great increase of the collagen II might, hence, be a consequence of the chondrocytes turning into a hypertrophic phenotype, however, further assessment of hypertrophic markers such as collagen X will be further analysed in Chapter 5 in order to obtain more conclusive results.

For the second part of this chapter, ovine MSCs, chondrocytes and de-differentiated chondrocytes were used to further examine the MICA potential for cartilage repair. Ovine cells were selected for this study with the intention of conducting a pre-clinical ovine trial, following the group work on an ovine model for bone repair. In the previous section, the TGF- $\beta$  was removed from the culture medium with the intention of testing the chondrogenic potential of MICA without adding one of the key differentiation factors. Nevertheless, the chondrogenesis on TRPV4 activated samples was observed to be similar with or without TGF- $\beta$ . For this reason, and with the aim of further understanding the relationship of TGF- $\beta$  and TRPV4 crosstalk, histological determination was performed on a 3D culture system. Moreover, TREK-1 and TRPV4 chondrogenic comparison was also assessed with the aim of selecting the more chondro-inductive pharmacological target for MICA activation. TGF- $\beta$  is a crucial factor for maintaining cartilage homeostasis and normal tissue development (321). However, it has been described to have both a protective and catabolic role (322). Despite the need for TGF- $\beta$  signalling for the healthy maintenance of cartilage and avoidance of the hypertrophic phenotype, it

has also been reported that in aged chondrocytes, the TGF- $\beta$  pathway often switches from the anabolic SMAD2/3 pathway to the catabolic SMAD1/5/8 pathway and therefore, the activation of the pathway might not be beneficial for aged patients (323).

For this study, samples cultured without TGF- $\beta$  showed similar chondrogenic potential for MICA activated samples, however, as previously observed in the eMSCs study, the effect was more enhanced when samples were cultured in a complete media. Moreover, this similarity was specially observed for TRPV4 activated pellets that showed similar levels of gene expression of the ECM markers. The relationship between TRPV4 and TGF- $\beta$ , is now beginning to be investigated. A study performed by O'Connor et al. reported increased TGF- $\beta$  expression for constructs under mechanical loading, or following TRPV4 activation with the agonist GSK101 (171). The lack of TGF- $\beta$  in the culture medium might be replaced by the activation of the growth factor expression directly by the mechanical stimulation of the constructs, and the TRPV4 pathway activation. Therefore, it was hypothesised that the similarity of the chondrogenic analysis in samples cultured without TGF- $\beta$  was due to the upregulation of TGF- $\beta$  in the cells following activation of the signalling pathway by MICA-induced mechanical activation of TRPV4. Nevertheless, long culture times without the presence of TGF- $\beta$  could potentially induce chondrocytes to undergo a final differentiation towards the hypertrophic state (300) and therefore the large increase observed in some cases for gene expression could be a result of the cells entering this state. A further study on samples cultured without TGF- $\beta$  and without MNPs or MICA activation could potentially elucidate this hypothesis.

Regardless of the enhanced chondrogenesis observed for samples cultured without TGF- $\beta$ , it was noted that the level of organisation of the ECM was higher for those groups cultured in complete media. There was a tendency observed for samples cultured in complete media to form an external ring of collagen and show GAGs deposited in the centre of the pellet sections. This could be correlated to the native tissue levels of organisation, being the superficial zone rich in collagen II and water, and the middle zone the richest region in proteoglycans (10). The higher organisation of the collagen fibres

was also supported by the polarised microscopy data, that showed a higher level of thickness and organisation for the collagen fibres produced by MICA activated samples cultured in complete chondrogenic media.

This study was performed on MSCs, de-differentiated chondrocytes and freshly isolated chondrocytes (Supplementary figure 3). Interestingly, freshly isolated chondrocytes did not show any chondrogenic markers. These results were attributed to a bad donor, given that chondrocytes on passage 1 should retain some of their natural properties. In contrast to this, MSCs and de-differentiated chondrocytes showed a good chondrogenic response, being moderately improved for the de-differentiated chondrocytes. This was thought to be due to the retention of the chondrogenic potential of chondrocytes, as this has been previously reported in other studies (324,325). The combination of the results from this chapter, and the homogeneity of the response, supported by the available literature reporting the role of TRPV4 in chondrogenesis (1), led to selection of this channel as the pharmacological target for the further study of MICA as novel tool for remote cartilage repair.

## 4.6 Conclusions

The targeting of the mechano-sensitive proteins RGD, TREK-1 and TRPV4 improved the chondrogenesis on micromass culture. TRPV4 was selected as the main mechano-inductive target for the duration of this work, due to the enhanced production of ECM markers compared to RGD and the homogeneity on the chondrogenic response compared to TREK-1, in addition to the solid research supporting the essential role performed during chondrogenesis. MICA activation of the TRPV4 channel resulted in improved chondrogenic performance for all studied cell types and conditions, when compared to culture in chondrogenic media without further stimulation. The enhanced production of ECM markers has led to further investigation of the potential of this technology for obtaining cartilage constructs with improved functionality, which are able to fulfil the mechanical requirements of the native tissue. The evidence provided by the collagen 2 reporter cell line, and the histological staining

led to continuation of the study of the MICA technology on TRPV4 activation for cartilage repair, however, alternative cell sources will be investigated in the next chapter to evaluate the chondrogenic response for a potential cell therapy.

---

# *Chapter 5*

---

*Human UC-MSCs as potential candidates for an injectable OA therapy*

## 5.1 Introduction

Current tissue engineering treatments for OA repair are based on the use of autologous chondrocytes obtained from non-load bearing healthy areas of the patient's own articular cartilage for regeneration of the damaged tissue. More novel approaches propose the delivery of autologous stem cells injections that aim to trigger intrinsic repair and resolve the inflammatory events. Despite the chondrogenic potential observed for these cells sources *in vitro*, the donor age and health status may reflect on the potential of the cells to expand and differentiate (326,327). Often the donor presents a defect that fails to meet the criteria for autologous cell therapy, hence, researchers are focusing on the study of the safety and efficacy of allogenic cell treatments as an alternative cell source, demonstrating a promising potential (62).

Adult stem cells can be obtained from several tissues such as adipose tissue, bone marrow, dental pulp, gastrointestinal tract, or synovial fluid. Despite the good chondrogenic response observed *in vitro* for bone marrow-derived MSCs, the invasive and painful method of extraction from the iliac crest or the pelvic bone, the variable amount of obtained cells and their donor-dependant expansion and differentiation potential, has set the focus on seeking for novel sources of MSCs. As an alternative, MSCs can also be obtained from extra-embryonic tissues such as the umbilical cord, the amniotic fluid or the placenta (328).

The use umbilical cord-derived stem cells do not involve ethical concerns given that the tissue is often discarded. In addition, the painless extraction of the cells and the early age of the donor source, make them excellent candidates for tissue engineering techniques. UC-MSCs share properties with both adult MSCs and ESCs although they do not form teratomas. The key element for this cell source cells, is the possibility that they may have immune-privileged status which would make them a safe candidate for allogenic OA therapy (329). The chondrogenic potential of UC-MSCs has been previously

assessed with promising outcomes and some recent studies have begun to investigate the potential for OA repair *in vivo* (330,331).

In terms of tissue engineering approaches for OA, articular chondrocyte implantation is among the most practiced treatments when aiming for not only symptomatic relief, but also self-regeneration of the damaged tissue. Despite the good outcomes reported after long-term follow-up on ACI patients, the limitations encountered with the donor site morbidity or the compromised success rate for defects bigger than 4.5 cm<sup>2</sup>, highlight the need for alternative therapies to be offered (332,333).

Injectable stem cell therapies are becoming increasingly popular due to the ease of the administration procedure, low invasiveness, low cost of the technical procedure, the elimination of the 2 surgery-step for healthy tissue collection and more importantly, the promising clinical outcomes reported (273,334). However, these therapies also encounter some limitations due to the autologous source of stem cells, that is restricted by the proliferative and differentiation potential of the patient's own cells. Hence, injectable therapies could potentially benefit from a novel stem cell source with high expansion capacity in order to achieve the required cell number. Moreover, the cell source should be able to successfully achieve chondrogenic differentiation, being able to generate native cartilage-like matrix, fulfilling the mechanical and functional needs of the tissue.

It is also of great importance to consider that the chondrogenic potential of stem cells *in vitro* is often studied under the effect of chondro-inductive cues such as TGF- $\beta$  or BMP-2. Nevertheless, following *in vivo* injection of the MSCs, cells are subjected to the local niche microenvironment and chondrogenic events rely on the paracrine effect of the cells, due to the lack of vascularisation in the tissue. The possibility of guiding the stem cell fate remotely could introduce an enormous advantage for cell-based therapies.

The work described in this chapter aims to study the chondrogenic potential of umbilical cord-derived stem cells in response to MICA stimulation and biochemical treatment, with the aim of studying UC-

MSCs as a potential allogenic source for an OA injectable therapy. The initial study was focused on *in vitro* differentiation of human primary UC-MSCs with the objective of potentially translating the study into an ovine model.

## 5.2 Aims

The aims of this chapter were:

- To study the chondrogenic potential of hUC-MSCs with the aid of biochemical factors and the use of the MICA technology in comparison with BM-MSCs
- To assess the variability on the chondrogenic response on 3 different donors
- To assess the length of MICA stimulation time required to induce chondrogenesis
- To design an injectable therapy with hUC-MSCs and MICA technology for a pre-clinical trial on an ovine model

## 5.3 Methods

### 5.3.1 Experimental design

The experiments performed for this chapter were done testing human UC-MSCs from 3 different donors, obtained from The Robert Jones and Agnes Hunt orthopaedic hospital, and treated as indicated in section 2.3.5. Due to the need of large number of cells for pellet formation, cells were expanded to passage 4 and 5.

Cells were cultured and expanded as described in section 2.3.5 and when achieved an optimal number of cells ( $2 \times 10^5$  cells per pellet), cells were labelled with TRPV4-MNPs and pellets were formed following the protocols in sections 2.5.4 and 2.3.7 and cultured in chondrogenic media for hUC-MSC (section 2.4). This process was repeated using stem cells from 3 different donors, and a fourth time combining the 3 donors together. For the pooled experiment, cells were labelled as described in section 2.11 with a tracking agent to assess the effect of the dye prior to carry *in vivo* experiments (Results not shown).

Pellets were studied at different culture time points: 24 hours after formation and at days 7, 10 (results not shown), 14 and 21 of culture. For each time point, cells were processed for further analysis and stored in appropriate conditions in order to perform the analysis at once, with the aim of avoiding variability on the results. Samples were stimulated with the magnetic force bioreactor as per described in 2.6 on a regime of 1 hour of stimulation for 5 days followed by 2 resting days. Pellets were firstly stimulated on the following day after formation (excepting for the 24-hour time point sample to be collected). Samples were stimulated for the same amount of days before the 2-day break in order to maintain homogeneity.

For the 3 repetitions of the experiment, some experimental groups were preserved, and new groups were incorporated with the aim of testing all possible experimental conditions (Table 5-1). The lack of repeats for some groups was caused by the limited amount of cells at a maximum determined passage with the aim of avoiding loss of potency of the cells. Hence, a decision had to be met to test certain groups for each donor to avoid from missing relevant culture conditions. For this reason, the positive control was only tested for 2 donors, and used for comparative purposes for donor 2 where it was found the highest limitation on cell number for pellet formation. For all groups except unlabelled MNPs, repeats were done in at least 2 donors. Cells were cultured in chondrogenic media described in section 2.4, containing 10% FBS, unless stated otherwise. An experimental group was also cultured with the TRPV4 chemical agonist, GSK101, following the protocol in section 2.4.1.

**Table 5-1. Experimental groups for the 2 different hUC-MSC donors.**

| Group                             | Donor 1 | Donor 2 | Donor 3 |
|-----------------------------------|---------|---------|---------|
| Cells                             | ✓       | ✓       | ✓       |
| Cells (1% FBS)                    |         | ✓       | ✓       |
| Cells + MNPs                      |         | ✓       |         |
| Cells + GSK101                    | ✓       |         | ✓       |
| Cells + TRPV4 MNPs Static         | ✓       |         | ✓       |
| Cells + TRPV4 MNPs (1% FBS)       |         | ✓       | ✓       |
| Cells + TRPV4 MNPs +MICA          | ✓       | ✓       | ✓       |
| Cells + TRPV4 MNPs +MICA (1% FBS) | ✓       | ✓       | ✓       |

With the aim of simplifying the experimental conditions for a potential *in vivo* experiment, the effects of a shorter MICA activation of the pellets was tested; 7 days of stimulation against 21 days (Supplementary figures 4 and 5). Analysis was performed on days 0, 7, 14 and 21. (Table 5-2). In addition, some samples were labelled with a cell tracker (section 2.11) to assess the effects of the tracking dye in the pellet formation and proliferation (Results not shown).

**Table 5-2. Pooled donors experimental conditions for each studied time point.**

| Group                                   | Day 7 | Day 14 | Day 21 |
|---|-------|--------|--------|
| Cells                                   | ✓     | ✓      | ✓      |
| Cells + GSK101                          | ✓     | ✓      | ✓      |
| Cells + TRPV4 MNPs Static               | ✓     | ✓      | ✓      |
| Cells + TRPV4 MNPs + <b>7-day</b> MICA  | ✓     | ✓      | ✓      |
| Cells + TRPV4 MNPs + <b>21-day</b> MICA |       |        | ✓      |

The area of the pellets from donor 1 was measured for 1 sample per group with the aim of evaluating any major changes of the pellet size before setting the culture conditions in future experiments. The

total area of the pellet was measured by hand-drawing the area around the sample and obtaining the area in  $\mu\text{m}$  by the software of the microscope EVOS M5000.

### 5.3.2 Histological and immunohistochemical analysis

The histological analysis of the pellets aimed to measure the chondrogenic potential of the UC-MSCs and the quality of the cartilage formed. For this purpose, the histological assessment was done in duplicate samples and 3 sections per sample (only shown results from 1 sample), for all 4 experiments, and samples were stained with toluidine blue (section 2.7.6), GAGs detection with alcian blue (section 2.7.7), picrosirius red for collagen visualisation (section 2.7.8) and safranin O for proteoglycan detection (section 2.7.10, results not shown). Samples were also stained with prussian blue for visualisation of the iron content of the MNPs (section 2.7.9) and haematoxylin and eosin for general observation (section 2.7.5, results not shown).

Immunohistochemistry was performed in order to visualise more specific cartilage markers. Following indications in section 2.9, one pellet per group and 3-4 sections per pellet were stained with Collagen II, Collagen X, SOX9 and Ki67 markers and imaged with the automated microscope Cytation 5. Settings were kept the same for all 4 experiments for comparative purposes. The fluorescent analysis was quantified by Image J by measuring the total fluorescent intensity in a designated area for all pictures taken per pellet (Section 2.9.5).

### 5.3.3 Gene expression and DNA / sGAGs analysis

Molecular biology and biochemical assays were restrained to certain experiments due to the lack of samples from each donor to perform all tests. For donor 1, a total of 5 pellets per group were digested, and RNA was extracted and converted to cDNA for gene expression analysis (sections 2.15 and 2.16). From each individual sample, 3 replicates were tested for statistical relevance. The expression of *COL2A1*, *ACAN*, *SOX9* and *COL10A1* was determined and normalised to *GAPDH* expression levels as per indicated in section 2.17.

For donor 3 and the experiment performed with the combination of cells from all 3 donors, the glycosaminoglycans were quantified relative to the amount of DNA present in the samples. From each experimental group, 3 samples were digested (section 2.12) and GAGs were measured by the DMMB assay in triplicates and normalised to the DNA measured by the PicoGreen™ assay (sections 2.13 and 2.14).

#### 5.3.4 Statistical analysis

Statistical analysis was performed as indicated in section 2.24.

## 5.4 Results

### 5.4.1 Pellet size analysis

The pellet total area was measured for the first donor for all time points studied (Figure 5-1). Samples measured 24 hours after inducing the pellet formation were on the process of curling in order to form a dense and rounded construct. For this reason, irregular-shaped structures were observed, corresponding to the sheet of cells that is formed prior to achieving the dense and rounded morphology of the pellet. Hence, the total area was seemingly bigger due to the non-uniform shape of the samples (results not shown).

In general, across the experimental groups, pellet size increased from day 7 to day 21 of culture with the greatest changes observed during the initial 2 weeks of culture. No statistical differences were found between the studied groups, however, there was a slight growth elevation of MICA activated pellets when cultured with 1% FBS. The overall increase in pellet size with culture time was further evaluated by histological means to determine the nature of the sample growth.

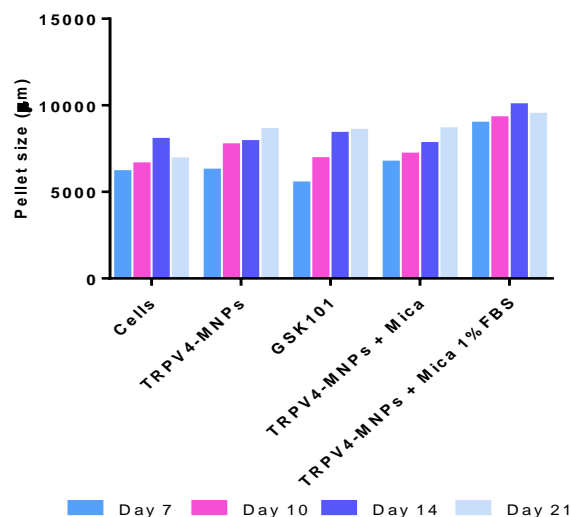


**Figure 5-1. Pellet size increases with culture time for all groups with a tendency for enhanced size in MICA activated samples cultured with 1% FBS.** Total area of the pellets manually delimited for all groups from donor 1 samples at all culture time points, n=1.

## 5.4.2 Pellet histology

### 5.4.2.1 Prussian blue

The presence of the MNPs was assessed on pellet sections. The distribution of the MNPs remained throughout the pellet for all groups until the termination of the experiment (Figure 5-2). Pellets labelled with TRPV4-MNPs cultured in 10% FBS in both static and MICA conditions showed some aggregation of MNPs in the form of darker stained areas, however, the distribution of the MNPs was homogeneous in the rest of the surface. For samples labelled with TRPV4-MNPs and cultured in low serum media, the presence of MNPs on the pellets seemed to be lower compared to the previous groups and there was less aggregation. No particles were detected in unlabelled samples.

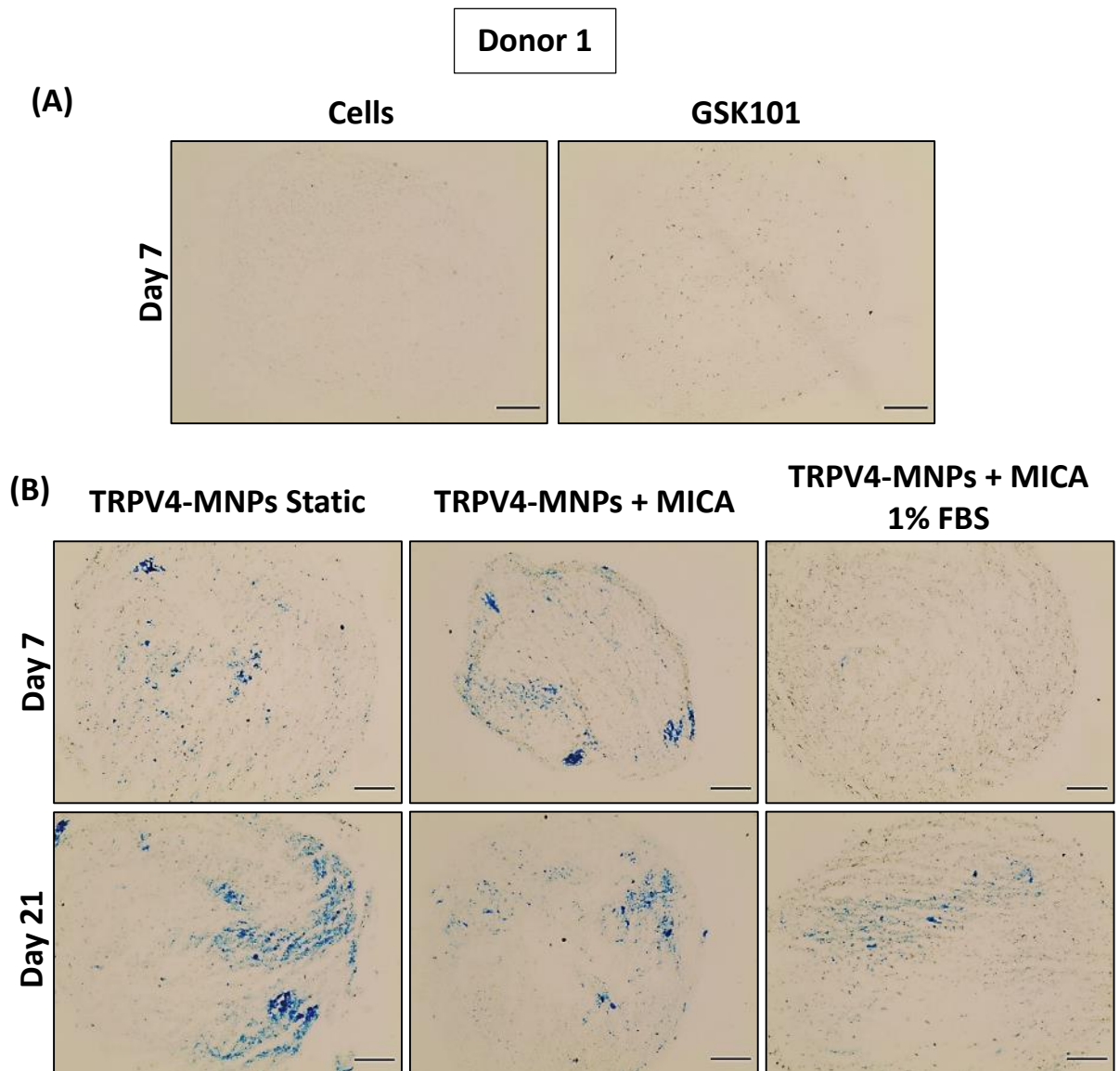


**Figure 5-2. MNPs were present after 21 days of culture with some areas of higher aggregation.** Representative images of MNPs stained with prussian blue on 7  $\mu\text{m}$  pellet sections from donor 1 at days 7 and 21 of culture on A) not labelled pellets and B) samples labelled with TRPV4-MNPs. The iron content of the MNPs is stained in blue. Scale bar = 100  $\mu\text{m}$ .

Pellets from donor 2 labelled with MNPs also showed presence of iron on the sample area with clear small clusters of MNPs in some areas and a general distribution of MNPs all over the sample (Figure 5-3). Samples cultured in 1% FBS seemed to match results from donor 1 with a lighter blue staining indicative of less aggregation of MNPs. No presence of particles was detected in unlabelled samples.

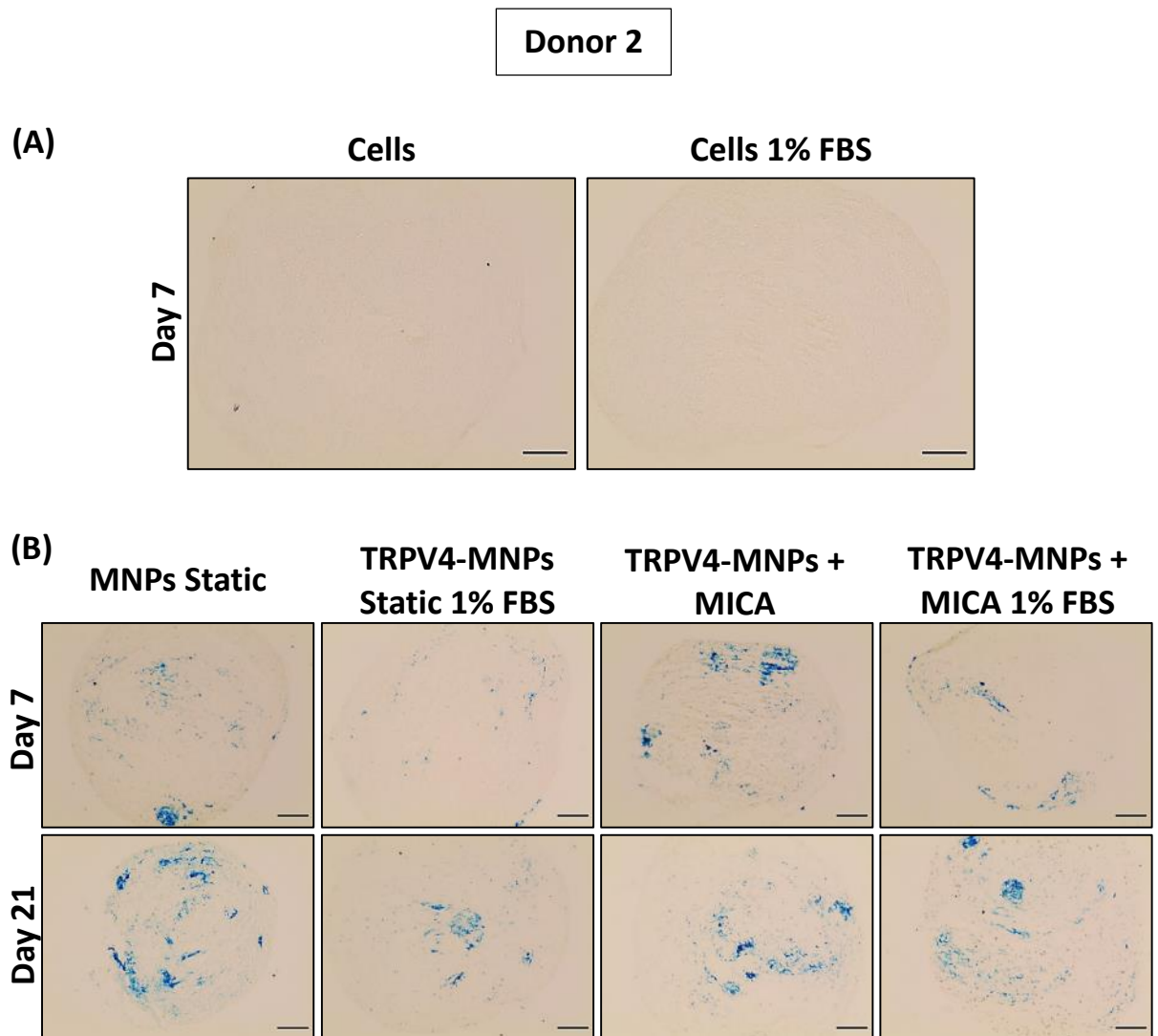


**Figure 5-3. Clustering of MNPs was present in all samples and similar concentration of particles was observed after 21 days of culture.** Representative images of Nanomag 250 nm stained with prussian blue on pellet sections from donor 2 of 7  $\mu\text{m}$  at days 7 and 21 of cultured on A) samples not labelled with MNPs and B) samples labelled with TRPV4-MNPs. The iron content of the magnetic nanoparticles is stained in blue. Scale bar = 100  $\mu\text{m}$ .

Samples from donor 3 showed a wide spread distribution of the MNPs across the pellet area with evident less aggregation than observed for previous donors (Figure 5-4). Little to no aggregation of MNPs was observed regardless of the group or the culture conditions. Samples not labelled with MNPs did not exhibit presence of MNPs.

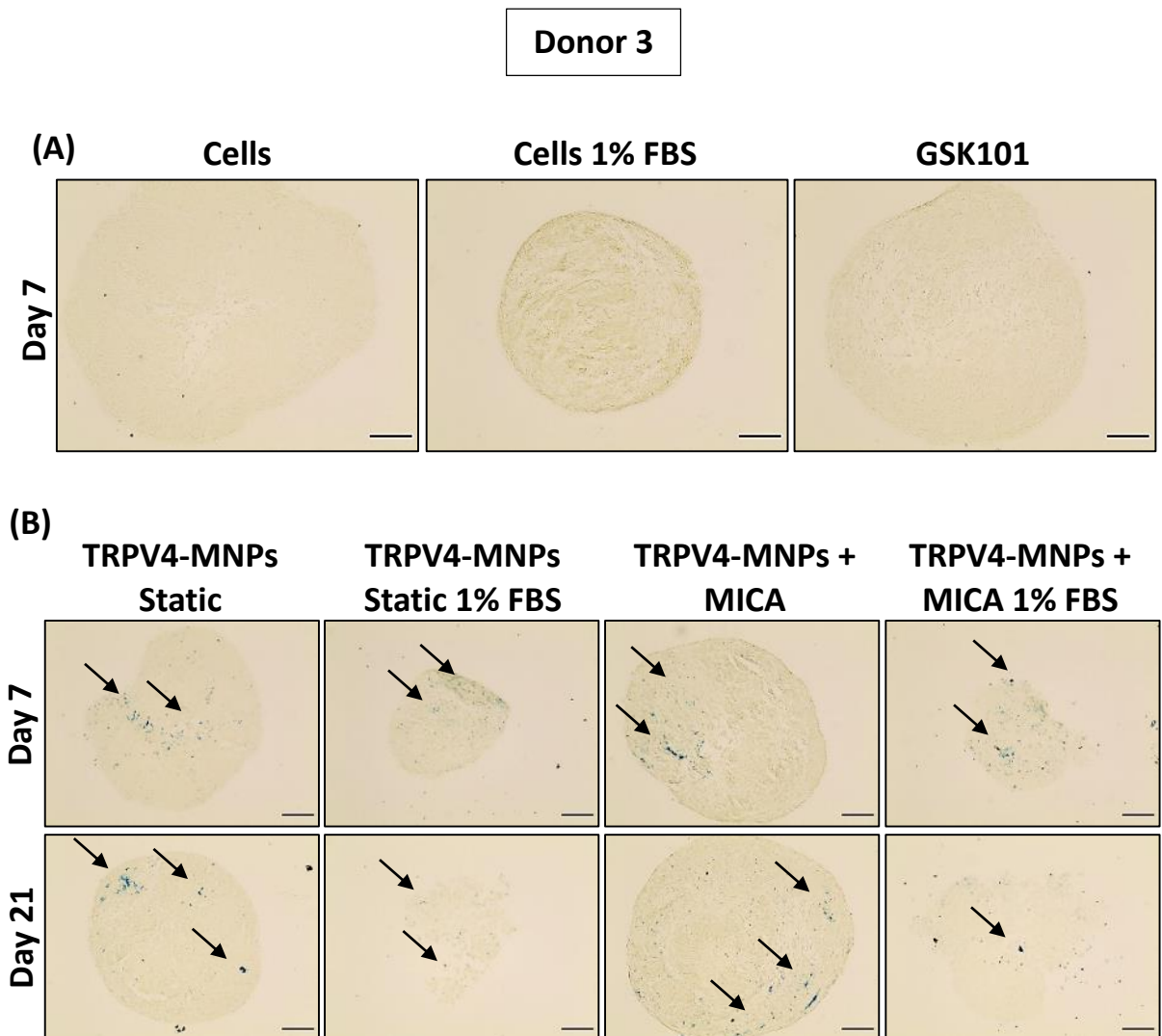


**Figure 5-4. MNPs were homogeneously distributed on the sections with little clustering observed.** Representative images of Nanomag 250 nm stained with prussian blue on pellet sections from donor 3 of 7  $\mu\text{m}$  at days 7 and 21 of cultured on A) samples not labelled with MNPs and B) samples labelled with TRPV4-MNPs. The iron content of the magnetic nanoparticles is stained in blue and indicated by black arrows. Scale bar = 100  $\mu\text{m}$ .

When analysing pellets formed of the combination of cells from the 3 donors, a homogeneous distribution of particles was also observed with little clustering of the MNPs (Figure 5-5). The data demonstrated little reduction of MNPs presence within the pellets over the time course of the experiment. As for the previous cases, no differences were observed among samples submitted to a magnetic field and samples under static conditions, indicating the lack of influence of the magnetic force on the particle distribution after pellet formation.

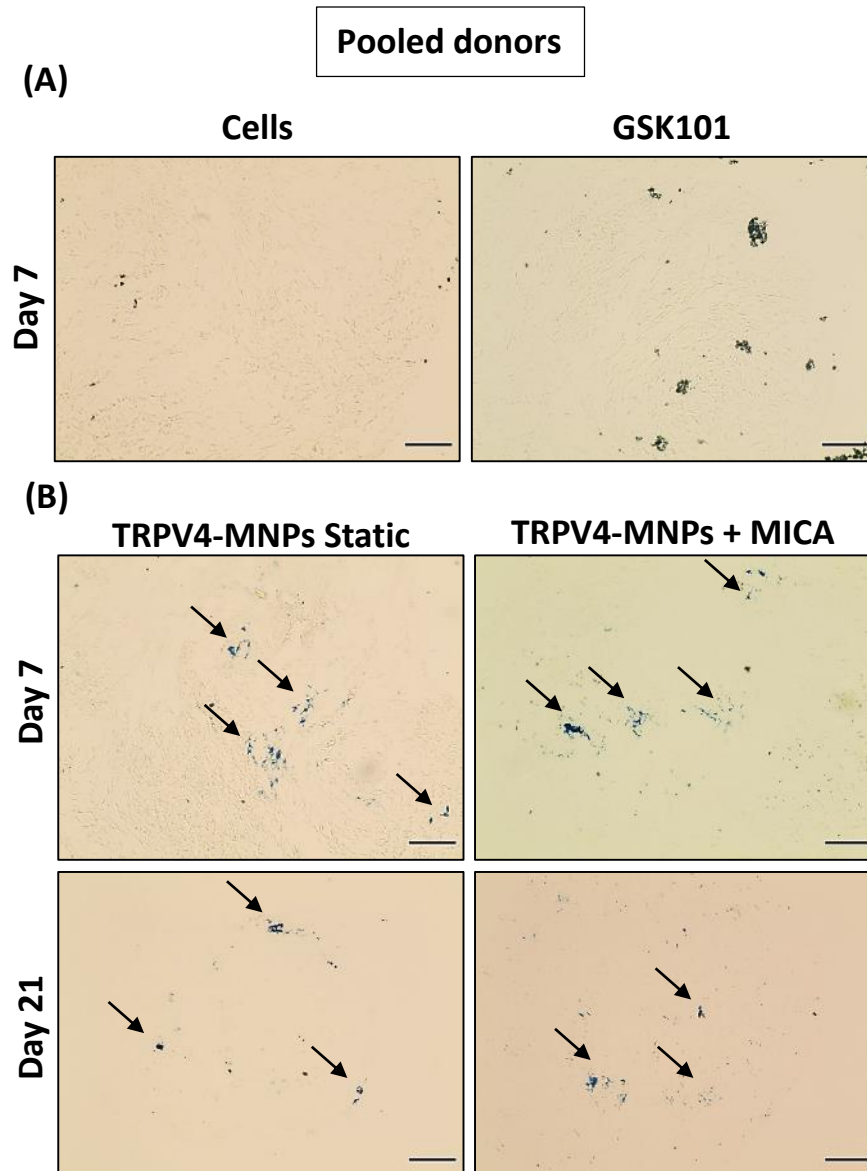


**Figure 5-5. Homogeneous distribution of MNPs observed on pellet sections from pooled donors.** Representative images of Nanomag 250 nm stained with prussian blue on pellet sections of 7  $\mu\text{m}$  at days 7 and 21 of cultured on A) samples not labelled with MNPs and B) samples labelled with TRPV4-MNPs. The iron content of the magnetic nanoparticles is stained in blue and indicated by black arrows. Scale bar = 100  $\mu\text{m}$ .

#### 4.4.2.2 Alcian blue: sulphated GAGs determination

Pellets were stained with alcian blue to reveal the presence of sulphated GAGs on the samples, correlated with an optimum cartilage ECM formation. Alcian blue at pH 1 stains for sulphated GAGs showing higher sGAG deposition with increased stained intensity. In order to compare the results to native tissue, human cartilage tissue sections were stained following the same procedure and control pellet samples were stained 24-hour after pellet setting for comparative purposes (Figure 5-6).

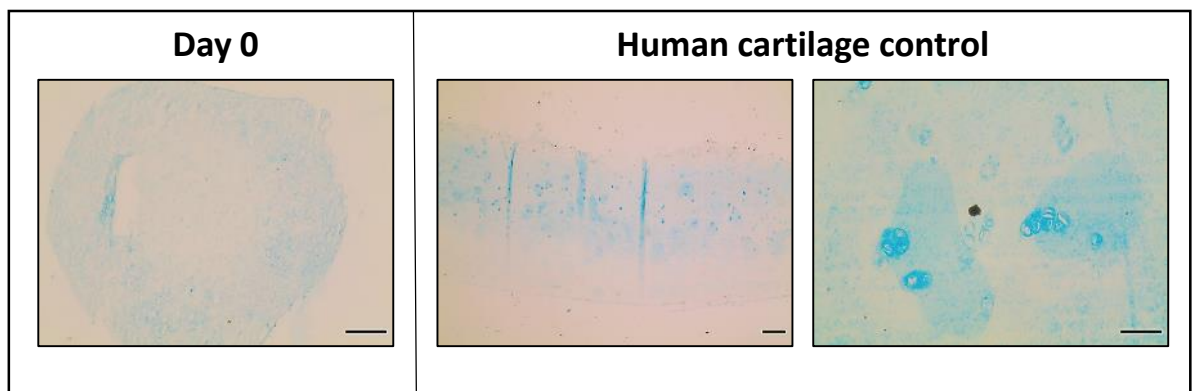


**Figure 5-6. Alcian blue staining of a pellet sample at day 0 of culture and human cartilage samples.** Sections of 7  $\mu\text{m}$  of pellets cultured for 24 hours were used for comparative purposes (scale bar = 100  $\mu\text{m}$ ). Native cartilage sections of 7  $\mu\text{m}$  were stained as positive control. Scale bars = 250 and 50  $\mu\text{m}$ .

Donors 1 and 2 shared very similar results after 21 days (Figures 5-7 and 5-8). Over the first week of culture, samples started to exhibit a discrete amount of stain, being more evident in TRPV4 stimulated samples either by addition of the chemical agonist, GSK101, or by magnetic activation. sGAGs deposition was imaged at days 10 and 14 of culture (results not shown) with similar trends until day 21 which was the time point when the biggest differences were observed. For donor 1, samples cultured in 10% FBS with GSK101 and MICA activation showed an increase in the intensity of the stain, indicating higher levels of sGAGs production. Donor 2 pellets matched the previous results with enhanced sGAGs in MICA activated samples. Interestingly, samples cultured in 1% FBS for both donors appear to have a reduced amount of GAGs regardless of the experimental conditions. When compared

to the human cartilage control, both groups, GSK101 and TRPV4 MNPs MICA-stimulated, exhibited a similar intensity of the stain. Nevertheless, at higher magnifications the pericellular structure observed in the positive controls was not able to be observed for the studied samples. Donor 3 pellet sections showed a different profile to the previous two donors (Figure 5-9). Overall, the intensity of the stain had a light appearance with no noticeable changes from initial time points until termination of the experiment. There was little variation between groups and no correlation was observed between samples cultured with 10% or 1% FBS. Higher magnification images showed a non-homogeneous distribution of sGAGs across the sections surface (results not shown).

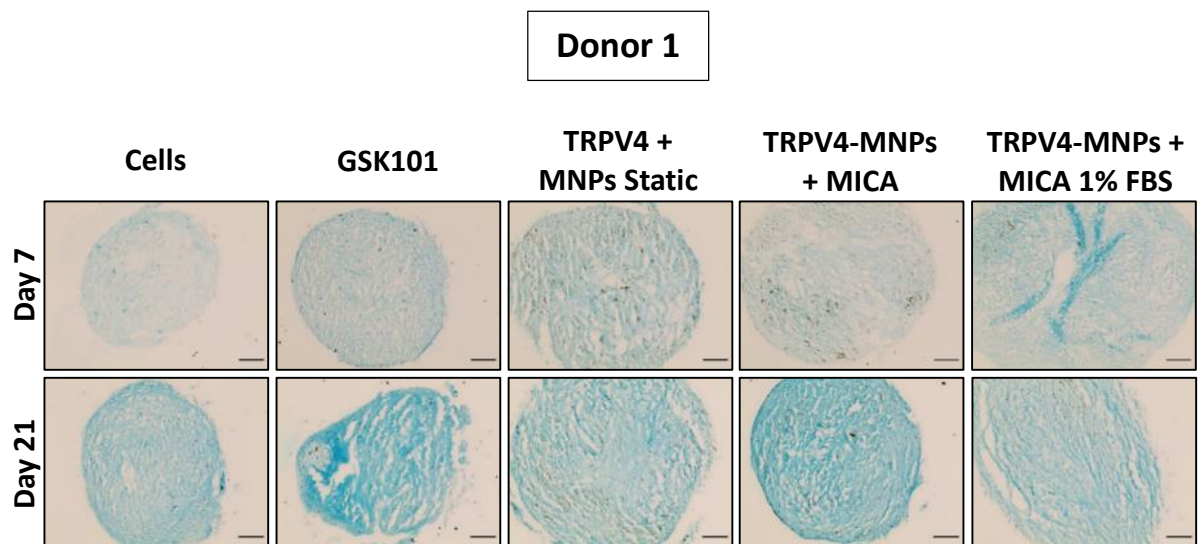


**Figure 5-7. TRPV4 activated samples showed enhanced sGAGs deposition.** Representative images of pellet sections of 7  $\mu\text{m}$  from donor 1 stained with alcian blue for sulphated GAGs reveal at days 7 and 21 of culture. The higher intensity of the colour of the stain reveals the presence of GAGs in the sections. Scale bar = 100  $\mu\text{m}$ .

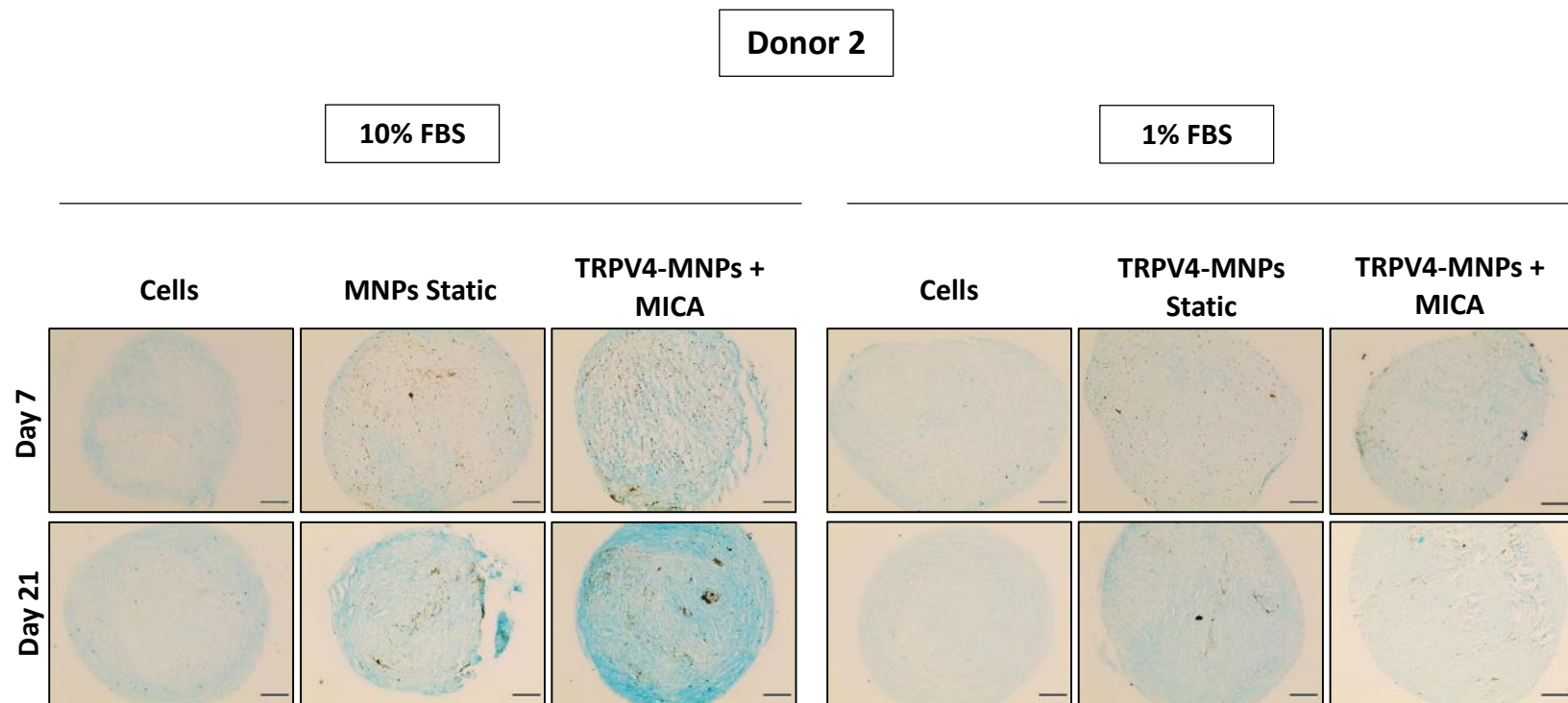


**Figure 5-8. MICA activated samples cultured in 10% FBS showed evident increase in sGAGs production.** Representative images of pellet sections of 7  $\mu$ m from donor 2 stained with alcian blue for sulphated GAGs reveal at days 7 and 21 of culture for samples cultured in 10% (left) and 1% FBS (right) The higher intensity of the colour of the stain reveals the presence of GAGs in the sections. Scale bar = 100  $\mu$ m.

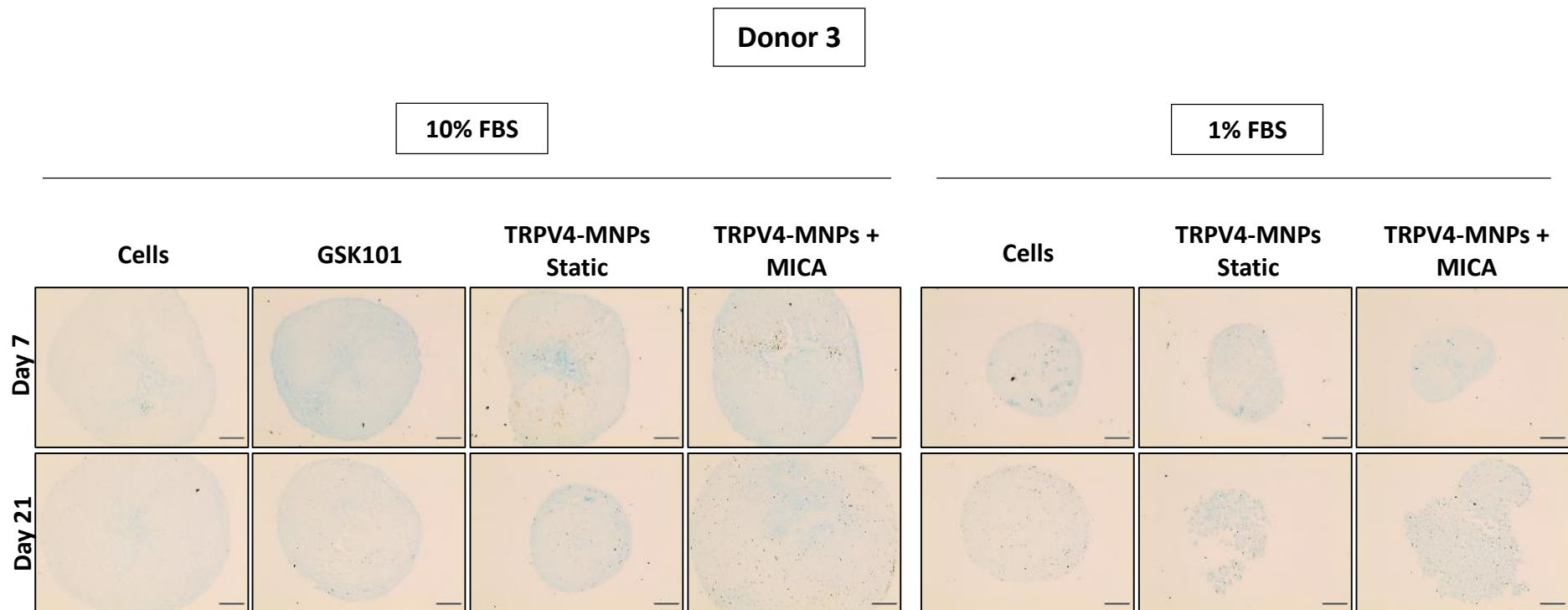


**Figure 5-9. Lower stain intensity was observed for all studied groups from donor 3 samples.** Representative images of pellet sections of 7  $\mu\text{m}$  from donor 3 stained with alcian blue for sulphated GAGs reveal at days 7 and 21 of culture for samples cultured in 10% (left) and 1% FBS (right). The higher intensity of the colour of the stain reveals the presence of GAGs in the sections. Scale bar = 100  $\mu\text{m}$ .

Pellets formed from pooling cells from all 3 donors showed overall similar results to donors 1 and 2, with increased sGAGs deposition over culture time (Figure 5-10). Chemically or mechanically TRPV4 activated samples showed increased sGAGs deposition when compared to the control pellets. The stain was homogeneously distributed on the pellet sections for all studied groups. Control samples exhibited little sGAG deposition. When comparing the MICA stimulated samples for 7 days alone (7 days of magnetic stimulation and 21 days of culture) with samples cultured and stimulated for 21 days, no evident differences were observed (Supplementary figure 4).

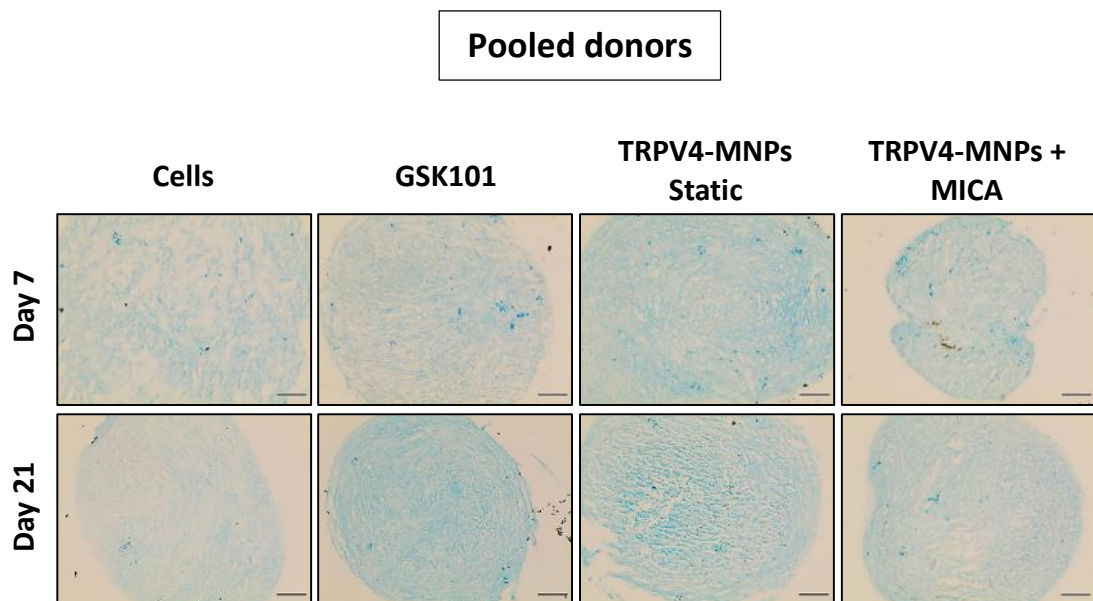


**Figure 5-10. Similar sGAG deposition to previous experiments was observed with lower stain intensity levels for control samples.** Representative images of pellet sections of 7  $\mu\text{m}$  from pooled donors stained with alcian blue for sulphated GAGs imaged at days 7 and 21 of culture. The higher intensity of the stain reveals the presence of GAGs in the sections. Scale bar = 100  $\mu\text{m}$ .

#### 5.4.2.3 Toluidine blue determination of proteoglycans

Samples were stained with toluidine blue, a dye that exposes the presence of proteoglycans in the sample by detecting a purple coloration on the sections and staining in blue the background structures. Human cartilage was stained as positive control as shown in Figure 5-11. The control clearly shows a purple coloration with chondrocytes arranged in columns. For comparative purposes, a section from a pellet cultured for 24 hours was used clearly showing a blue coloration and lack of GAGs present at this early time of culture.

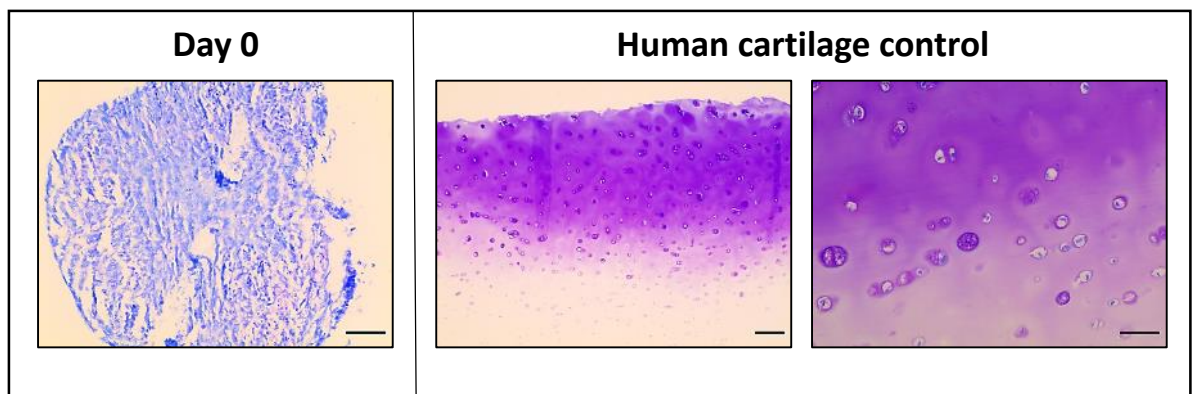


**Figure 5-11. Toluidine blue staining of negative and positive controls.** Representative fluorescence images of 7  $\mu\text{m}$  sections of a 24-hour cultured pellet section (scale bar = 100  $\mu\text{m}$ ) and native cartilage tissue (scale bars = 50  $\mu\text{m}$  and 150  $\mu\text{m}$ ) with toluidine blue staining GAGs. The stain shows a purple colouring when bound to GAGs and a blue tone for the rest of the structures.

Pellet sections from all 3 donors were stained with toluidine blue after 24 hours of culture, and at day 7, 10, 14 (results not shown) and 21 of culture to observe the proteoglycan production on the pellets. At day 7 the purple stain was not observed, however, by day 21, there was an increase in the metachromatic purple stain, observed for all 3 donors. As previously detected with alcian blue staining of sGAGs, high similarity of responses among the samples from donor 1 and donor 2 was observed (Figures 5-12 and 5-13). Samples cultured in 10% FBS that were activated by GSK101 or MICA showed enhanced proteoglycan deposition, as observed by the presence of a purple metachromatic staining

pattern spread across the sample. This was not observed for samples stimulated or unstimulated when cultured in 1% FBS. Control samples cultured in both serum conditions did not show enhanced proteoglycan production. A thin outer purple ring was observed on the samples with higher GAG deposition, however, the metachromatic purple stain was also observed across all the surface of these samples. This was not the case of samples having lower presence of the marker, which was mostly located peripherally. All 3 donors had a greater production of proteoglycans for the 10 % FBS MICA-treated samples, however, donor 3 samples appeared to overall have a much lower production of GAGs. Donor 3 pellets showed already from early time points less stain intensity and this phenomenon was observed throughout the culture period (Figure 5-14). Interestingly, at day 21, some samples appeared to have loss some of the stain intensity becoming difficult to visualise, especially for the TRPV4 static group cultured in 1% FBS.

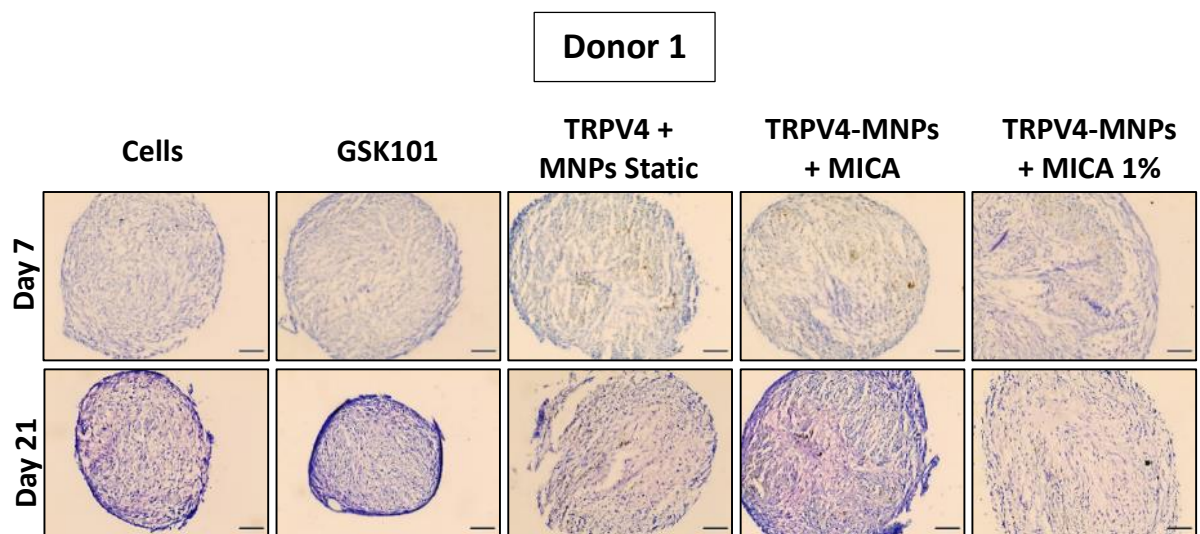


**Figure 5-12. Enhanced proteoglycan production observed for TRPV4 stimulated samples.** Representative images of pellet sections of 7 µm from donor 1 stained with toluidine blue for GAGs detection at days 7 and 21 of culture. The stain shows a purple colouring when bound to GAGs and a blue tone for the rest of the structures. Scale bar = 100 µm.

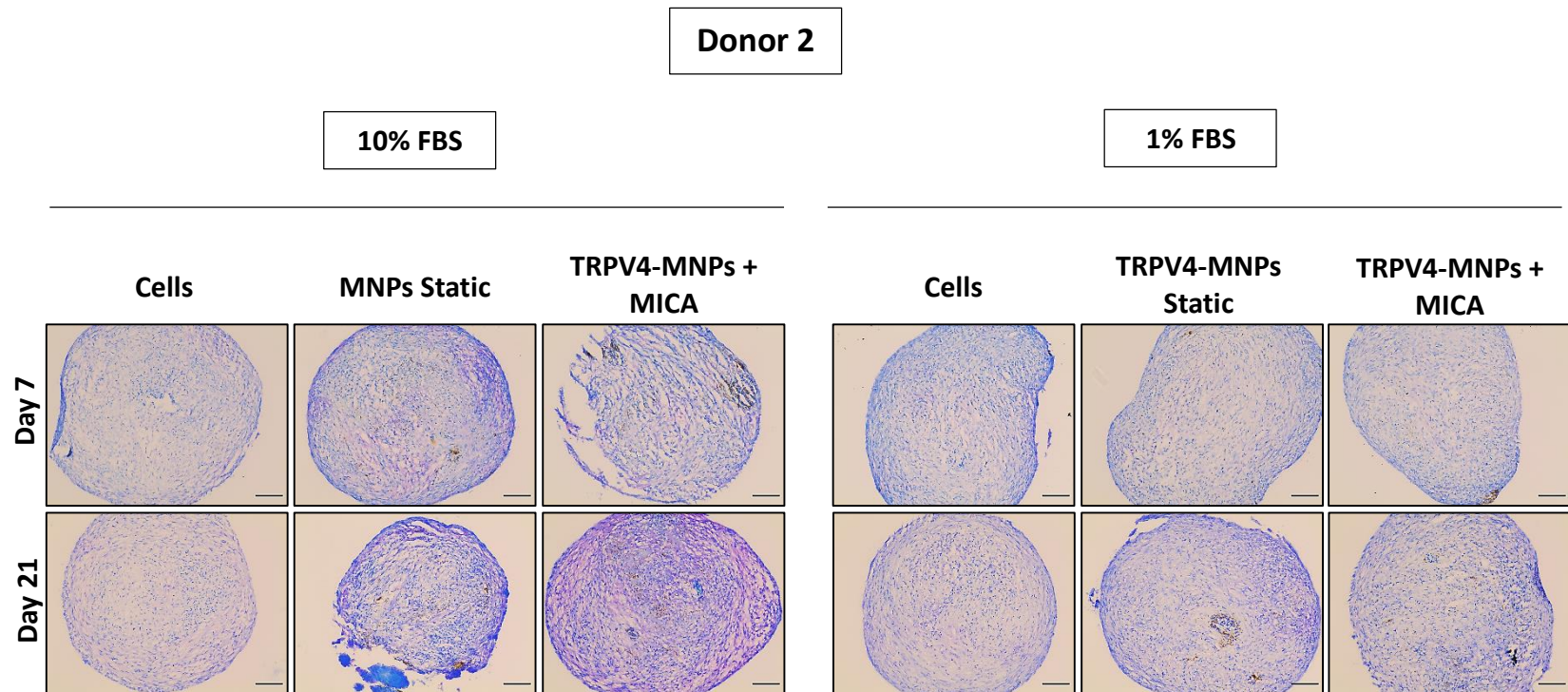


**Figure 5-13. Higher GAGs production for groups cultured in 10% FBS than for the same groups cultured in 1% FBS.** Representative images of pellet sections cultured in 10% FBS (left) and 1% FBS (right) of 7  $\mu\text{m}$  from donor 2 stained with toluidine blue for GAGs detection at days 7 and 21 of culture. The stain shows a purple colouring when bound to GAGs and a blue tone for the rest of the structures. Scale bar = 100  $\mu\text{m}$ .

Donor 3

10% FBS

1% FBS

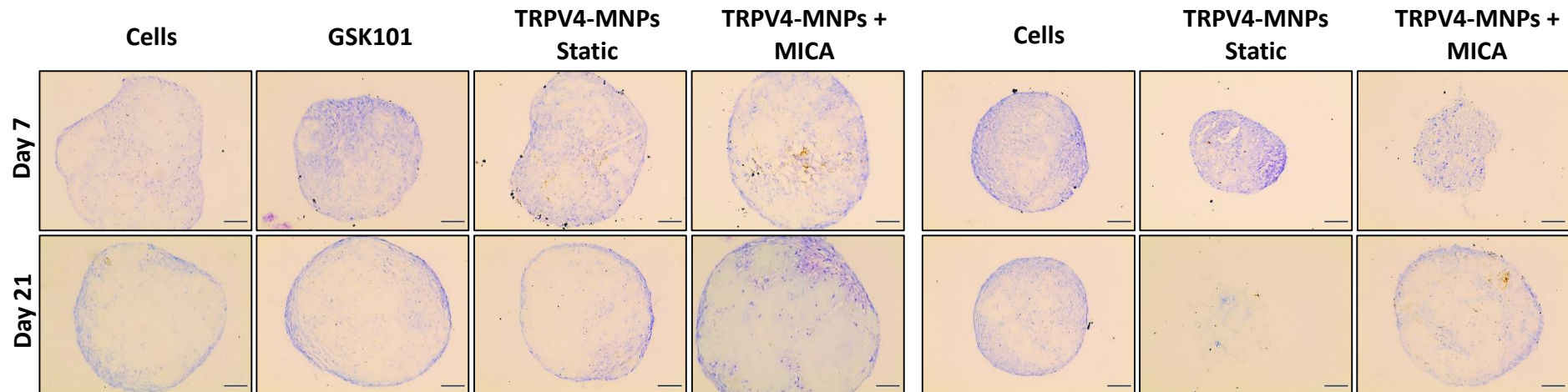


**Figure 5-14. Lower intensity of the stain was found in donor 3 for all studied groups when compared to previous donors.** Representative images of pellet sections of 7  $\mu\text{m}$  from donor 3 cultured in 10% FBS (left) and 1% FBS (right) stained with toluidine blue for GAGs detection at days 7 and 21 of culture. The stain shows a purple colouring when bound to GAGs and a blue tone for the rest of the structures. Scale bar = 100  $\mu\text{m}$ .

Pellets formed from pooled donors reflected the results observed from the individual donors, with exception of the low chondrogenic potential observed in donor 3 (Figure 5-15). Proteoglycans were able to be visualised already by day 7, with a patchy distribution over the pellet area, especially for TRPV4 stimulated groups. The GAG deposition continued to increase until day 21 when an almost uniform production was observed on the pellet sections. The control sample without MNPs or stimulation had the lower amount of metachromatic purple stain. Pellets cultured with GSK101 and pellets labelled with TRPV4 MNPs cultured under static conditions exhibited a homogeneous distribution of the marker. The MICA group showed increased GAG deposition when compared to the other groups. The purple stain was observed in the whole section surface, however, the central area appeared to have increased intensity of the metachromatic stain.

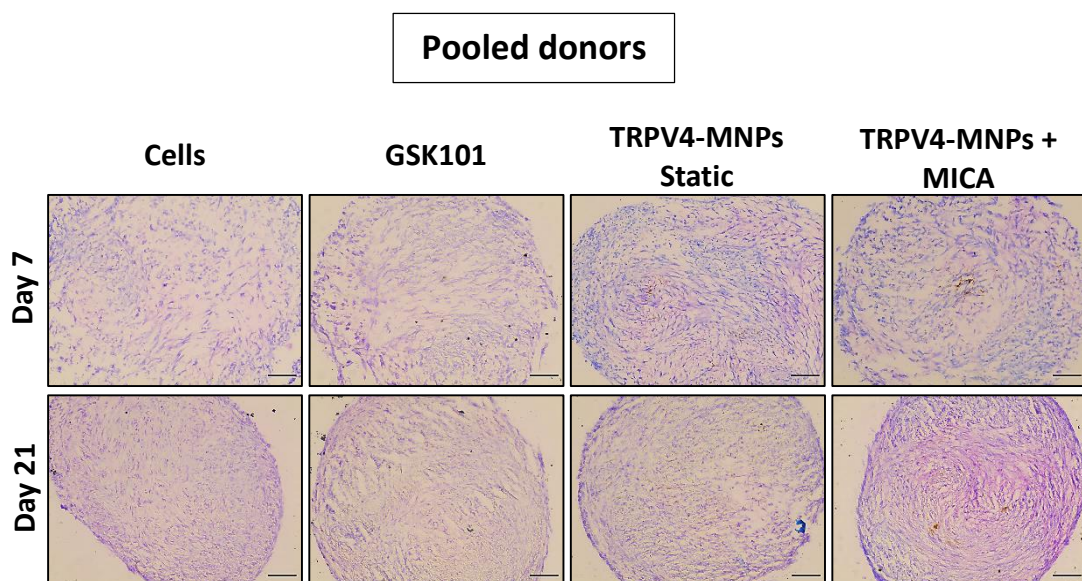


**Figure 5-15. MICA stimulated samples showed evident enhanced GAGs production.** Representative images of pellet sections of 7  $\mu\text{m}$  from pooled donors stained with toluidine blue for GAGs detection at days 7 and 21 of culture. The stain shows a purple colouring when bound to GAGs and a blue tone for the rest of the structures. Scale bar = 100  $\mu\text{m}$ .

#### 5.4.2.4 Collagen production study: Picrosirius red, collagen II and X analysis

The production of collagen on the cartilage constructs was measured through histological staining with picrosirius red, which stains collagen fibres with a red tone while the background is stained in yellow by the picric acid of the stain. In addition, it allows for observation of the collagen fibres under polarised light giving information of the fibre thickness and orientation, due to the birefringent nature of the stain. This is due to the different amount of absorption of polarised light by the collagen dye, dependant on the orientation of the collagen fibres (335). For a more complete analysis, collagen II and collagen X production were visualised through immunohistochemical analysis and the fluorescent intensity was quantified by Image J software analysis. Day 0 sections of the pellets and human cartilage control sections were also stained with picrosirius red (Figure 5-16). As expected, a zonal staining of collagen was observed in human cartilage with more intense staining on the parallel fibres of the surface (bottom of the images) and less intense staining on the calcified zone (top area of the images). No collagen was detected at day 0 being able to only visualise the yellow background stain from the picric acid.

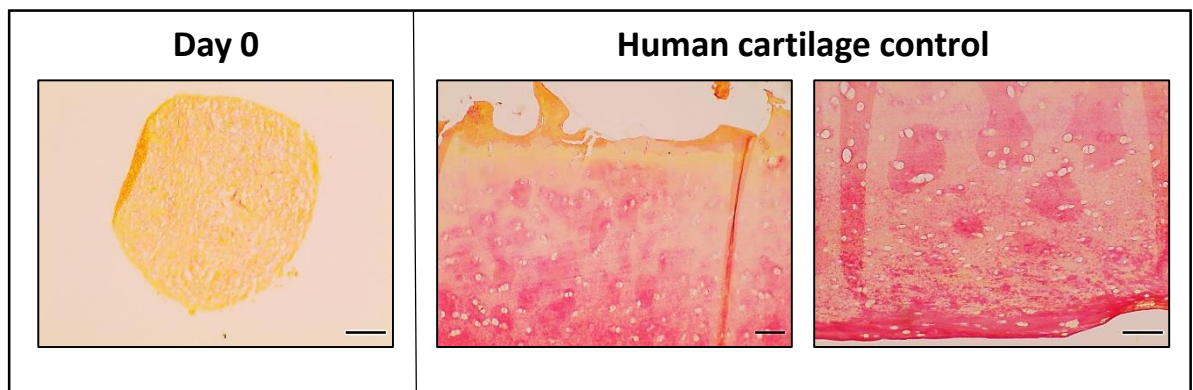


**Figure 5-16. Picrosirius red staining of collagen of day 0 pellet and human cartilage controls.** Representative images of collagen stained with picrosirius red of a day 0 pellet section of 7  $\mu\text{m}$  (scale bar = 100  $\mu\text{m}$ ) and of 7  $\mu\text{m}$  human cartilage samples (scale bars = 150 and 100  $\mu\text{m}$ ). Collagen fibres are shown in a red colour and the background in yellow.

Histological analysis with picosirius red revealed for all 3 donors an increased production of collagen in TRPV4 MICA-activated and GSKS101 groups when cultured in 10 % FBS (Figures 5-17, 5-18 and 5-19). The red colouring of the stain was able to be noticed from early culture time points for most samples. Collagen was present as individual fibres dispersed among the pellet area. The deposition of the marker was observed to greatly increase by day 21 of culture. By the termination of the experiment, all samples presented some level of collagen deposition although variable among studied groups. The collagen distribution on the pellets was variable, observing an almost homogeneous distribution of the marker for the TRPV4 MICA and GSK101 groups cultured in 10% FBS for donors 1 and 3. The remaining studied groups and all samples from donor 2 showed, however, a localised deposition of the marker. Nevertheless, none of the samples exhibited the same homogeneity of the staining observed in native cartilage tissue controls, being always present some degree of fibre patches. Overall samples cultured in 1% FBS presented lower collagen deposition than the same groups cultured in 10% FBS.

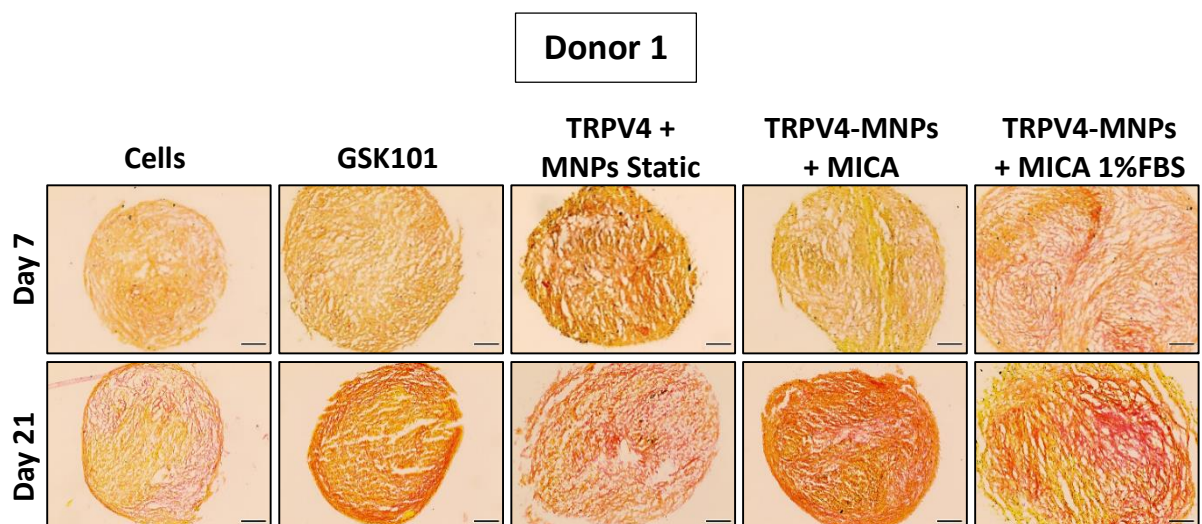


**Figure 5-17. Higher collagen deposition for TRPV4 activated samples with a homogeneous distribution.** Representative images of 7 µm pellet sections stained with picosirius red from donor 1 of all groups cultured in 10% FBS (left) and 1% FBS (right) were stained at day 7 and day 21 of culture. Collagen fibres are shown in a red colour and the background in yellow. Scale bar = 100 µm.

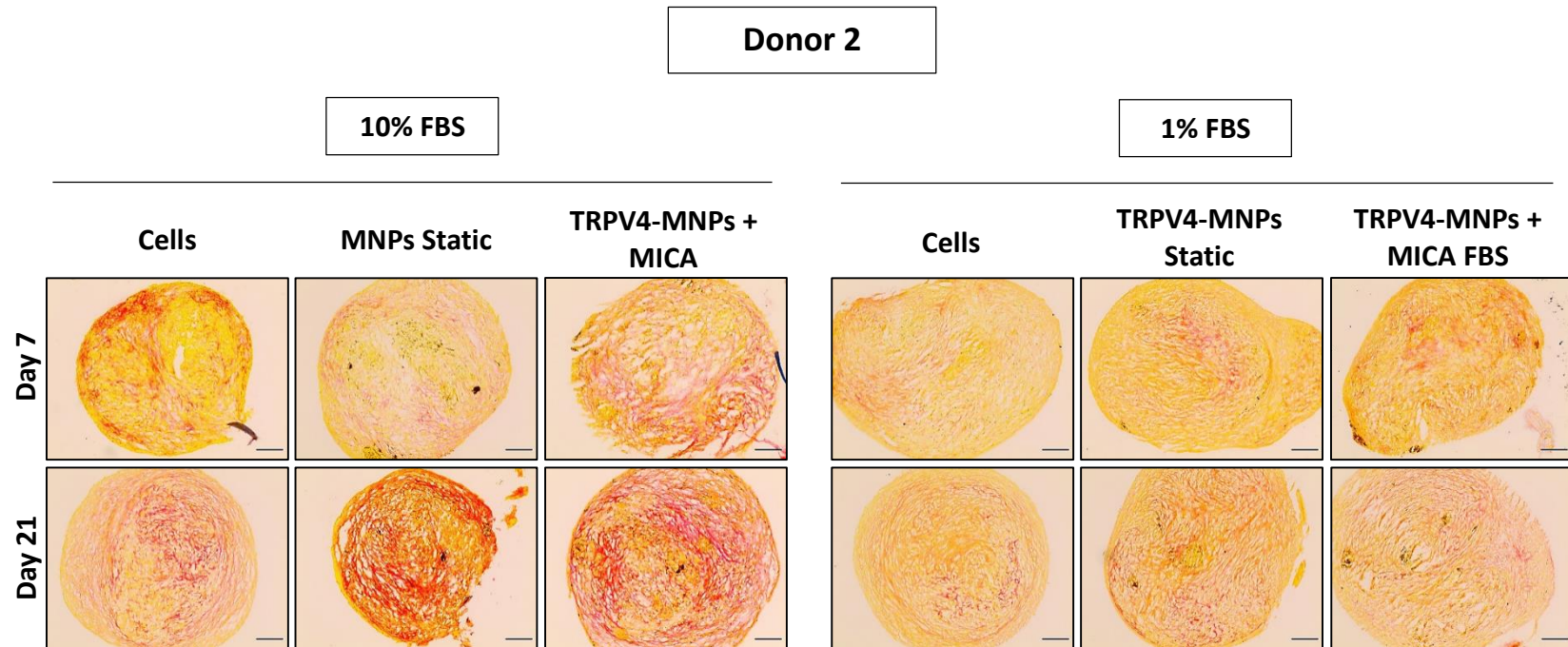


**Figure 5-18.** Samples cultured in 10% FBS showed higher collagen production than the homologous groups cultured in 1% FBS. Representative images of pellet sections from donor 2 of 7  $\mu\text{m}$  from all groups cultured in 10% FBS (left) and 1% FBS (right) were stained with picosirius red at day 7 and day 21 of culture. Collagen fibres are shown in a red colour and the background in yellow. Scale bar = 100  $\mu\text{m}$ .

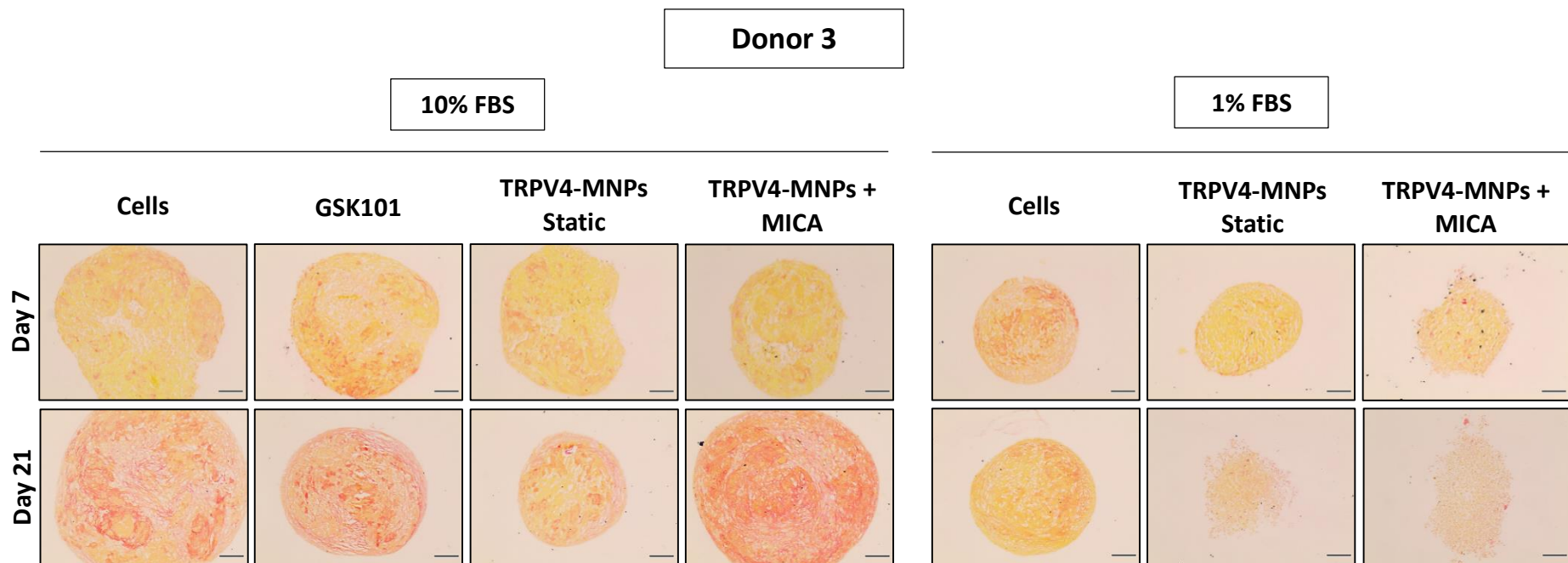


**Figure 5-19. Higher collagen production for samples cultured in 10% FBS with MICA stimulated group showing an increased production of the marker.** Representative images of pellet sections from donor 3 of 7  $\mu\text{m}$  from all groups cultured in 10% FBS (left) and 1% FBS (right) were stained with picosirius red at day 7 and day 21 of culture. Collagen fibres are shown in a red colour and the background in yellow. Scale bar = 100  $\mu\text{m}$ .

Samples from combined donors showed higher collagen deposition at early time points than observed from the individual donors (Figure 5-20). Oposing to the observations from individual donors, the collagen production was evident for all groups by day 7, with higher presence of the stain than previously observed. The collagen produced was distributed in fibre bundles without any apparent level of organisation. Similar intensity of the stain was observed for all groups at all compared time points, with differences being found among the distribution pattern of the red stain. After 21 days of culture, the collagen deposition was observed to have increased resulting in a more homogeneous distribution. Nevertheless, the collagen produced by the control sample was observed to be accumulated in some areas of the pellet with an uneven distribution, unlike observed for TRPV4 stimulated samples. MICA activated samples had an irregular distribution of the stain for early time points that covered the whole surface of the sample after 21 days of culture.

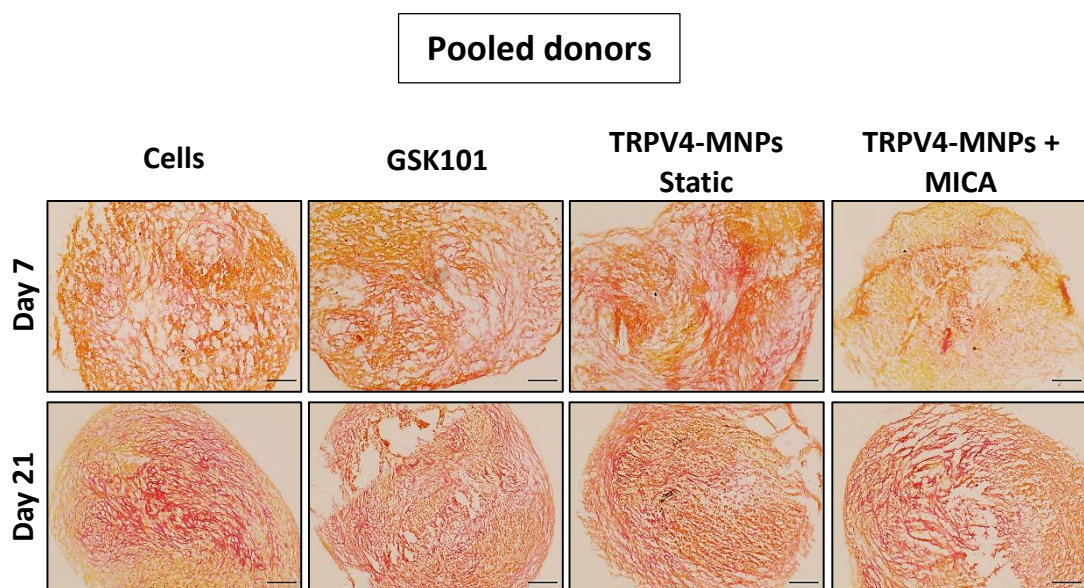


**Figure 5-20. Enhanced collagen production at early time points for all studied groups.** Pellet sections of 7 µm from all groups were stained with picosirius red at day 7 and day 21 of culture. Collagen fibres are shown in a red colour and the background in yellow. Scale bar = 100 µm.

Immunohistochemical analysis was performed on the pellet sections for all time points with the aim of studying the production of collagen II, considered a key marker of native cartilage (Figure 5-21). Collagen X expression was also studied to observe if activation of TRPV4 induced hypertrophy on the constructs. To enable comparison, day 0 pellet sections were stained for both markers and native cartilage tissue was used as a gold-standard positive control. No collagen production of any type was observed in pellets from day 0. Human cartilage samples showed evident and homogeneous collagen II stain, with increased intensity on the borders of the section. Little to no collagen X was observed in the native tissue.

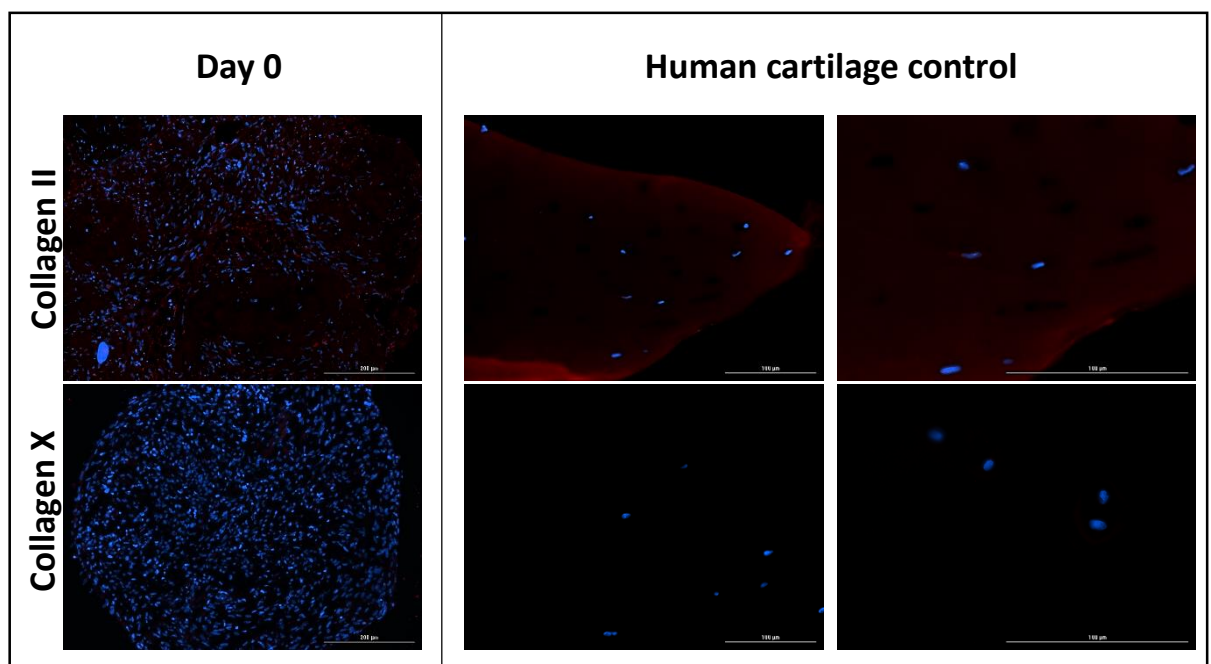


**Figure 5-21. Day 0 pellet and cartilage positive control.** Representative immunofluorescence images of 7  $\mu\text{m}$  sections stained with collagen II (top) and collagen X (bottom) of pellets cultured for 24 hours (scale bar = 200  $\mu\text{m}$ ) and of human native cartilage (scale bars = 100  $\mu\text{m}$ ). Collagen II and X are shown as red and DAPI as blue.

Matching the results observed previously, all 3 donors' samples were observed to exhibit a higher production of collagen II for the TRPV4 MICA group when cultured in 10 % FBS (Figures 5-22, 5-23 and 5-24). The majority of samples had some levels of collagen II production by day 7, being less noticeable in the cells only controls. After 21 days, the increase on the marker production was evident for all

cases, being also present in the control groups cultured in chondrogenic media. Donors 1 and 3 appeared to have a greater collagen II production when compared to donor 2. Overall, samples cultured in 1% FBS had a lower intensity of the stain, matching with previous histological results. The distribution of the collagen II was observed to be relatively homogeneous for most of the sections as observed in the human cartilage control samples. There was no collagen X in day 7 samples with the exception of TRPV4 MICA-stimulated samples cultured in 1% FBS, that presented mild signs of fluorescence for donor 2. Little to no changes on collagen production were observed after 21 days for any of the donors, being only noticeable some levels of collagen X deposition on samples labelled with unspecific MNPs. Overall, a small amount of fluorescent stain was detected for the samples cultured in 1% FBS being relatively low compared with the fluorescent levels displayed for collagen II staining.

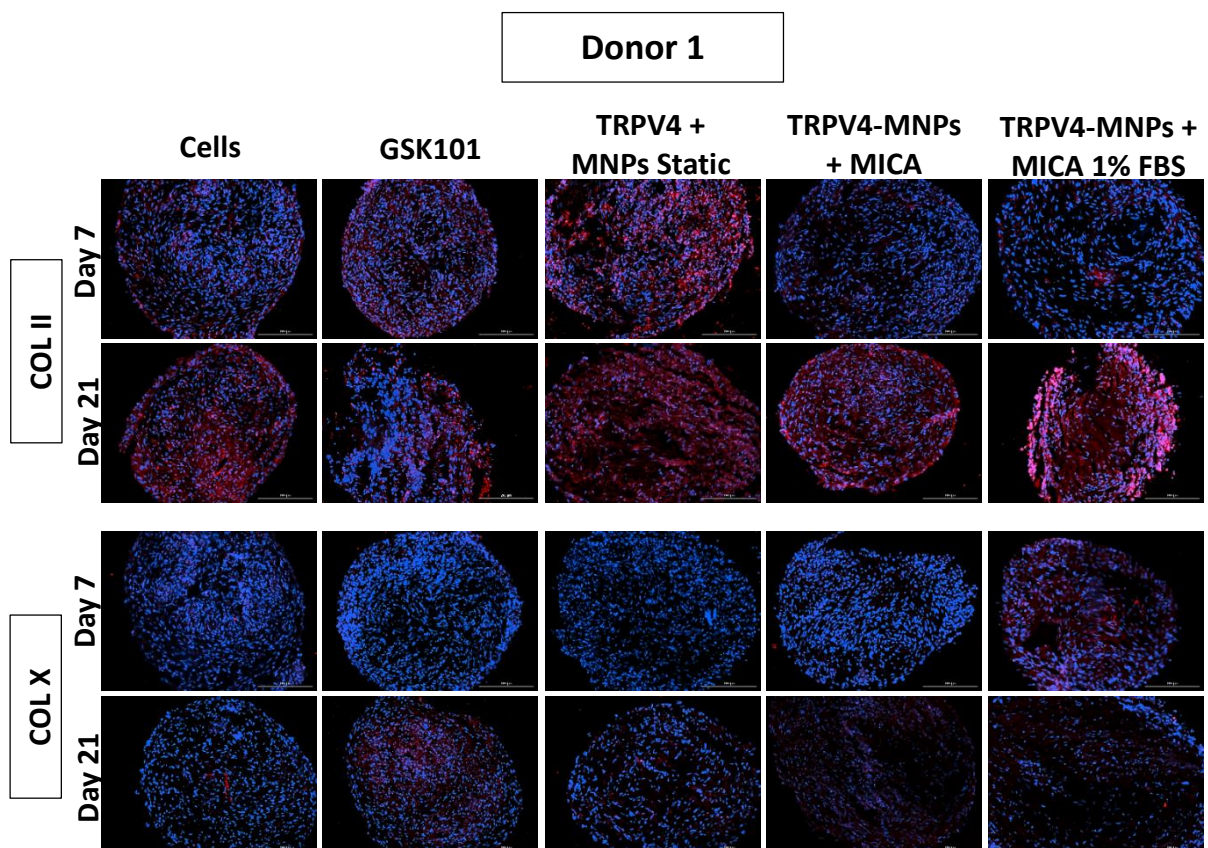


**Figure 5-22. TRPV4 activated samples showed enhanced collagen II production and little collagen X was detected after 21 days.** Representative immunohistochemical fluorescence images of pellet sections of 7  $\mu$ m at days 7 and 21 for all groups cultured in 10% FBS (left) and 1% FBS (right) from donor 1 pellets. Collagen II (top) and X (bottom) are shown read and DAPI stains nuclei in blue. Scale bar = 200  $\mu$ m.

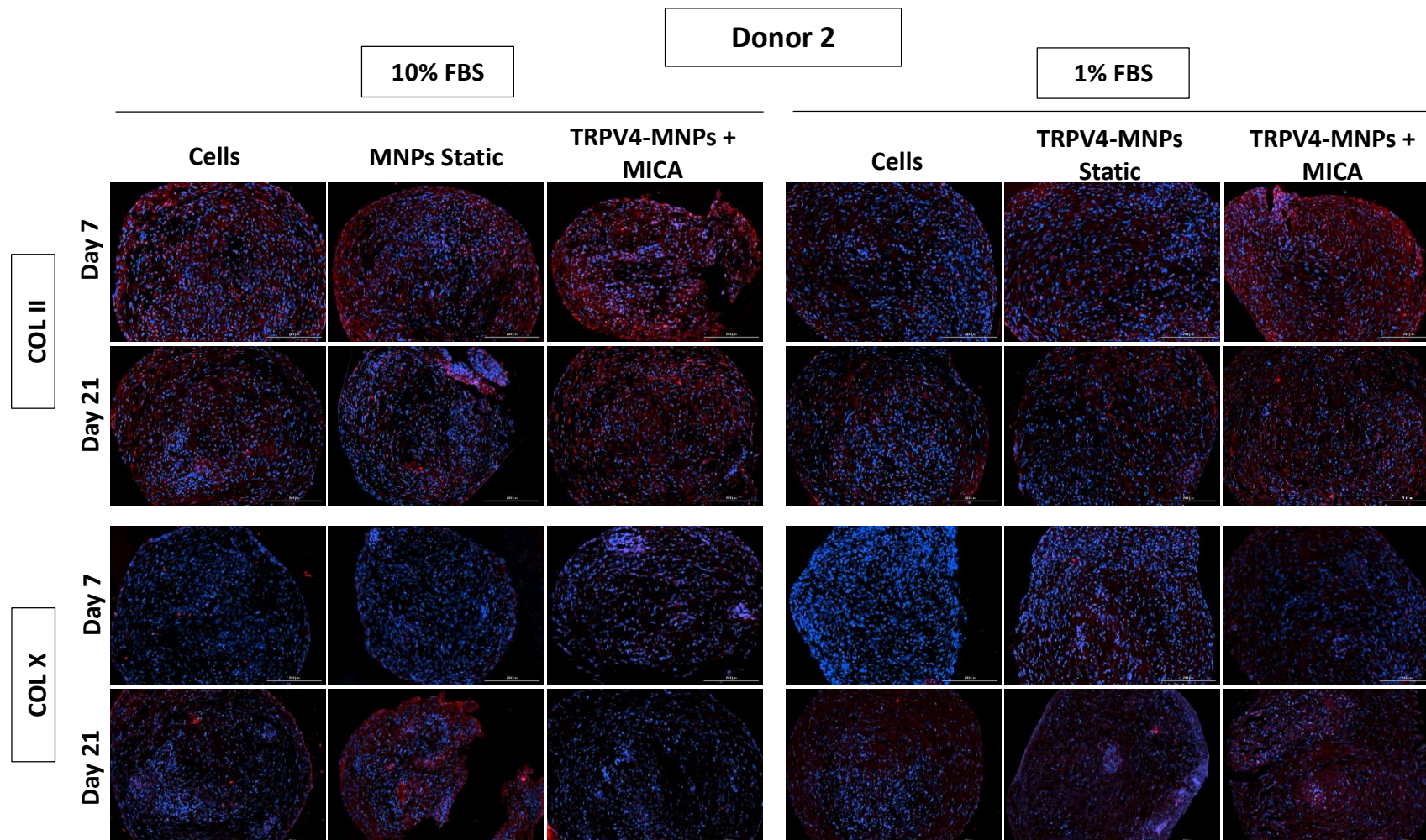


Figure 5-23. Lower general production of collagen II with enhanced production on MICA activated groups and mild presence of collagen X detected for samples after 21 days of culture. Representative immunohistochemical fluorescence images of pellet sections of 7  $\mu$ m at days 7 and 21 for all groups cultured in 10% FBS (left) and 1% FBS (right) from donor 2 pellets. Collagen II (top) and X (bottom) are shown read and DAPI stains nuclei in blue. Scale bar = 200  $\mu$ m.

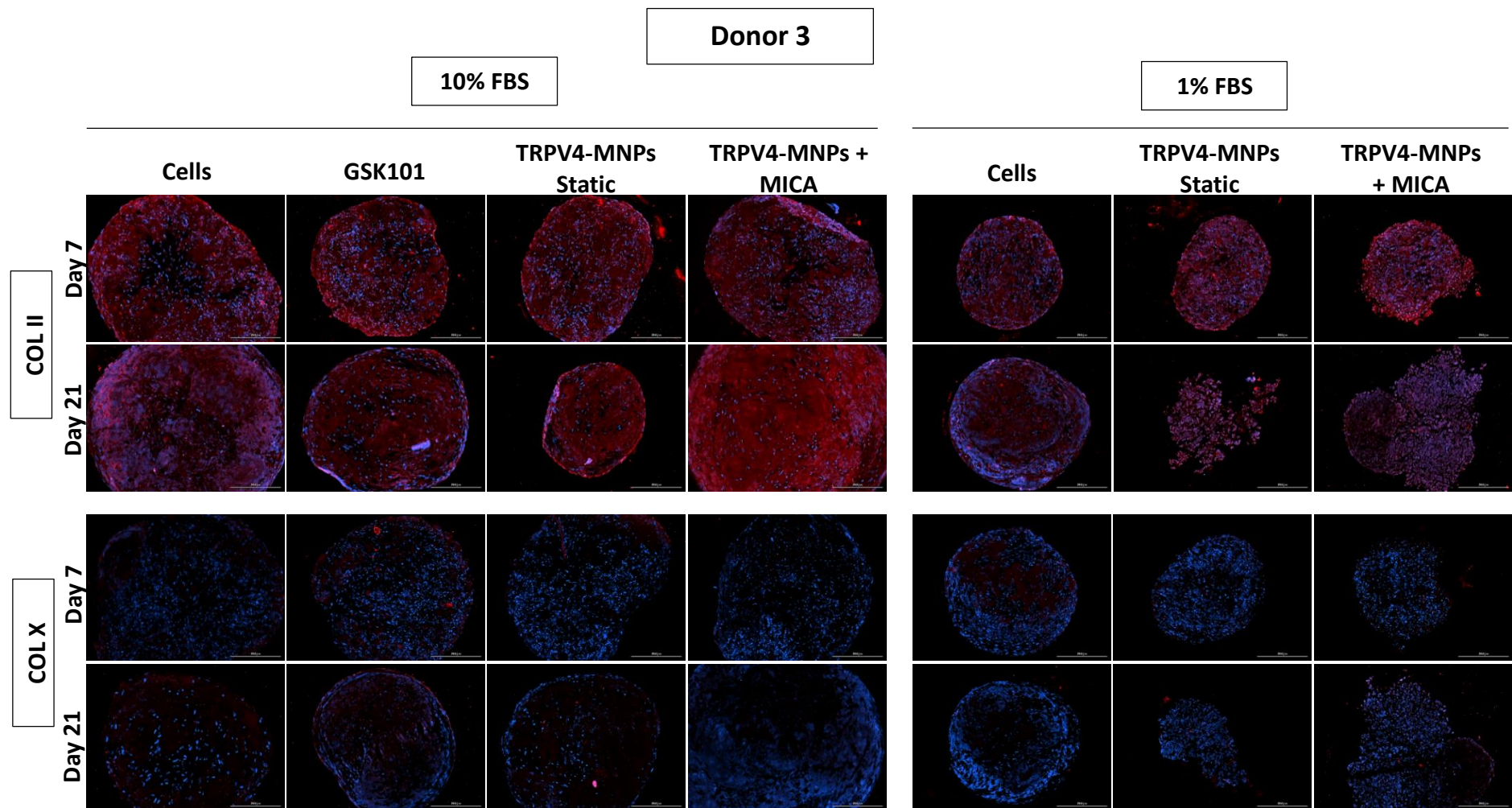
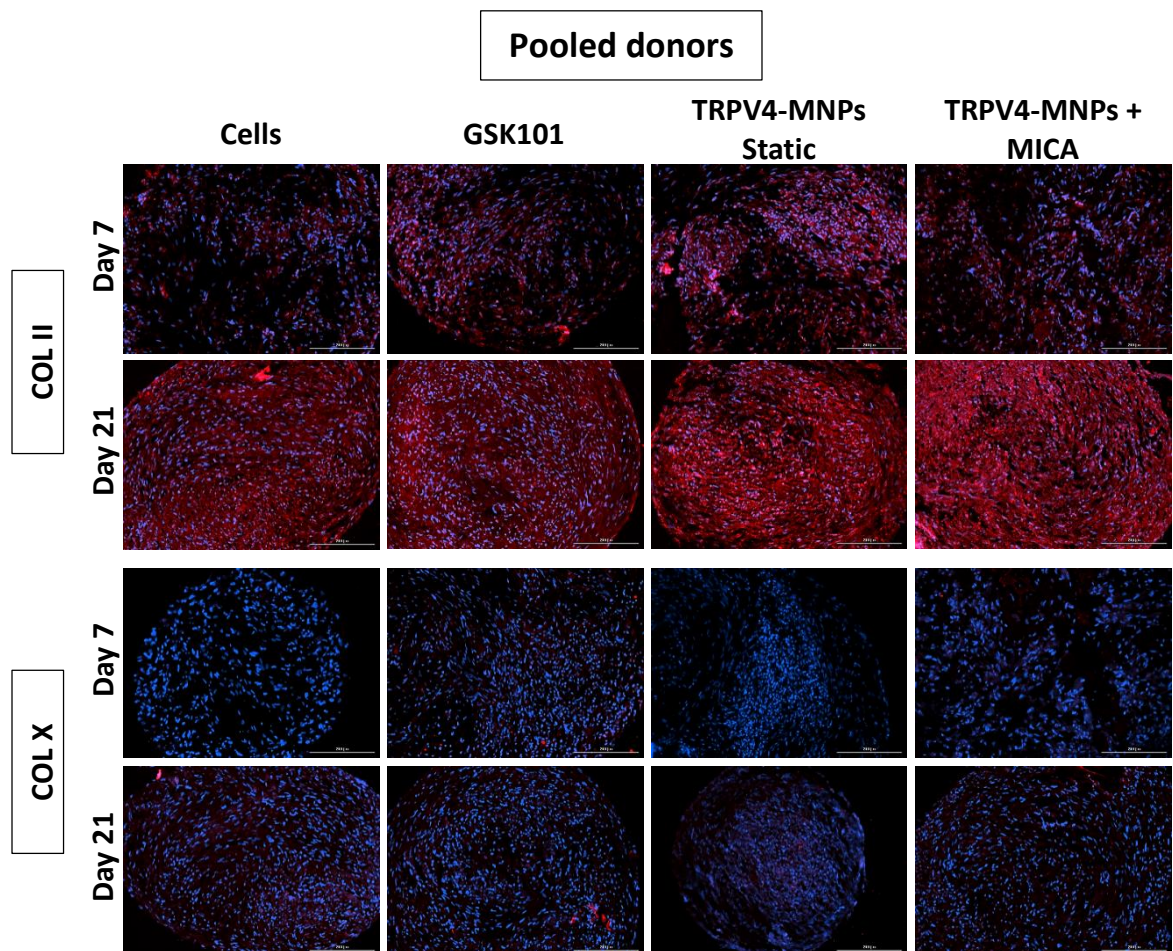


Figure 5-24. High levels of collagen II were detected with more pronounced production of MICA samples cultured in 10 % FBS and low overall collagen X production. Representative immunohistochemical fluorescence images of pellet sections of 7  $\mu$ m at days 7 and 21 for all groups cultured in 10% FBS (left) and 1% FBS (right) from donor 3 pellets. Collagen II (top) and X (bottom) are shown red and DAPI stains nuclei in blue. Scale bar = 200  $\mu$ m.

The results observed in pellets from combined donors followed the same general pattern observed from individual donors. Collagen II production was observed from early time points for all groups, being slightly less noticeable on the cells control group (Figure 5-25). Matching with previous results, the intensity of the fluorescent stain increased by day 21 for all groups. The higher marker production was observed in TRPV4-MNPs labelled samples with or without magnetic stimulation. As previously observed, collagen X was not present by day 7 and a mild production was observed by day 21, being more evident in the cells control group and in samples stimulated with GSK101.



**Figure 5-25. Increased levels of collagen II with culture time, with higher presence in TRPV4 MNPs-labelled samples and low detection of collagen X.** Representative immunohistochemical fluorescence images of pellet sections of 7  $\mu\text{m}$  at days 7 and 21 for all groups from combined donors. Collagen II (top) and X (bottom) are shown read and DAPI stains nuclei in blue. Scale bar = 200  $\mu\text{m}$ .

The fluorescence intensity of the samples stained with collagen II was quantified by Image J for each of the 3 sections imaged per studied group and for all 4 time points (Figure 5-26). This procedure was not applied to collagen X due to low levels of the marker detected. The differences between groups were higher in samples from donors 1 and 3 as previously observed in the images. Overall, both donors 1 and 2 had higher collagen II production in TRPV4 MICA-stimulated samples cultured in 10 % FBS. Samples stimulated with the chemical agonist GSK101 had increased fluorescence values when compared to the remaining groups, however, the intensity was always lower than the TRPV4 MICA group. Samples cultured in 1% FBS had lower values when compared to samples cultured in 10% FBS. Donor 2 fluorescence analysis showed reduced statistical differences among groups, with higher expression observed for TRPV4 MNPs-labelled samples cultured in both 10 % and 1 % FBS and samples labelled with unspecific MNPs. Analysis from pooled donors showed a similar tendency to donors 1 and 2 with higher expression observed for chemically and mechanically activated TRPV4 groups.

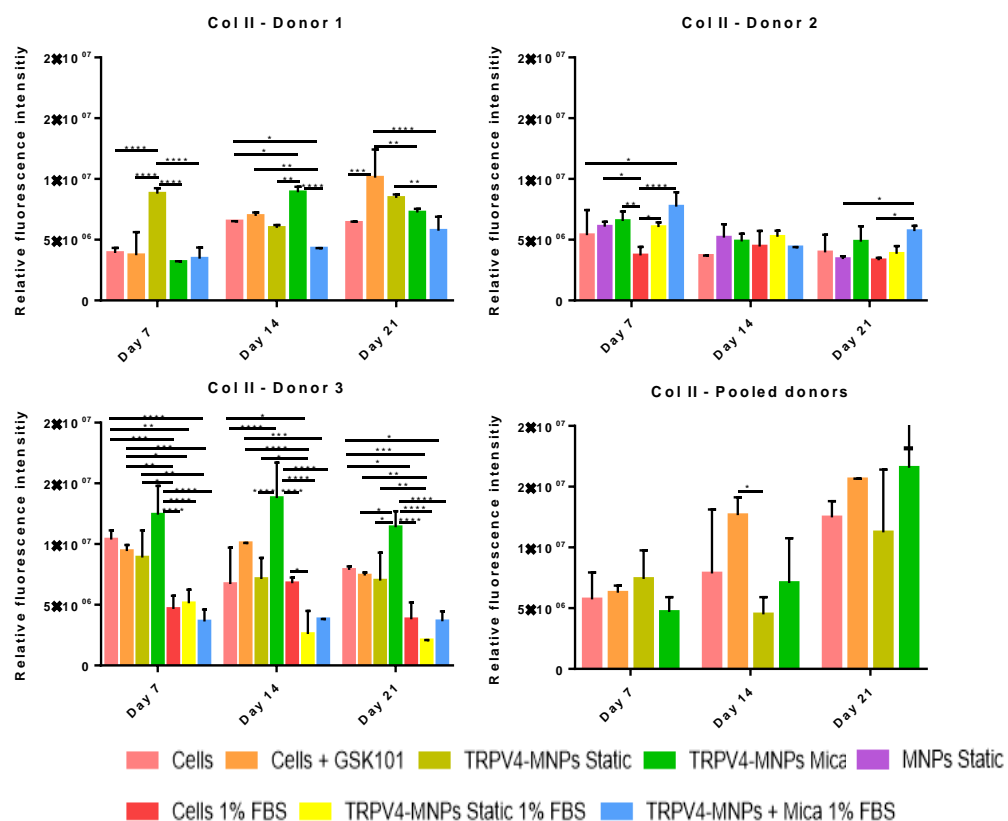


**Figure 5-26. Lower collagen II production in samples cultured in 1% FBS.** Collagen II quantified data was obtained from 3 images from each group and quantified by Image J. Data is expressed as the mean  $\pm$  standard deviation, \* $p < 0.05$ , \*\* $p < 0.01$ , \*\*\* $p < 0.001$  and \*\*\*\* $p < 0.0001$ .

#### 5.4.2.5 SOX9 immunohistochemistry

The presence of the well-studied chondrogenic marker was analysed through immunohistochemical analysis. SOX9 is responsible for collagen II and aggrecan production, being a key factor involved in chondrogenic differentiation. This transcription factor is an early marker, being often observed from the first days of culture. Control samples of day 0 pellets and human native cartilage were stained following the same procedure as for the experimental samples. The chondrogenic marker was observed after 24 hours of culture in chondrogenic media (Figure 5-27). In human adult cartilage, the presence of the marker was limited to the cell periphery located near the nuclei stained with DAPI.

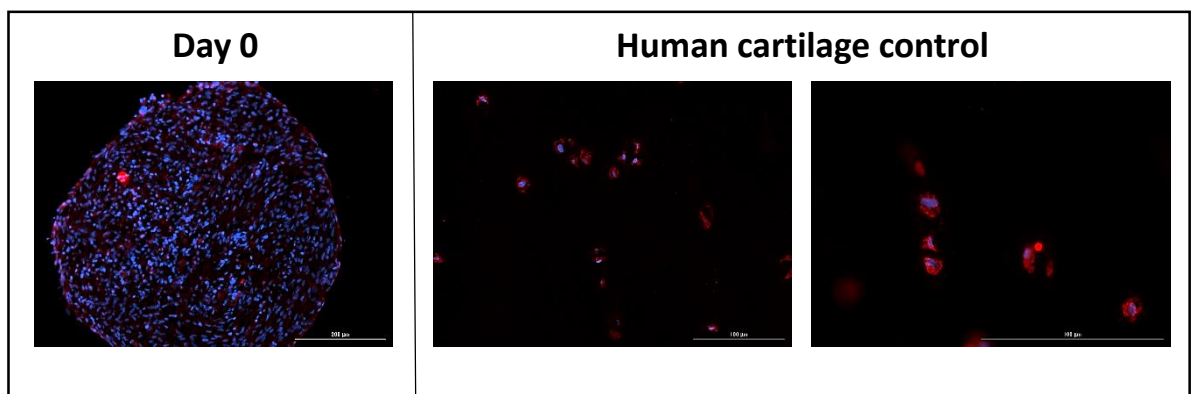


**Figure 5-27. Day 0 pellet and cartilage positive control.** Representative immunofluorescence images of SOX9 on a 7  $\mu\text{m}$  pellet section cultured for 24 hours (scale bar = 200  $\mu\text{m}$ ) and 7  $\mu\text{m}$  sections of human native cartilage (scale bars = 100  $\mu\text{m}$ ). SOX9 is shown as red and DAPI as blue.

Immunohistochemical staining of pellets from each of the individual donors revealed a similar pattern for all cases (Figures 5-28, 5-29 and 5-30). Early production of SOX9 was observed in TRPV4 stimulated samples with MICA or GSK101 cultured in both 10% and 1% FBS by day 7. The intensity of the stain was reduced after 21 days of culture for these groups, as expected by the early-expressing nature of the studied marker. While stimulated groups peaked on day 7, control groups cultured alone with chondrogenic media had some SOX9 production by day 7 that continued to increase and peaked at later time points. Samples cultured with the TRPV4 chemical agonist GSK101, peaked by day 7 and maintained the same intensity until day 14, followed by an evident decrease of the presence of the

marker after 21 days. The production of SOX9 was distributed in patches, always located near the nucleus stained with DAPI. Little difference was observed between samples cultured in 10% and 1% FBS, being slightly higher the fluorescent intensity for the samples cultured in higher serum conditions. Donors 1 and 2 showed similar level of fluorescence intensity for the same groups, however, donor 3 was observed to overall have higher intensity for each of the groups. The stain distribution was patchy, close to the nuclei stained with DAPI, however, some samples were observed to have a greater production of the marker on the periphery of the section. This was the case for the samples that had higher fluorescence intensity, TRPV4 MICA static and dynamic groups and GSK101 samples. Some individual dots of stain were observed for these samples being attributed to unwashed antibody.

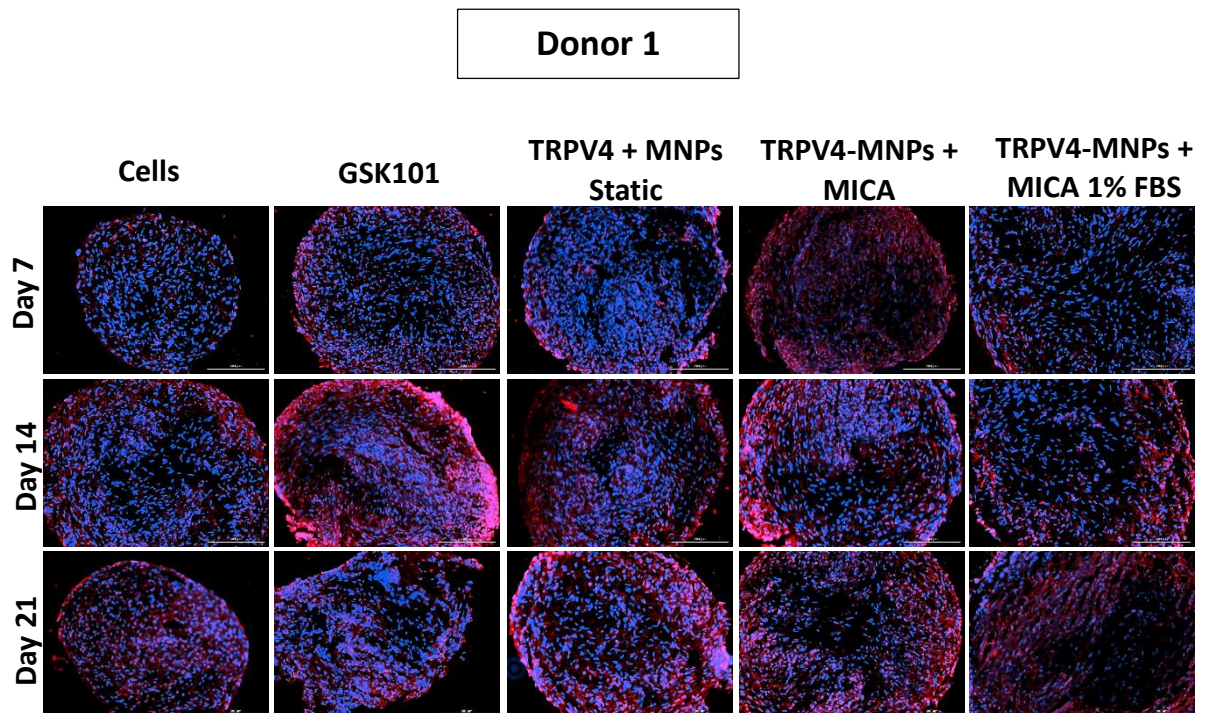


**Figure 5-28. SOX9 was detected from early time points for MICA activated group cultured in 10% FBS that increased with culture time.** Representative immunohistochemical fluorescence images of pellet sections of 7  $\mu\text{m}$  at days 7, 14 and 21 for all groups from donor 1. SOX9 is shown red and DAPI stains nuclei in blue. Scale bar = 200  $\mu\text{m}$ .

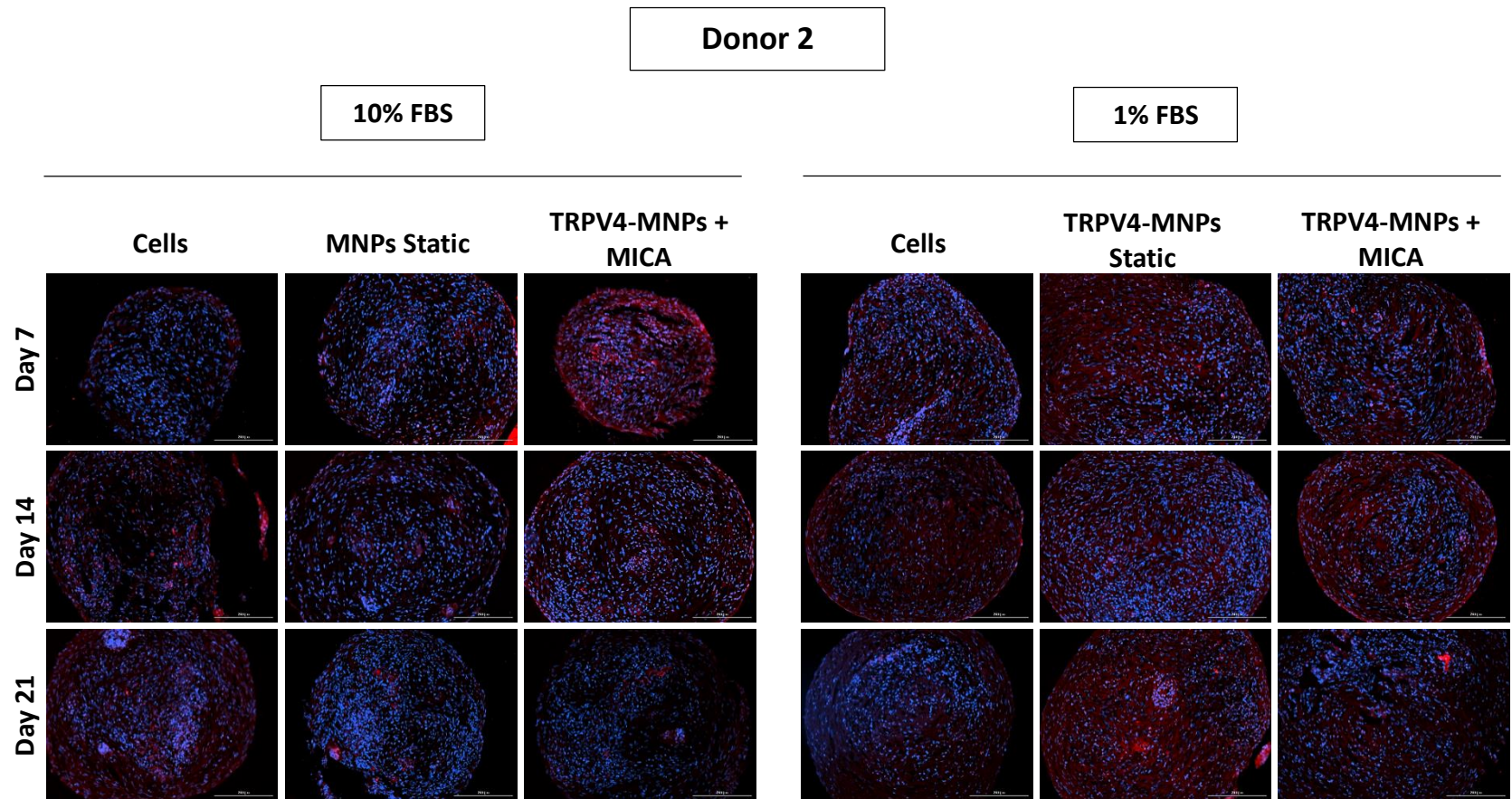


**Figure 5-29.** Early detection of SOX9 in TRPV4 MICA samples cultured in 10% FBS with low overall production over culture time for all groups. Representative immunohistochemical fluorescence images of pellet sections of 7  $\mu\text{m}$  at days 7, 14 and 21 for all groups from donor 2 cultured in 10% FBS (left) and 1% FBS (right). SOX9 is shown red and DAPI stains nuclei in blue. Scale bar = 200  $\mu\text{m}$ .

Donor 3

10% FBS

1% FBS

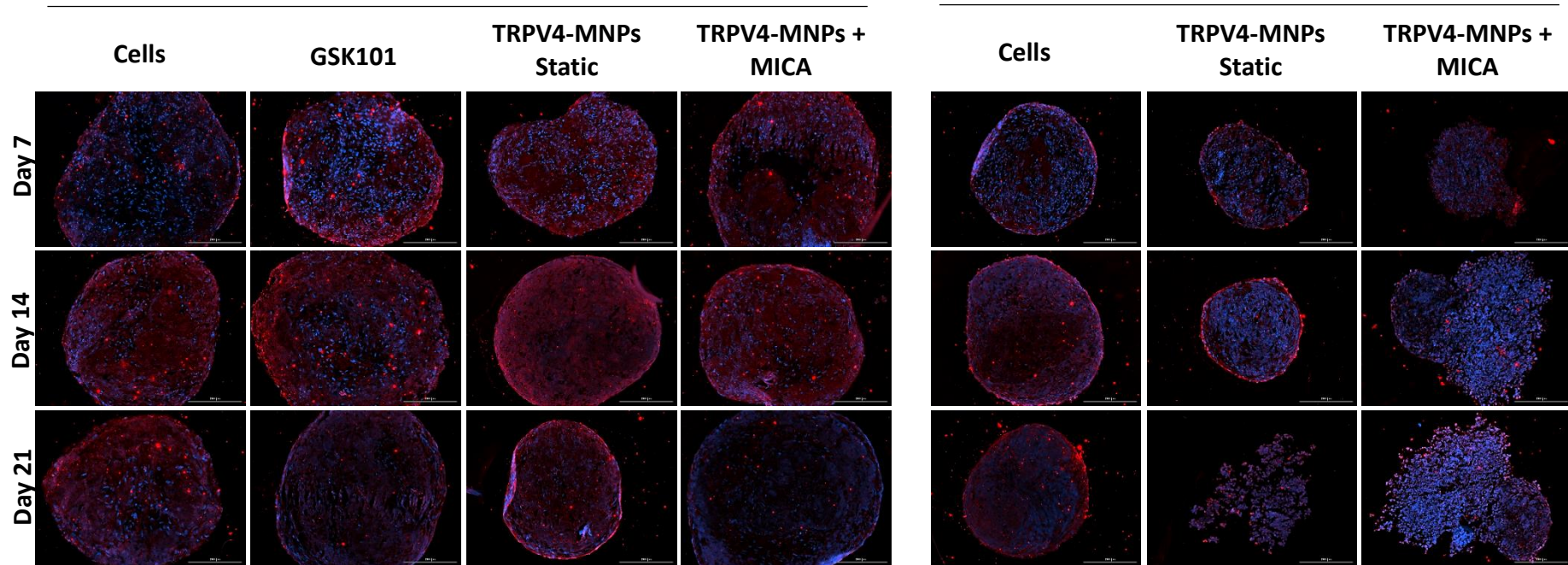
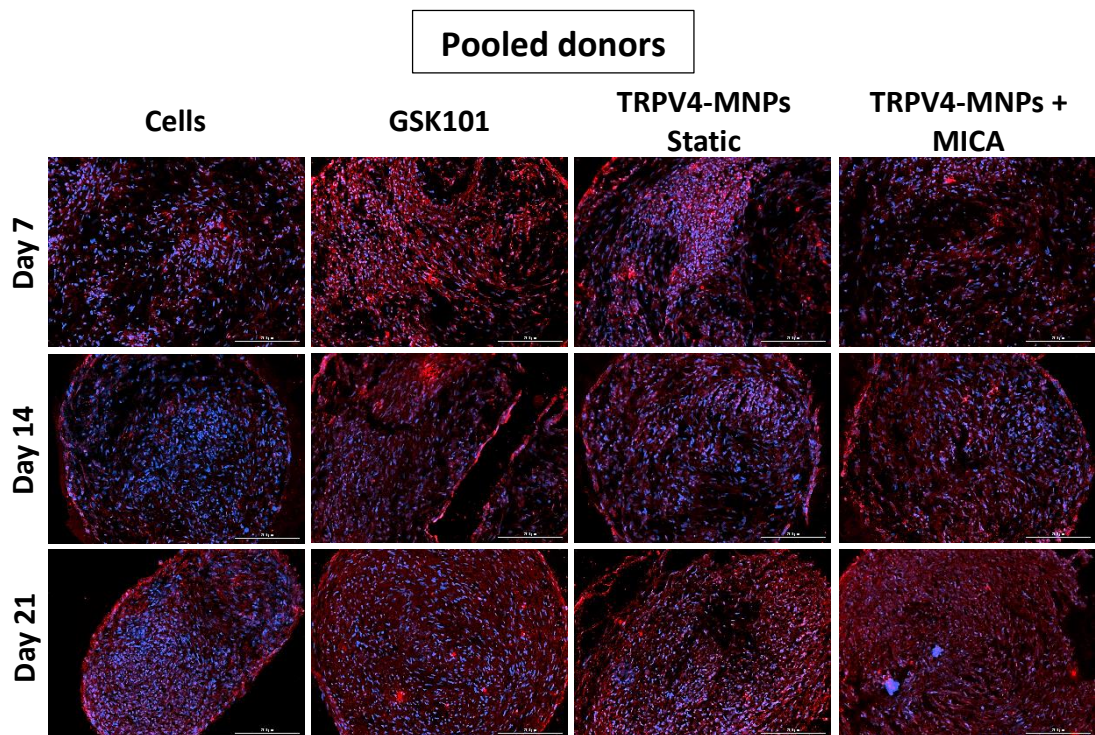


Figure 5-30. Higher SOX9 expression from early time points that was maintained with culture time for all samples cultured in 10% FBS. Representative immunohistochemical fluorescence images of pellet sections of 7  $\mu\text{m}$  at days 7 14 and 21 for all groups from donor 3 cultured in 10% FBS (left) and 1% FBS (right). SOX9 is shown red and DAPI stains nuclei in blue. Scale bar = 200  $\mu\text{m}$ .

The results for the immunohistochemical staining of SOX9 seen in samples from combined donors were similar to the ones observed from individual donors (Figure 5-31). All groups except for the cells control exhibited a moderate to high intensity of the fluorescence at day 7. The control group with cells only showed increased production of SOX9 with culture time peaking by day 21. Unlike previous observations, where intensity decreased by day 21, pellets cultured with TRPV4-MNPs and GSK101 had a sustained or increased intensity of the stain over the culture time. The localisation of the marker was not homogeneous and it was generally produced located near to the nuclei.



**Figure 5-31. High presence of SOX9 was detected from day 7 for all groups except for the control with a continuous growth over culture time.** Representative immunohistochemical fluorescent images of pellet sections of 7  $\mu\text{m}$  at days 7, 14 and 21 for all groups from samples made from pooled donors. SOX9 is shown red and DAPI stains nuclei in blue. Scale bar = 200  $\mu\text{m}$ .

The quantitative analysis of the fluorescence intensity from SOX9 pellet sections (Figure 5-32) revealed that GSK101, TRPV4-MNPs static and TRPV4-MNPs MICA groups cultured in 10% FBS presented the higher fluorescence peaks. Statistical analysis revealed significant differences between these groups and the controls cultured in both serum conditions and the remaining groups cultured in 1% FBS. Samples cultured with unspecific MNPs also had a significant reduction of the intensity when

compared to TRPV4 stimulated groups. Pellets cultured with TRPV4 MNPs under static conditions, however, presented higher variability between the 3 sections that were compared from each donor. Some of the groups showing higher fluorescence intensity peaked at day 14 decreasing by the next time point whereas others had continuous growth of the intensity signal that continued until day 21. Samples cultured in 1% FBS and the control cultured in 10% FBS showed lower intensity than other groups, with a tendency to maintain or decrease the intensity over culture time. Nevertheless, samples cultured in 1% FBS presented variability of the results, showing higher intensity on donor 2 experiment when compared to donor 3 and hence, a conclusion could not be met.

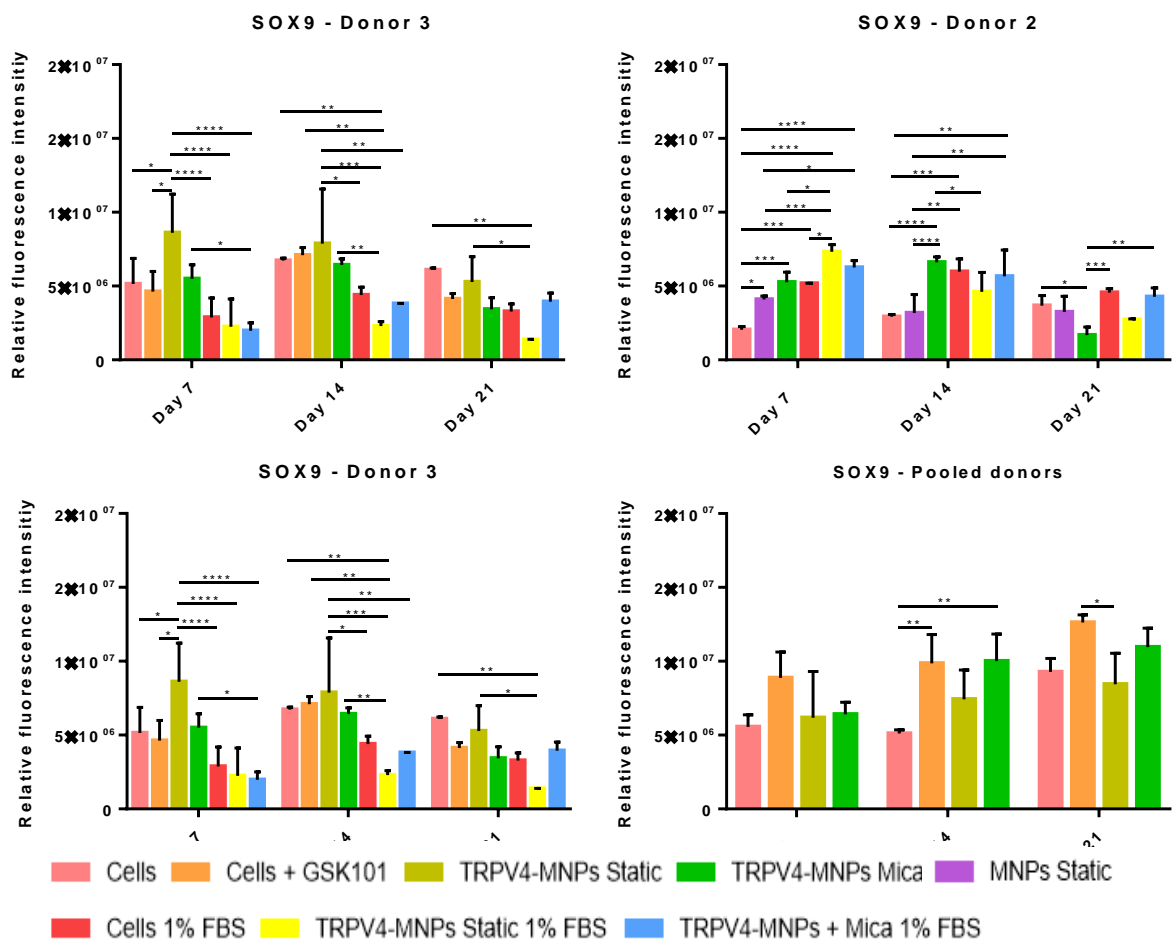


**Figure 5-32. Variability observed in the results with more consistency found among TRPV4 activated groups.** Data was obtained from 3 images of each group and quantified by Image J. Data is expressed as the mean  $\pm$  standard deviation, \* $p < 0.05$ , \*\* $p < 0.01$ , \*\*\* $p < 0.001$  and \*\*\*\* $p < 0.0001$ .

#### 5.4.2.6 Ki67 immunohistochemistry: A proliferation study

The proliferative status of the pellets was studied by immunohistochemical fluorescence analysis of the Ki67 marker. Ki67 is a nuclear protein commonly used as a proliferation marker in multiple types of cancers. It has been described to be highly expressed in cycling cells and strongly down-regulated in cells resting in G0 (336). For comparative purposes, immunohistochemistry of Ki67 was performed in day 0 pellet sections showing a homogeneous distribution of the marker on the section (Figure 5-33). Nevertheless, the samples were cultured for 24 hours in chondrogenic media, hence, some levels of differentiation were expected reducing the rate of proliferative cells. Adult human cartilage samples were also stained showing little to no presence of the marker as expected due to the low proliferative nature of the adult tissue.

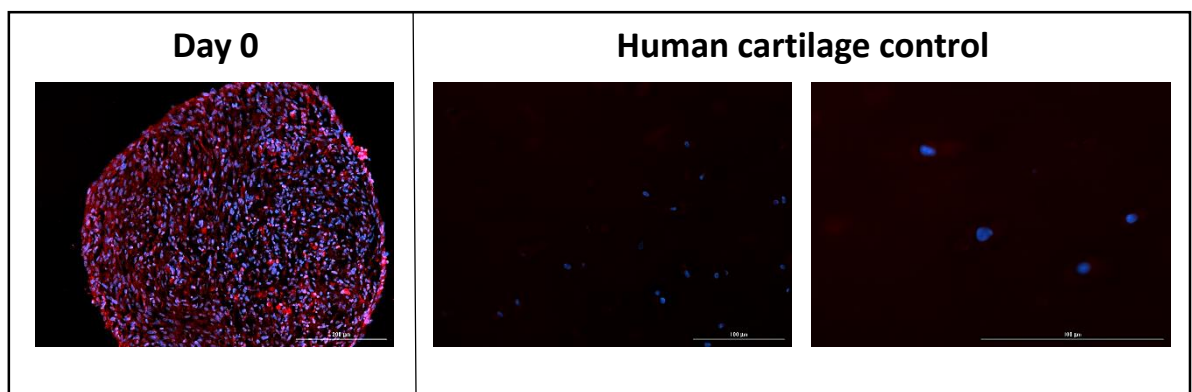


**Figure 5-33. Day 0 pellet and cartilage positive control.** Representative immunofluorescence images of Ki67 on a 7 µm pellet section cultured for 24 hours (scale bar = 200 µm) and 7 µm sections of human native cartilage (scale bars = 100 µm). Ki67 is shown as red and DAPI as blue.

Pellet sections from each of the individual donors were analysed for their proliferative potential with the aim of observing the effect of the different culture conditions on the ability for the cells to proliferate. All 3 donors showed similar results with a general increase of the presence of the proliferation marker with culture time (Figures 5-34, 5-35 and 5-36). All samples showed proliferating cells for all time points studied with the exception for donor 3 samples labelled with TRPV4 MNPs

cultured in 1% FBS which showed low levels of proliferation after 21 days. The pellet sections from this group showed an abnormal appearance and hence, the low proliferation was attributed to the individual samples and not the culture conditions. The presence of MNPs alone or labelled with TRPV4 did not showed signs of reducing the proliferation of the cells. On the contrary, samples containing nanoparticles showed higher fluorescence intensity when compared to controls. This was also the case for samples stimulated with the TRPV4 agonist GSK101. Overall, it was observed that both samples cultured with GSK101 and TRPV4 MNPs MICA-activated cultured in 10% FBS showed higher proliferation signs with increased signal intensity over culture time. The rest of the groups showed a peak on the fluorescence intensity at day 14, followed by a variable decrease of the intensity by day 21. The stain distribution was observed to not be homogeneous on the pellet sections for any of the groups. Some groups presented more intensity of the stain in the periphery and other groups had higher fluorescence on the middle of the sections.

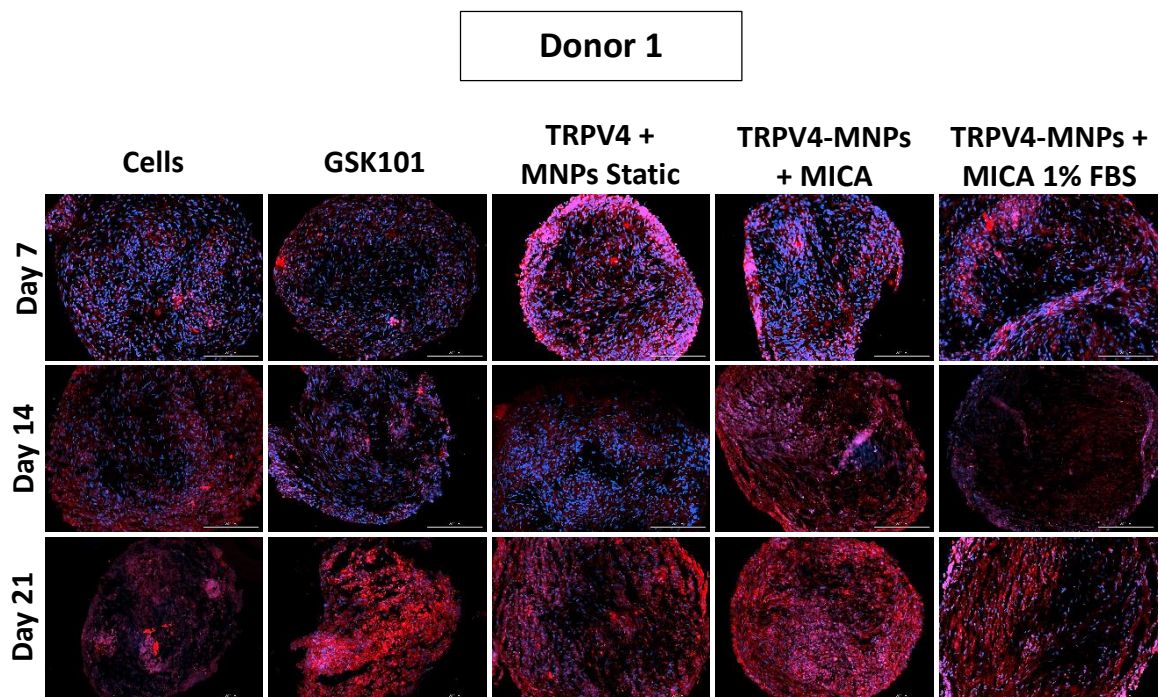


**Figure 5-34. Increased Ki67 presence over culture time for all groups with enhanced presence in TRPV4 activated samples cultured in 10% FBS.** Representative immunohistochemical fluorescence images of pellet sections of 7  $\mu$ m at days 7, 14 and 21 for all groups from donor 1. Ki67 is shown read and DAPI stains nuclei in blue. Scale bar = 200  $\mu$ m.

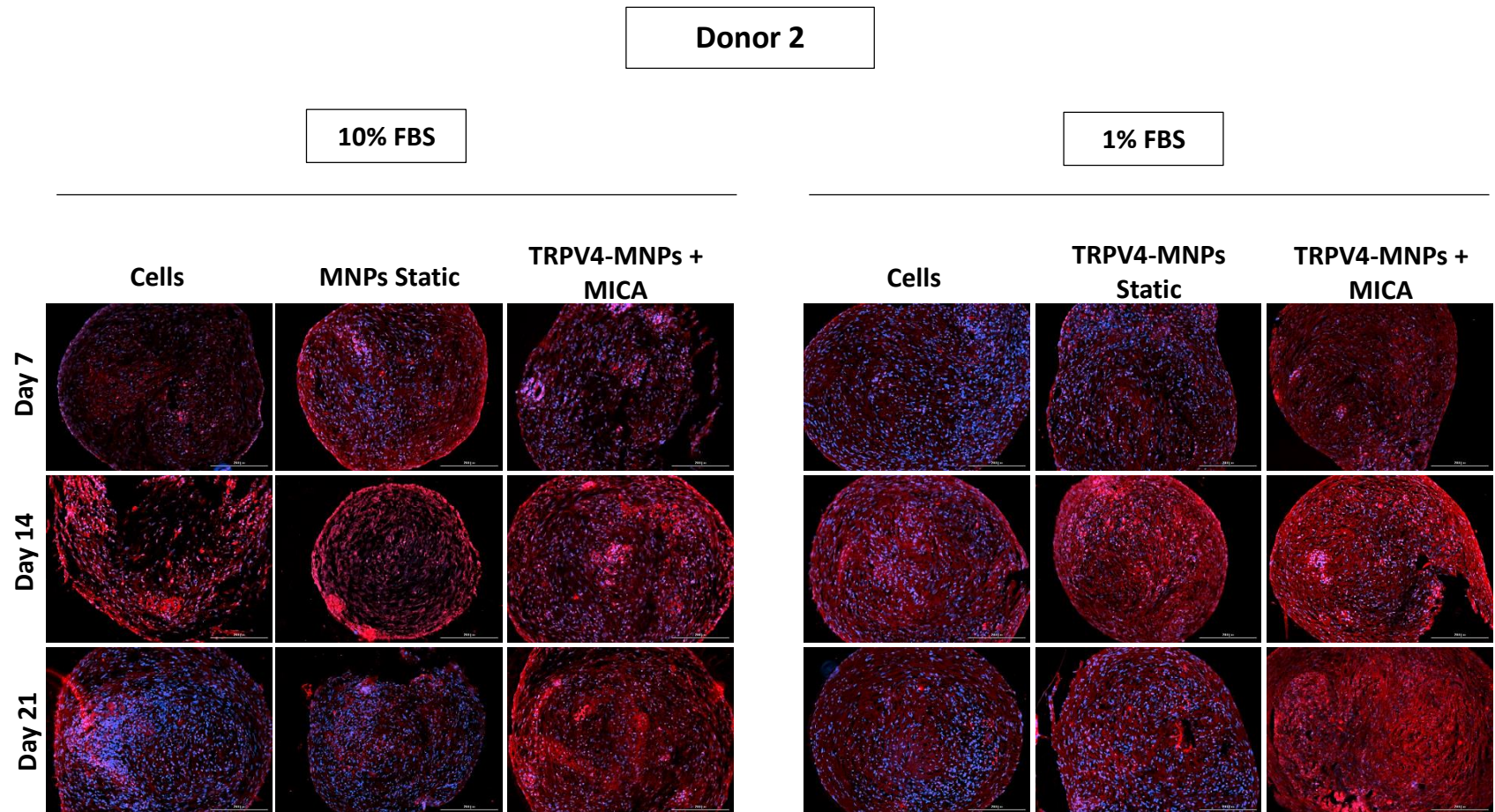


**Figure 5-35. Increased Ki67 production with culture time for samples labelled with TRPV4 MNPs.** Representative immunohistochemical fluorescence images of pellet sections of 7  $\mu$ m at days 7, 14 and 21 for all groups from donor 2 cultured in 10% FBS (left) and 1% FBS (right). Ki67 is shown red and DAPI stains nuclei in blue. Scale bar = 200  $\mu$ m.

Donor 3

10% FBS

1% FBS

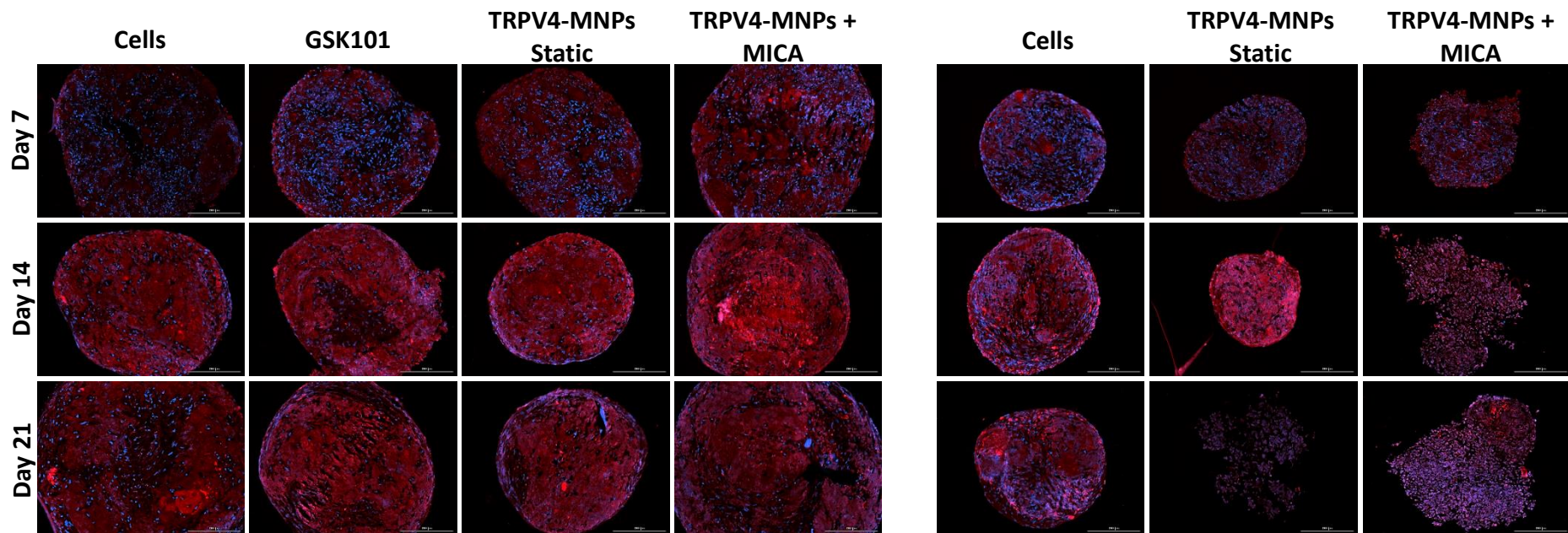
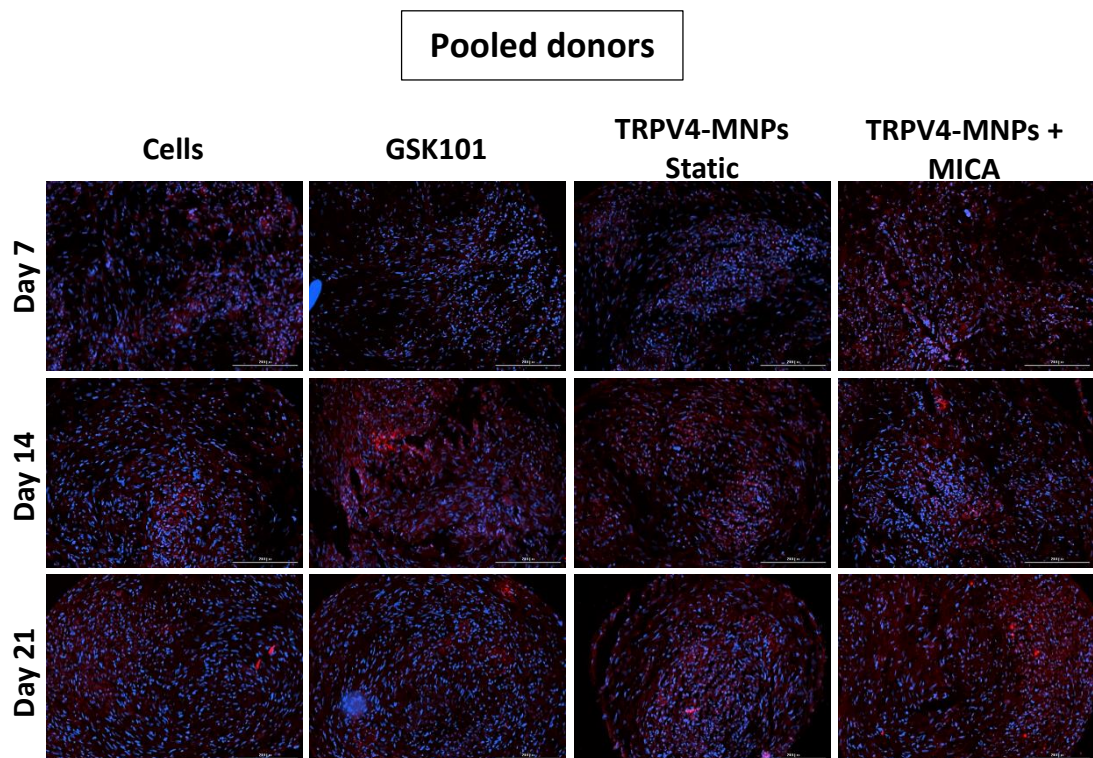


Figure 5-36. Increased production of Ki67 over culture time with enhanced presence on TRPV4 activated samples and TRPV4 static group cultured in 10% FBS. Representative immunohistochemical fluorescence images of pellet sections of 7  $\mu$ m at days 7, 14 and 21 for all groups from donor 3 cultured in 10% FBS (left) and 1% FBS (right). Ki67 is shown red and DAPI stains nuclei in blue. Scale bar = 200  $\mu$ m.

The immunohistochemical analysis of Ki67 in combined donors pellet sections revealed a lower proliferation for all groups when compared to individual donors, as observed by the reduced intensity of the stain (Figure 5-37). The variation between groups was also reduced, observing a lower presence of the marker in the cells only control group. Matching with previous results, visual analysis of the images showed slightly higher fluorescence stain in samples stimulated with MICA and GSK101, being more evident for day 14-time point for the GSK101 group, and earlier, at day 7 for TRPV4 MICA group. After 21 days, all studied groups had increased presence of the marker, being also higher for the TRPV4 MICA group. Despite the lower fluorescence levels, the results found for this experiment matched the trend observed previously confirming the positive effect of TRPV4 activation on cell proliferation.



**Figure 5-37. Lower levels of Ki67 presence observed when compared to individual donors, with a higher presence in MICA activated samples.** Representative immunohistochemical fluorescent images of pellet sections of 7  $\mu\text{m}$  at days 7, 14 and 21 for all groups from samples made of pooled donors. Ki67 is shown red and DAPI stains nuclei in blue. Scale bar = 200  $\mu\text{m}$ .

The quantitative analysis of the fluorescence intensity of Ki67 confirmed the previous visual observations (Figure 5-38). The presence of the proliferative marker was observed to increase with culture time, especially from the first to second weeks of culture. Overall, results from all 4 experiment showed that pellets labelled with TRPV4 MNPs stimulated with MICA and cultured in 10% FBS had higher fluorescence intensity, being constant for all cases. Samples cultured with GSK101 and with TRPV4 MNPs under static conditions and cultured in 10% FBS, also exhibited high levels of fluorescence. Variability was observed for pellets cultured in 1% FBS and for control samples cultured in both serum conditions, showing overall lower signal than other studied groups. As previously stated, all 3 donors showed higher levels of fluorescence than the samples from combined donors.

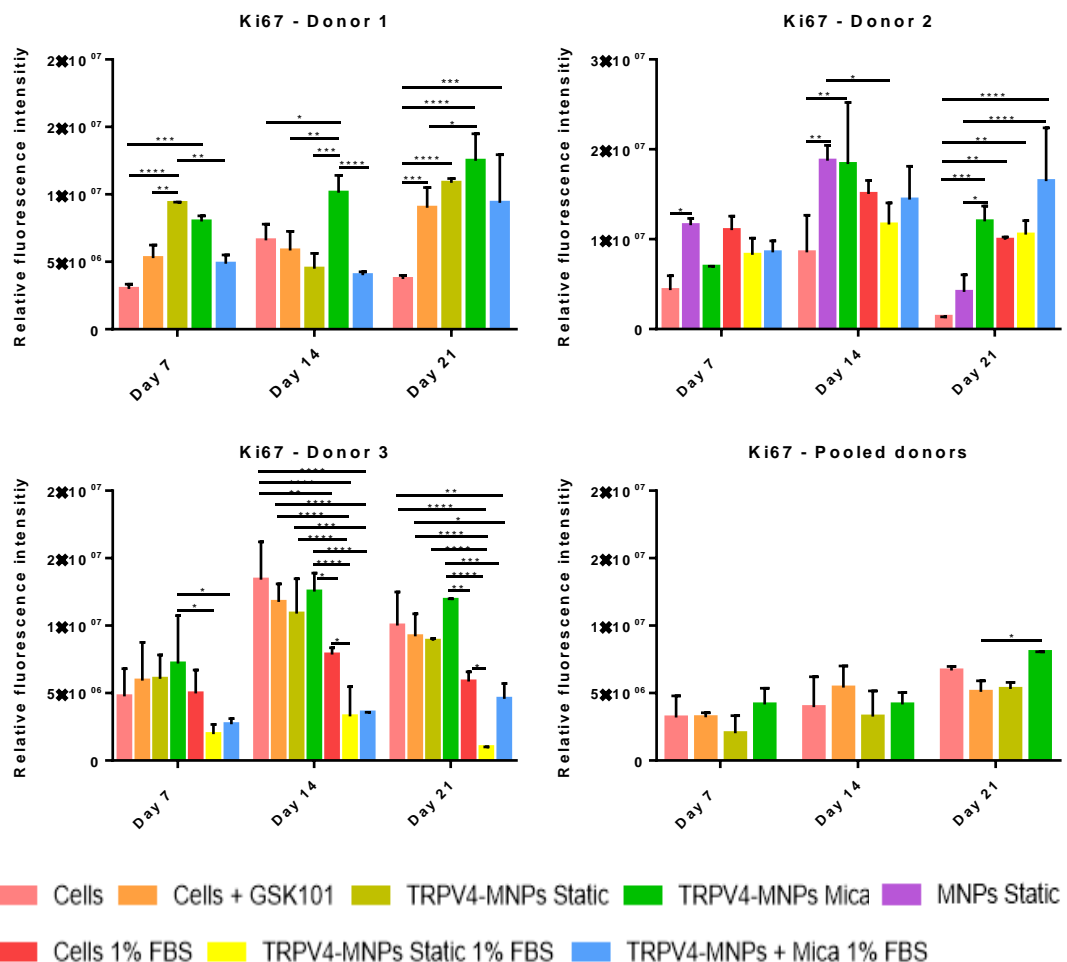


**Figure 5-38. Increased proliferation with culture time for samples cultured in 10% FBS.** Data was obtained from 3 images of each group and quantified by Image J. Data is expressed as the mean  $\pm$  standard deviation, \* $p < 0.05$ , \*\* $p < 0.01$ , \*\*\* $p < 0.001$  and \*\*\*\* $p < 0.0001$ .

### 5.4.3 Pellets sGAGs and DNA production

The concentration of sGAGs and DNA was quantified in samples from donor 3 and samples from all 3 combined donors following the spectrophotometric DMMB and PicoGreen™ assays for days 0 (24 hours of culture), 7, 10, 14 and 21 (Figure 5-39). Quantification was performed after digestion of the pellets in a proteinase K solution. Donor 3 samples cultured in 10% FBS had a significantly higher ( $p < 0.0001$ ) production of sGAGs when compared to samples cultured in 1% FBS for all studied time points. TRPV4 activated samples with MICA and GSKS101 cultured in 10% FBS presented overall, the highest level of sGAGs production. A tendency for increased sGAGs levels with advanced culture time was observed for these groups, however, the remaining of the studied groups showed no clear trend. Results from samples cultured in 1% FBS showed inferior levels of sGAGs than those observed for day 0 pellets. Evaluation of sGAG in pooled donors showed no statistical differences among samples, however, the amount of sGAGs detected for these samples was much higher than samples from donor 3. PicoGreen™ analysis of DNA revealed for both experiments an initial high concentration of DNA that was reduced by day 7 and continued to increase with culture time. Interestingly, donor 3 samples showed significantly higher concentration of DNA ( $p < 0.0001$ ) for the control groups cultured in 1% FBS when compared to the remaining groups, with the exception of TRPV4-activated samples with MICA and GSK101 cultured in 10% FBS. The remaining groups cultured in 1% FBS showed reduced DNA concentration compared to all studied groups ( $p < 0.0001$ ). Samples from combined donors also followed a similar trend among groups as found in donor 3 samples cultured in 10% FBS. Nevertheless, concentration levels were again much higher than the ones for the individual donor. The sGAGs data normalised to DNA revealed a higher production of sGAG for samples cultured in 10% FBS stimulated with MICA, especially at initial time points ( $p < 0.0001$ ). However, over culture time the statistical differences only remained for samples cultured in 1% FBS which presented low production of sGAGs. Results from pooled donors also showed a similar trend for samples cultured in 10% FBS with no statistical differences among majority of the studied groups.

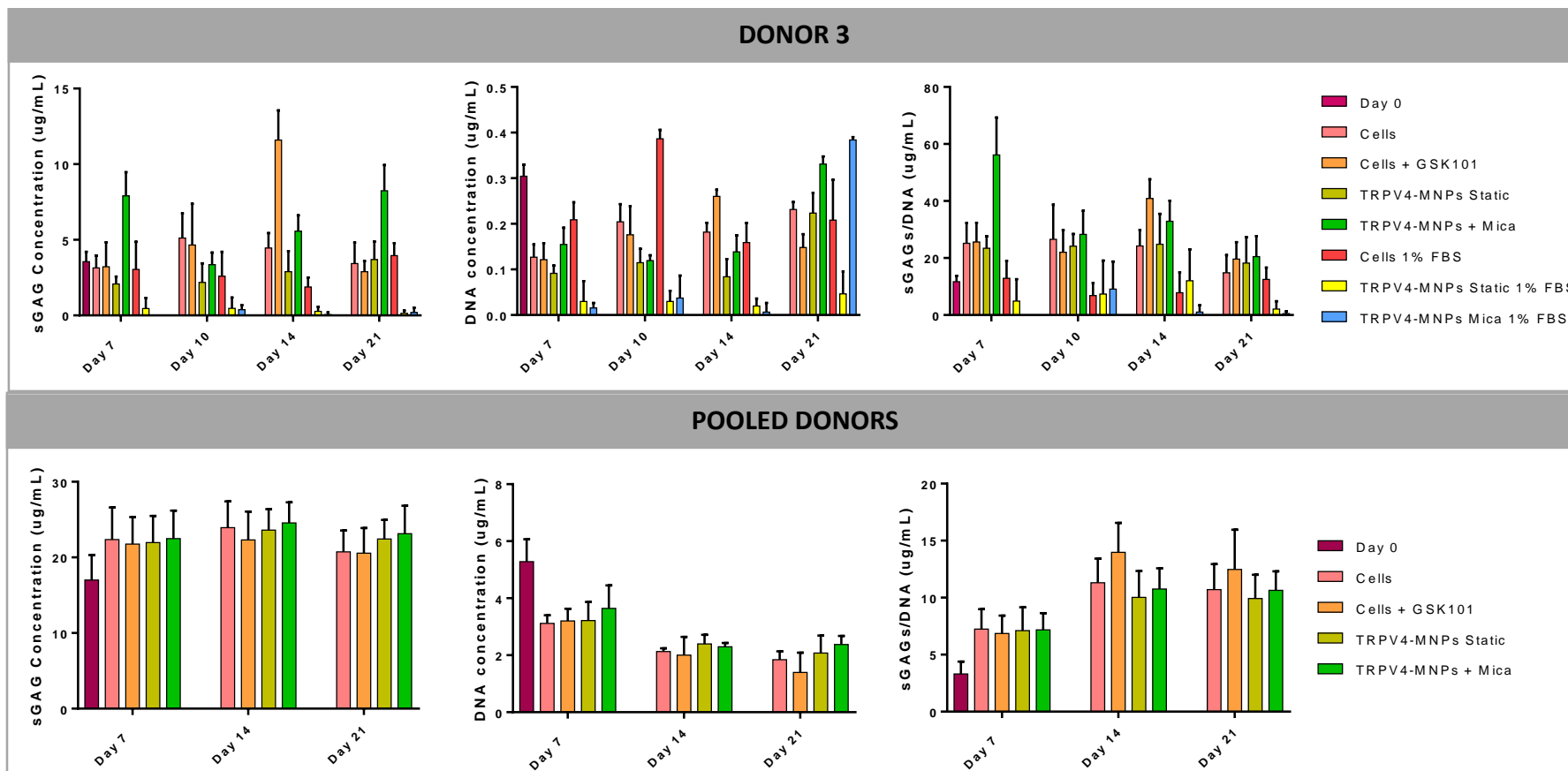


**Figure 5-39. Samples cultured in 10% FBS showed higher sGAGs production.** SGAGs and DNA were quantified at days 0, 7, 10, 14 and 21 of culture for pellets formed of cells from donor 3 and the combined donors. Normalised data are expressed as a ratio sGAGs/DNA. Data is expressed as the mean  $\pm$  standard deviation in n=2-3 repeats for 3 different samples per group.

Table 5-3. Statistical analysis of donor 3 Figure 5-39 (Top).

| DONOR 3 – sGAGs Concentration (µg/mL)                 |             |              |              |              |
|---|-------------|--------------|--------------|--------------|
| Group   | Day 7<br>P< | Day 10<br>P< | Day 14<br>P< | Day 21<br>P< |
| Cells vs. GSK101                                      |             |              | ****         |              |
| Cells vs. TRPV4 MNPs Static                           |             | ***          |              |              |
| Cells vs. TRPV4-MNPs + Mica                           | ****        |              |              | ****         |
| Cells vs. Cells 1% FBS                                |             | **           | **           |              |
| Cells vs. TRPV4-MNPs Static 1% FBS                    | **          | ****         | ****         | ***          |
| Cells vs. TRPV4-MNPs + Mica 1% FBS                    | ***         | ****         | ****         | ***          |
| GSK101 vs. TRPV4 MNPs Static                          |             | **           | ****         |              |
| GSK101 vs. TRPV4-MNPs + Mica                          | ****        |              | ****         | ****         |
| GSK101 vs. Cells 1% FBS                               |             |              | ****         |              |
| GSK101 vs. TRPV4-MNPs Static 1% FBS                   | **          | ****         | ****         | **           |
| GSK101 vs. TRPV4-MNPs + Mica 1% FBS                   | ***         | ****         | ****         | **           |
| TRPV4 MNPs Static vs. TRPV4-MNPs + Mica               | ****        |              | **           | ****         |
| TRPV4 MNPs Static vs. TRPV4-MNPs Static 1% FBS        |             |              | **           | ****         |
| TRPV4 MNPs Static vs. TRPV4-MNPs + Mica 1% FBS        |             |              | **           | ****         |
| TRPV4-MNPs + Mica vs. Cells 1% FBS                    | ****        |              | ****         | ****         |
| TRPV4-MNPs + Mica vs. TRPV4-MNPs Static 1% FBS        | ****        | **           | ****         | ****         |
| TRPV4-MNPs + Mica vs. TRPV4-MNPs + Mica 1% FBS        | ****        | ***          | ****         | ****         |
| Cells 1% FBS vs. TRPV4-MNPs Static 1% FBS             | **          | *            |              | ****         |
| Cells 1% FBS vs. TRPV4-MNPs + Mica 1% FBS             | ****        | *            |              | ****         |
| DONOR 3 – DNA Concentration (µg/mL)                   |             |              |              |              |
| Group   | Day 7<br>P< | Day 10<br>P< | Day 14<br>P< | Day 21<br>P< |
| Cells vs. GSK101                                      |             |              | ***          | ****         |
| Cells vs. TRPV4 MNPs Static                           |             | ****         | ****         |              |
| Cells vs. TRPV4-MNPs + Mica                           |             | ****         |              | ****         |
| Cells vs. Cells 1% FBS                                | ****        | ****         |              |              |
| Cells vs. TRPV4-MNPs Static 1% FBS                    | ****        | ****         | ****         | ****         |
| Cells vs. TRPV4-MNPs + Mica 1% FBS                    | ****        | ****         | ****         | ****         |
| GSK101 vs. TRPV4 MNPs Static                          |             | **           | ****         | ***          |
| GSK101 vs. TRPV4-MNPs + Mica                          |             | *            | ****         | ****         |
| GSK101 vs. Cells 1% FBS                               | ****        | ****         | ****         | **           |
| GSK101 vs. TRPV4-MNPs Static 1% FBS                   | ****        | ****         | ****         | ****         |
| GSK101 vs. TRPV4-MNPs + Mica 1% FBS                   | ****        | ****         | ****         | ****         |
| TRPV4 MNPs Static vs. TRPV4-MNPs + Mica               | **          |              | *            | ****         |
| TRPV4 MNPs Static vs. Cells 1% FBS                    | ****        | ****         | ***          |              |
| TRPV4 MNPs Static vs. TRPV4-MNPs Static 1% FBS        | **          | ****         | **           | ****         |
| TRPV4 MNPs Static vs. TRPV4-MNPs + Mica 1% FBS        | ***         | ***          | ***          | ****         |
| TRPV4-MNPs + Mica vs. Cells 1% FBS                    | *           | ****         |              | ****         |
| TRPV4-MNPs + Mica vs. TRPV4-MNPs Static 1% FBS        | ****        | ****         | ****         | ****         |
| TRPV4-MNPs + Mica vs. TRPV4-MNPs + Mica 1% FBS        | ****        | ****         | ****         | *            |
| Cells 1% FBS vs. TRPV4-MNPs Static 1% FBS             | ****        | ****         | ****         | ****         |
| Cells 1% FBS vs. TRPV4-MNPs + Mica 1% FBS             | ****        | ****         | ****         | ****         |
| TRPV4-MNPs Static 1% FBS vs. TRPV4-MNPs + Mica 1% FBS |             |              |              | ****         |

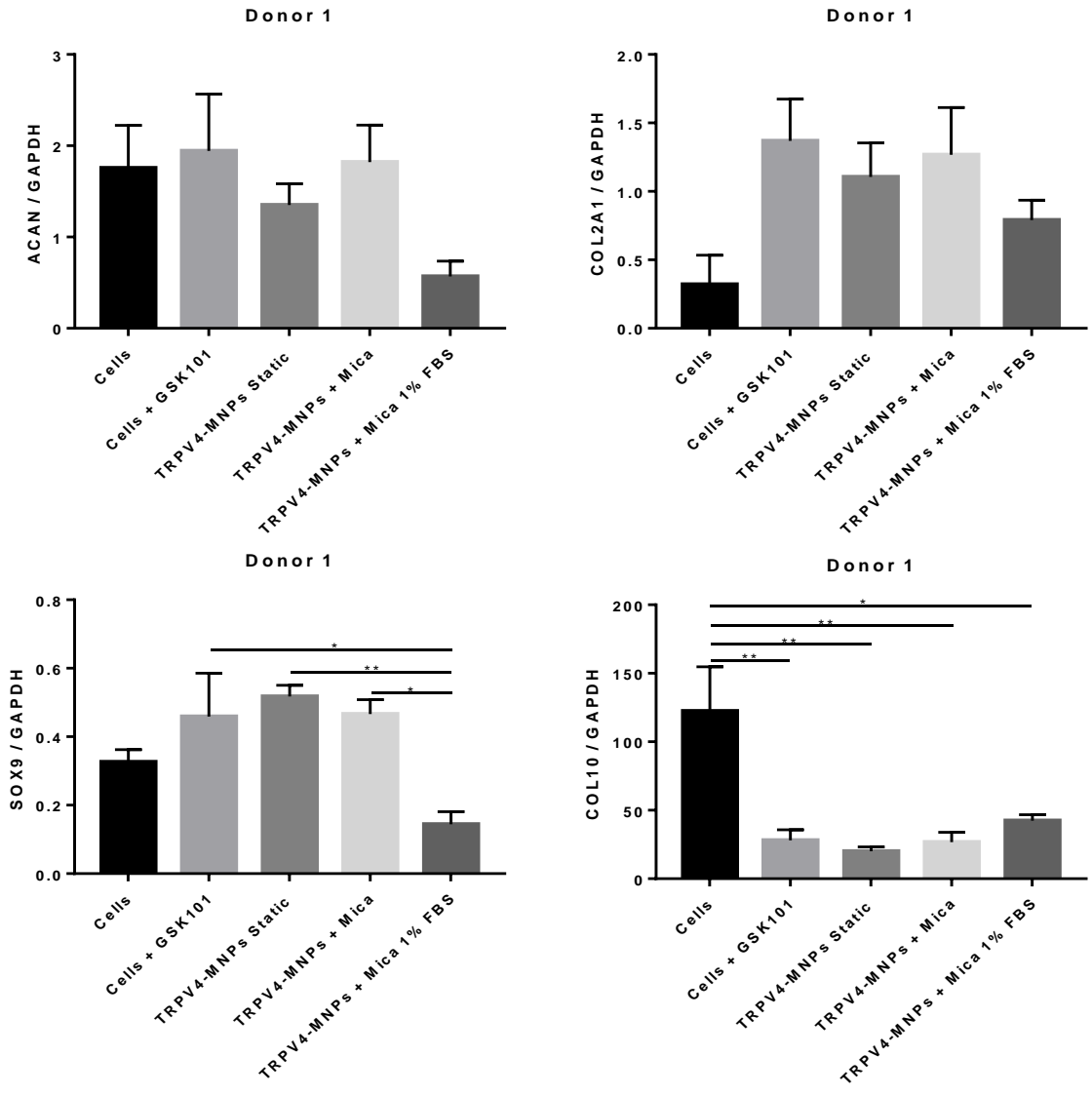
| DONOR 3 – sGAGs / DNA ( $\mu\text{g}/\text{mL}$ ) |             |              |              |              |
|---|-------------|--------------|--------------|--------------|
| Group   | Day 7<br>P< | Day 10<br>P< | Day 14<br>P< | Day 21<br>P< |
| Cells vs. GSK101                                  |             |              | **           |              |
| Cells vs. TRPV4-MNPs + Mica                       | ****        |              |              |              |
| Cells vs. Cells 1% FBS                            |             | ***          | **           |              |
| Cells vs. TRPV4-MNPs Static 1% FBS                | ***         | ***          |              |              |
| Cells vs. TRPV4-MNPs + Mica 1% FBS                | ****        | **           | ****         | *            |
| GSK101 vs. TRPV4 MNPs Static                      |             |              | **           |              |
| GSK101 vs. TRPV4-MNPs + Mica                      | ****        |              |              |              |
| GSK101 vs. Cells 1% FBS                           |             | *            | ****         |              |
| GSK101 vs. TRPV4-MNPs Static 1% FBS               | ****        | *            | ****         | **           |
| GSK101 vs. TRPV4-MNPs + Mica 1% FBS               | ****        | *            | ****         | ***          |
| TRPV4 MNPs Static vs. TRPV4-MNPs + Mica           | ****        |              |              |              |
| TRPV4 MNPs Static vs. Cells 1% FBS                |             | **           | **           |              |
| TRPV4 MNPs Static vs. TRPV4-MNPs Static 1% FBS    | ***         | **           |              | **           |
| TRPV4 MNPs Static vs. TRPV4-MNPs + Mica 1% FBS    | ****        | *            | ****         | **           |
| TRPV4-MNPs + Mica vs. Cells 1% FBS                | ****        | ****         | ****         |              |
| TRPV4-MNPs + Mica vs. TRPV4-MNPs Static 1% FBS    | ****        | ****         | ****         | ***          |
| TRPV4-MNPs + Mica vs. TRPV4-MNPs + Mica 1% FBS    | ****        | ****         | ****         | ***          |

Table 5-4. Statistical analysis of pooled donors Figure 5-39 (bottom).

| Pooled donors – DNA concentration ( $\mu\text{g}/\text{mL}$ ) |             |              |              |              |
|---|-------------|--------------|--------------|--------------|
| Group   | Day 7<br>P< | Day 10<br>P< | Day 14<br>P< | Day 21<br>P< |
| GSK101 vs. TRPV4-MNPs Static                                  |             |              |              | *            |
| GSK101 vs TRPV4-MNPs + Mica                                   |             |              |              | ***          |
| Pooled donors – sGAGs / DNA ( $\mu\text{g}/\text{mL}$ )       |             |              |              |              |
| Group   | Day 7<br>P< | Day 10<br>P< | Day 14<br>P< | Day 21<br>P< |
| GSK101 vs. TRPV4-MNPs Static                                  |             |              |              | *            |

#### 5.4.4 Chondrogenic gene expression

Gene expression was quantified by qRT-PCR for genes related to chondrogenic events and ECM deposition, *COL2A1*, *ACAN*, *COL10A1* and *SOX9* (Figure 5-40). The analysis was performed in samples from donor 1 alone as a preliminary study of the chondrogenic markers expressed by hUC-MSCs. For the analysis, 5 pellets per group were measured at day 0 as a basal control and day 7 of culture. Each group was compared to day 0 for the analysis. The expression of all markers except for *SOX9* was relatively low at day 7, matching the results observed in the histological study. *ACAN* analysis did not revealed any statistical differences among the compared groups, however, the expression profile matches the results observed for sGAGs quantitative measurement at day 7. Collagen 2 is a well-defined chondrogenic marker known to peak at day 17. The expression analysis of an early time point, did not shown any significant differences among compared groups indicating nevertheless, a higher trend for TRPV4 chemically and mechanically activated groups in 10% FBS. The analysis of *SOX9*, an early expression marker, presented statistical variations between the samples labelled with TRPV4 MNPs MICA-activated cultured in 1% FBS and the TRPV4 activated groups with GSK101 and MICA ( $p < 0.05$ ) and TRPV4-MNPs static ( $p < 0.01$ ) cultured in 10% FBS, also showing a lower expression trend for the cells only control. The expression analysis of the hypertrophic marker *COL10A1* revealed higher expression for the control group when compared to all other studied groups ( $p < 0.01$ ), however, the expression levels of this marker were low enough to consider the expression negligible.



**Figure 5-40. Gene expression analysis revealed higher expression on TRPV4 activated groups for the *SOX9* transcription factor and reduction in *COLX*.** qRT-PCR performed on pellets from donor 1 after 7 days of culture. Results expressed as fold change relative to day 0 samples and normalised to GAPDH. Data is expressed as mean  $\pm$  standard error, n=5 (n=3 technical repeats), \*p<0.05, \*\*p<0.01.

## 5.5 Discussion

The potential of umbilical cord-derived stem cells as an immune-privileged source for allogenic cell therapy has highlighted the need for studies to determine the differentiation capacity of these cells. OA tissue engineering treatments are currently based on the use of autologous MSCs with promising outcomes (337). However, these clinical autologous approaches have common limitations such as cell number yield from each patient, as well as the variability observed in the chondrogenic potential of MSCs from different donors (338,339). Recently, researchers have focused on the study of UC-MSCs as a potential source to replace MSCs. The use of foetal derived-MSCs eliminates the problem encountered by the limited proliferative ability of adult MSCs and preliminary studies have determined a promising chondrogenic potential for UC-MSCs (331,340,341). Despite the increasing interest on UC-MSCs for OA tissue engineering approaches, little studies have been performed comparing the variability of the proliferative and differentiation potential encountered among different donors. In addition, the chondrogenic potential of these cells has mostly been studied *in vitro* following the supplementation of chondro-inductive factors that are unavailable for *in vivo* adult models given the lack of vascularisation of the cartilage.

The possibility of remotely controlling the stem cell fate was studied *in vitro* prior to set a pre-clinical ovine study for an injectable stem cell therapy with the possibility to remotely control the stem cells behaviour and track the migration of cells during the treatment via MRI. For this purpose, the MICA technology was studied in 3 different donors and variable culture conditions were set to assess the quality of the cartilage formed. The original pre-clinical study was designed to receive a combination of cells from all 3 donors therefore, an experiment was performed with pellets form of pooled donors. With the aim of simplifying the study, the differences of MICA stimulation regimes were studied for this experiment reducing to 7 days the stimulation period regardless of the duration of the culture time. The chondrogenic study was performed in 3D culture following the technique used in Chapter

3, and results were compared to the chondrogenic events observed for human MSCs treated in the same conditions.

Measurements of the pellet size did not brought evidences of the effect of each culture condition on the influence of the cells proliferative potential or ECM formation. The limitation on the available cell number hindered the further study of the pellet size with more precise techniques. Nevertheless, no statistical differences were found among groups or time points, however, there was a clear tendency indicative of pellet growth with increased culture time. Measures from samples corresponding to day 0 were not considered valid due to the ongoing process of pellet formation. The cell sheet formed following cell centrifugation was observed to begin to curl over the first 24 hours of culture, however, the pellets initially formed are often the result of a low-density layer of cells and take up to 48 hours to acquire the condensed nature of the chondrogenic 3D pellets. The size of the pellets was measured by manually limiting the contour of the sample due to the irregular shape that some samples acquired, precluding the measurement of the X and Y axes that would have induced to erroneous conclusions. In addition, the presence of secondary smaller form of pellets was observed for some samples. This event is proposed to be consequence of the attachment of cells to the centrifuge tube walls during pellet formation that ultimately formed secondary forms of pellets.

Limitations to perform quantitative studies due to restricted cell number and the need for several replicates were encountered for this study and hence, variable analysis was applied for each donor. Nevertheless, the pellet formation protocols and culture conditions were rigorously mimicked to ensure the comparability of the studies. The pellet size measurements from donor 1 correlated with the DNA concentration study performed in donor 3. The initial elevated cell number from day 0 samples was expected to moderately drop over the first days of culture, as previously reported by pellet culture studies (67,342). Recovery of the cell number was observed over culture time with an evident increase in the proliferative rate after the initial 2 weeks of culture. This event matches with previous studies reporting the low proliferation rates of cells while undergoing chondrogenic events

that take place initially during the differentiation process (266,326,343). Chondrogenic events have been described to be observed over 21 days of culture (344), however, studies on MICA technology have attributed an early initiation of these events with a peak of expression on day 14, as reported in Chapter 4. These results matched with the immunohistochemical findings showing increased proliferation with culture time and a clear augmented proliferation rate after the second week of culture.

In addition to the cell proliferation contributing towards an increased pellet size with culture time, the formation of the ECM specially during the first 2 weeks of culture, is also noted to increase the size (268). The quantification of sulphated GAGs was an indicative of matrix production, endorsed by the histological analysis revealing GAGs deposition with more evident presence in both analyses for samples that undergo chemical or mechanical stimulation of TRPV4. The histological observation also evidenced the production of classical chondrogenic markers with a notable production of collagen and proteoglycans. The production of sGAGs on the combined donor samples differ in that differences found among groups were not significant, however, most of the differences encountered by donor 3 were found among samples cultured in different concentrations of FBS. Nevertheless, a tendency of increased sGAGs production with culture time was also observed for these samples.

The variation of culture media was studied with the aim of determining the best option to enhance the chondrogenesis. Interestingly, this study revealed the benefit of culturing cells with higher concentrations of FBS (10%) as opposed to common protocols used to induct human chondrogenesis containing 1% FBS. The media formulation was based on a modification of the protocol from Mennan *et al.* (345). The original protocol was initially used, however, 48 hours after pellet formation, disaggregation of the samples was observed due to apoptosis of the cells and samples were discarded. The protocol used for all the experiments performed with UC-MSCs was based on the chondrogenic media for chondrocytes (228) with the substitution of TGF- $\beta$ 1 for TGF- $\beta$ 3 due to the optimal chondrogenesis previously observed with various cell types tested in our group. Lower percentages of

FBS resulted in poor chondrogenesis with almost a non-existent production of sGAGs being similar to those results obtained from day 0 samples, even after normalisation to the DNA amount. This data was reinforced by the histological observation showing an evident difference of GAGs and collagen production after 21 days, when compared to the groups with the same conditions cultured in 10% FBS. Immunohistochemical analysis also brought evidence of the poor chondrogenesis of samples cultured with lower FBS with overall low detection of collagen II and SOX9 when compared to the same groups cultured in higher FBS. The analysis of the proliferative marker Ki67 endorsed the data obtained from the DNA analysis, with lower proliferation for samples cultured in 1% FBS. Interestingly, the control group in lower serum presented higher DNA and Ki67 values than the other groups and hence, the effects observed were hypothesised to be a direct cause of the MNPs presence. Moreover, donor 3 samples cultured in low serum and labelled with MNPs were observed to disaggregate after 2 weeks of culture and the usual pellet consistency was lost, finding fragile samples that crumbled when sectioning. This was attributed to a low ECM production that did not sustain the structure of the pellet.

The sustained presence of MNPs on the samples was demonstrated by iron staining with prussian blue. The labelling dose was set to enable the presence of 5-6 MNPs per cell, that was hypothesised to generate enough force under an external magnetic field to trigger the activation of the channel (120,209). To ensure an optimal distribution of the MNPs, samples are often mixed while labelling, however, visual observation allowed to set differences among the labelled groups for samples cultured with higher and lower FBS concentration. The presence of higher percentage of serum was observed to cause mild levels of MNPs aggregations. This event was not observed for samples cultured in 1% FBS that showed apparent lower presence of MNPs due to the spread distribution of the individual particles across the section surface. The cells are labelled in serum free media, to avoid the aggregation of the MNPs during the process (346), nevertheless, once the pellets are formed they are set in chondrogenic media and the presence of serum in the sample might interfere with the pellet

formation. During the formation of the pellet, it is possible that the MNPs attract other labelled cells, finding the areas of higher density of MNPs. It was also hypothesized that after labelling the cells when the 10 % FBS chondrogenic media was added, there might have been a corona formation on the MNPs. The biomolecular corona is referred to the layer of adsorbed biomolecules on the particle surface. The formation of the corona can alter the functional properties of the MNPs, although the lack of further analysis did not allow to elucidate if this was the cause for the MNPs aggregation, or the attraction between labelled cells (347). Leaving the labelled cells for 24 hours in serum free media might have solved this issue. This should be further addressed if aiming for in vivo translation, given that the corona formation might lead to MNPs crossing the blood barrier (348). However, if the MNPs were aggregated due to attraction between labelled cells, the effect of this concentration of MNPs might be of benefit for the stimulation with MICA. This aggregation could have generated stronger forces on the channel, at the same time as physically contracting the pellet and hence, favouring the mechanical activation of signalling pathways that support chondrogenesis.

The stimulation of the TRPV4 receptor with either magnetically activated MNPs or the chemical agonist GSK101 was observed to enhance chondrogenesis, cell proliferation and ECM deposition. Histological analysis clearly revealed an enhanced production of GAGs and collagen that was noticeable from early culture time points. The uniform distribution of the markers was seen as an indicative of a good diffusion of oxygen and nutrient across the pellets. This event has been broadly discussed with some studies suggesting that hypoxic conditions are beneficial to chondrogenesis (349,350). Nevertheless, other studies suggest the negative effects of the poor diffusion events with the inevitable necrosis of the centre of the pellet (270). Despite the homogeneity observed on the marker's distribution, the pellets had a stiff consistency that hindered the digestion for RNA extraction even after mechanical disaggregation of the samples. This was consistent with both the histological and immunohistochemical analysis evidencing the formation of a consistent matrix for all TRPV4

stimulated samples cultured in higher serum. The presence of the chondrogenic markers collagen II and SOX9 was observed from the first week of culture, being more evident in TRPV4 stimulated groups. The marker production continued to increase with culture time showing a deposition pattern resembling to that of native articular cartilage. SOX9 is a highly regulated transcription factor tightly regulated and closely involved in chondrogenic events (351). The production of the marker was evident by day 7 of culture and peaked on day 14 with higher production observed for TRPV4 activated groups as expected. The presence of the marker was maintained or moderately increased after 21 days of culture, matching with results from available literature (306). TRPV4 channel activity has been broadly related to SOX9 activation through specific signalling pathways (1) and mechanical loading has also been described as an activator of the transcription factor (352). The activation of the channel with a chemical agonist and direct mechanical stimulation of the channel with MNPs are hypothesised to be responsible for the higher production of the marker among the various tested conditions (165,353,354).

Great variation was found among samples labelled with TRPV4 MNPs not submitted to any external magnetic field. Histological analysis revealed for some samples marker deposition levels resembling to those of MICA activated groups, and other samples showed results resembling more to those found in the controls. These events were also observed for the immunohistochemical analysis, being more evident for SOX9 production. The variability found among different samples from the same group was attributed to the effect of the MNPs directly attached to the mechano-sensitive domain of the channel. Despite the lack of external forces, the MNPs binding alone might be exerting some levels of channel activation that could be modifying the channel activity. This would potentially explain the similarity on the results with the MICA activated groups, always considering that the magnetically activated groups showed consistency on the chondrogenic events, while the static group showed slightly lower chondrogenic activity. The similarity of both groups was previously observed in Chapters 3 and 4, and hence it was not attributed to random events.

MSCs obtained from adult donors for OA treatments have been widely reported to show variability on the proliferative and differentiation potential, often related to donor's age. The variability of hUC-MSCs has been studied among cells extracted with differential techniques or from variable locations of the umbilical cord (345,355). Few studies have analysed the variability among donors, some of them reporting variable effects (275) and opposing studies finding low variability among donors in the proliferative and differentiation capacity (356). In this study, some levels of variability were found among 3 different donors. With the aim of reducing any variability introduced by differential culture conditions, all experiments were performed with identical protocols and culture times. Nevertheless, due to unforeseen circumstances both donors 2 and 3 expansion processes varied from the standard expansion from donor 1 and pooled donors. Due to laboratory shutdown during COVID-19 pandemic, the pooled donor experiment had to be performed prior to donor 3 experiment, given the importance of testing this condition prior to the animal study. Hence donor 3 experiment was performed following frozen storage of the cells for 3 months. Moreover, donor 2 cells had to be further expanded due to technical issues, having more population doublings in order to manage sufficient cell number to perform the minimum required groups for this experiments. Analysis performed for all 3 donors revealed a similarity pattern for donors 1 and 3 and variable results for donor 2. It is believed that the longer expansion for cells from donor 2 might have generated stress on the cells that did not show the same chondrogenic behaviour than the compared donors. The limitations encountered with cell number prevented the possibility to conduct a more thorough study with all culture conditions studied in all 3 donors, however, groups were repeated at least for 2 different donors, with the exception of the group labelled with unspecific MNPs that was introduced merely to analyse the effect of unspecific MNP binding and needed no further study. Donors 1 and 3 shared similarities in the histological and immunohistochemical results nevertheless, variation among the levels of markers production was found being higher for donor 1. Donors 1 and 2 were found to express similar levels of chondrogenic markers in terms to production level, however, some of the shared groups were found to vary.

Moreover, differences on the proliferation rates were found among donors when expanding the cells. These findings lead to suggest the existence of variability in the proliferation and chondrogenic potential of hUC-MSCs from different donors. Further studies with a higher number of donors would be required to examine changes in the surface markers and a more detailed chondrogenic assessment to obtain more definitive conclusions.

The pre-clinical study design for OA repair was proposed to be delivered via an injectable solution of hUC-MSCs from all 3 donors combined. With this aim an *in vitro* experiment with cells from all 3 pooled donors was performed. The samples containing MNPs were stimulated mechanically 7 days and continued normal culture for 21 days with the aim of simplifying the experimental design (Supplementary figures 4 and 5). The mechanical activation for 7 days, did not alter the chondrogenic response of the samples showing similar responses compared to samples stimulated with MICA for 21 days. This might be an indicator of the mechanism of action of the MICA technology being effective over the initial phases of the differentiation process. Given the growth and the production of a stiff ECM, the magnetic stimulation might only be acting over initial culture times when the samples have a less dense matrix and the MNPs can exert the pulling effect of the membrane when attracted to a magnetic field. Samples from the combined donors were also labelled with a cell tracker to test the effect of the dye in proliferation and differentiation seeing no adverse effects (Results not shown) as previously demonstrated by members of the group (222).

TRPV4 chemical and mechanical stimulation was seen to also induce higher expression of *COL2A1*, *ACAN* and *SOX9* at a gene expression level, coordinating with previous histological and immunohistochemical findings. The expression of *COL10A1*, related with a hypertrophy or maturation during endochondral ossification, was only detected in low levels for the control samples (357). Nevertheless, the overall expression levels for all genes and transcription factors measured had low expression ranges. The complications encountered to disaggregate the pellets for RNA extraction were suspected to be responsible for the low gene expression profile. Despite mechanically disrupting the

pellets, the RNA yield and purity was not satisfactory and only samples from day 7 yielded enough RNA to qualify for qRT-PCR analysis.

## 5.6 Conclusions

Selecting the cell source for an injectable OA therapy is a key element for a successful outcome. The broad variability encountered among BM-MSCs was not shared by UC-MSCs, nevertheless, assessment of the chondrogenic ability of different donors showed some levels of variation. The variability was above all encountered among production levels of markers, however, identical groups followed a trend for all donors tested. These findings suggest the need for a preliminary study of the proliferative and chondrogenic ability of individual donors prior to selecting the specific donor for *in vivo* applications. The chondrogenic performance of the cells evaluated for UC-MSCs was satisfactory when TRPV4 was activated and overpassed the quality of the cartilage constructs produced with BM-MSCs on Chapter 3. Nevertheless, the culture of the cells alone with chondro-inductive media was not sufficient to enhance the production of a cartilage-like matrix. Further evaluation of the gene expression profile would highly contribute to conclusively determine the chondrogenic potential of this cell source. The mechanical activation of the TRPV4 was an enhancer of the chondrogenesis and matrix formation obtaining constructs with similar properties to those of native cartilage. Introducing this technology for the pre-clinical trial could be of great benefit to remotely guide the differentiation of UC-MSCs in addition to introduce the possibility of *in vivo* tracking and locating the cells.

---

# *Chapter 6*

---

## *Discussion, future work and concluding remarks*

## 6.1 Summative discussion

Articular damage and degeneration is a condition affecting millions of people worldwide, and an effective gold standard treatment has yet to be developed. Current therapeutic approaches range from symptomatic treatment to joint replacement. Despite the improvement of life quality and pain reduction following joint replacement, the economic burden and the invasiveness of the procedure have necessitated the search for alternative treatments. The development of new lines of therapy in recent years has focused on targeting the degeneration of cartilage and aimed to develop approaches that intend to stop disease progression, while attempting to regenerate the damaged tissue. Clinically approved techniques based on tissue engineering approaches are now being successfully performed. These techniques are based on the use of autologous chondrocytes harvested from healthy tissue, and the posterior implantation at the injury site, with the hope that the microniche generated within the joint will promote the integration of the cells into the tissue and the following regeneration of the damaged tissue. Despite the promising outcomes reported (358,359), current tissue engineering approaches have some common limitations. One of the major disadvantages met is the limitation of the cell number available. Given the fact that cells are often affected by the patient's age or life quality, the cells obtained often do not perform adequately for their attributed functions and fail to integrate within the damaged tissue. Histological assessment of the newly formed tissue is usually graded as fibrocartilage, and the regenerated tissue tends to not match the functional and mechanical properties of the native tissue. Moreover, harvesting of the cells from healthy tissue is often associated with donor site morbidity. These limitations have led researchers to primarily focus on the selection of an alternative cell source. Stem cells have emerged as a promising alternative for tissue engineering approaches. The plasticity of the cells together with the immuno-modulatory properties and the multiple sources of extraction, have made stem cells the preferred candidate for cartilage therapy. Stem cell research has offered promising potential for cartilage tissue engineering, with multiple clinical trials in place (284,360). Among the variety of stem cells, adult MSCs have emerged

as the most studied in the field. The lack of ethical concerns surrounding their extraction, and the well-defined tri-lineage differentiation ability make them excellent candidates for regenerative medicine. Nevertheless, the source tissue of extraction is still a topic of discussion and often the cell number obtained is also seen as a limitation. Alternative stem cell sources range from ESCs, iPSCs or UC-MSCs. Both ESCs and iPSCs have great advantages, such as the unlimited expansion and the greater differentiation potential, however, ethical concerns surround the use of both cell types and the potential teratoma formation poses a significant risk (361,362). Over the past few years, UC-MSCs have emerged as a possible source of allogenic therapy for tissue engineering. The cells from the umbilical cord can be harvested painlessly from discarded tissue and thus, no ethical concerns are raised. Moreover, given the young age of the source, they have a great expansion and differentiation potential. In addition, they have been demonstrated to possess an immune-privileged status making them excellent candidates of study for future clinical applications.

The purpose of this study was to define the bases for a novel cartilage tissue engineering approach, gathering the use of stem cells and bioreactors. This was performed firstly, by studying the chondrogenic potential of a range of mechano-inducible targets under the effect of MICA activation. Secondly, once a potential target for cartilage repair was selected, the scope of the MICA technology on the TRPV4 channel activation for chondrogenic differentiation was assessed and optimised. Thirdly, and following studies on a variety of cell types, UC-MSCs were studied as a potential source for a preclinical ovine trial that was planned and designed for an injectable therapy for OA repair. Unfortunately, the crisis originated by the Covid pandemic precluded the continuation of the trial just before the start. Despite the growing number of studies focused on the chemical or mechanical activation of TRPV4, this thesis is the first report to selectively target the TRPV4 channel via labelling with MNPs and magnetically activating the channel for enhancing chondrogenic differentiation. Moreover, this is the first study where TRPV4 activation for chondrogenic purposes has been tested in UC-MSCs. This work demonstrated in Chapter 4 the enhancement of chondrogenesis, introduced

by the MICA technology, and further on Chapter 5, the potential of the activation of TRPV4 in UC-MSCs for driving the cells towards a chondrogenic phenotype for future injectable therapies for OA repair. This chapter demonstrated that the selective mechanical activation of the channel showed similar chondrogenic response to the direct activation of the channel with the GSK101 agonist.

One of the major concerns surrounding the use of MNPs for medical approaches is the toxicity reported by some studies (363–365) following the systemic delivery of the nanoparticles and especially after MNP degradation. Multiple viability studies were performed during Chapter 3, widely demonstrating the safety of the MNPs after 21 days of culture. This is of great importance, considering that our lab has previously reported, for the same commercially available MNPs, degradation under lysosomal conditions after 1 week. Nevertheless, *in vitro* assessment of the MNPs demonstrated the presence of the nanoparticle's iron in the samples after 21 days of culture, for both for the micromasses and the 3D culture systems. Retention of the MNPs within the cells is key for the efficacy of the MICA technology, however, the stimulation of the cells for 21 days presented a similar outcome to that obtained for samples stimulated over the first week of culture, that were kept in culture for 21 days (Supplementary figures 4 and 5). This is not surprising considering the early chondrogenic response obtained from MICA activated samples, suggesting the activation of the TRPV4 receptor has a key role in the initiation of the chondrogenic response, as is also suggested by the available literature (1,157,171). Moreover, the MNPs underwent internalisation shortly after labelling, in agreement with the reported endocytosis of the receptor following activation (250). Gathering all the evidence, it is believed that the magnetic activation of TRPV4 influences the initiation of the chondrogenic response. For this reason, and in order to simplify the treatment for potential future applications, the pre-clinical animal trial was designed to supply 1 week of magnetic stimulation rather than 21 days. Nevertheless, the limited access to the TEM equipment hindered the further study on the MNPs fate. The process following the culture of cells with unlabelled MNPs was not studied for this work. However, the work performed by our group suggests that unlabelled MNPs are rapidly phagocytised. Further study should

be carried in order to elucidate if the internalisation of the TRPV4-MNPs was an effect of the receptor recycling following activation or if this event was due to phagocytic events.

The study of *in vitro* chondrogenesis is widely practiced by many research groups. A variation of culture conditions has been used with differential outcomes, nevertheless, most protocols agree on the importance of TGF- $\beta$ , in addition to dexamethasone and ascorbic acid, for an effective chondrogenic induction of the constructs. Initially the aim of removing the growth factor from the culture medium was intended for analysing the scope of the MICA activation without one of the key elements for chondrogenesis. Nevertheless, the results observed following the removal of the factor led to further investigation of the constructs generated in the absence of TGF- $\beta$ . The growth factor has been widely described as having an essential role in cartilage formation and healthy maintenance of the tissue, by preventing cells from undergoing terminal hypertrophic differentiation. In Chapter 4, the removal of the factor from the culture environment did not seem to negatively affect the chondrogenesis in terms of ECM production, and similar results were obtained from those samples cultured with a complete chondrogenic media, when under MICA stimulation. Nevertheless, the presence of hypertrophy markers was not assessed. Notably, the samples not exposed to TGF- $\beta$  did not form an organised matrix, and thus it was included in the culture medium for future experiments. The good chondrogenic response, as evidenced by ECM deposition, was believed to be achieved by the recently discovered role of TRPV4 enhancing the production of TGF- $\beta$  following chemical or mechanical activation. The gene expression analysis, revealing a great increase of the collagen II and aggrecan production in TRPV4 activated samples following MICA activation and an absence of TGF- $\beta$ , was attributed to production of the growth factor under the effect of both mechanical stimulation and activation of the TRPV4 receptor. Following this line of reasoning, it was expected that TRPV4 activated samples cultured with the complete chondrogenic medium would show an enhanced effect in comparison to samples cultured without TGF- $\beta$ . Nevertheless, TRPV4 MICA-activated samples in complete media formed a thick outer collagen ring, which hugely hindered the disaggregation of the

sample for RNA extraction and thus, great limitations were encountered for the digestion with a low RNA yield, and lower quality of the obtained RNA, affecting the results from the gene expression analysis.

The selection of the cell source for tissue engineering approaches has long been debated among the scientific community. Chondrocytes have always been the obvious choice, and current clinically approved therapies are based on the use of autologous chondrocytes. Nevertheless, chondrocytes have widely been described to lose their phenotype when cultured in monolayer, and these techniques require the *in vitro* expansion of the cells. Adding to the existing concern raised for chondrocytes from OA patients to retain a predisposition for disease development, the major limitation encountered is the limited cell number and the complications for pharmaceutical manufacturing. Therefore, research has focused on the study of MSCs as a potential candidate for cartilage repair. The source of MSCs has also been greatly discussed with bone marrow and adipose tissue being the most popular sources. The tri-lineage differentiation potential for both cell sources has been widely demonstrated, however, donor features such as age or health status influence the performance and proliferative capacity of the cells (338). Allogenic donation of MSCs would avoid these limitations, however, despite the immune-modulatory properties of the stem cells, issues regarding the use of allogenic cell therapy are still common. The chondrogenic potential of bone marrow and adipose-derived MSCs was demonstrated in this work, mainly by histological determination of the ECM components. Measurement of the chondrogenic activity was achieved with the collagen II reporter cell line, which allowed for a clear visualisation of the enhancement of collagen II production following MICA activation. The use of the reporter cell line aided selection of the best chondro-inductive target for MICA activation, and revealed the lack of response of RGD that showed similar results to those observed for samples cultured without MNPs. TREK-1 and TRPV4 activation showed a similar pattern of collagen II expression and thus further analysis was done to select the more adequate target. The slight increased expression of collagen II observed for the TRPV4 activated

samples, together with the histological assessment led to the selection of the calcium channel as the main target for this work. Despite the favourable outcomes observed for TREK-1 activation, a homogeneity on the chondrogenic response was observed for all the assessments performed on TRPV4 activation. Moreover, the existing literature highlights the fundamental role of TRPV4 in cartilage formation and homeostasis, whereas no studies were found that link TREK-1 with cartilage.

Regardless of the demonstrated chondrogenic potential of adult MSCs during this work, the differentiation ability of UC-MSCs was initially assessed, with the aim of overcoming the previously mentioned issues encountered among the selection of adult MSCs for a clinical therapy. An initial experiment testing the chondrogenic potential of the cells with and without TRPV4 activation was performed, with promising outcomes for those samples where the channel was chemically or mechanically activated. Enhanced matrix deposition was found among stimulated samples, with increased histological properties compared to those found with human MSCs. Due to the lack of vascularisation in native tissue, conventional human chondrogenic protocols often use low percentages of FBS (228,345,366), hence, all experiments were performed with high and low concentration of FBS. Regardless of the popularity of low serum protocols, it was consistently found among this work that samples cultured with 10% FBS exhibited improved chondrogenesis. The experiment was repeated three times with different donors to observe the variability on the chondrogenic response and indeed, some levels of performance variation were found among donors, however, all compared donors exhibited chondrogenic response to some extent. The introduction of different experimental groups aimed to optimise the best conditions for driving differentiation, prior to the realisation of the animal study. The pre-clinical trial was designed to deliver combined cells from all 3 donors and thus, a last repeat of the experiment was carried with the combined cells, and the 7-day MICA activation protocol, against the 21-day activation. A lower chondrogenic response was observed for the combination of the donor's cells, however, this was attributed to the need for an additional cycle of freeze-thawing due to the issues encountered with the lab closure during the

pandemic. Overall, the in-depth histological and immunohistochemical analysis indicated the potential of UC-MSCs for cartilage regeneration approaches, and this was the selected cell source for the pre-clinical study.

The delivery of mechanical forces targeted specifically towards a mechano-responsive element of the cells could introduce great advantages for cartilage repair approaches. The labelling of the cells with MNPs allows for *in vivo* tracking and visualisation of cell fate following injection by MRI assessment. In addition, this technology would allow to remotely control the stem cell fate while delivering external mechanical forces to aid the stem cells to differentiate towards a chondrogenic lineage while ensuring the retention of the cells in the injury site by the design of a magnetic bandage.

## 6.2 Future work

The work performed during this thesis has left some optimisation of the MICA technology that could be of benefit for an improved result for potential clinical translation. In Chapter 3, characterisation of the cells and MNPs used for the duration of this work was performed. Although the work was conducted following previous research on the topic from the lab's group and current literature, a repeated in depth characterisation would have ensured the adequate basis of the MICA technology. MNPs internalised by cells in suspension were demonstrated by our group to be metabolised after 7 days in lysosomal conditions. Assessment after termination of the experiment of the iron content left on the 3D culture systems under physiological conditions, would have been beneficial to understand if the delivery of magnetic stimulus is needed following the first week of activation, since the magnetic activation would only be of benefit if MNPs remain intact. The cells were labelled differently according to the method of culture. The preferred method of culture for this work was the formation of 3D pellets, where cells were labelled in suspension prior to pellet formation. This method of labelling was performed with the aim of avoiding an extra passage of the cells with the added stress, nevertheless, labelling in monolayer was observed to be more efficient for MNP uptake. The assessment of the MNP

uptake was performed in a simple experiment with prussian blue staining of the iron content. This detection method was not powerful enough to detect the uptake of MNPs in the samples due to the lack of availability of a more powerful microscope, and there was no certainty that the particles were engulfed by the cells. Therefore, it was not possible to optimise the most efficient labelling method. Regarding the MNPs characterisation, the dose of MNPs selected was based on previous studies from the group claiming that the chosen concentration was optimal for delivering the units of force needed to activate the cells, and the amount of MNPs needed to exert this force (5-6 MNPs per cells). This dose was also shown to bring about no cytotoxicity. Given the variability of the toxicological results on viability studies, a dose-dependent effect-viability study would have ensured the optimal dose of MNPs for every different experiment performed.

The TRPV4 channel was targeted with MNPs that were attached to the intracellular N-terminal domain, which is reported to have the mechano-sensitive control of the channel (141). The attachment of the MNPs to the mechano-responsive domain ensured the activation of the channel following MNPs labelling, nevertheless, several inconveniences were met during this work. Targeting an intracellular domain required the administration of a transfection agent for the internalisation of the MNPs, which could become an obstacle if the transfection is not effectively performed. In addition, targeting the control domain of the mechanical activation could have caused desensitisation of the channel, by the constant indirect activation of the channel with the MNPs wiggle movement. It was proposed for future work to compare the effect of MICA activation targeting an extracellular region of the channel against labelling the N-terminal domain. Despite being able to demonstrate by TEM the successful uptake of the MNPs, a dual co-localisation experiment targeting the MNPs and the TRPV4 channel, would have further supported the effective targeting of the channel. The effect of TRPV4 mechanical and chemical activation on chondrogenic enhancement was fully demonstrated for the duration of this work. Regardless of the mechanisms of TRPV4 activation being reported by the literature to be actuated by the initiation of downstream signalling events with initial increase of the

intracellular [Ca], a study measuring the effects following the channel activation such as measuring the phosphorylation of the PKC protein or the fluctuations of the intracellular calcium levels, could have helped to further elucidate the mechanism behind the MICA activation of TRPV4.

The assessment of the chondrogenesis in Chapter 4 was performed using a novel system based on the quantification of collagen II expression by a reporter cell line. The visual analysis of the GFP-collagen II cell line was successfully performed, however, the quantification of the secreted luciferase needed for further optimisation with the CMV control cell line. The chondrogenesis study was also performed with and without the effect of TGF- $\beta$ , however, the exact relationship between TRPV4 and the growth factor remained unclear. Gene expression analysis of TGF- $\beta$  following chemical, mechanical or static conditions, would have been beneficial to elucidate if, as proposed by the literature, the growth factor expression is activated by both mechanical stimulation and TRPV4 activation. In addition to analysing the gene expression of TGF- $\beta$ , an improved digestion method for the RNA extraction would ensure the success of the qRT-PCR, often hindered during the duration of this work by the thickness of the ECM and the subsequent low RNA yield.

The assessment of the chondrogenic potential of UC-MSCs was mainly done by histological and molecular analysis of the ECM markers. Mechanical testing of the constructs could have added information regarding the quality of the 3D constructs and the mechanical properties. In addition, analysis of the different markers by flow cytometry could have further supported the chondrocyte-acquired phenotype of the UC-MSCs. Due to the unforeseen circumstances, it was not possible to resume the animal pre-clinical trial for the duration of this work. However, the experimental design was completed for the initiation of the trial. UC-MSCs pooled from all 3 donors and labelled with TRPV4-MNPs were to be delivered into medial meniscus defects of 7 sheep, followed by 7 days of MICA activation with a magnetic bandage designed by Dr. Hareklea Markides. In addition, 7 sheep were to be injected with SPION-labelled cells and not receive any magnetic stimulation and Dr. Claire Mennan was delivering cells alone to other 7 animals. The analysis was mainly based on MRI imaging

of the defect and histological assessment. The progression of this trial would have been a great opportunity to study the potential of MICA technology as future remote control healing therapy.

### 6.3 Concluding remarks

The work conducted during this thesis studied the potential of the MICA technology as a proposed tool for cartilage repair by activating a mechano-sensitive structure within the cells. Mechanical activation of TRPV4 enhanced the chondrogenic response obtained with the aid of biochemical cues and produced 3D constructs with an enhanced cartilage matrix deposition. In addition, UC-MSCs were firstly studied for the mechanical activation of TRPV4 resulting in a potential cell source for cartilage therapies. The promising results of the MICA activation of TRPV4 open the door to explore potential applications for cartilage repair, eliminating the invasiveness of the current procedures and offering the novel principle of *in vivo* remote control of the cells.

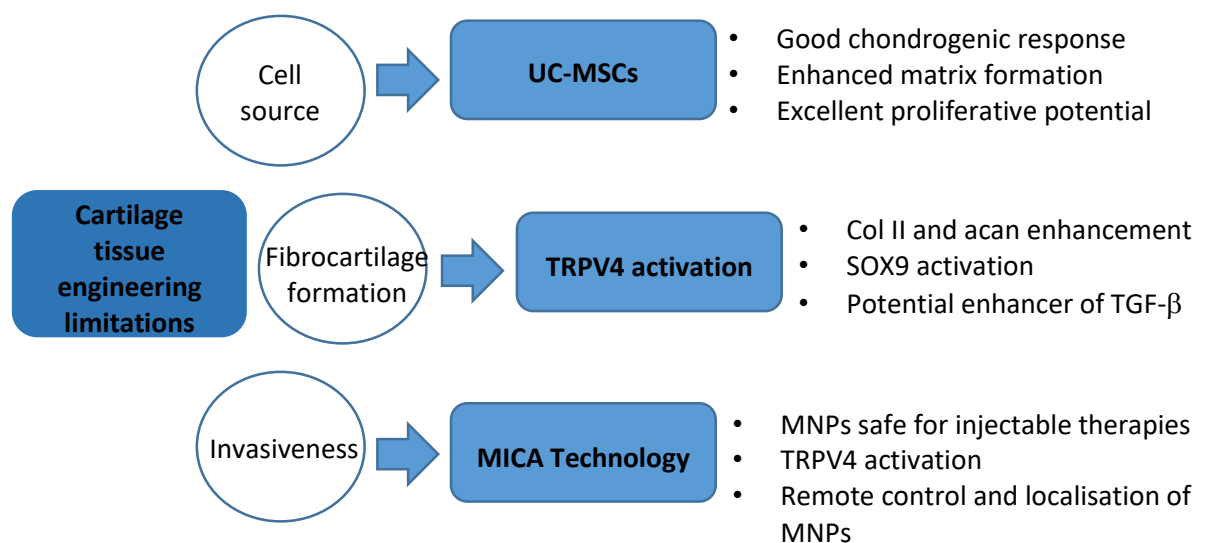


**Figure 6-1. Summative conclusion diagram.** Limitations to current tissue engineering approaches and potential possibilities to overcome these difficulties, offered by the work described for this thesis.

---

# *References*

---

1. Muramatsu S, Wakabayashi M, Ohno T, Amano K, Ooishi R, Sugahara T, et al. Functional gene screening system identified TRPV4 as a regulator of chondrogenic differentiation. *J Biol Chem.* 2007;282(44):32158–67.
2. Graaff KMVD, Strete D, Creek CH. *Van De Graaf Human Anatomy.* McGraw Hill Higher Education. 2001.
3. Molnar C, Gair J. *Concepts of Biology-1st Canadian Edition.* Vol. 1, *Concepts of Biology-1st Canadian Edition.* 2015. 1007 p.
4. Mow VC, Ratcliffe A, Robin Poole A. Cartilage and diarthrodial joints as paradigms for hierarchical materials and structures. *Biomaterials.* 1992;13(2):67–97.
5. Nygaard G, Firestein GS. Restoring synovial homeostasis in rheumatoid arthritis by targeting fibroblast-like synoviocytes. *Nat Rev Rheumatol.* 2020;16:316–33.
6. Sophia Fox AJ, Bedi A, Rodeo SA. The basic science of articular cartilage: Structure, composition, and function. *Sports Health.* 2009;1(6):461–8.
7. Watkins J. Biomechanics of Musculoskeletal Adaptation. In: *Comprehensive Biomedical Physics.* Elsevier B.V.; 2014. p. 1–37.
8. Marchiori G, Berni M, Boi M, Bianchi M, Filardo G. Cartilage mechanical tests: Evolution of current standards for cartilage repair and tissue engineering. A literature review. *Clin Biomech.* 2019;68:58–72.
9. Hunziker EB, Quinn TM, Häuselmann HJ. Quantitative structural organization of normal adult human articular cartilage. *Osteoarthr Cartil.* 2002;10(7):564–72.
10. Buckwalter JA, Mankin HJ, Grodzinsky AJ. *Articular Cartilage and Osteoarthritis.* 2005. p. 465–80.

11. Becerra J, Andrades JA, Guerado E, Zamora-Navas P, Lopez-Puertas JM, Reddi AH. Articular Cartilage : Structure and Regeneration. *Tissue Eng Part B*. 2010;16(6):617–617.
12. Usami Y, Gunawardena AT, Iwamoto M, Enomoto-Iwamoto M. Wnt signaling in cartilage development and diseases: Lessons from animal studies. *Lab Investig*. 2016;96(2):186–96.
13. Wong M, Wuethrich P, Eggli P, Hunziker E. Zone-Specific Cell Biosynthetic Activity in Mature Bovine Articular Cartilage : A New Method Using Confocal Microscopic Stereology and Quantitative Autoradiography. *J Orthop Res*. 1996;14(3):424–32.
14. Buckwalter A. Joseph, Nancy LE. Athletics and Osteoarthritis. *Am J Sports Med*. 1997;25(6):873–81.
15. Wu JP, Kirk TB, Zheng MH. Study of the collagen structure in the superficial zone and physiological state of articular cartilage using a 3D confocal imaging technique. 2008;11:1–11.
16. Bhosale AM, Richardson JB. Articular cartilage : structure , injuries and review of management. *Br Med Bull*. 2008;87:77–95.
17. Eyre D. Collagen of articular cartilage. *Arthritis Res*. 2002;4(1):30–5.
18. van Weeren PR, Firth EC. Future Tools for Early Diagnosis and Monitoring of Musculoskeletal Injury: Biomarkers and CT. *Vet Clin North Am - Equine Pract*. 2008;24(1):153–75.
19. He B, Wu JP, Kirk TB, Carrino JA, Xiang C, Xu J. High-resolution measurements of the multilayer ultra-structure of articular cartilage and their translational potential High-resolution measurements of the multilayer ultra-structure of articular cartilage and their translational potential. *Arthritis Res Ther*. 2014;16(205).
20. Akkiraju H, Nohe A. Role of chondrocytes in cartilage formation, progression of osteoarthritis and cartilage regeneration. *J Dev Biol*. 2015;3(4):177–92.

21. Masuda K, Sah RL, Hejna MJ, Thonar EJMA. A novel two-step method for the formation of tissue-engineered cartilage by mature bovine chondrocytes: The alginate-recovered-chondrocyte (ARC) method. *J Orthop Res.* 2003;21(1):139–48.
22. Carballo CB, Nakagawa Y, Rodeo SA. *Basic Science of Articular Cartilage.* 2017;36:413–25.
23. Landinez-Parra NS, Garzon-Alvarado DA, Venegas-Acosta JC. Mechanical Behavior of Articular Cartilage. In: *Injury and Skeletal Biomechanics.* 2012.
24. Guilak F, Jones WR, Ting-Beall PH, Less GM. The deformation behavior and mechanical properties of chondrocytes in articular cartilage. 1999;59–70.
25. Wilson W, Van Donkelaar CC, Van Rietbergen B, Huiskes R. A fibril-reinforced poroviscoelastic swelling model for articular cartilage. *J Biol Chem.* 2005;38:1195–204.
26. Roughley PJ, Mort JS. The role of aggrecan in normal and osteoarthritic cartilage. *J Exp Orthop.* 2014;1(1):1–11.
27. Felson DT, Hodgson R. Identifying and treating preclinical and early osteoarthritis. *Rheum Dis Clin North Am.* 2014;40(4):699–710.
28. L. Brody Thein. Physical Therapy in Sport Knee osteoarthritis : Clinical connections to articular cartilage structure and function. *Phys Ther Sport.* 2015;16(4):301–16.
29. Vina ER, Kent Kwoh C. Epidemiology of Osteoarthritis: Literature Update Ernest. *Physiol Behav.* 2018;30(2):160–7.
30. Chen A, Gupte C, Akhtar K, Smith P, Cobb J. The Global Economic Cost of Osteoarthritis: How the UK Compares. *Arthritis.* 2012;2012(October):1–6.
31. Xia B, Di Chen, Zhang J, Hu S, Jin H, Tong P. Osteoarthritis Pathogenesis: A Review of Molecular Mechanisms. *Calcif Tissue Int.* 2014;95(6):495–505.

32. Glyn-Jones S, Palmer AJR, Agricola R, Price AJ, Vincent TL, Weinans H, et al. Osteoarthritis. *Lancet*. 2015;386(9991):376–87.
33. Filardo G, Kon E, Martino A Di, Patella S, Altadonna G, Balboni F, et al. Second-generation arthroscopic autologous chondrocyte implantation for the treatment of degenerative cartilage lesions. *Knee Surgery, Sport Traumatol Arthrosc*. 2012;20(9):1704–13.
34. Mort JS, Billington CJ. Articular cartilage and changes in arthritis matrix degradation. *Arthritis Res*. 2001;3(6):337–41.
35. van den Borne MPJ, Raijmakers NJH, Vanlauwe J, Victor J, de Jong SN, Bellemans J, et al. International Cartilage Repair Society (ICRS) and Oswestry macroscopic cartilage evaluation scores validated for use in Autologous Chondrocyte Implantation (ACI) and microfracture. *Osteoarthr Cartil*. 2007;15(12):1397–402.
36. Pritzker KPH, Gay S, Jimenez SA, Ostergaard K, Pelletier JP, Revell K, et al. Osteoarthritis cartilage histopathology: Grading and staging. *Osteoarthr Cartil*. 2006;14(1):13–29.
37. Hunter DJ, March L, Chew M. Osteoarthritis in 2020 and beyond: a Lancet Commission. *Lancet*. 2020;396(10264):1711–2.
38. Zhang W, Moskowitz RW, Nuki G, Abramson S, Altman RD, Arden N, et al. OARSI recommendations for the management of hip and knee osteoarthritis, Part II: OARSI evidence-based, expert consensus guidelines. *Osteoarthr Cartil*. 2008;16(2):137–62.
39. Hochberg MC, Altman ROYD, April KT, Benkhalti M, Guyatt G, Gowan JMC, et al. American College of Rheumatology 2012 Recommendations for the Use of Nonpharmacologic and Pharmacologic Therapies in Osteoarthritis of the Hand , Hip , and Knee. 2012;64(4):465–74.
40. Richter DL, Jr RCS, Wascher DC. Knee Articular Cartilage Repair and Restoration Techniques : A Review. 2015;8(2):153–60.

41. Steadman JR, Rodkey WG, Rodrigo JJ. Microfracture : Surgical Technique and Rehabilitation to Treat Chondral Defects. 2001;(391):362–9.
42. Kwon H, Brown WE, Lee CA, Wang D, Paschos N, Hu JC, et al. Surgical and tissue engineering strategies for articular cartilage and meniscus repair. 2020;15(9):550–70.
43. Hangody L, Gabor GK, Rathonyi K, Duska S, Vasarhelyi G, P.Fules, et al. Autologous Osteochondral Mosaicplasty. J Bone Jt Surg Am. 2003;85-A(Suppl 2):25–32.
44. Dunkin BS, Latterman C. New and Emerging Techniques in Cartilage Repair: MACI. 2013;21(2):100–7.
45. Jakobsen RB, Engebretsen L, Slauterbeck JR. An analysis of the quality of cartilage repair studies. J Bone Jt Surg - Ser A. 2005;87(10):2232–9.
46. De Bari C, Roelofs AJ. Stem cell-based therapeutic strategies for cartilage defects and osteoarthritis. Curr Opin Pharmacol. 2018;40(Figure 1):74–80.
47. Solheim E, Hegna J, Inderhaug E. The Knee Long-term clinical follow-up of microfracture versus mosaicplasty in articular cartilage defects of medial femoral condyle. Knee. 2017;6–11.
48. Cournil-Henrionnet C, Huselstein C, Wang Y, Galois L, Mainard D, Decot V, et al. Phenotypic analysis of cell surface markers and gene expression of human mesenchymal stem cells and chondrocytes during monolayer expansion. Biorheology. 2008;45(3–4):513–26.
49. Murphy CL, Polak JM. Control of Human Articular Chondrocyte Differentiation by Reduced Oxygen Tension. J Cell Physiol. 2004;199(3):451–9.
50. Guerne P -a, Blanco F, Kaelin A, Desgeorges A, Lotz M. Growth factor responsiveness of human articular chondrocytes in aging and development. Arthritis Rheum. 1995;38(7):960–8.
51. Kolios G, Moodley Y. Introduction to Stem Cells and Regenerative Medicine. Respiration.

- 2013;(85):3–10.
52. Alison MR, Poulosom R, Forbes S, Wright NA. An introduction to stem cells. *J Pathol.* 2002;197(4):419–23.
  53. Salgado A, Oliveira J, Pedro A, Reis R. Adult Stem Cells in Bone and Cartilage Tissue Engineering. *Curr Stem Cell Res Ther.* 2006;1(3):345–64.
  54. Denham M, Conley B, Olsson F, Cole TJ. Stem Cells : An Overview. 2005;1–18.
  55. Trohatou O, Roubelakis MG. Mesenchymal Stem/Stromal Cells in Regenerative Medicine: Past, Present, and Future. 2017;19(0):1–8.
  56. Pers YM, Ruiz M, Noel D, Jorgensen C. Mesenchymal stem cells for the management of inflammation in osteoarthritis : state of the art and perspectives. 2015;23:2027–35.
  57. Ghannam S, Bouffi C, Djouad F, Jorgensen C, Noël D. Immunosuppression by mesenchymal stem cells : mechanisms and clinical applications. *Stem Cell Res Ther.* 2010;1:1–7.
  58. Papadopoulou A, Yiangou M, Athanasiou E, Kaloyannidis P, Batsis I, Fassas A, et al. Mesenchymal stem cells are conditionally therapeutic in preclinical models of rheumatoid arthritis. *Ann Rheum Dis.* 2012;71(10):1733–40.
  59. Djouad F, Charbonnier LM, Bouffi C, Louis-Plence P, Bony C, Apparailly F, et al. Mesenchymal Stem Cells Inhibit the Differentiation of Dendritic Cells Through an Interleukin-6-Dependent Mechanism. 2007;33(0):2025–32.
  60. Murphy JM, Dixon K, Beck S, Fabian D, Feldman A, Barry F. Reduced Chondrogenic and Adipogenic Activity of Mesenchymal Stem Cells From Patients With Advanced Osteoarthritis. 2002;46(3):704–13.
  61. Chen L, Tredget EE, Liu C, Wu Y. Analysis of Allogenicity of Mesenchymal Stem Cells in
-

- Engraftment and Wound Healing in Mice. 2009;4(9):3–9.
62. Griffin MD, Ryan AE, Alagesan S, Lohan P, Treacy O, Ritter T. Anti-donor immune responses elicited by allogeneic mesenchymal stem cells : what have we learned so far ? 2013;(October 2012):40–51.
  63. Vega A, Martín-ferrero MA, Canto F Del, Alberca M, García V, Munar A, et al. Treatment of Knee Osteoarthritis With Allogeneic Bone Marrow Mesenchymal Stem Cells: A Randomized Controlled Trial. 2015;99(8):1681–90.
  64. Gupta PK, Chullikana A, Rengasamy M, Shetty N, Pandey V, Agarwal V, et al. Efficacy and safety of adult human bone marrow-derived, cultured, pooled, allogeneic mesenchymal stromal cells (Stempeucel®): Preclinical and clinical trial in osteoarthritis of the knee joint. *Arthritis Res Ther*. 2016;18(1):1–18.
  65. Prockop DJ, Ph.D. The Exciting Porspects of New Therapies with Mesenchymal Stromal Cells. 2016;19(1):1–8.
  66. Jorgensen C, Noël D. Mesenchymal stem cells in osteoarticular diseases. *Regen Med*. 2011;6:44–51.
  67. Vidal MA, Robinson S, Lopez MJ, Paulsen DB, Borkhsenius O, Johnson JR, et al. Comparison of Chondrogenic Potential in Equine Mesenchymal Stromal Cells Derived from Adipose Tissue and Bone Marrow. *Bone*. 2008;23(1):1–7.
  68. Saw KY, Hussin P, Loke SC, Azam M, Chen HC, Tay YG, et al. Articular Cartilage Regeneration With Autologous Marrow Aspirate and Hyaluronic Acid: An Experimental Study in a Goat Model. *Arthrosc - J Arthrosc Relat Surg*. 2009;25(12):1391–400.
  69. Saw KY, Anz A, Siew-Yoke Jee C, Merican S, Ching-Soong Ng R, Roohi SA, et al. Articular cartilage regeneration with autologous peripheral blood stem cells versus hyaluronic acid: A

- randomized controlled trial. *Arthrosc - J Arthrosc Relat Surg*. 2013;29(4):684–94.
70. Nam HY, Karunanithi P, Loo WCP, Naveen S V., Chen HC, Hussin P, et al. The effects of staged intra-articular injection of cultured autologous mesenchymal stromal cells on the repair of damaged cartilage: A pilot study in caprine model. *Arthritis Res Ther*. 2013;15(5):1.
71. Richardson SM, Kalamegam G, Pushparaj PN, Matta C, Memic A, Khademhosseini A, et al. Mesenchymal stem cells in regenerative medicine : Focus on articular cartilage and intervertebral disc regeneration. *Methods*. 2016;99:69–80.
72. Chang CJ, Yen ML, Chen YC, Cien CC, Huang HI, Bai CH, et al. Placenta-Derived Multipotent Cells Exhibit Immunosuppressive Properties That Are Enhanced in the Presence of Interferon. *Stem Cells*. 2006;24:2466–77.
73. Pappa KI, Anagnou NP. Novel sources of fetal stem cells : where do they fit on the developmental continuum ? 2009;4:423–33.
74. Safari F, Fani N, Eglin D, Alini M, Stoddart MJ, Eslaminejad MB. Human umbilical cord-derived scaffolds for cartilage tissue engineering. *J Biomed Mater Res Part A*. 2019;107A:1793–802.
75. Liang H, Suo H, Wang Z, Feng W. Progress in the treatment of osteoarthritis with umbilical cord stem cells. *Hum Cell*. 2020;33(3):470–5.
76. Harris DT. Umbilical Cord Tissue Mesenchymal Stem Cells : Characterization and Clinical Applications. *Curr Stem Cell Res*. 2013;8(5):394–9.
77. Reppel L, Schiavi J, Charif N, Leger L, Yu H, Pinzano A, et al. Chondrogenic induction of mesenchymal stromal / stem cells from Wharton ' s jelly embedded in alginate hydrogel and without added growth factor : an alternative stem cell source for cartilage tissue engineering. *Stem Cell Res Ther*. 2015;6:260:1–13.
78. Park YB, Ha CW, Lee CH, Yoon YC, Park YG. Cartilage Regeneration in in Osteoarthritic

Osteoarthritic Patients by Composite of Allogeneic Umbilical Cord Blood-Derived Mesenchymal Stem Hyaluronate Hydrogel : Results from Trial for Safety and Proof-of-Concept with 7 Years of Extended Follow-Up. *Stem Cells Transl Med.* 2017;6:613–21.

79. Zaim M, Karaman S, Cetin G, Isik S. Donor age and long-term culture affect differentiation and proliferation of human bone marrow mesenchymal stem cells. *Ann Hematol.* 2012;91(8):1175–86.
80. Song J, Hong K, Kim N, Jung J, Park H, Heon S, et al. Implantation of allogenic umbilical cord blood-derived mesenchymal stem cells improves knee osteoarthritis outcomes : Two-year follow- up. *Regen Ther.* 2020;14:32–9.
81. Dilogio IH, Feby A, Alberto C, Hanitya L. Umbilical cord - derived mesenchymal stem cells for treating osteoarthritis of the knee : a single - arm , open - label study. *Eur J Orthop Surg Traumatol.* 2020;(0123456789):12–5.
82. Gupta PK, Das AK, Chullikana A, Majumdar AS. Mesenchymal stem cells for cartilage repair in osteoarthritis. *Stem Cell Res Ther.* 2012;3(25):1–9.
83. Darling EM, Athanasiou KA. Biomechanical Strategies for Articular Cartilage Regeneration. *Ann Biomed Eng.* 2003;31:1114–24.
84. Freed LE, Guilak F, Guo XE, Gray ML, Tranquillo R, Holmes JW, et al. Advanced Tools for Tissue Engineering: Scaffolds, Bioreactors and Signaling. *Tissue Eng.* 2006;12(12):3285–305.
85. Athanasiou KA, Rajalakshmanan E, Hadidi P, Hu JC. Self-Organization and the Self-Assembling Process in Tissue Engineering. *Physiol Behav.* 2019;176(3):139–48.
86. Chiang E, Ma H, Wang J, Liu C. Allogeneic Mesenchymal Stem Cells in Combination with Hyaluronic Acid for the Treatment of Osteoarthritis in Rabbits. *PLoS One.* 2016;11(2):1–15.
87. Gilbert TW, Sellaro TL, Badylak SF. Decellularization of tissues and organs. 2006;27:3675–83.

88. Plunkett N, O'Brien FJ. Bioreactors in tissue engineering. *Technol Heal Care*. 2011;19:55–69.
89. Farrell MJ, Shin JI, Smith LJ, Mauck RL. Functional consequences of glucose and oxygen deprivation on engineered mesenchymal stem cell-based cartilage constructs. *Osteoarthr Cartil*. 2015;23(1):134–42.
90. Boeuf S, Steck E, Pelttari K, Hennig T, Buneß A, Benz K, et al. Subtractive gene expression profiling of articular cartilage and mesenchymal stem cells : serpins as cartilage-relevant differentiation markers. *Osteoarthr Cartil*. 2008;16:48–60.
91. Farrell MJ, Farrell MJ, Comeau ES, Mauck RL. Mesenchymal Stem Cells Produce Functional Cartilage Matrix in Three-Dimensional Culture in Regions of Optimal Nutrient Supply. *Eur Cells Mater*. 2012;23:425–40.
92. Ahmed S, Chauhan VM, Ghaemmaghami AM, Aylott JW. New generation of bioreactors that advance extracellular matrix modelling and tissue engineering. *Biotechnol Lett*. 2019;41(1):1–25.
93. Glowacki J, Mizuno S, Greenberger JS. Perfusion Enhances Functions of Bone Marrow Stromal Cells in Three-Dimensional Culture. *Cell Transplant*. 1998;7(3):319–26.
94. Robins JC, Akeno N, Mukherjee A, Dalal RR, Aronow BJ, Koopman P, et al. Hypoxia induces chondrocyte-specific gene expression in mesenchymal cells in association with transcriptional activation of Sox9. *Bone*. 2005;37(3):313–22.
95. Sheehy EJ, Buckley CT, Kelly DJ. Biochemical and Biophysical Research Communications Oxygen tension regulates the osteogenic , chondrogenic and endochondral phenotype of bone marrow derived mesenchymal stem cells. *Biochem Biophys Res Commun*. 2012;417(1):305–10.
96. Buckley CT, Meyer EG, Kelly DJ. The Influence of Construct Scale on the Composition and

Functional Properties of Cartilaginous Tissues Engineered Using Bone Marrow-Derived Mesenchymal Stem Cells. *Tissue Eng Part A*. 2012;18:34–9.

97. Daly AC, Sathy BN, Kelly DJ. Engineering large cartilage tissues using dynamic bioreactor culture at defined oxygen conditions. *J Tissue Eng*. 2018;9:1–12.
98. Winter A, Breit S, Parsch D, Benz K, Steck E, Hauner H, et al. Cartilage-Like Gene Expression in Differentiated Human Stem Cell Spheroids A Comparison of Bone Marrow – Derived and Adipose Tissue – Derived Stromal Cells. *Arthritis Rheum*. 2003;48(2):418–29.
99. Huang AH, Farrel MJ, Kim M, Mauck RL. Long-Term Dynamic Loading Improves the Mechanical Properties of Chondrogenic Mesenchymal Stem Cell-Laden Hydrogels. *Eur Cell Mater*. 2010;19:72–85.
100. Foster NC, Henstock JR, Reinwald Y, El Haj AJ. Dynamic 3D culture: Models of chondrogenesis and endochondral ossification. *Birth Defects Res Part C - Embryo Today Rev*. 2015;105(1):19–33.
101. Anderson DE, Johnstone B. Dynamic mechanical compression of chondrocytes for tissue engineering: A critical review. *Front Bioeng Biotechnol*. 2017;5(DEC):1–20.
102. Huang AH, Farrell MJ, Mauck RL. Mechanics and Mechanobiology of Mesenchymal Stem Cell-Based Engineered Cartilage. *J Biomech*. 2010;43(1):1–21.
103. Chen CS, Ingber DE. Tensegrity and mechanoregulation : from skeleton to cytoskeleton. *Osteoarthr Cartil*. 1999;7(1):81–94.
104. O’Conor CJ, Case N, Guilak F. Mechanical regulation of chondrogenesis. *Stem Cell Res Ther*. 2013;4(4):1.
105. Ingber DE. Tensegrity I. Cell structure and hierarchical systems biology. *J Cell Sci*. 2003;116(7):1157–73.

106. Ingber DE. Tensegrity and Mechanotransduction. *J Bodyw Mov Ther.* 2008;12(3):198–200.
107. Ingber DE. The architecture of life. *Sci Am.* 1998;278(1):48–57.
108. Wang N, Donald E. Probing transmembrane mechanical coupling and cytomechanics using magnetic twisting cytometry. *Biochem Cell Biol.* 1995;73:327–35.
109. Chen CS, Chen CS, Mrksich M, Huang S, Whitesides GM, Ingber DE. Geometric Control of Cell Life and Death. *Science (80- ).* 1997;276:1425–8.
110. Ingber DE. Tensegrity II . How structural networks influence cellular information processing networks. *J Cell Sci.* 2003;116(8):1397–408.
111. Alenghat FJ, Ingber DE. Mechanotransduction : All Signals Point to Cytoskeleton , Matrix , and Integrins. *Sci STKE.* 2002;119(PE6):1–5.
112. Davies PF. Flow-mediated endothelial mechanotransduction. *Physiol Rev.* 1995;75(3):519–60.
113. Wary KK, Mariotti A, Zurzolo C, Giancotti FG. A requirement for caveolin-1 and associated kinase Fyn in integrin signaling and anchorage-dependent cell growth. *Cell.* 1998;94(5):625–34.
114. Wang N, Butler JP, Ingber DE. Mechanotransduction Across the Cell Surface and Through the Cytoskeleton. *Science (80- ).* 1993;260(May):1124–8.
115. Ruoslahti E. RGD and other recognition sequences for integrins. *Annu Rev Cell Dev Biol.* 1996;12:697–715.
116. Huettner N, Dargaville TR, Forget A. Discovering Cell-Adhesion Peptides in Tissue Engineering: Beyond RGD. *Trends Biotechnol.* 2018;36(4):372–83.
117. Jeschke B, Meyer J, Jonczyk A, Kessler H, Adamietz P, Meenen NM, et al. RGD-peptides for tissue engineering of articular cartilage. *Biomaterials.* 2002;23(16):3455–63.

118. Martin JA, Buckwalter JA. Effects of fibronectin on articular cartilage chondrocyte proteoglycan synthesis and response to insulin-like growth factor-I. *J Orthop Res.* 1998;16(6):752–7.
119. Kock LM, Schulz RM, van Donkelaar CC, Thümmeler CB, Bader A, Ito K. RGD-dependent integrins are mechanotransducers in dynamically compressed tissue-engineered cartilage constructs. *J Biomech.* 2009;42(13):2177–82.
120. Cartmell SH, Dobson J, Verschueren SB, El Haj AJ. Development of magnetic particle techniques for long-term culture of bone cells with intermittent mechanical activation. *IEEE Trans Nanobioscience.* 2002;1(2):92–7.
121. Hughes S, Dobson J, El Haj AJ. Magnetic targeting of mechanosensors in bone cells for tissue engineering applications. *J Biomech.* 2007;40(SUPPL. 1):96–104.
122. Chen JL, Duan L, Zhu W, Xiong J, Wang D. Extracellular matrix production in vitro in cartilage tissue engineering. *J Transl Med.* 2014;12(1):1–9.
123. Enyedi P, Czirják G. Molecular background of leak K<sup>+</sup> currents: Two-pore domain potassium channels. *Physiol Rev.* 2010;90(2):559–605.
124. Honoré E. The neuronal background K<sup>2</sup>P channels: Focus on TREK1. *Nat Rev Neurosci.* 2007;8(4):251–61.
125. Maingret F, Lauritzen I, Patel AJ, Heurteaux C, Reyes R, Lesage F, et al. TREK-1 is a heat-activated background K<sup>+</sup> channel. *EMBO J.* 2000;19(11):2483–91.
126. Martinac B. Mechanosensitive ion channels : molecules of mechanotransduction. *J Cell Sci.* 2004;117:2449–60.
127. Patel AJ, Honoré E, Maingret F, Lesage F, Fink M, Duprat F, et al. A mammalian two pore domain mechano-gated S-like K<sup>+</sup> channel. *EMBO J.* 1998;17(15):4283–90.

128. Honore E, Patel AJ, Chemin J, Suchyna T, Sachs F. Desensitization of mechano-gated K<sup>2</sup>P channels. *Proc Natl Acad Sci.* 2006;103(18):6859–64.
129. Maingret F, Patel AJ, Lesage F, Lazdunski M, Honoré E. Lysophospholipids open the two-pore domain mechano-gated K<sup>+</sup> channels TREK-1 and TRAAK. *J Biol Chem.* 2000;275(14):10128–33.
130. Honoré E, Maingret F, Lazdunski M, Patel AJ. An intracellular proton sensor commands lipid- and mechano-gating of the K<sup>+</sup> channel TREK-1. *EMBO J.* 2002;21(12):2968–76.
131. Lauritzen I, Chemin J, Honoré E, Jodar M, Guy N, Lazdunski M, et al. Cross-talk between the mechano-gated K<sup>2</sup>P channel TREK-1 and the actin cytoskeleton. *EMBO Rep.* 2005;6(7):642–8.
132. Hughes S, Mcbain S, Dobson J, Haj AJ El. Selective activation of mechanosensitive ion channels using magnetic particles. *J R Soc Interface.* 2008;5:855–63.
133. Kanczler JM, Sura HM, Magnay J, Green D, Oreffo ROC, Phil D, et al. Controlled Differentiation of Human Bone Marrow Stromal Cells Using Magnetic Nanoparticle Technology. *Tissue Eng Part A.* 2010;16(10):3241–50.
134. Walker RG, Willingham AT, Zuker CS. A *Drosophila* Mechanosensory Transduction Channel. *Science (80- ).* 2000;287:2229–34.
135. Christensen AP, Corey DP. TRP channels in mechanosensation: Direct or indirect activation? *Nat Rev Neurosci.* 2007;8(7):510–21.
136. Montell C. The TRP superfamily of cation channels. *Sci STKE.* 2005;(272).
137. Ranade SS, Syeda R, Ardem P. Mechanically activated ion channels. *Neuron.* 2016;87(6):1162–79.
138. Güler AD, Lee H, Iida T, Shimizu I, Tominaga M, Caterina M. Heat-Evoked Activation of the Ion

- Channel, TRPV4. *J Neurosci*. 2002;22(15):6408–14.
139. Nilius B, Watanabe H, Vriens J. The TRPV4 channel: Structure-function relationship and promiscuous gating behaviour. *Pflugers Arch Eur J Physiol*. 2003;446(3):298–303.
140. Everaerts W, Nilius B, Owsianik G. The vanilloid transient receptor potential channel TRPV4: From structure to disease. *Prog Biophys Mol Biol*. 2010;103(1):2–17.
141. Mamenko M, Zaika O, Boukelmoune N, O’Neil RG, Pochynyuk O. Deciphering physiological role of the mechanosensitive TRPV4 channel in the distal nephron. *Am J Physiol - Ren Physiol*. 2015;308(4):F275–86.
142. Colbert HA, Smith TL, Bargmann CI. OSM-9, a novel protein with structural similarity to channels, is required for olfaction, mechanosensation, and olfactory adaptation in *Caenorhabditis elegans*. *J Neurosci*. 1997;17(21):8259–69.
143. Liedtke W, Choe Y, Martí-Renom MA, Bell AM, Denis CS, AndrejŠali, et al. Vanilloid receptor-related osmotically activated channel (VR-OAC), a candidate vertebrate osmoreceptor. *Cell*. 2000;103(3):525–35.
144. Cuajungco MP, Grimm C, Oshima K, D’Hoedt D, Nilius B, Mensenkamp AR, et al. PACSINs bind to the TRPV4 cation channel: PACSIN 3 modulates the subcellular localization of TRPV4. *J Biol Chem*. 2006;281(27):18753–62.
145. Strotmann R, Schultz G, Plant TD. Ca<sup>2+</sup>-dependent potentiation of the nonselective cation channel TRPV4 is mediated by a C-terminal calmodulin binding site. *J Biol Chem*. 2003;278(29):26541–9.
146. Nishimura G, Lausch E, Savarirayan R, Shiba M, Spranger J, Zabel B, et al. TRPV4-associated skeletal dysplasias. *Am J Med Genet Part C Semin Med Genet*. 2012;160 C(3):190–204.
147. Guilak F, Leddy HA, Liedtke W. Transient receptor potential vanilloid 4: The sixth sense of the

- musculoskeletal system? *Ann N Y Acad Sci.* 2010;1192(Skeletal Biology and Medicine):404–9.
148. Erickson GR, Alexopoulos LG, Guilak F. Hyper-osmotic stress induces volume change and calcium transients in chondrocytes by transmembrane, phospholipid, and G-protein pathways. *J Biomech.* 2001;34(12):1527–35.
149. Chao PHG, West AC, Hung CT. Chondrocyte intracellular calcium, cytoskeletal organization, and gene expression responses to dynamic osmotic loading. *Am J Physiol - Cell Physiol.* 2006;291(4):718–25.
150. Phan MN, Leddy HA, Votta BJ, Kumar S, Levy DS, Lipshutz DB, et al. Functional Characterization of TRPV4 As an Osmotically Sensitive Ion Channel in Articular Chondrocytes. *Arthritis Rheum.* 2010;60(10):3028–37.
151. Nilius B, Prenen J, Wissenbach U, Bödding M, Droogmans G. Differential activation of the volume-sensitive cation channel TRP12 (OTRPC4) and volume-regulated anion currents in HEK-293 cells. *Pflugers Arch Eur J Physiol.* 2001;443(2):227–33.
152. O’Neil RG, Heller S. The mechanosensitive nature of TRPV channels. *Pflugers Arch Eur J Physiol.* 2005;451(1):193–203.
153. Bi W, Deng JM, Zhang Z, Behringer RR, De Crombrughe B. Sox9 is required for cartilage formation. *Nat Genet.* 1999;22(1):85–9.
154. Sekiya I, Tsuji K, Koopman P, Watanabe H, Yamada Y, Shinomiya K, et al. SOX9 enhances aggrecan gene promoter/enhancer activity and is up-regulated by retinoic acid in a cartilage-derived cell line, TC6. *J Biol Chem.* 2000;275(15):10738–44.
155. Akiyama H, Chaboissier MC, Martin JF, Schedl A, De Crombrughe B. The transcription factor Sox9 has essential roles in successive steps of the chondrocyte differentiation pathway and is required for expression of Sox5 and Sox6. *Genes Dev.* 2002;16(21):2813–28.

156. Auer-grumbach M, Olschewski A, Papić L, Kremer H, Meriel E. Alterations in the ankyrin domain of TRPV4 cause congenital distal SMA, scapulo-peroneal SMA and HMSN2C. *Nat Genet.* 2010;42(2):160–4.
157. McNulty AL, Leddy HA, Liedtke W, Guilak F. TRPV4 as a Therapeutic Target for Joint Diseases. *Naunyn-Schmiedeberg's Arch Pharmacol.* 2015;388(4):437–50.
158. Nilius B, Voets T. The puzzle of TRPV4 channelopathies. *EMBO Rep.* 2013;14(2):152–63.
159. Rock MJ, Prenen J, Funari VA, Funari TL, Merriman B, Nelson SF, et al. Gain-of-function mutations in TRPV4 cause autosomal dominant brachyolmia. *Nat Genet.* 2008;40(8):999–1003.
160. Chikuda H, Kugimiya F, Hoshi K, Ikeda T, Ogasawara T, Shimoaka T, et al. Cyclic GMP-dependent protein kinase II is a molecular switch from proliferation to hypertrophic differentiation of chondrocytes. *Genes Dev.* 2004;18(19):2418–29.
161. Foster JW, Dominguez-Steglich MA, Guioli S, Kwok C, Weller PA, Stevanovic M, et al. Campomelic dysplasia and autosomal sex reversal caused by mutations in a SRY-related gene. *Nature.* 1994;372(6505):525–30.
162. Clark AL, Votta BJ, Kumar S, Liedtke W, Guilak F. Chondroprotective role of the osmotically-sensitive ion channel TRPV4: Age- and sex-dependent progression of osteoarthritis in *Trpv4* deficient mice. *Arthritis Rheum.* 2010;62(10):2973–83.
163. O'Connor CJ, Griffin TM, Liedtke W, Guilak F. Increased susceptibility of *Trpv4*-deficient mice to obesity and obesity-induced osteoarthritis with very high-fat diet. *Ann Rheum Dis.* 2013;72(2):300–4.
164. O'Connor CJ, Ramalingam S, Zelenski NA, Benefield HC, Rigo I, Little D, et al. Cartilage-Specific Knockout of the Mechanosensory Ion Channel TRPV4 Decreases Age-Related Osteoarthritis.

- Sci Rep. 2016;6(July):1–10.
165. Corrigan MA, Johnson GP, Stavenschi E, Riffault M. TRPV4-mediates oscillatory fluid shear mechanotransduction in mesenchymal stem cells in part via the primary cilium. *Sci Rep.* 2018;8:1–13.
  166. Itoh Y, Hatano N, Hayashi H, Onozaki K, Miyazawa K, Muraki K. An environmental sensor, TRPV4 is a novel regulator of intracellular Ca<sup>2+</sup> in human synoviocytes. *Am J Physiol - Cell Physiol.* 2009;297(5):1082–90.
  167. Fu S, Meng H, Inamdar S, Das B, Gupta H, Wang W, et al. Activation of TRPV4 by mechanical, osmotic or pharmaceutical stimulation is anti-inflammatory blocking IL-1 $\beta$  mediated articular cartilage matrix destruction. *Osteoarthr Cartil.* 2021;29(1):89–99.
  168. Stanczyk J, Ospelt C, Karouzakis E, Filer A, Raza K, Kolling C, et al. Altered expression of microRNA-203 in rheumatoid arthritis synovial fibroblasts and its role in fibroblast activation: Commentary. *Arthritis Rheum.* 2011;63:373–81.
  169. Horwich MD, Zamore PD. Design and delivery of antisense oligonucleotides to block microRNA function in cultured *Drosophila* and human cells. *Nat Protoc.* 2008;3(10):1537–49.
  170. Eleswarapu S V., Athanasiou KA. TRPV4 channel activation improves the tensile properties of self-assembled articular cartilage constructs. *Acta Biomater.* 2013;9(3):5554–61.
  171. O’Conor CJ, Leddy HA, Benefield HC, Liedtke WB, Guilak F. TRPV4-mediated mechanotransduction regulates the metabolic response of chondrocytes to dynamic loading. *PNAS.* 2014;111(4):1316–21.
  172. Nims RJ, Pferdehirt L, Ho NB, Savadipour A, Lorentz J, Sohi S, et al. A synthetic mechanogenetic gene circuit for autonomous drug delivery in engineered tissues. *Sci Adv.* 2021;7(5):1–13.

173. Akbarzadeh A, Samiei M, Davaran S. Magnetic nanoparticles: preparation, physical properties, and applications in biomedicine. *Nanoscale Res Lett.* 2012;7(1):144.
174. Lovejoy D, Lovejoy D. Magnetic particles, their characteristics and application. In: *Magnetic Particle Inspection.* 1993. p. 117–47.
175. Tapeinos C. Magnetic Nanoparticles and Their Bioapplications. In: *Smart Nanoparticles for Biomedicine.* Elsevier Inc.; 2018. p. 131–42.
176. Williams HM. The application of magnetic nanoparticles in the treatment and monitoring of cancer and infectious diseases. *Biosci Horizons Int J Student Res.* 2017;10:1–10.
177. Colombo M, Carregal-Romero S, Casula MF, Gutiérrez L, Morales MP, Böhm IB, et al. Biological applications of magnetic nanoparticles. *Chem Soc Rev.* 2012;41(11):4306–34.
178. Spain E, Venkatanarayanan A. Review of Physical Principles of Sensing and Types of Sensing Materials. In: *Comprehensive Materials Processing.* Elsevier; 2014. p. 5–46.
179. Krishnan KM. Biomedical nanomagnetism: A spin through possibilities in imaging, diagnostics, and therapy. *IEEE Trans Magn.* 2010;46(7):2523–58.
180. Sechovsky V. Encyclopedia of Materials: Science and Technology : Magnetism in Solids: General Introduction. In: Elsevier Science Ltd. 2000. p. 1–15.
181. Frank R. Handbook of modern sensors: physics, designs, and applications. *Anal Bioanal Chem.* 2005;382(1):8–9.
182. Schenck JF. The role of magnetic susceptibility in magnetic resonance imaging: MRI magnetic compatibility of the first and second kinds. *Med Phys.* 1996;23(6):815–50.
183. Veisheh O, Gunn JW, Zhang M. Design and fabrication of magnetic nanoparticles for targeted drug delivery and imaging. *Adv Drug Deliv Rev.* 2010;62(3):284–304.

184. Chouly C, Pouliquen D, Lucet I, Jeune JJ, Jallet P. Development of superparamagnetic nanoparticles for MRI: Effect of particle size, charge and surface nature on biodistribution. *J Microencapsul.* 1996;13(3):245–55.
185. Zhang Y, Kohler N, Zhang M. Surface modification of superparamagnetic iron oxide nanoparticles and their intracellular uptake. *Biomaterials.* 2002;23:1553–61.
186. Reddy LH, Arias JL, Nicolas J, Couvreur P. Magnetic nanoparticles: Design and characterization, toxicity and biocompatibility, pharmaceutical and biomedical applications. *Chem Rev.* 2012;112(11):5818–78.
187. Berry CC. Possible exploitation of magnetic nanoparticle – cell interaction for biomedical applications. *J Mater Chem.* 2005;15:543–7.
188. Weissleder R, Stark DD, Engelstad BL, Bacon BR, Compton CC, White DL, et al. Superparamagnetic iron oxide: Pharmacokinetics and toxicity. *Am J Roentgenol.* 1989;152(1):167–73.
189. Harrison RP, Chauhan VM, Onion D, Aylott JW, Sottile V. Intracellular processing of silica-coated superparamagnetic iron nanoparticles in human mesenchymal stem cells. *RSC Adv.* 2019;9(6):3176–84.
190. Arruebo M, Fernández-Pacheco R, Ibarra MR, Santamaría J. Magnetic nanoparticles for drug delivery. *Nano Today.* 2007;2(3):22–32.
191. Yin H, Too HP, Chow GM. The effects of particle size and surface coating on the cytotoxicity of nickel ferrite. *Biomaterials.* 2005;26(29):5818–26.
192. Karlsson HL, Gustafsson J, Cronholm P, Möller L. Size-dependent toxicity of metal oxide particles-A comparison between nano- and micrometer size. *Toxicol Lett.* 2009;188(2):112–8.
193. Klausner RD, Rouault TA, Harford JB. Regulating the fate of mRNA: The control of cellular iron

- metabolism. *Cell*. 1993;72(1):19–28.
194. Elias A, Tsourkas A. Imaging circulating cells and lymphoid tissues with iron oxide nanoparticles. *Hematol Am Soc Hematol Educ Progr*. 2009;1:720–6.
195. Lunov O, Syrovets T, Röcker C, Tron K, Ulrich Nienhaus G, Rasche V, et al. Lysosomal degradation of the carboxydextran shell of coated superparamagnetic iron oxide nanoparticles and the fate of professional phagocytes. *Biomaterials*. 2010;31(34):9015–22.
196. Markides H, Rotherham M, El Haj AJ. Biocompatibility and toxicity of magnetic nanoparticles in regenerative medicine. *J Nanomater*. 2012;2012:13–5.
197. Jordan A, Scholz R, Maier-Hauff K, van Landeghem FKH, Waldoefner N, Teichgraber U, et al. The effect of thermotherapy using magnetic nanoparticles on rat malignant glioma. *J Neurooncol*. 2006;78(1):7–14.
198. Albarqi HA, Demessie AA, Sabei FY, Moses AS, Hansen MN, Dhagat P, et al. Systemically delivered magnetic hyperthermia for prostate cancer treatment. *Pharmaceutics*. 2020;12(11):1–14.
199. Singh S, Barick KC, Bahadur D. Inactivation of bacterial pathogens under magnetic hyperthermia using Fe<sub>3</sub>O<sub>4</sub>-ZnO nanocomposite. *Powder Technol*. 2015;269:513–9.
200. Choi JW, Park JW, Na Y, Jung SJ, Hwang JK, Choi D, et al. Using a magnetic field to redirect an oncolytic adenovirus complexed with iron oxide augments gene therapy efficacy. *Biomaterials*. 2015;65:163–74.
201. Wang C, Ding C, Kong M, Dong A, Qian J, Jiang D, et al. Tumor-targeting magnetic lipoplex delivery of short hairpin RNA suppresses IGF-1R overexpression of lung adenocarcinoma A549 cells in vitro and in vivo. *Biochem Biophys Res Commun*. 2011;410(3):537–42.
202. Wimpenny I, Markides H, Haj AJ El. Orthopaedic applications of nanoparticle-based stem cell

- therapies. *Stem Cell Res Ther.* 2012;3(13).
203. Markides H, Kehoe O, Morris RH, El Haj AJ. Whole body tracking of superparamagnetic iron oxide nanoparticle-labelled cells - A rheumatoid arthritis mouse model. *Stem Cell Res Ther.* 2013;4(5):1.
204. Harrison R, Lockett J, Marsh S, Leija HAL, Salih S, Alkharji R, et al. Magnetically assisted control of stem cells applied in 2D, 3D and in situ models of cell migration. *Molecules.* 2019;24(8):1–18.
205. Landázuri N, Tong S, Suo J, Joseph G, Weiss D, Sutcliffe DJ, et al. Magnetic targeting of human mesenchymal stem cells with internalized superparamagnetic iron oxide nanoparticles. *Small.* 2013;9(23):4017–26.
206. Lewin M, Carlesso N, Tung CH, Tang XW, Cory D, Scadden DT, et al. Tat peptide-derivatized magnetic nanoparticles allow in vivo tracking and recovery of progenitor cells. *Nat Biotechnol.* 2000;18(4):410–4.
207. Arbab AS, Yocum GT, Rad AM, Khakoo AY, Fellowes V, Read EJ, et al. Labeling of cells with ferumoxides-protamine sulfate complexes does not inhibit function or differentiation capacity of hematopoietic or mesenchymal stem cells. *NMR Biomed.* 2005;18(8):553–9.
208. Balakumaran A, Pawelczyk E, Ren J, Sworder B, Chaudhry A, Sabatino M, et al. Superparamagnetic iron oxide nanoparticles labeling of bone marrow stromal (Mesenchymal) cells does not affect their “stemness.” *PLoS One.* 2010;5(7).
209. Dobson J, Cartmell SH, Keramane A, El Haj AJ. Principles and design of a novel magnetic force mechanical conditioning bioreactor for tissue engineering, stem cell conditioning, and dynamic in vitro screening. *IEEE Trans Nanobioscience.* 2006;5(3):173–7.
210. Kobayashi T, Ochi M, Yanada S, Ishikawa M, Adachi N, Deie M, et al. A Novel Cell Delivery

- System Using Magnetically Labeled Mesenchymal Stem Cells and an External Magnetic Device for Clinical Cartilage Repair. *Arthrosc - J Arthrosc Relat Surg*. 2008;24(1):69–76.
211. Kobayashi T, Ochi M, Yanada S, Ishikawa M, Adachi N, Deie M, et al. Augmentation of Degenerated Human Cartilage In Vitro Using Magnetically Labeled Mesenchymal Stem Cells and an External Magnetic Device. *Arthrosc - J Arthrosc Relat Surg*. 2009;25(12):1435–41.
212. Hughes S, El Haj AJ, Dobson J. Magnetic micro- and nanoparticle mediated activation of mechanosensitive ion channels. *Med Eng Phys*. 2005;27(9):754–62.
213. Cromer Berman SM, Walczak P, Bulte JWM. Tracking stem cells using magnetic nanoparticles. *Wiley Interdiscip Rev Nanomedicine Nanobiotechnology*. 2011;3(4):343–55.
214. Wang N, Stamenović D. Contribution of intermediate filaments to cell stiffness, stiffening, and growth. *Am J Physiol - Cell Physiol*. 2000;279(1 48-1):188–94.
215. El Haj AJ, Wood MA, Thomas P, Yang Y. Controlling cell biomechanics in orthopaedic tissue engineering and repair. *Pathol Biol*. 2005;53(10):581–9.
216. Dobson J. Remote control of cellular behaviour with magnetic nanoparticles. *Nat Nanotech*. 2008;3:139–43.
217. Jagodzinski M, Drescher M, Zeichen J, Hankemeier S, Krettek C, Bosch U, et al. Effects of cyclic longitudinal mechanical strain and dexamethasone on osteogenic differentiation of human bone marrow stromal cells. *Eur Cells Mater*. 2004;7:35–41.
218. Hu B, El Haj AJ, Dobson J. Receptor-targeted, magneto-mechanical stimulation of osteogenic differentiation of human bone marrow-derived mesenchymal stem cells. *Int J Mol Sci*. 2013;14(9):19276–93.
219. Markides H, McLaren JS, El Haj AJ. Overcoming translational challenges - The delivery of mechanical stimuli in vivo. *Int J Biochem Cell Biol*. 2015;69:162–72.

220. Henstock JR, Rotherham M, Rashidi H, Shakesheff KM, El Haj AJ. Remotely Activated Mechanotransduction via Magnetic Nanoparticles Promotes Mineralization Synergistically With Bone Morphogenetic Protein 2: Applications for Injectable Cell Therapy. *Stem Cells Transl Med.* 2014;3:1363–74.
221. Rotherham M, Haj AJE. Remote activation of the Wnt/ $\beta$ -catenin signalling pathway using functionalised magnetic particles. *PLoS One.* 2015;10(3):1–18.
222. Markides H, McLaren JS, Telling ND, Alom N, Al-Mutheffer EA, Oreffo ROC, et al. Translation of remote control regenerative technologies for bone repair. *npj Regen Med.* 2018;3(9).
223. Rotherham M, Henstock JR, Qutachi O, El Haj AJ. Remote regulation of magnetic particle targeted Wnt signaling for bone tissue engineering. *Nanomedicine Nanotechnology, Biol Med.* 2018;14(1):173–84.
224. Henstock JR, Rotherham M, El Haj AJ. Magnetic ion channel activation of TREK1 in human mesenchymal stem cells using nanoparticles promotes osteogenesis in surrounding cells. *J Tissue Eng.* 2018;9:1–10.
225. Gonçalves AI, Rotherham M, Markides H, Rodrigues MT, Reis RL, Gomes ME, et al. Triggering the activation of Activin A type II receptor in human adipose stem cells towards tenogenic commitment using mechanomagnetic stimulation. *Nanomedicine Nanotechnology, Biol Med.* 2018;14(4):1149–59.
226. Hayman DM, Blumberg TJ, Scott CC, Athanasiou KA. The effects of isolation on chondrocyte gene expression. *Tissue Eng.* 2006;12(9):2573–81.
227. Martin-Pena A, Porter RM, Plunton G, McCarrel TM, Morton AJ, Guijarro M V., et al. Lentiviral-based reporter constructs for profiling chondrogenic activity in primary equine cell populations. *Eur Cell Mater.* 2019;36(3):156–70.

228. Mennan C, Garcia J, Roberts S, Hulme C, Wright K. A comprehensive characterisation of large-scale expanded human bone marrow and umbilical cord mesenchymal stem cells. *Stem Cell Res Ther.* 2019;10(1):1–15.
229. Heidari B, Shirazi A, Akhondi MM, Hassanpour H, Behzadi B, Naderi MM, et al. Comparison of proliferative and multilineage differentiation potential of sheep mesenchymal stem cells derived from bone marrow, liver, and adipose tissue. *Avicenna J Med Biotechnol.* 2013;5(2):104–17.
230. Mackay AM, Beck SC, Murphy JM, Barry FP, Chichester CO, Pittenger MF. Chondrogenic differentiation of cultured human mesenchymal stem cells from marrow. *Tissue Eng.* 1998;4(4):415–28.
231. Vincent F, A.J. Duncton M. TRPV4 Agonists and Antagonists. *Curr Top Med Chem.* 2011;11(17):2216–26.
232. Sridharan G, Shankar AA. Toluidine blue: A review of its chemistry and clinical utility. *J Oral Maxillofac Pathol.* 2012;16(2):251–5.
233. Layton C, Bancroft JD. Classification of carbohydrates. *J Franklin Inst.* 1943;235(5):525–6.
234. Rittié L. Method for picrosirius red-polarization detection of collagen fibers in tissue sections. *Methods Mol Biol.* 2017;1627:395–407.
235. Drury R. Theory and Practice of Histotechnology. *J Clin Pathol.* 1981;34(12):1406–1406.
236. Alibegović A, Blagus R, Martinez IZ. Safranin O without fast green is the best staining method for testing the degradation of macromolecules in a cartilage extracellular matrix for the determination of the postmortem interval. *Forensic Sci Med Pathol.* 2020;16(2):252–8.
237. Narayanaswamy V, Sambasivam S, Saj A, Alaabed S, Issa B, Al-Omari IA, et al. Role of Magnetite Nanoparticles Size and Concentration on Hyperthermia under Various Field

- Frequencies and Strengths. *Molecules*. 2021;26(4):1–14.
238. Barcena C, Sra AK, Gao J. Nanoscale magnetic materials and applications. *Nanoscale Magnetic Materials and Applications*. 2009. 1–719 p.
239. Markides H, Newell KJ, Rudolf H, Ferreras LB, Dixon JE, Morris RH, et al. Ex vivo MRI cell tracking of autologous mesenchymal stromal cells in an ovine osteochondral defect model. *Stem Cell Res Ther*. 2019;10(1):1–15.
240. Bulte JWM, Daldrup-Link HE. Clinical tracking of cell transfer and cell transplantation: *Tu. Radiology*. 2018;289(3):604–15.
241. Belanova AA, Gavalas N, Makarenko YM, Belousova MM, Soldatov A V., Zolotukhin P V. Physicochemical Properties of Magnetic Nanoparticles: Implications for Biomedical Applications in Vitro and in Vivo. *Oncol Res Treat*. 2018;41(3):139–43.
242. Mülhopt S, Diabaté S, Dilger M, Adelhelm C, Anderlohr C, Bergfeldt T, et al. Characterization of nanoparticle batch-to-batch variability. *Nanomaterials*. 2018;8(5).
243. Desai N. Challenges in development of nanoparticle-based therapeutics. *AAPS J*. 2012;14(2):282–95.
244. Wolfram J, Zhu M, Yang Y, Shen J, Gentile E, Paolino D, et al. Safety of nanoparticles in medicine HHS Public Access This mini-review addresses the safety considerations for nanoparticles in medicine. *Curr Drug Targets*. 2015;16(14):1671–81.
245. Vakili-Ghartavol R, Momtazi-Borojeni AA, Vakili-Ghartavol Z, Aiyelabegan HT, Jaafari MR, Rezayat SM, et al. Toxicity assessment of superparamagnetic iron oxide nanoparticles in different tissues. *Artif Cells, Nanomedicine Biotechnol*. 2020;48(1):443–51.
246. Molday RS, Mackenzie D. Immunospecific ferromagnetic iron-dextran reagents for the labelling and magnetic separation of cells. *J Immunol Methods*. 1982;52:353–67.

247. Lu AH, Salabas EL, Schüth F. Magnetic nanoparticles: Synthesis, protection, functionalization, and application. *Angew Chemie - Int Ed.* 2007;46(8):1222–44.
248. Karimi Z, Karimi L, Shokrollahi H. Nano-magnetic particles used in biomedicine: Core and coating materials. *Mater Sci Eng C.* 2013;33(5):2465–75.
249. Foroozandeh P, Aziz AA. Insight into Cellular Uptake and Intracellular Trafficking of Nanoparticles. *Nanoscale Res Lett.* 2018;13.
250. Baratchi S, Keov P, Darby WG, Lai A, Khoshmanesh K, Thurgood P, et al. The TRPV4 agonist GSK1016790A regulates the membrane expression of TRPV4 channels. *Front Pharmacol.* 2019;9(JAN):1–12.
251. Jin P, Jan LY, Jan Y-N. Mechanosensitive ion channels: Structural features relevant to mechanotransduction mechanisms. *Annu Rev Neurosci.* 2020;43(6):207–29.
252. He L, Ahmad M, Perrimon N. Mechanosensitive channels and their functions in stem cell differentiation. *Exp Cell Res.* 2019;374(2):259–65.
253. Dedman A, Sharif-Naeini R, Folgering JHA, Duprat F, Patel A, Honoré E. The mechano-gated K2P channel TREK-1. *Eur Biophys J.* 2009;38(3):293–303.
254. Fillion MC, Phillips NC. Toxicity and immunomodulatory activity of liposomal vectors formulated with cationic lipids toward immune effector cells. *Biochim Biophys Acta - Biomembr.* 1997;1329(2):345–56.
255. Li L, Jiang W, Luo K, Song H, Lan F, Wu Y, et al. Superparamagnetic iron oxide nanoparticles as MRI contrast agents for non-invasive stem cell labelling and tracking. *Theranostics.* 2013;3(8):595–615.
256. Mudalige T, Qu H, Van Haute D, Ansar SM, Paredes A, Ingle T. Characterization of Nanomaterials: Tools and Challenges. *Nanomaterials for Food Applications.* Elsevier Inc.;

2018. 313–353 p.
257. Sandler SE, Fellows B, Thompson Mefford O. Best Practices for Characterization of Magnetic Nanoparticles for Biomedical Applications. *Anal Chem.* 2019;91(22):14159–69.
258. Tonigold M, Simon J, Estupiñán D, Kokkinopoulou M, Reinholz J, Kintzel U, et al. Pre-adsorption of antibodies enables targeting of nanocarriers despite a biomolecular corona. *Nat Nanotechnol.* 2018;13(9):862–9.
259. Minelli C, Garcia-Diez R, Sikora AE, Gollwitzer C, Krumrey M, Shard AG. Characterization of igg-protein-coated polymeric nanoparticles using complementary particle sizing techniques. *Surf Interface Anal.* 2014;46(10–11):663–7.
260. Worsley GJ, Kumarswami N, Minelli C, Noble JE. Characterisation of antibody conjugated particles and their influence on diagnostic assay response. *Anal Methods.* 2015;7(22):9596–603.
261. Gupta AK, Gupta M. Synthesis and surface engineering of iron oxide nanoparticles for biomedical applications. *Biomaterials.* 2005;26(18):3995–4021.
262. Lin JN, Andrade JD, Chang IN. The influence of adsorption of native and modified antibodies on their activity. *J Immunol Methods.* 1989;125(1–2):67–77.
263. Malhotra N, Lee JS, Liman RAD, Ruallo JMS, Villaflore OB, Ger TR, et al. Potential toxicity of iron oxide magnetic nanoparticles: A review. *Molecules.* 2020;25(14):1–26.
264. Naqvi S, Samim M, Abdin MZ, Ahmed FJ, Maitra AN, Prashant CK, et al. Concentration-dependent toxicity of iron oxide nanoparticles mediated by increased oxidative stress. *Int J Nanomedicine.* 2010;5(1):983–9.
265. Yang CY, Hsiao JK, Tai MF, Chen ST, Cheng HY, Wang JL, et al. Direct labeling of hMSC with SPIO: The long-term influence on toxicity, chondrogenic differentiation capacity, and

- intracellular distribution. *Mol Imaging Biol.* 2011;13(3):443–51.
266. Ruijtenberg S, van den Heuvel S. Coordinating cell proliferation and differentiation: Antagonism between cell cycle regulators and cell type-specific gene expression. *Cell Cycle.* 2016;15(2):196–212.
267. Zhou Y, Fujisawa I, Ino K, Matsue T, Shiku H. Metabolic suppression during mesodermal differentiation of embryonic stem cells identified by single-cell comprehensive gene expression analysis. *Mol Biosyst.* 2015;11(9):2560–7.
268. Lewis MC, MacArthur BD, Tare RS, Oreffo ROC, Please CP. Extracellular matrix deposition in engineered micromass cartilage pellet cultures: Measurements and modelling. *PLoS One.* 2016;11(2):1–12.
269. Watts AE, Ackerman-Yost JC, Nixon AJ. A comparison of three-dimensional culture systems to evaluate in vitro chondrogenesis of equine bone marrow-derived mesenchymal stem cells. *Tissue Eng - Part A.* 2013;19(19–20):2275–83.
270. Li S, Oreffo ROC, Sengers BG, Tare RS. The effect of oxygen tension on human articular chondrocyte matrix synthesis: Integration of experimental and computational approaches. *Biotechnol Bioeng.* 2014;111(9):1876–85.
271. Baratchi S, Khoshmanesh K, Woodman OL, Potocnik S, Peter K, McIntyre P. Molecular Sensors of Blood Flow in Endothelial Cells. *Trends Mol Med.* 2017;23(9):850–68.
272. Gilchrist CL, Leddy HA, Kaye L, Case ND, Rothenberg KE, Little D, et al. TRPV4-mediated calcium signaling in mesenchymal stem cells regulates aligned collagen matrix formation and vinculin tension. *Proc Natl Acad Sci U S A.* 2019;116(6):1992–7.
273. Prodromos C, Finkle S, Rumschlag T, Lotus J. Autologous Mesenchymal Stem Cell Treatment is Consistently Effective for the Treatment of Knee Osteoarthritis: The Results of a Systematic

- Review of Treatment and Comparison to a Placebo Group. *Medicines*. 2020;7(8):42.
274. Le H, Xu W, Zhuang X, Chang F, Wang Y, Ding J. Mesenchymal stem cells for cartilage regeneration. *J Tissue Eng*. 2020;11.
275. Kang I, Lee BC, Choi SW, Lee JY, Kim JJ, Kim BE, et al. Donor-dependent variation of human umbilical cord blood mesenchymal stem cells in response to hypoxic preconditioning and amelioration of limb ischemia. *Exp Mol Med*. 2018;50(4).
276. Holtzer H, Abbott J, Lash J, Holtzer S. The Loss of Phenotypic Traits By Differentiated Cells in Vitro, I. Dedifferentiation of Cartilage Cells. *Proc Natl Acad Sci*. 1960;46(12):1533–42.
277. Yoo JU, Barthel TS, Nishimura K, Solchaga L, Caplan AI, Goldberg VM, et al. The chondrogenic potential of human bone-marrow-derived mesenchymal progenitor cells. *J Bone Jt Surg - Ser A*. 1998;80(12):1745–57.
278. Fahy N, Alini M, Stoddart MJ. Mechanical stimulation of mesenchymal stem cells: Implications for cartilage tissue engineering. *J Orthop Res*. 2018;36(1):52–63.
279. Papachristou D, Pirttiniemi P, Kantomaa T, Agnantis N, Basdra EK. Fos- and Jun-related transcription factors are involved in the signal transduction pathway of mechanical loading in condylar chondrocytes. *Eur J Orthod*. 2006;28(1):20–6.
280. Hong E, di Cesare PE, Haudenschild DR. Role of c-maf in chondrocyte differentiation: A review. *Cartilage*. 2011;2(1):27–35.
281. Woods S, Humphreys PA, Bates N, Richardson SA, Kuba SY, Brooks IR, et al. Regulation of TGF $\beta$  Signalling by TRPV4 in Chondrocytes. *Cells*. 2021;10(4).
282. Huang B, He Y, Li S, Wei X, Liu J, Shan Z, et al. The RCAN1.4-calcineurin/NFAT signaling pathway is essential for hypoxic adaption of intervertebral discs. *Exp Mol Med*. 2020;52(5):865–75.

283. Neybecker P, Henrionnet C, Pape E, Grossin L, Mainard D, Galois L, et al. Respective stemness and chondrogenic potential of mesenchymal stem cells isolated from human bone marrow, synovial membrane, and synovial fluid. *Stem Cell Res Ther.* 2020;11(1):1–12.
284. Zhang R, Ma J, Han J, Zhang W, Ma J. Mesenchymal stem cell related therapies for cartilage lesions and osteoarthritis. *Am J Transl Res.* 2019;11(10):6275–89.
285. DiBartola AC, Everhart JS, Magnussen RA, Carey JL, Brophy RH, Schmitt LC, et al. Correlation between histological outcome and surgical cartilage repair technique in the knee: A meta-analysis. *Knee.* 2016;23(3):344–9.
286. Armiento AR, Alini M, Stoddart MJ. Articular fibrocartilage - Why does hyaline cartilage fail to repair? *Adv Drug Deliv Rev.* 2019;146:289–305.
287. Neginhal V, Kurtz W, Schroeder L. Patient satisfaction, functional outcomes, and survivorship in patients with a customized posterior-stabilized total knee replacement. *JBJS Rev.* 2020;8(7):1–6.
288. Weber M, Craiovan B, Woerner ML, Schwarz T, Grifka J, Renkawitz TF. Predictors of Outcome After Primary Total Joint Replacement. *J Arthroplasty.* 2018;33(2):431–5.
289. Lamo-Espinosa JM, Blanco JF, Sánchez M, Moreno V, Granero-Moltó F, Sánchez-Guijo F, et al. Phase II multicenter randomized controlled clinical trial on the efficacy of intra-articular injection of autologous bone marrow mesenchymal stem cells with platelet rich plasma for the treatment of knee osteoarthritis. *J Transl Med.* 2020;18(1):1–9.
290. Yves-Marie Pers, Lars rackwitz, Rosanna ferreira, Oliver Pullig, Chrostophe Delfour, Frank Barry, Luc Sensebe, Louis Casteilla, Sandrine Fleury, Joachim schrauth, Daniel Haddad Sophie Domergue, Ulruch Noeth C jorgensen. Adipose Mesenchymal Stromal Cell-Based Therapy for Severe Osteoarthritis of the Knee : A phase I Dose-Escalation Trial. *Stemcells Transl Med.*

2016;7(5):847–56.

291. Djillani A, Mazella J, Heurteaux C, Borsotto M. Role of TREK-1 in health and disease, focus on the central nervous system. *Front Pharmacol.* 2019;10(APR):1–15.
292. Salifu AA, Obayemi JD, Uzonwanne VO, Soboyejo WO. Mechanical stimulation improves osteogenesis and the mechanical properties of osteoblast-laden RGD-functionalized polycaprolactone/hydroxyapatite scaffolds. *J Biomed Mater Res - Part A.* 2020;108(12):2421–34.
293. Kafi MA, Aktar K, Todo M, Dahiya R. Engineered chitosan for improved 3D tissue growth through Paxillin-FAK-ERK activation. *Regen Biomater.* 2020;7(2):141–51.
294. Sahu N, Budhiraja G, Subramanian A. Preconditioning of mesenchymal stromal cells with low-intensity ultrasound: influence on chondrogenesis and directed SOX9 signaling pathways. *Stem Cell Res Ther.* 2020;11(1):1–15.
295. Du G, Li L, Zhang X, Liu J, Hao J, Zhu J, et al. Roles of TRPV4 and piezo channels in stretch-evoked Ca<sup>2+</sup> response in chondrocytes. *Exp Biol Med.* 2020;245(3):180–9.
296. Soul J, Dunn SL, Anand S, Serracino-Inglott F, Schwartz JM, Boot-Handford RP, et al. Stratification of knee osteoarthritis: two major patient subgroups identified by genome-wide expression analysis of articular cartilage. *Ann Rheum Dis.* 2018;77(3):423.
297. Matsunobu T, Torigoe K, Ishikawa M, de Vega S, Kulkarni AB, Iwamoto Y, et al. Critical roles of the TGF- $\beta$  type I receptor ALK5 in perichondrial formation and function, cartilage integrity, and osteoblast differentiation during growth plate development. *Dev Biol.* 2009;332(2):325–38.
298. Allen JL, Cooke ME, Alliston T. ECM stiffness primes the TGF $\beta$  pathway to promote chondrocyte differentiation. *Mol Biol Cell.* 2012;23(18):3731–42.

299. Nakao A, Imamura T, Souchelnytskyi S, Kawabata M, Ishisaki A, Oeda E, et al. TGF- $\beta$  receptor-mediated signalling through Smad2, Smad3 and Smad4. *EMBO J.* 1997;16(17):5353–62.
300. Wang W, Rigueur D, Lyons KM. TGF $\beta$  signaling in cartilage development and maintenance. *Birth Defects Res Part C - Embryo Today Rev.* 2014;102(1):37–51.
301. Savadipour A, Nims RJ, Katz DB, Guilak F. Regulation of chondrocyte biosynthetic activity by dynamic hydrostatic pressure: the role of TRP channels. *Connect Tissue Res.* 2021;00(00):1–13.
302. Servin-Vences MR, Moroni M, Lewin GR, Poole K. Direct measurement of TRPV4 and PIEZO1 activity reveals multiple mechanotransduction pathways in chondrocytes. *Elife.* 2017;6:1–24.
303. Gao Y, Liu S, Huang J, Guo W, Chen J, Zhang L, et al. The ECM-cell interaction of cartilage extracellular matrix on chondrocytes. *Biomed Res Int.* 2014;2014:8 pages.
304. Garcia-Carvajal ZY, Garciadiego-Czares D, Parra-Cid C, Aguilar-Gaytn R, Velasquillo C, Ibarra C, et al. Cartilage Tissue Engineering: The Role of Extracellular Matrix (ECM) and Novel Strategies. *Regen Med Tissue Eng.* 2013;365–97.
305. Waldstein W, Perino G, Gilbert SL, Maher SA, Windhager R, Boettner F. OARSI osteoarthritis cartilage histopathology assessment system: A biomechanical evaluation in the human knee. *J Orthop Res.* 2016;34(1):135–40.
306. Yi SW, Kim HJ, Oh HJ, Shin H, Lee JS, Park JS, et al. Gene expression profiling of chondrogenic differentiation by dexamethasone-conjugated polyethyleneimine with SOX trio genes in stem cells. *Stem Cell Res Ther.* 2018;9(1):1–13.
307. Tallheden T, Karlsson C, Brunner A, van der Lee J, Hagg R, Tommasini R, et al. Gene expression during redifferentiation of human articular chondrocytes. *Osteoarthr Cartil.* 2004;12(7):525–35.

308. Yoon IS, Chung CW, Sung JH, Cho HJ, Kim JS, Shim WS, et al. Proliferation and chondrogenic differentiation of human adipose-derived mesenchymal stem cells in porous hyaluronic acid scaffold. *J Biosci Bioeng.* 2011;112(4):402–8.
309. Huang JI, Zuk PA, Jones NF, Zhu M, Lorenz HP, Hedrick MH, et al. Chondrogenic potential of multipotential cells from human adipose tissue. *Plast Reconstr Surg.* 2004;113(2):585–94.
310. Erickson GR, Gimble JM, Franklin DM, Rice HE, Awad H, Guilak F. Chondrogenic potential of adipose tissue-derived stromal cells in vitro and in vivo. *Biochem Biophys Res Commun.* 2002;290(2):763–9.
311. Ravalli S, Szychlinska MA, Lauretta G, Musumeci G. New insights on mechanical stimulation of mesenchymal stem cells for cartilage regeneration. *Appl Sci.* 2020;10(8).
312. Ouyang X, Xie Y, Wang G. Mechanical stimulation promotes the proliferation and the cartilage phenotype of mesenchymal stem cells and chondrocytes co-cultured in vitro. *Biomed Pharmacother.* 2019;117(May):109146.
313. Mueller MB, Fischer M, Zellner J, Berner A, Dienstknecht T, Prantl L, et al. Hypertrophy in mesenchymal stem cell chondrogenesis: Effect of TGF- $\beta$  isoforms and chondrogenic conditioning. *Cells Tissues Organs.* 2010;192(3):158–66.
314. Cao S, Anishkin A, Zinkevich NS, Nishijima Y, Korishettar A, Wang Z, et al. Transient receptor potential vanilloid 4 (TRPV4) activation by arachidonic acid requires protein kinase A-mediated phosphorylation. *J Biol Chem.* 2018;293(14):5307–22.
315. Weissenberger M, Weissenberger MH, Gilbert F, Groll J, Evans CH, Steinert AF. Reduced hypertrophy in vitro after chondrogenic differentiation of adult human mesenchymal stem cells following adenoviral SOX9 gene delivery. *BMC Musculoskelet Disord.* 2020;21(1):1–14.
316. Legendre F, Ollitrault D, Gomez-Leduc T, Bouyoucef M, Hervieu M, Gruchy N, et al. Enhanced

- chondrogenesis of bone marrow-derived stem cells by using a combinatory cell therapy strategy with BMP-2/TGF- $\beta$ 1, hypoxia, and COL1A1/HtrA1 siRNAs. *Sci Rep.* 2017;7(1):1–16.
317. Lu TJ, Chiu FY, Chiu HY, Chang MC, Hung SC. Chondrogenic differentiation of mesenchymal stem cells in three-dimensional chitosan film culture. *Cell Transplant.* 2017;26(3):417–27.
318. Gale AL, Linardi RL, McClung G, Mammone RM, Ortved KF. Comparison of the chondrogenic differentiation potential of equine synovial membrane-derived and bone marrow-derived mesenchymal stem cells. *Front Vet Sci.* 2019;6(JUN):1–10.
319. Desancé M, Contentin R, Bertoni L, Gomez-Leduc T, Branly T, Jacquet S, et al. Chondrogenic differentiation of defined equine mesenchymal stem cells derived from umbilical cord blood for use in cartilage repair therapy. *Int J Mol Sci.* 2018;19(2).
320. Thorpe SD, Buckley CT, Vinardell T, O'Brien FJ, Campbell VA, Kelly DJ. Dynamic compression can inhibit chondrogenesis of mesenchymal stem cells. *Biochem Biophys Res Commun.* 2008;377(2):458–62.
321. Serra R, Johnson M, Filvaroff EH, LaBorde J, Sheehan DM, Derynck R, et al. Expression of a truncated, kinase-defective TGF- $\beta$  type II receptor in mouse skeletal tissue promotes terminal chondrocyte differentiation and osteoarthritis. *J Cell Biol.* 1997;139(2):541–52.
322. Bush JR, Beier F. TGF- $\beta$  and osteoarthritis - The good and the bad. *Nat Med.* 2013;19(6):667–9.
323. Van Der Kraan PM, Goumans MJ, Blaney Davidson E, Ten Dijke P. Age-dependent alteration of TGF- $\beta$  signalling in osteoarthritis. *Cell Tissue Res.* 2012;347(1):257–65.
324. Benya PD, Shaffer JD. Dedifferentiated chondrocytes reexpress the differentiated collagen phenotype when cultured in agarose gels. *Cell.* 1982;30(1):215–24.
325. Angelozzi M, Penolazzi L, Mazzitelli S, Lambertini E, Lolli A, Piva R, et al. Dedifferentiated

- chondrocytes in composite microfibers as tool for cartilage repair. *Front Bioeng Biotechnol.* 2017;5(June).
326. Dexheimer V, Mueller S, Braatz F, Richter W. Reduced reactivation from dormancy but maintained lineage choice of human mesenchymal stem cells with donor age. *PLoS One.* 2011;6(8).
327. Wu CL, Diekmann BO, Jain D, Guilak F. Diet-induced obesity alters the differentiation potential of stem cells isolated from bone marrow, adipose tissue and infrapatellar fat pad: The effects of free fatty acids. *Int J Obes.* 2013;37(8):1079–87.
328. Hipp J, Atala A. Sources of stem cells for regenerative medicine. *Stem Cell Rev.* 2008;4(1):3–11.
329. Marino L, Castaldi MA, Rosamilio R, Ragni E, Vitolo R, Fulgione C, et al. Mesenchymal stem cells from the Wharton's jelly of the human umbilical cord: Biological properties and therapeutic potential. *Int J Stem Cells.* 2019;12(2):218–26.
330. Li X, Duan L, Liang Y, Zhu W, Xiong J, Wang D. Human Umbilical Cord Blood-Derived Mesenchymal Stem Cells Contribute to Chondrogenesis in Coculture with Chondrocytes. *Biomed Res Int.* 2016;2016.
331. Contentin R, Demoor M, Concari M, Desancé M, Audigié F, Branly T, et al. Comparison of the Chondrogenic Potential of Mesenchymal Stem Cells Derived from Bone Marrow and Umbilical Cord Blood Intended for Cartilage Tissue Engineering. *Stem Cell Rev Reports.* 2020;16(1):126–43.
332. Pareek A, Carey JL, Reardon PJ, Peterson L, Stuart MJ, Krych AJ. Long-Term Outcomes after Autologous Chondrocyte Implantation: A Systematic Review at Mean Follow-Up of 11.4 Years. *Cartilage.* 2016;7(4):298–308.

333. Niemeyer P, Laute V, Zinser W, Becher C, Diehl P, Kolombe T, et al. Clinical outcome and success rates of ACI for cartilage defects of the patella: a subgroup analysis from a controlled randomized clinical phase II trial (CODIS study). *Arch Orthop Trauma Surg.* 2020;140(6):717–25.
334. Huang R, Li W, Zhao Y, Yang F, Xu M. Clinical efficacy and safety of stem cell therapy for knee osteoarthritis: A meta-analysis. *Medicine (Baltimore).* 2020;99(11):e19434.
335. Lattouf R, Younes R, Lutomski D, Naaman N, Godeau G, Senni K, et al. Picrosirius Red Staining : A Useful Tool to Appraise Collagen Networks in Normal and Pathological Tissues. *J Histochem Cytochem.* 2020;62(10):751–8.
336. Sun X, Kaufman PD, Biology C. Ki-67: more than a proliferation marker Xiaoming. *HHS Public Access.* 2019;127(2):175–86.
337. Song Y, Zhang J, Xu H, Lin Z, Chang H, Liu W, et al. Mesenchymal stem cells in knee osteoarthritis treatment: A systematic review and meta-analysis. *J Orthop Transl.* 2020;24(March):121–30.
338. Trivedi A, Miyazawa B, Gibb S, Valanoski K, Vivona L, Lin M, et al. Bone marrow donor selection and characterization of MSCs is critical for pre-clinical and clinical cell dose production. *J Transl Med.* 2019;17(1):1–16.
339. Siegel G, Kluba T, Hermanutz-Klein U, Bieback K, Northoff H, Schäfer R. Phenotype, donor age and gender affect function of human bone marrow-derived mesenchymal stromal cells. *BMC Med.* 2013;11(1).
340. Gómez-Leduc T, Hervieu M, Legendre F, Bouyoucef M, Gruchy N, Poulain L, et al. Chondrogenic commitment of human umbilical cord blood-derived mesenchymal stem cells in collagen matrices for cartilage engineering. *Sci Rep.* 2016;6(August):1–17.

341. Chang YH, Wu KC, Wang CC, Ding DC. Enhanced chondrogenesis of human umbilical cord mesenchymal stem cells in a gelatin honeycomb scaffold. *J Biomed Mater Res - Part A*. 2020;108(10):2069–79.
342. Liu J, Yu C, Chen Y, Cai H, Lin H, Sun Y, et al. Fast fabrication of stable cartilage-like tissue using collagen hydrogel microsphere culture. *J Mater Chem B*. 2017;5(46):9130–40.
343. Myster DL, Duronio RJ. Cell cycle: To differentiate or not to differentiate? *Curr Biol*. 2000;10(8):302–4.
344. Pfeifer CG, Berner A, Koch M, Krutsch W, Kujat R, Angele P, et al. Higher ratios of hyaluronic acid enhance chondrogenic differentiation of human MSCs in a hyaluronic acid-gelatin composite scaffold. *Materials (Basel)*. 2016;9(5).
345. Mennan C, Wright K, Bhattacharjee A, Balain B, Richardson J, Roberts S. Isolation and characterisation of mesenchymal stem cells from different regions of the human umbilical cord. *Biomed Res Int*. 2013;2013.
346. Eberbeck D, Wiekhorst F, Steinhoff U, Trahms L. Aggregation behaviour of magnetic nanoparticle suspensions investigated by magnetorelaxometry. *J Phys Condens Matter*. 2006;18(38).
347. Ahsan SM, Rao CM, Ahmad MF. Nanoparticle-protein interaction: The significance and role of protein corona. *Adv Exp Med Biol*. 2018;1048:175–98.
348. Mahmoudi M, Sheibani S, Milani AS, Rezaee F, Gauberti M, Dinarvand R, et al. Crucial role of the protein corona for the specific targeting of nanoparticles. *Nanomedicine*. 2015;10(2):215–26.
349. Markway BD, Tan GK, Brooke G, Hudson JE, Cooper-White JJ, Doran MR. Enhanced chondrogenic differentiation of human bone marrow-derived mesenchymal stem cells in low

- oxygen environment micropellet cultures. *Cell Transplant*. 2010;19(1):29–42.
350. Samal JRK, Rangasami VK, Samanta S, Varghese OP, Oommen OP. Discrepancies on the Role of Oxygen Gradient and Culture Condition on Mesenchymal Stem Cell Fate. *Adv Healthc Mater*. 2021;10(6).
351. Song H, Park KH. Regulation and function of SOX9 during cartilage development and regeneration. *Semin Cancer Biol*. 2020;67(May):12–23.
352. Lefebvre V D-GM. SOX9 and the many facets of its regulation in the chondrocyte lineage. 2017;58(1):2–14.
353. Ogawa Y, Takahashi N, Takemoto T, Nishiume T, Suzuki M, Ishiguro N, et al. Hyaluronan promotes TRPV4-induced chondrogenesis in ATDC5 cells. *PLoS One*. 2019;14(8):1–15.
354. Hattori K, Takahashi N, Terabe K, Ohashi Y, Kishimoto K, Yokota Y, et al. Activation of transient receptor potential vanilloid 4 protects articular cartilage against inflammatory responses via CaMKK/AMPK/NF- $\kappa$ B signaling pathway. *Sci Rep*. 2021;11(1):1–9.
355. Dalous J, Larghero J, Baud O. Transplantation of umbilical cord-derived mesenchymal stem cells as a novel strategy to protect the central nervous system: technical aspects, preclinical studies, and clinical perspectives. *Pediatr Res*. 2012;71(4 Pt 2):482–90.
356. Raileanu VN, Whiteley J, Chow T, Kollara A, Mohamed A, Keating A, et al. Banking Mesenchymal Stromal Cells from Umbilical Cord Tissue: Large Sample Size Analysis Reveals Consistency Between Donors. *Stem Cells Transl Med*. 2019;8(10):1041–54.
357. Lu Y, Qiao L, Lei G, Mira RR, Gu J, Zheng Q. Col10a1 gene expression and chondrocyte hypertrophy during skeletal development and disease. *Front Biol (Beijing)*. 2014;9(3):195–204.
358. Ogura T, Mosier BA, Bryant T, Minas T. A 20-Year Follow-up after First-Generation Autologous

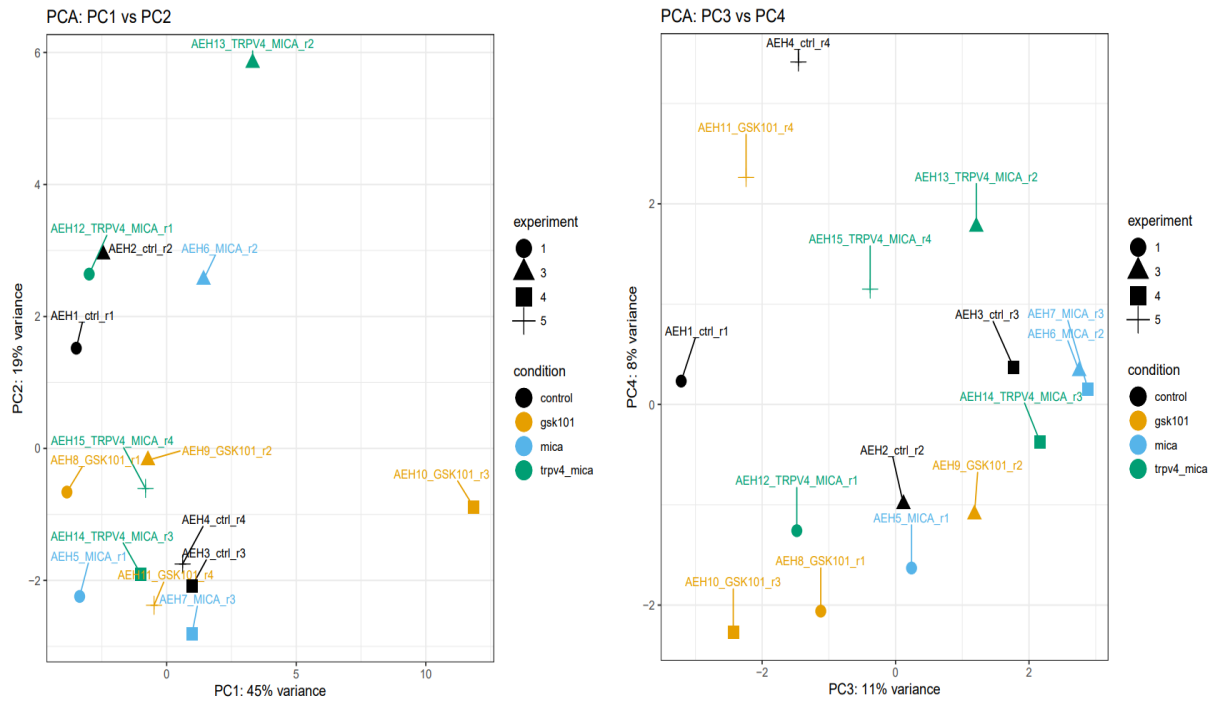
- Chondrocyte Implantation. *Am J Sports Med.* 2017;45(12):2751–61.
359. Peterson L, Vasiliadis HS, Brittberg M, Lindahl A. Autologous chondrocyte implantation: A long-term follow-up. *Am J Sports Med.* 2010;38(6):1117–24.
360. Arshi A, Petrigliano FA, Williams RJ, Jones KJ. Stem Cell Treatment for Knee Articular Cartilage Defects and Osteoarthritis. *Curr Rev Musculoskelet Med.* 2020;13(1):20–7.
361. Toh WS, Lee EH, Cao T. Potential of Human Embryonic Stem Cells in Cartilage Tissue Engineering and Regenerative Medicine. *Stem Cell Rev Reports.* 2011;7(3):544–59.
362. Gutierrez-Aranda I, Ramos-Mejia V, Bueno C, Munoz-Lopez M, Real PJ, Mácia A, et al. Human induced pluripotent stem cells develop teratoma more efficiently and faster than human embryonic stem cells regardless the site of injection. *Stem Cells.* 2010;28(9):1568–70.
363. Szalay B, Tátrai E, Nyíró G, Vezér T, Dura G. Potential toxic effects of iron oxide nanoparticles in in vivo and in vitro experiments. *J Appl Toxicol.* 2012;32(6):446–53.
364. Li J, Liu Y, Cha R, Ran B, Mou K, Wang H, et al. The biocompatibility evaluation of iron oxide nanoparticles synthesized by a one pot process for intravenous iron supply. *RSC Adv.* 2016;6(17):14329–34.
365. Nune SK, Gunda P, Thallapally PK, Lin Y-Y, Forrest LM, Berkland CJ. Nanoparticles for medical imaging. *Expert Opin Drug Deliv.* 2009;6(11):1175–94.
366. Solchaga LA, Penick KJ, Welter JF. Chondrogenic differentiation of bone marrow-derived mesenchymal stem cells: tips and tricks. Vol. 698, *Methods in molecular biology* (Clifton, N.J.). 2011. 253–278 p.

---

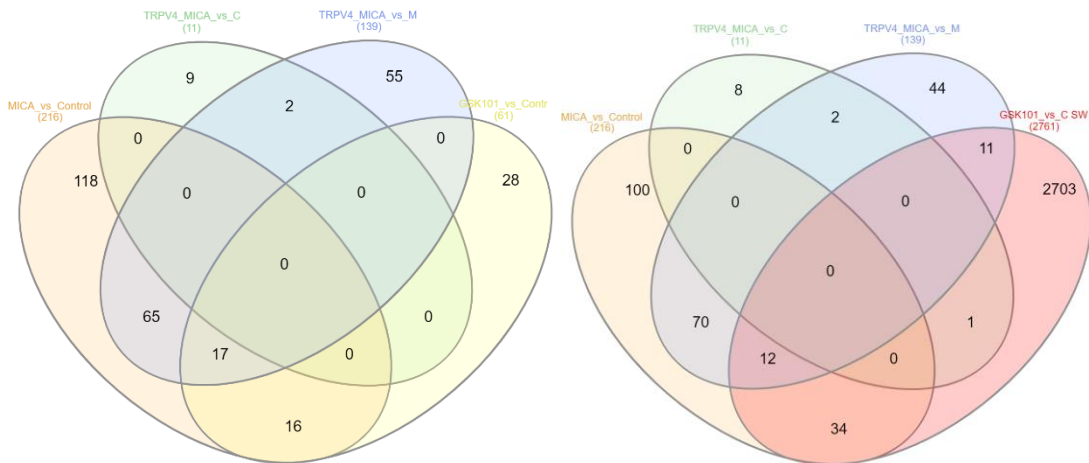
# *Appendices*

---

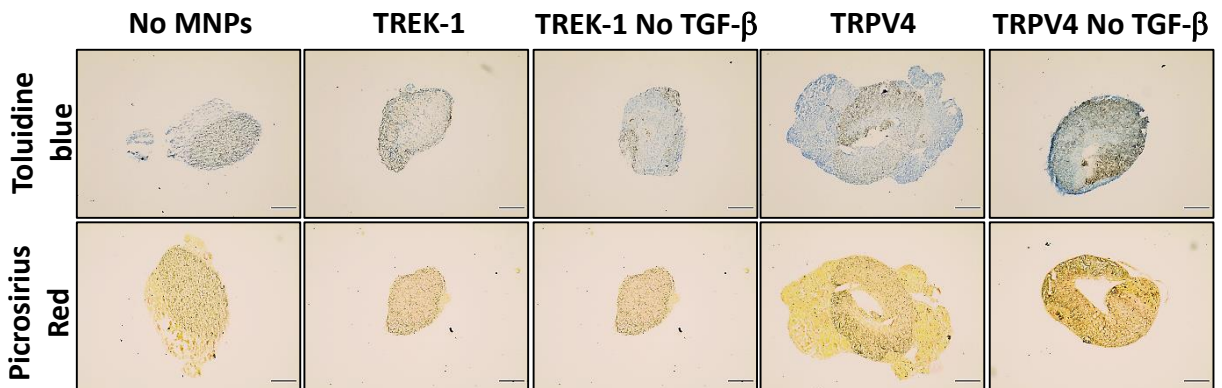
## Supplementary figures



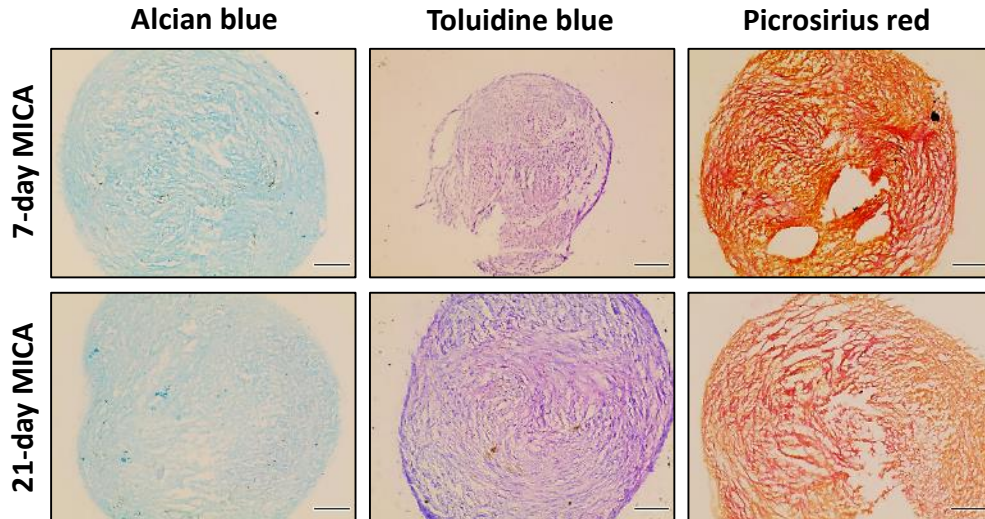
**Supplementary figure 1. Higher variability was found among experiments than among experimental conditions.** RNAseq principal component analysis (PCA) of experiments 1, 2, 3 and 4. N= 4 (1 sample per group per experiment) (n=1 technical repeats). Data generated by Dr. Steven Woods and Prof. Sue Kimber.



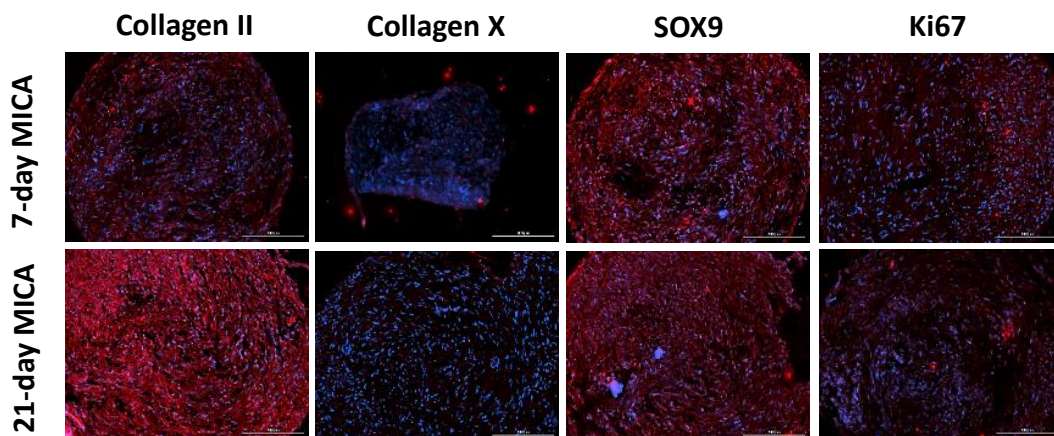
**Supplementary figure 2. DEGs in common between comparisons shown few genes matching the mechanical and chemical activation of TRPV4.** The RNA extracted from monolayers without MNPs under static and dynamic (MICA) conditions, TRPV4-MNPs labelled samples MICA-stimulated and TRPV4 activated samples with GSK101 was analysed by RNA seq. All groups show the genes matching with other experimental groups on each section of the diagram. Right diagram has included GSK101 results from the collaborators' previous experiment. Data generated by Dr. Steven Woods and Prof. Sue Kimber.



**Supplementary figure 3. No signs of collagen or proteoglycan presence were detected on P0 chondrocytes sections after 21 days of culture.** Representative images of ovine P0 chondrocytes pellet 7  $\mu\text{m}$  sections stained with toluidine blue for sGAGs detection and picrosirius red for collagen detection. Scale bar = 200  $\mu\text{m}$ .



**Supplementary figure 4. Little differences were found among samples MICA activated for 7 days and 21 days.** Representative images of 7  $\mu\text{m}$  pellet sections of hUC-MSCs TRPV4-labelled, cultured for 21 days and stimulated for 7 and 21 days. Sections were stained with alcian blue for sGAGs detection, toluidine blue for proteoglycan detection and picrosirius red for collagen evaluation. Scale bar = 200  $\mu\text{m}$ .



**Supplementary figure 5. Similar expression found among samples MICA-activated for 7 days and 21 days with the exception of collagen II.** Representative images of immunohistochemical sections of 7  $\mu\text{m}$  hUC-MSCs TRPV4-labelled pellet sections cultured for 21 days and stimulated for 7 and 21 days. Sections were stained with collagen II, collagen X, SOX9 and Ki67. Scale bar = 200  $\mu\text{m}$ .